Silver as a Novel Tracer for Late Quaternary Southern Ocean Biological and Geophysical Processes

by

Meghan Elizabeth Wagner

A dissertation submitted in partial fulfillment
of the requirements for the degree of
Doctor of Philosophy
(Earth and Environmental Sciences)
in the University of Michigan
2013

Doctoral Committee:

Associate Professor Ingrid L. Hendy, Chair
Research Professor Jeffrey C. Alt
Assistant Professor Gregory J. Dick
Professor Adam J. Matzger
Assistant Professor Nathan D. Sheldon

Acknowledgements

First and foremost, this dissertation would not have been possible without the help, guidance, and immense patience of my advisor, Ingrid Hendy. Thank you for giving me a second chance at the amazing world of research, and for opening my eyes to the fascinating worlds of geochemistry and paleoceanography. You have been a role model and an inspiration. I have also benefitted from having a great committee to work with. Greg Dick always seemed to have a solution to my research problems where I found myself lacking the proper equipment. Jeff Alt was a source of simple, powerful ideas and questions. Nathan Sheldon spent many hours with me in reading group, class, the laboratory, etc. Adam Matzger gave me an opportunity in his laboratory and entertained my crazy research ideas.

Additionally my collaborators Jennifer McKay and Tom Pedersen patiently read through many drafts of Chapter 2, and probably will do the same for Chapter 3. Thank you for all your insight and hard work.

This dissertation would also not have been possible without the help and encouragement of many people within the Department of Earth and Environmental Sciences. Some who have made an especially notable contribution include: Becky Lange and Anne Hudon, who helped me to find my way into the department when I changed my field of study midway through graduate school (a decision I have never regretted); Ted Huston, who has been a patient and diligent teacher in all things mass spec; and Janine Taylor, who took care of all my computer needs.

I owe a big thank you to my parents for a lifetime's worth of love and support. Thank you also to friends and extended family that have supported and encouraged me. You have seen me

through good times and bad. I am lucky to have had your strong shoulders to lean on in the bad times, and I have been overwhelmed by your generosity. Because I will probably leave someone out if I try to list names, I will only say that you know who you are. Grandpa, although you couldn't be here to see me finish my degree, I still wanted to tell you: I did it! First Ph.D. in the Poel family!

I am also grateful to many people at the Asian Martial Arts Studio (including the Chinese Lion Dance Troupe) for helping me to grow in martial arts and in life, and for giving me an outlet for any frustrations. The dojo has been a second home to me, and I will miss being part of the school. Special thanks go to Eric, who taught me the value of deliberateness and how to stand taller. You have been an incredible teacher and positive force in my life, as well as my friend. I could not have gotten through this last year without you. Thank you also to "Iron Lady" Laura, a true friend and inspiration. I have enjoyed being your lion dance teammate and partner for stirring up trouble at the dojo. You have taught me an enormous amount about how to learn and how to conquer problems.

Finally, I was supported by a Rackham Dissertation Writing Fellowship during Winter 2013, and BP provided fellowship support during three terms.

Table of Contents

List of Tables

List of Figures

List of Appendices

List of Acronyms

	ACRONYM
Antarctic Bottom Water	AABW
Antarctic Circumpolar Current	ACC
Antarctic Cold Reversal	ACR
Antarctic Polar Front	APF
Antarctic Polar Frontal Zone	APFZ
Antarctic Zone	AZ
Deep Western Boundary Current	DWBC
Glacial North Atlantic Intermediate Water	GNAIW
High-Nutrient, Low-Chlorophyll	HNLC
Indian Deep Water	IDW
Indonesian Throughflow	ITF
Inductively Coupled Plasma-Mass Spectrometry	ICP-MS
Inductively Coupled Plasma-Optical Emission Spectrometry	ICP-OES
Isotope Dilution	ID
Last Glacial Maximum	LGM
Lower Circumpolar Deep Water	LCDW
Marine Isotope Stage	MIS
North Atlantic Deep Water	NADW

North Pacific Intermediate Water	NPIW
Oxygen Penetration Depth	OPD
Pacific Deep Water	PDW
Particulate Organic Carbon	POC
Relative Standard Deviation	RSD
Southern Antarctic Circumpolar Current Front	SACCF
Subantarctic Front	SAF
Subantarctic Zone	SAZ
Upper Circumpolar Deep Water	UCDW
West Antarctic Peninsula	WAP
X-Ray Fluorescence	XRF

Abstract

The global air-sea CO_2 balance is set within the Southern Ocean through deep water formation, upwelling, and the biological pump. Diatoms dominate Southern Ocean primary productivity and export large amounts of C_{org}. However, past changes in Southern Ocean biological pump strength are presently not well understood because conventional proxies for export production can be biased by particle degradation. This dissertation explores Ag as a novel, potentially more robust proxy for diatom (paleo)productivity. The reliability of Ag and its delivery mechanism to sediments are investigated in Southern Ocean sediments and by laboratory studies on pure diatom cultures.

To test whether sedimentary Ag enrichment occurs underlying oceanic regions of high diatom productivity, Ag and redox-sensitive trace metal fluxes were measured alongside conventional productivity proxy fluxes in Southern Ocean surface sediments. In the open ocean Pacific sector, increased Ag and productivity proxy fluxes coincide with the highly productive opal belt. Along the West Antarctic Peninsula continental margin, high regional surface productivity and nonlithogenic trace metal concentrations strongly suggest suboxic sediments maintained by seasonally elevated export production.

Having demonstrated that Ag records diatom productivity patterns, Ag and redox-sensitive trace metals were measured in two South Atlantic cores to determine whether glacial-age deep waters contained greater CO_2/lower O_2 concentrations. Results reveal a shift in pore water chemistry from poorly oxygenated during the Last Glacial Maximum and deglaciation, to well oxygenated during the late Holocene. Sedimentary suboxia resulting from high C_{org} flux and

lower bottom water O_2 concentrations implies that glacial Lower Circumpolar Deep Water was more isolated and stored more CO_2 compared to present day.

Accurately interpreting Ag as a paleoproxy requires understanding how diatom debris delivers Ag to sediments. To probe this mechanism, diatoms were fed Ag in culture and subsequently analyzed in bulk and as single cells to determine Ag storage location. Results indicate that diatoms store Ag in organic matter with little to no Ag in frustules. Although biogenic particle degradation and Ag scavenging during particle water column transit likely affect the amount of Ag delivered to sediments, Ag shows considerable potential to serve as a reliable qualitative proxy for diatom (paleo)productivity.

Chapter 1

Introduction

1. Biogeochemical Cycles

Chemical elements are continually transferred from one component of the Earth to another. At Earth's surface, natural processes partition elements among the atmosphere (gases), hydrosphere (water), cryosphere (ice), geosphere (rocks and sediments), and biosphere (living things). The mass of an element stored in a given reservoir at any one time coupled with its rate of transfer to a different reservoir is known as biogeochemical cycling. Understanding an element's biogeochemical cycling can be used as a tool for interpreting the geological record in terms of perturbations to a system and the feedbacks that follow. Insights gained from past changes can reveal how the system works, how one system interacts with another, and how the systems we know today might change in the future.

For example, the biogeochemical cycling of carbon has particular importance because the carbon stored in the atmospheric reservoir as carbon dioxide (CO_2) is a primary driver of climate through the greenhouse effect. Atmospheric CO_2 levels have fluctuated throughout Earth's history, with warmer intervals having higher atmospheric CO_2 concentrations and vice versa [*Royer et al.*, 2007]. Presently, anthropogenic perturbation of carbon biogeochemical cycling is occurring as large volumes of CO_2 enter the atmosphere each year due to fossil fuel burning. Assessments of future climate impacts rely on accurate modeling of carbon biogeochemical cycling. To understand how the climate system responds to perturbations, one commonly

employed strategy is to study past events where large masses of carbon were redistributed among reservoirs. One such event considered in **Chapter 4** is the Last Glacial Maximum, at which time the atmosphere contained ~80-100 ppm CO_2 less than interglacial periods [*Sigman and Boyle*, 2000]. Because the deep ocean reservoir is approximately 60 times larger than the atmospheric reservoir and the deep ocean exchanges carbon on millennial timescales, it is assumed to have stored glacial CO_2 [*Broecker*, 1982]. However, the mechanisms underlying this change have still not been fully worked out.

2. Silver (Ag) and the Biological Pump

This dissertation mainly investigates Ag biogeochemical cycling and its intersection with the biological pump, the process by which atmospheric CO_2 is transferred to the deep ocean using marine organic matter as an intermediary. The biological pump has been invoked as a potential mechanism for drawing down atmospheric CO_2 during Pleistocene glacial intervals [*Martin*, 1990] and for ameliorating the effects of anthropogenic CO_2 emissions [e.g., *Martin et al.*, 1990]. Export production—organic matter that sinks below the thermocline—that is respired back to CO_2 (i.e., remineralized) in deep waters can be isolated from the atmosphere for hundreds of years. A relatively small portion of export production survives remineralization during water column transit to be buried in sediments, effectively removing that carbon from the atmosphere for a longer time [*Sarmiento and Gruber*, 2006]. Insights into the past strength of the biological pump and its effect on climate have largely come from biogenic particles (e.g., organic matter, microfossils, etc.) preserved in marine sediments that serve as proxies for export production. A proxy is a chemical or physical characteristic preserved in the geological record that substitutes for direct measurements of past conditions. However, biogenic particles are rapidly remineralized by decomposers in the water column and in sediments, leaving a

potentially incomplete record.

As described in **Chapter 2**, prior experimental work and observations suggested that Ag might function as a novel proxy to overcome these limitations. Furthermore, Ag has been hypothesized to act as a diatom-specific proxy. Diatoms are single-celled eukaryotic phytoplankton that are distinctive for their construction of a hydrated silica ($SiO_2 \bullet nH_2O$) shell, termed a frustule. Their structure is similar to a petri dish, with one, larger half of the frustule (the epitheca) overlapping the other, smaller half (hypotheca) [*Round et al.*, 1990]. Diatoms evolved during the Mesozoic era and the fossil record indicates that they began to radiate by the Early Cretaceous [*Falkowski et al.*, 2004]. Diatoms thrive where nutrient levels are high, such as in upwelling regions. Their ability to accumulate and store nutrients under these conditions allows them to outcompete other phytoplankton groups [*Falkowski et al.*, 2004] such that diatom silica forms major sedimentary deposits under coastal upwelling areas and in the Subarctic Pacific and Southern Oceans [*Nelson et al.*, 1995]. More importantly concerning the biological pump, diatoms are responsible for ~40% of global marine primary productivity and more than 50% of organic carbon exported to the ocean interior [*Katz et al.*, 2004], firmly establishing their significance in modern marine carbon cycling.

The research comprising this dissertation aims to test the reliability and usefulness of Ag as a (paleo)productivity proxy. Additionally, in **Chapters 2-4** sedimentary enrichments of redox-sensitive trace metals (Cd, Re, and Mo) are measured alongside Ag to explore diagenetic and environmental controls on redox chemistry and to track paleoceanographic changes. Diagenesis refers to the combined effect of all chemical, physical, and/or biological processes that change a sediment subsequent to its deposition in water [*Berner*, 1980]. Redox chemistry describes reactions in which one or more electrons are transferred between reactants. The decomposition of

organic matter is a redox reaction, as organic carbon is oxidized (electrons lost) by a series of oxidizing agents (electrons gained) [*Froelich et al.*, 1979]. Decomposition using O_2 yields the greatest free energy change, followed by MnO_2, NO_3^-, Fe_2O_3 or FeOOH, SO_4^{2-}, and methanogenesis. Trace metals are useful for reconstructing the intensity of organic matter decomposition in sediments because their relative enrichment or depletion depends on how reducing sediments are—in other words, how much of the available oxidizing agents are used up.

The research presented here was undertaken with the idea that effective use of Ag depends on a thorough understanding of its marine geochemical cycling. Because diatoms are the dominant phytoplankton group in the Southern Ocean [*Ragueneau et al.*, 2000], we began our investigations by examining Southern Ocean sediments. The Southern Ocean is an atypical location in which to search for sedimentary trace metal enrichments given its well-oxygenated bottom waters and the fact that the trace metals (Ag, Cd, Re, and Mo) are preserved under reducing conditions. Nevertheless, this dissertation demonstrates that trace metal enrichments occur in modern and ancient Southern Ocean sediments.

Chapter 2 examines sedimentary enrichments of Ag and other trace metals compared to commonly used productivity proxies and surface productivity patterns in the open ocean of the Pacific sector. Within the opal belt, biogenic silica-rich sediments provide evidence for strong export production by diatoms, and establish the first test of whether increased Ag fluxes to underlying sediments will occur as a result. At the time of writing, this chapter is in revision at *Earth and Planetary Science Letters.* **Chapter 3** utilizes the same proxy tools, but instead investigates trace metal enrichments along the continental shelf west of the Antarctic Peninsula. Trace metal concentrations in this environment are compared to those from more commonly studied regions (e.g., oxygen minimum zones), and a strategy for interpreting paleoredox records

along the West Antarctic Peninsula margin is proposed. Having established that Ag enrichments concur with productivity proxies and surface productivity, **Chapter 4** applies Ag and other trace metals to unraveling the interplay between ocean ventilation changes and organic carbon export in the South Atlantic Ocean over the last ~30,000 years. This chapter is currently in review at *Paleoceanography*. Finally, **Chapter 5** provides the first real test of the assumption that Ag is located in diatom frustules using culture studies. The marine biogeochemical cycling of Ag dictates its interpretation as a paleoproductivity proxy, since its delivery to sediments depends on the particle carrier and the partitioning of Ag between particulate and dissolved phases. Hence these experiments provide significant insight into how Ag is delivered to sediments.

3. Ag Geochemistry

Because Ag biogeochemical cycling underlies all of the work presented in this dissertation, its known geochemistry is briefly discussed here. Figure 1.1 presents a simplified version of global Ag geochemical cycling. Native Ag deposits occur worldwide, although Ag is also found associated with other metals. The principal Ag minerals typically contain sulfur either as sulfides (e.g., argentite, acanthite) or sulfosalts (e.g., proustite, tennantite), but chlorides (chlorargyrite) and sulfates (argentojarosite) are also known [*Smith and Carson,* 1977]. Silver occurs at concentrations of 70 ppb in shales [*Turekian and Wedepohl,* 1961], 50 ppb in Earth's upper continental crust [*Taylor and McLennan,* 1985], and 100 ppb in typical basalts [*Taylor,* 1964]. Surface ocean Ag concentrations are on the order of a few pM (10^{-12} mol/L) [e.g., *Ranville and Flegal*, 2005]. In marine and brackish waters, Ag speciation is dominated by chloride complexation $[AgCl_n]^{1-n}$ (n = 1-4) [*Cowan et al.*, 1985; *Miller and Bruland,* 1995]. In fresh and estuarine waters, organic and inorganic sulfides are hypothesized to be the Ag carrier

phases. Dissolved Ag appears to be dominated by colloidal Ag species, while particulate Ag is primarily associated with Fe and Mn oxyhydroxides and sulfides [*Wen et al.*, 1997].

4. Isotope Dilution

The isotope dilution technique was used to determine trace metal concentrations in **Chapters 2-4**. During sample preparation, an elemental spike of known concentration that is artificially enriched in one isotope is added to the sample. The resulting isotopic mixture is then a combination of the natural isotopic composition of the sample plus the isotopic composition of the spike. By measuring the ratio of the spike (enriched) isotope to a reference isotope, the concentration of the analyte in the sample can then be determined by the following equation:

$$\frac{N_W}{M} = \frac{S_W\left(\frac{W_N}{W_S}\right)\left[\frac{Ab_S^A - R_m Ab_S^B}{R_m Ab_N^B - Ab_N^A}\right]}{M}$$

where N_W is mass of the analyte; M is mass of the sample; S_W is the mass of the added spike; W_N is the atomic weight of the analyte in the sample; W_S is the atomic weight of the analyte in the spike; Ab is the abundance of isotope A or B in the spike (S) or sample (N); and R_m is the ratio of isotopes A and B in the mixture. Derivation of the isotope dilution equation and further discussion of the technique are given in Faure and Mensing [2005].

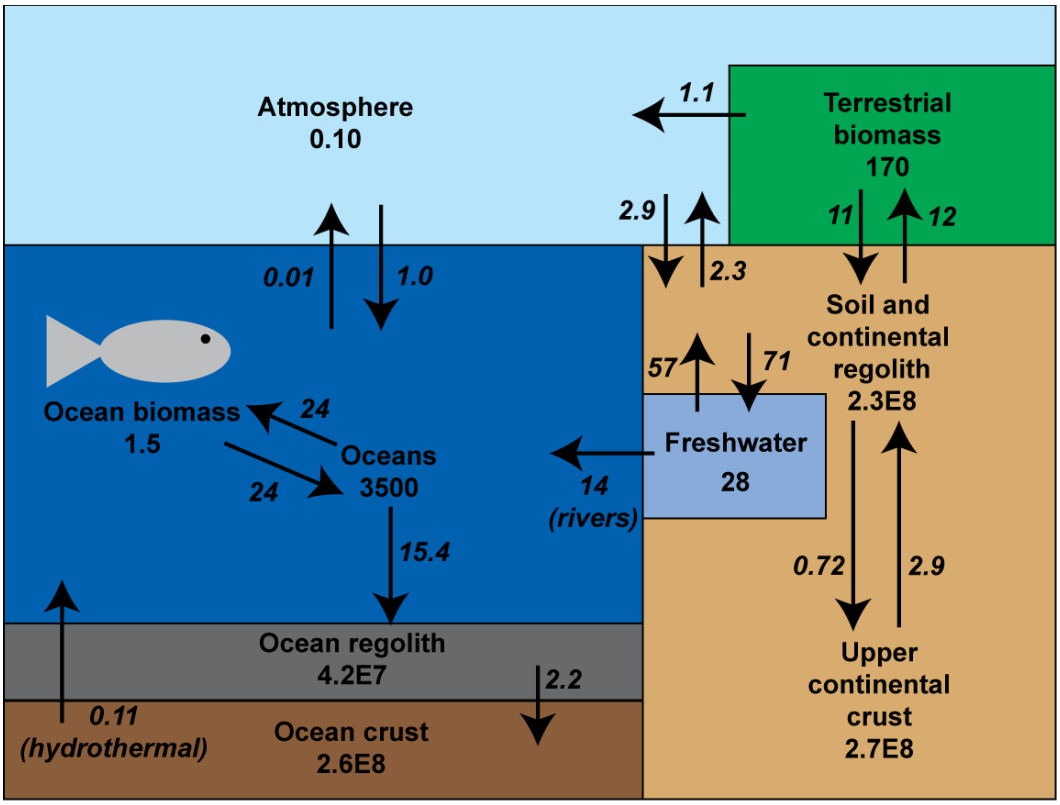

Reservoir size in 10^9 g Ag
Fluxes in 10^9 g Ag/yr

Figure 1.1. A simplified version of the global Ag geochemical cycle (after Rauch and Pacyna [2009] with data from Alt [2003]).

REFERENCES

Alt, J. C. (2003), Hydrothermal fluxes at mid-ocean ridges and on ridge flanks, *Comptes Rendus Geoscience*, *335*(10-11), 853-864.

Berner, R. A. (1980), *Early Diagenesis: A Theoretical Approach*, 241 pp., Princeton University Press, Princeton, NJ.

Broecker, W. S. (1982), Glacial to interglacial changes in ocean chemistry, *Progress in Oceanography*, *11*(2), 151-197.

Cowan, C. E., E. A. Jenne, and E. A. Crecelius (1985), Silver speciation in seawater: The importance of sulfide and organic complexation, in *Marine and Estuarine Geochemistry*, edited by A. C. Sigleo and A. Hattori, pp. 285-303, Lewis Publishers, Inc., Chelsea, MI.

Falkowski, P. G., M. E. Katz, A. H. Knoll, A. Quigg, J. A. Raven, O. Schofield, and F. J. R. Taylor (2004), The evolution of modern eukaryotic phytoplankton, *Science*, *305*(5682), 354-360.

Faure, G., and T. M. Mensing (2005), *Isotopes: principles and applications*, 3rd ed., Wiley, Hoboken.

Froelich, P. N., G. P. Klinkhammer, M. L. Bender, N. A. Luedtke, G. R. Heath, D. Cullen, P. Dauphin, D. Hammond, B. Hartman, and V. Maynard (1979), Early oxidation of organic matter in pelagic sediments of the eastern equatorial Atlantic: suboxic diagenesis, *Geochimica et Cosmochimica Acta*, *43*(7), 1075-1090.

Katz, M. E., Z. V. Finkel, D. Grzebyk, A. H. Knoll, and P. G. Falkowski (2004), Evolutionary trajectories and biogeochemical impacts of marine eukaryotic phytoplankton, *Annual Review of Ecology, Evolution, and Systematics*, *35*, 523-556.

Martin, J. H. (1990), Glacial-interglacial CO_2 change: the iron hypothesis, *Paleoceanography*, *5*(1), 1-13.

Martin, J. H., R. M. Gordon, and S. E. Fitzwater (1990), Iron in Antarctic waters, *Nature*, *345*(6271), 156-158.

Miller, L. A., and K. W. Bruland (1995), Organic speciation of silver in marine waters, *Environmental Science and Technology*, *29*(10), 2616-2621.

Nelson, D. M., P. Treguer, M. A. Brzezinski, A. Leynaert, and B. Queguiner (1995), Production and dissolution of biogenic silica in the ocean-revised global estimates, comparison with regional data and relationship to biogenic sedimentation, *Global Biogeochemical Cycles*, *9*(3), 359-372.

Ragueneau, O., et al. (2000), A review of the Si cycle in the modern ocean: recent progress and missing gaps in the application of biogenic opal as a paleoproductivity proxy, *Global and Planetary Change*, *26*(4), 317-365.

Ranville, M. A., and A. R. Flegal (2005), Silver in the North Pacific Ocean, *Geochemistry Geophysics Geosystems*, *6*(3), Q03M01, doi: 10.1029/2004GC000770.

Rauch, J. N., and J. M. Pacyna (2009), Earth's global Ag, Al, Cr, Cu, Fe, Ni, Pb, and Zn cycles, *Global Biogeochemical Cycles*, *23*, GB2001, doi: 2010.1029/2008GB003376.

Round, F. E., R. M. Crawford, and D. G. Mann (1990), *The Diatoms: Biology and Morphology of the Genera*, 747 pp., Cambridge University Press, New York.

Royer, D. L., R. A. Berner, and J. Park (2007), Climate sensitivity constrained by CO_2 concentrations over the past 420 million years, *Nature*, *446*(7135), 530-532.

Sarmiento, J. L., and N. Gruber (2006), *Ocean Biogeochemical Dynamics*, 503 pp., Princeton University Press, Princeton.

Sigman, D. M., and E. A. Boyle (2000), Glacial/interglacial variations in atmospheric carbon dioxide, *Nature*, *407*(6806), 859-869.

Smith, I. C., and B. L. Carson (1977), *Trace Metals in the Environment*, 469 pp., Ann Arbor Science Publishers Inc., Ann Arbor.

Taylor, S. R. (1964), Abundance of chemical elements in the continental crust: a new table, *Geochimica et Cosmochimica Acta*, *28*(8), 1273-1285.

Taylor, S. R., and S. M. McLennan (1985), *The Continental Crust: its Composition and Evolution*, Blackwell Scientific Publications, Boston.

Turekian, K. K., and K. H. Wedepohl (1961), Distribution of the elements in some major units of the earth's crust, *Geological Society of America Bulletin*, *72*(2), 175-192.

Wen, L.-S., P. H. Santschi, G. A. Gill, C. L. Paternostro, and R. D. Lehman (1997), Colloidal and particulate silver in river and estuarine waters of Texas, *Environmental Science and Technology*, *31*(3), 723-731.

Chapter 2

Influence of Biological Productivity on Silver and Redox-Sensitive Trace Metal Accumulation in Southern Ocean Surface Sediments, Pacific Sector

Abstract

Accurate interpretation of paleoproductivity proxies in the Southern Ocean requires "ground truthing" these proxies. Here the concentrations of total Ba, organic carbon (C_{org}), and biogenic silica (Si_{bio}), along with other redox-sensitive trace metals (Cd, Re, and Mo), are compared with the distribution of silver (Ag) in core top sediments from the Pacific sector of the Southern Ocean. Conventional thinking holds that enrichment of trace metals should be muted or absent in Southern Ocean sediments despite high export of C_{org} from surface waters because deposition under well-oxygenated bottom waters inhibits accumulation of reduced metal phases. While our data support this prediction, detectable preserved vertical fluxes of Ag, Cd, and Re exist beneath the opal belt and faithfully record surface productivity patterns. Therefore we suggest Ag fluxes into Southern Ocean sediments occur via biodetritus associated with high export production rather than accumulation by redox-driven diagenetic processes. Sedimentary Ag concentrations are likely altered at the seafloor by biogenic particle remineralization due to high bottom water O_2. Nevertheless, zonal Ag fluxes are similar to surface productivity patterns, highlighting the potential of Ag to serve as a proxy for diatom export production.

1. Introduction

The accumulation of redox-sensitive trace metals in marine sediments has the capacity to record subtle shifts in the O_2 content of oceanic bottom waters, sedimentary pore waters, or both [*Calvert and Pedersen*, 1993; *Morford and Emerson*, 1999; *Tribovillard et al.*, 2006]. These changes are often tied to the biological pump—a process by which carbon is fixed as organic matter in surface waters by phytoplankton, and subsequently transferred to the deep ocean where it is respired back to CO_2. Because respiration consumes O_2, changes in the strength of the biological pump can indirectly influence redox-sensitive trace metal accumulation, allowing some trace metals—particularly those delivered to sediments with biogenic particles—to act as proxies for past export production. However, trace metals accumulated under reducing conditions are susceptible to remobilization if sediments are subsequently re-oxygenated. In comparison, conventional evaluations of past changes in the biological pump rely on measuring biogenic proxies that accumulate in sediments, such as organic carbon and biogenic silica [e.g., *Bareille et al.*, 1998; *Charles et al.*, 1991; *Mortlock et al.*, 1991]. These proxies suffer from rapid degradation (i.e., remineralization) in the water column and at the sediment-water interface, with only ~1% of organic carbon [*Jahnke*, 1996] and ~10% of biogenic silica [*Ragueneau et al.*, 2000] produced in surface waters arriving at the seafloor. Differential rates of remineralization therefore result in a globally observed decoupling of organic carbon and biogenic silica, diagnosed by highly variable Si:C ratios in sediments. Hence biogenic particle remineralization complicates an accurate determination of the relationship between sediment composition and export production.

Because every proxy is subject to individual biases during production, water column transit, and deposition, a suite of proxies provides a better estimate of past export production. In this study we apply such a multiproxy approach and investigate the coherence between known

modern surface productivity patterns, conventional productivity proxies (organic carbon [C_{org}], biogenic silica [Si_{bio}], and Ba), and redox proxies (Cd, Re, and Mo) preserved in Southern Ocean core top sediments sampled from 18 cores along a north-south transect in the Pacific sector (Figure 2.1). Moreover we explore application of a novel potential proxy for diatom export production: preserved Ag fluxes to sediments. Previous culture studies [*Fisher and Wente*, 1993] and open ocean water column measurements of dissolved Ag versus dissolved silica [*Flegal et al.*, 1995] suggested that Ag is associated with silica, ergo diatoms. Southern Ocean surface sediments were thus chosen for this study because diatoms dominate regional primary production [*Ragueneau et al.*, 2000]. This study is the first to examine trace metal enrichments (with the exception of U) in an open ocean, seasonally productive, and well-oxygenated environment, and extends known conditions under which Ag may be considered a reliable proxy for diatom export production.

2. Background

2.1 Trace Metal Proxies for Sedimentary Redox Conditions

Measurement of trace metal enrichments has become a common technique to infer (paleo) pore water redox conditions [*Tribovillard et al.*, 2006]. Following Berner [1981], we classify sediments whose pore waters contain no *measurable* dissolved oxygen or dissolved sulfide as suboxic, and those that contain measurable dissolved sulfide as anoxic. A variety of delivery mechanisms transfer redox-sensitive trace metals to sediments from overlying waters, so a suite of metals is required to differentiate the processes driving pore water suboxia/anoxia. Below we describe the known geochemistry of trace metals used in this study.

2.1.1 Silver

Silver geochemical cycling in the marine environment is presently not well understood. It

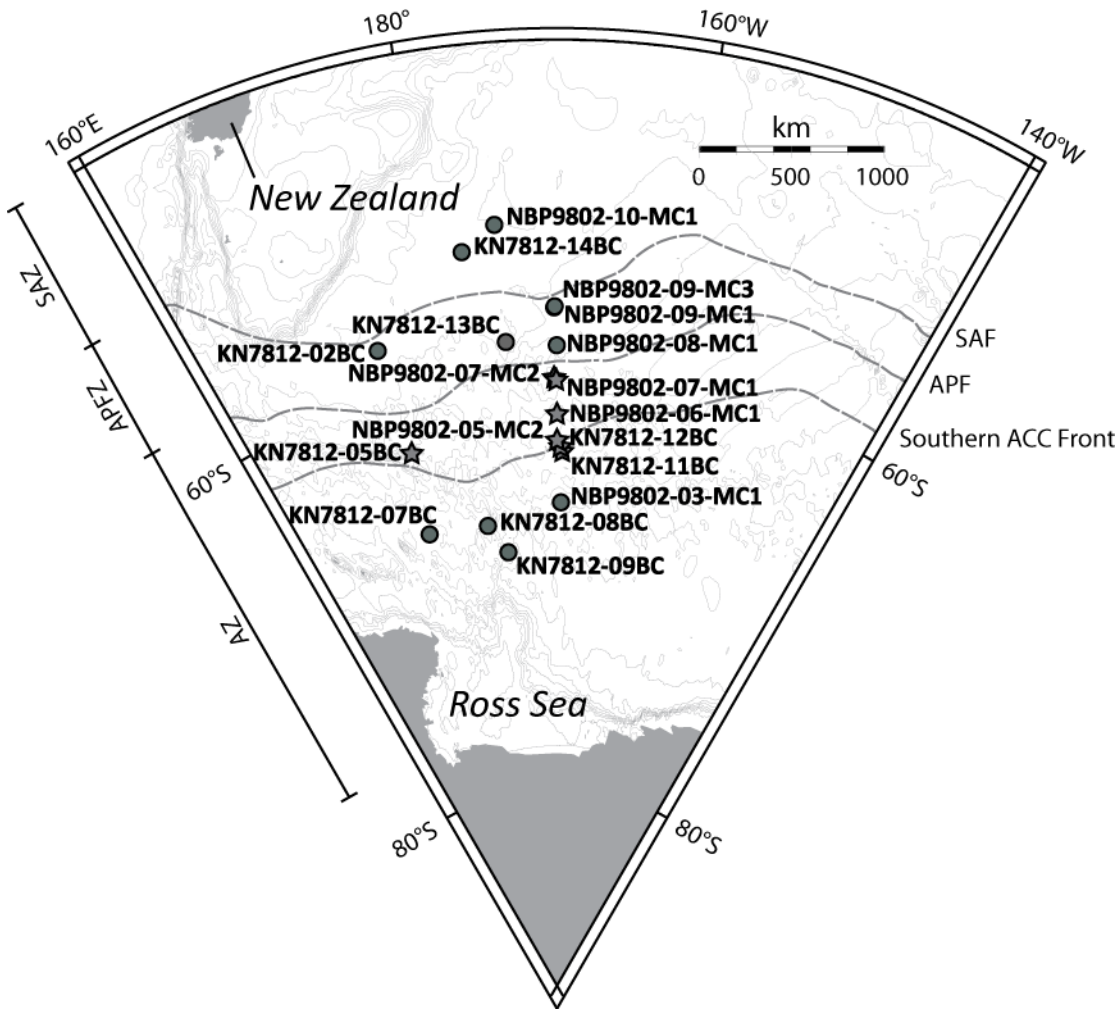

Figure 2.1. Core locations, with stars indicating sites with highest ^{230}Th-normalized proxy concentrations. Fronts of the Antarctic Circumpolar Current (ACC) are indicated by dashed grey lines (after Orsi et al. [1995]). APFZ—Antarctic Polar Frontal Zone; AZ—Antarctic Zone; SAZ—Subantarctic Zone; APF—Antarctic Polar Front; SAF—Subantarctic Front.

appears to have an intermediate behavior that resembles nutrient-type and scavenged elements [*Masuzawa et al.*, 1989]. Water column profiles that show increasing dissolved Ag concentrations with depth, and deep water Ag concentrations that increase along the path of the "conveyor belt" [*Flegal et al.*, 1995; *Kramer et al.*, 2011; *Martin et al.*, 1983; *Ndung'u et al.*, 2001; *Ranville and Flegal*, 2005; *Rivera-Duarte et al.*, 1999; *Zhang et al.*, 2001; *Zhang et al.*, 2004], suggest that Ag participates in biogeochemical cycles. However, sedimentary Ag concentrations increase with water depth, implying concurrent Ag scavenging by sinking

particles [*McKay and Pedersen*, 2008; *Morford et al.*, 2008]. Due to its inferred association with biogenic particles, Ag has been proposed as a proxy for diatom export production [*Crusius and Thomson*, 2003; *Friedl and Pedersen*, 2001; *Hendy and Pedersen*, 2005]. Following Friedl and Pedersen [2001], we hypothesize that diatoms take up Ag in surface waters and sequester it in their tests. This silica-bound Ag is subsequently delivered to sediments by sinking diatom debris, released during silica dissolution, and precipitated as highly insoluble Ag_2S in the presence of trace quantities of sulfide. Thus, preserved Ag_2S would record diatom export production even as diatom frustules are remineralized during early diagenesis in surface sediments and thereby circumvent uncertainties in reconstructing export productivity from biogenic silica that may be caused by diatom dissolution. Silver fluxes higher than those expected from lithogenic background have been suggested to indicate that a high flux of organic matter drove past reducing conditions in sediments [*Hendy and Pedersen*, 2005]. Authigenic Ag_2S precipitation directly from seawater appears to be negligible except in severely anoxic sediments where significant sulfate reduction occurs [*McKay and Pedersen*, 2008].

2.1.2 Cadmium

Similar water column profiles of Cd and PO_4^{3-} [*Boyle et al.*, 1976; *de Baar et al.*, 1994] suggest Cd cycling with biogenic particles that subsequently deliver Cd to the sediment-water interface. It is then released during early diagenesis, diffusing downward to the redox front where it is preserved as CdS in the presence of trace amounts of dissolved sulfide [*Rosenthal et al.*, 1995b]. Like Ag, high Cd fluxes relative to the expected lithogenic contribution should indicate a high flux of organic matter capable of producing suboxic conditions and low-level sulfide generation in sediments [*Hendy and Pedersen*, 2005]. Cadmium displays a strong tendency toward authigenic precipitation within sediments where reducing conditions occur

close to the sediment-water interface [*Calvert and Pedersen*, 1993; *Pedersen et al.*, 1989; *Rosenthal et al.*, 1995b].

2.1.3 Rhenium

Rhenium enrichment—like Ag and Cd—indicates pore water suboxia [*Crusius et al.*, 1996]. Rhenium displays conservative behavior in seawater [*Anbar et al.*, 1992] and exists in pM concentrations as the perrhenate anion [ReO_4^-] [*Colodner et al.*, 1993]. It diffuses into sediments along concentration gradients and precipitates directly from seawater under reducing conditions, possibly as ReO_2 [*Crusius et al.*, 1996], although the probability for this reaction to proceed spontaneously in typical seawater has recently been questioned [*Helz and Dolor*, 2012; and references therein]. Due to its low crustal concentrations, nearly all sedimentary Re is authigenically precipitated [*Crusius et al.*, 1996], such that Re enrichment in the absence of Ag and/or Cd indicates that low bottom water oxygen concentrations rather than high organic matter delivery were responsible for suboxia in underlying sediments.

2.1.4 Molybdenum

In seawater Mo is present as the conservative molybdate anion (MoO_4^{2-}). Under oxic conditions, Mo associates with Mn-oxyhydroxides [*Calvert and Pedersen*, 1993; *Zheng et al.*, 2000] which produces low-level enrichments unrelated to reductive processes. When redox conditions become favorable to Mn-oxyhydroxide reduction, adsorbed Mo can be released to pore waters [*Crusius et al.*, 1996], decreasing preserved solid-phase Mo. Molybdenum enrichments indicating reducing sediments are controlled by pore water H_2S concentrations [*Helz et al.*, 1996; *Zheng et al.*, 2000]. Accumulation of authigenic Mo in continental margin sediments has been shown to significantly correlate with organic carbon delivery and burial [*McManus et al.*, 2006], suggesting coupled biogeochemical cycling. In non-euxinic settings

where sulfide is restricted to sedimentary pore waters, sedimentary Mo concentrations range up to tens of ppm [*Scott and Lyons*, 2012]. Similar to Re, elevated Mo fluxes not coupled with increased Ag and/or Cd fluxes indicate that low bottom water oxygen—rather than high organic carbon flux to sediments—caused anoxic conditions in pore waters.

2.2 Oceanographic Setting

Box cores and multicores used in this study present an opportunity to study productivity proxy preservation and redox-sensitive trace metal behavior in surface sediments across the major frontal zones of the Antarctic Circumpolar Current (ACC). The ACC is an extremely wide and deep current powered by the southern hemisphere westerly winds [*Pickard and Emery*, 1990]. Within the ACC, three major fronts exist around the entire circumpolar region [*Orsi et al.*, 1995]: the Antarctic Polar Front (APF); the Subantarctic Front (SAF), which marks the northernmost limit of the ACC; and the Southern ACC Front, which approximately coincides with, but is distinct from, the southern boundary of the ACC. Frontal systems of the ACC are characterized by fast-moving jets of water that sharply delineate water masses of different properties [*Trull et al.*, 2001] and account for most of the water transport of the ACC[*Orsi et al.*, 1995; *Whitworth and Nowlin*, 1987]. Eddy generation at the fronts is significant and helps to mix nutrients to the surface [*Moore and Abbott*, 2000]. Maximum upwelling of low oxygen, nutrient-rich Upper Circumpolar Deep Water (UCDW) occurs just south of the APF [*Anderson et al.*, 2009; *Trull et al.*, 2001], resulting in high phytoplankton productivity. Oxic bottom waters (> 4.8 mL/L) are present across the predominantly north-south transect traced by the cores studied. Bottom water [O_2] is highest to the south (~5.5 mL/L), reflecting Antarctic Bottom Water (AABW) as the dominant water mass. The Pacific-Antarctic Ridge acts as a barrier to water

mass exchange, separating AABW from lower oxygen (~4.8 mL/L) Lower Circumpolar Deep Water (LCDW) to the north [*Gille et al.,* 2004; *Hall et al.,* 2003; *Orsi et al.,* 1999].

The annual advance and retreat of sea ice plays a crucial role in Southern Ocean ecosystem dynamics and therefore exerts control over biogenic particle production. Phytoplankton blooms have long been observed at the sea ice edge [e.g., *Comiso et al.,* 1993; *Smith and Nelson,* 1985]. Spring melts are thought both to stabilize the water column [*Constable et al.,* 2003; *Smith and Nelson,* 1986] and possibly provide seed populations of diatoms from which to begin the growing season bloom [*Smith and Nelson,* 1985]. In the Pacific sector, maximum sea ice extent occurs during September-October and reaches northward to near 60°S, while the minimum occurs during February following rapid ice retreat during the previous summer months [*Cavalieri and Parkinson,* 2008]. The spring/summer diatom bloom tends to follow the retreating ice edge [*Brzezinski et al.,* 2001].

2.3 Southern Ocean Primary Productivity Patterns

The Southern Ocean is one of the world ocean's three major high-nutrient, low-chlorophyll (HNLC) regions [*Falkowski et al.,* 1998], areas in which phytoplankton productivity is low despite unused major nutrients. Southern Ocean phytoplankton productivity is neither spatially nor temporally homogeneous, as shown by satellite data that first mapped the distribution and abundance of phytoplankton stocks across the entire Southern Ocean [*Boyd,* 2002; *Comiso et al.,* 1993]. High chlorophyll concentrations occur along coastal and near shelf areas, and in open ocean regions overlying bathymetric highs [*Comiso et al.,* 1993]. Phytoplankton productivity may be further enhanced where frontal systems interact with bottom topography [*Moore et al.,* 1999], as in the Southwest Pacific where the Southern ACC Front coincides with the Pacific-Antarctic Ridge. High phytoplankton productivity in open ocean

regions between the APF and the northern extent of winter sea ice (~59-62°S in the Pacific sector) has created the most recognized feature of Southern Ocean sediments, the circum-Antarctic "opal belt," [*Diekmann*, 2007] a band of sediments consisting of diatomaceous opal ooze. Phytoplankton blooms have also been observed near the sea ice edge during episodes of ice melting and retreat [*Comiso et al.*, 1993; *Moore and Abbott*, 2000]. Melt water is hypothesized to stabilize the water column and prevent mixing of phytoplankton away from optimum irradiance levels [*Constable et al.*, 2003]. Seasonal Ekman upwelling is also positively correlated with chlorophyll [*Comiso et al.*, 1993], and acts to sustain high nutrient concentrations. Conversely, low productivity occurs in open ocean areas subject to high wind stress where mixing removes phytoplankton from the optimum irradiance zone [*Comiso et al.*, 1993; *Sallée et al.*, 2010].

3. Materials and Methods

3.1 Cores and Laboratory Methods

Core top sediments were obtained from the Oregon State University Marine Geology Repository. Core locations are mapped in Figure 2.1 and listed in Table 2.1 alongside water depths and sampling depths. Concentrations of Ag, Cd, Re, and Mo for all samples were determined at the University of Victoria by isotope dilution inductively coupled plasma-mass spectrometry (ID ICP-MS) using a Thermo X Series 2 quadrupole mass spectrometer. Prior to analysis, samples were freeze dried and homogenized, then spiked and subjected to total microwave digestion in Teflon vessels using an acid cocktail of trace metal grade HF, HCl, and HNO_3 (SeaStar), following Crusius et al. [1996]. An aliquot was removed from digested samples for Cd, Ag, and Re analysis and passed through a column of Dowex 1X-8 resin to remove interfering isotopes. Working spike concentrations and ratios of $^{109}Ag/^{107}Ag$, $^{111}Cd/^{113}Cd$, $^{185}Re/^{187}Re$, and $^{95}Mo/^{98}Mo$ were calibrated using natural element solutions (High-Purity

Standards). Total Ba and Al concentrations were measured at the University of Michigan's Environmental and Analytical Geochemistry Laboratory (EAGL) using a Jobin Yvon Horiba inductively coupled plasma-optical emission spectrometer (ICP-OES). Samples were prepared using the flux method [*Murray et al.*, 2000] and dissolved in 10% HNO_3. Reproducibility of measurements for trace metals, Ba, and Al, based on repeated analysis of the sediment standard MESS-3, are presented in Table 2.2. Biogenic silica (Si_{bio}) concentrations were determined by the method of Mortlock and Froelich [1989] (2% RSD). Organic carbon (C_{org}) was calculated as the difference of weight percent total carbon minus weight percent inorganic carbon (6% RSD). Total carbon was measured at Oregon State University using a Carlo Erba NA1500 Series 1 elemental analyzer. Inorganic carbon was measured by coulometry at EAGL using a UIC, Inc. Coulometrics instrument. Relative standard deviations of Si_{bio} and C_{org} concentrations are based on 1-2 repeat measurements of ~10% of samples.

3.2 Data Normalization

Large changes in sediment composition across the transect—from primarily lithogenic at the northern and southern extremes, to primarily biogenic silica near the Southern ACC Front [*Sayles et al.*, 2001]—necessitate some form of data normalization to establish a baseline for comparison. However, because every normalization tool relies on a set of assumptions, an ideal normalization method does not exist. This study aims to improve our understanding of Ag biogeochemistry, and because Ag appears to be delivered to sediments as part of the biogenic particle flux, normalizing concentrations of trace metals and biogenic components (Si_{bio}, C_{org}) to particle flux using ^{230}Th (which is highly particle-reactive and delivered to sediments by sinking particles [*Francois et al.*, 2004]) is a reasonable choice. Furthermore, ^{230}Th normalization has the advantage of correcting for sediment redistribution effects—which can deposit up to 20 times

more sediment than the vertical rain in the Southern Ocean [*Chase et al.*, 2003b; *Dezileau et al.*, 2000; *Francois et al.*, 1993]—and estimating fluxes of elements to the sediment-water interface [*Francois et al.*, 2004]. Although Re and Mo are not delivered to sediments as part of the particle flux, they are still susceptible to redistribution by bottom currents and dilution by biogenic silica in the opal belt. Hence we have chosen to use ^{230}Th normalization for these elements as well, while acknowledging that these elements are authigenically precipitated. Further information about the various methods of comparing sedimentary concentrations that were considered and our choice of ^{230}Th normalization is available in the Supplementary Information (Appendix A).

Thorium-230 has a known production rate in the water column, and its expected flux to sediments is entirely a function of water depth. Preserved vertical fluxes of sedimentary components are calculated from measured excess ^{230}Th and normalized to the expected flux of ^{230}Th to sediments [*Francois et al.*, 2004]:

$$F_i = (\beta \times z \times f_i)/{}^{230}_{xs}Th_0$$

where F_i is the preserved vertical flux of component *i*; β is the production rate of ^{230}Th in the water column (2.63×10^{-5} dpm/cm^3/kyr); z is water depth in cm; f_i is the weight fraction of component *i*; and ${}^{230}_{xs}Th_0$ is the measured sedimentary ^{230}Th not associated with the detrital component. We have used published ${}^{230}_{xs}Th_0$ concentrations for *R/V N.B. Palmer* cores [*Chase et al.*, 2003b]. In many cases, sediment sample depths used in this study did not overlap those with reported ${}^{230}_{xs}Th_0$ data, and the data point with the nearest sample depth ($\leq$ 1 cm offset for all *R/V N.B. Palmer* cores) was used instead (Table 2.3). We justify this approach by noting that sedimentation rates within the opal belt are ~8 cm/kyr [*Sayles et al.*, 2001], and that there is little variation in ${}^{230}_{xs}Th_0$ values over the upper 5 cm of each multicore (see Supplementary Information). Cores recovered by the *R/V Knorr* have no measured ${}^{230}_{xs}Th_0$ concentrations, and

instead data were taken from *R/V N.B. Palmer* cores as follows: Cores KN7812-11BC and KN7812-12BC were recovered at nearly the same location as NBP9802-05-MC2 (Figure 2.1), hence the $^{230}_{xs}Th_0$ value from the *R/V N. B. Palmer* core was used for the *R/V Knorr* cores. For the remaining *R/V Knorr* cores, they were assigned $^{230}_{xs}Th_0$ values by considering 1) whether the core is sited within the Antarctic Zone, Antarctic Polar Frontal Zone, or Subantarctic Zone; 2) water depth similarity; 3) similarity in Al content; and 3) similarity in other proxy concentrations. Chosen $^{230}_{xs}Th_0$ values and estimated uncertainties are listed in Table 2.3.

Total metal concentrations were normalized to ^{230}Th instead of excess concentrations because the provenance and composition of the lithogenic material was unknown for each site. However, increases in Ag fluxes occur within the opal belt, where sediment composition has been estimated at ~2-4% lithogenic [*Sayles et al.*, 2001], and therefore trace metal input via lithogenic sediment is negligible. In other words, because the opal belt is the oceanic region of interest, omitting a correction for lithogenic input does not affect our conclusions.

4. Results

All trace metal and Al data reported here are newly generated. We also determined total Ba, weight percent Si_{bio}, and weight percent C_{org} for all surface sediment samples. Productivity proxy results generally agree with previously reported data [*Chase et al.*, 2003b; *Eagle et al.*, 2003]. Fluxes of the commonly-used productivity proxies C_{org}, Ba, and Si_{bio} are shown in Figure 2.2a. Barium fluxes are less than 1000 µg cm^{-2} kyr^{-1} both north and south of 60-65°S; inside this zone fluxes increase, and a maximum flux of 2035 µg cm^{-2} kyr^{-1} occurs at 62°S (core NBP9802-06-MC1). Similarly, Si_{bio} flux is low outside the zone of 60-65°S, but it is significantly higher between these latitudes with the maximum (1.6 g cm^{-2} kyr^{-1}) occurring at site NBP9802-06-MC1. Organic carbon (C_{org}) flux follows a similar pattern to both Ba and Si_{bio} with lower fluxes

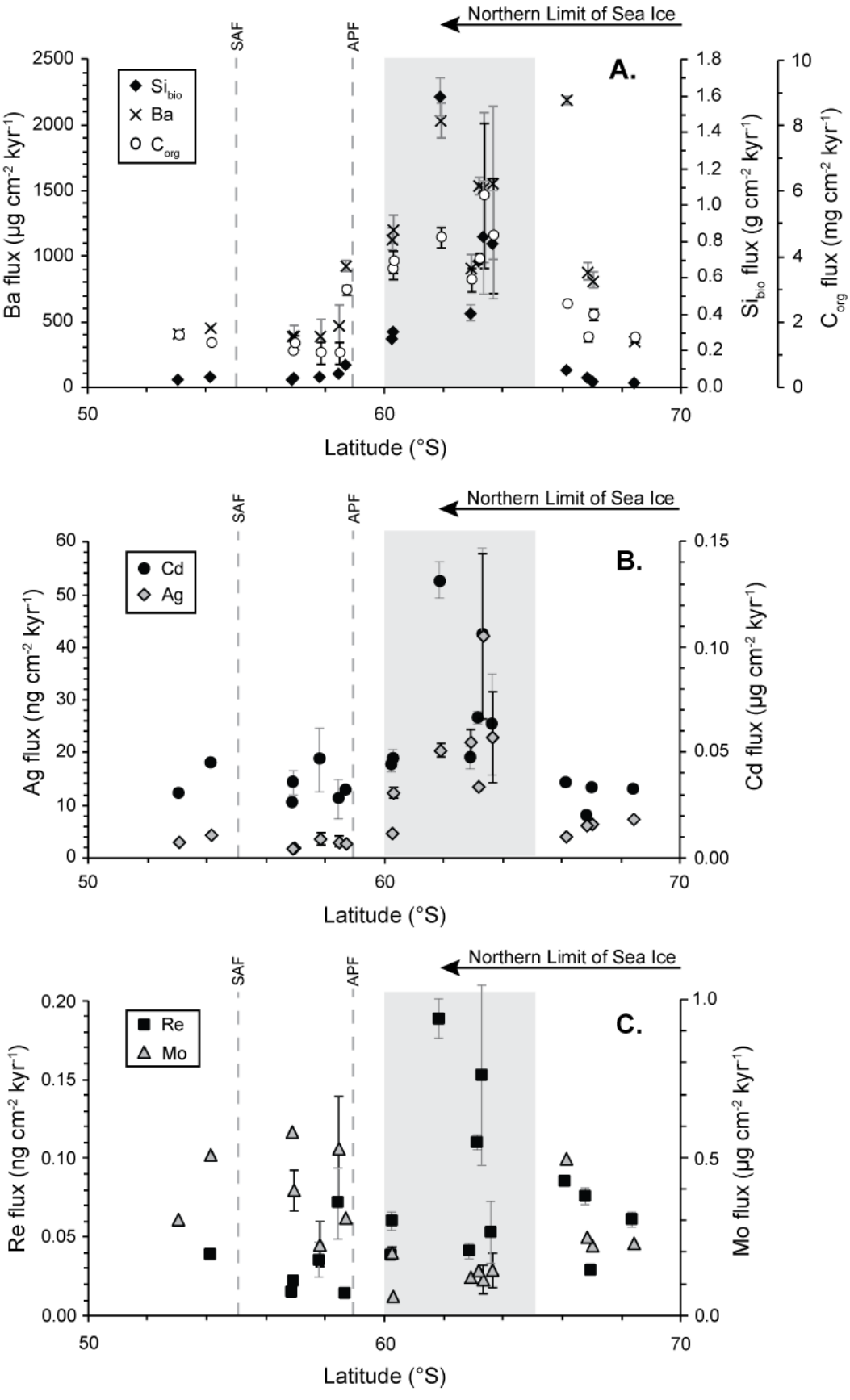
A.
Northern Limit of Sea Ice
SAF
APF
Si$_{bio}$
Ba
C$_{org}$
Ba flux (µg cm^{-2} kyr^{-1})
Si$_{bio}$ flux (g cm^{-2} kyr^{-1})
C$_{org}$ flux (mg cm^{-2} kyr^{-1})
Latitude (°S)
B.
Cd
Ag
Ag flux (ng cm^{-2} kyr^{-1})
Cd flux (µg cm^{-2} kyr^{-1})
C.
Re
Mo
Re flux (ng cm^{-2} kyr^{-1})
Mo flux (µg cm^{-2} kyr^{-1})

Figure 2.2. (Previous page) Productivity proxy and trace metal fluxes estimated from ^{230}Th normalization. A: Productivity proxies barium (Ba), biogenic silica (Si_{bio}), and organic carbon (C_{org}). B: Productivity-influenced trace metals silver (Ag) and cadmium (Cd). C: Authigenic trace metals rhenium (Re) and molybdenum (Mo). Error bars denote range of fluxes expected from uncertainty in $^{230}_{xs}Th_0$, as given in Table 2.3 and discussed in Supplementary Information (Appendix A). If no error bars are shown, then they are smaller than the symbol. Dashed vertical lines mark approximate locations of the Subantarctic Front (SAF) and the Antarctic Polar Front (APF). Grey shaded box from 60-65°S highlights region of highest ^{230}Th-normalized proxy concentrations, excluding Mo which decreases in this zone. Arrow at the top of the figure indicates the northern extent of winter sea ice. Well oxygenated (> 5 mL/L) Antarctic Bottom Water bathes sites south of the Pacific-Antarctic Ridge (~62°S), while slightly less well oxygenated (~4.8 mL/L) Lower Circumpolar Deep Water bathes sites north of the ridge. Oxygen data from http://www.nodc.noaa.gov/OC5/SELECT/dbsearch/dbsearch.html.

outside 60-65°S. Within this region, a maximum flux of 5.9 mg cm^{-2} kyr^{-1} occurs at ~63°S (core KN7812-12BC). In all cases, the highest proxy fluxes to the sediment (Figure 2.2a) are concentrated near 62-63°S, a few degrees south of the Antarctic Polar Front (APF) and approximately coincident with both the northern limit of winter sea ice and the Pacific-Antarctic Ridge axis. This increase in biogenic proxies marks the Pacific sector location of the "opal belt"—the band of biogenic silica-rich sediments that encircles Antarctica [*Diekmann*, 2007].

Trace metal fluxes (Ag, Cd, Re, and Mo) for surface sediments are plotted in Figures 2.2b and 2.2c. The pattern of Ag and Cd fluxes (Figure 2.2b) resembles that observed for Ba, Si_{bio}, and C_{org}. Fluxes are lower north and south of ~60-65°S, while within this region, fluxes abruptly increase. Silver flux reaches a maximum of 42 ng cm^{-2} kyr^{-1} in core KN7812-12BC, and Cd flux reaches a maximum of 0.13 µg cm^{-2} kyr^{-1} in core NBP9802-06-MC1. Rhenium fluxes (Figure 2.2c) also resemble those observed for Ba, Si_{bio}, and C_{org}, and peak ~62°S in core NBP9802-06-MC1 with a value of 0.19 ng cm^{-2} kyr^{-1}. Molybdenum fluxes are dissimilar to the patterns observed for productivity proxies and the other trace metals. In the Antarctic Zone, Mo fluxes attain a local maximum (0.5 µg cm^{-2} kyr^{-1}) at ~66°S, then decrease northward to a minimum ~62°S, where the Mo concentration is sufficiently low (data point not shown) that it cannot be distinguished from a procedural blank. Molybdenum fluxes increase again north of

60°S and attain a maximum of 0.6 μg cm^{-2} kyr^{-1} near 57°S. Fluxes remain between ~0.3-0.6 μg cm^{-2} kyr^{-1} through the northernmost section of the transect.

Preserved vertical fluxes of Ag and Cd (trace metals associated with biogenic particles), and productivity proxies were compared with surface productivity patterns by plotting their fluxes alongside particulate organic carbon (POC) and Si net production [*Nelson et al.*, 2002] (Figure 2.3). Because Southern Ocean biogeochemical properties are more zonally homogeneous, Nelson et al. [2002] divide the Pacific sector into the Northern ACC (55-59°S), the Polar Frontal Region (59-61.5°S), the Southern ACC (61.5-65.5°S), and the Ross Gyre (65.5-68.5°S). Consequently, trace metal and productivity proxy fluxes estimated in this study were averaged within these latitudes to facilitate comparison to surface productivity data. POC production, Si net production, and productivity proxy fluxes are lower in the Northern ACC and Ross Gyre than in the Polar Frontal Zone and Southern ACC. Highest POC and Si net production occur within the Southern ACC, corresponding to maximum Ag and Cd fluxes. The zonal pattern of Ag and Cd fluxes more closely resembles that of Si net production, with the maximum amount of change occurring from the Polar Frontal Region to the Southern ACC. POC and Si net production patterns follow C_{org} and Si_{bio} fluxes, respectively. Barium fluxes also more closely resemble POC production in that the maximum amount of change occurs from the Northern ACC to the Polar Frontal Region, and a smaller change occurs from the Polar Frontal Region to the Southern ACC.

5. Discussion

5.1 Conventional Productivity Proxies and Southern Ocean Productivity

We measured total Ba, C_{org}, and Si_{bio} concentrations in Pacific sector surface sediments to test whether these commonly-used productivity proxies accurately record surface productivity

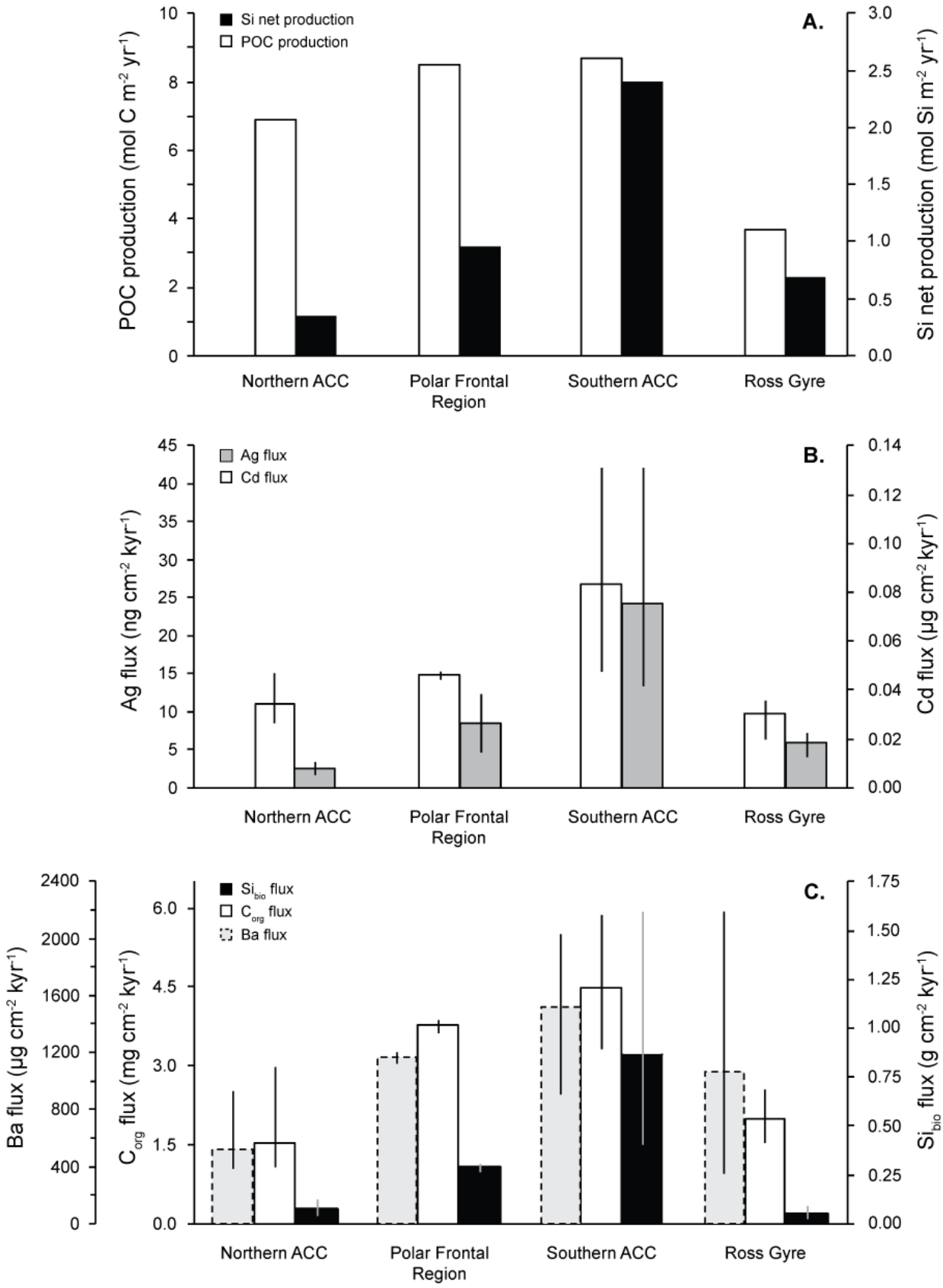
A.
Si net production
POC production
POC production (mol C m-2 yr-1)
Si net production (mol Si m-2 yr-1)
Northern ACC
Polar Frontal Region
Southern ACC
Ross Gyre
B.
Ag flux
Cd flux
Ag flux (ng cm-2 kyr-1)
Cd flux (µg cm-2 kyr-1)
C.
Sibio flux
Corg flux
Ba flux
Ba flux (µg cm-2 kyr-1)
Corg flux (mg cm-2 kyr-1)
Sibio flux (g cm-2 kyr-1)

Figure 2.3. (Previous page) A: Surface productivity [*Nelson et al.*, 2002] compared to productivity proxies (B: Ag and Cd fluxes; C: Ba, C_{org}, and Si_{bio} fluxes). Latitudinal zones labeled on x-axis after Nelson et al. [2002]. Vertical bars indicate range of fluxes rather than measurement uncertainty.

patterns. Barite ($BaSO_4$) accumulation in Southern Ocean sediments has previously been shown to have a strong correlation with carbon export and primary production [*Eagle et al.*, 2003]. Moreover, total Ba and excess Ba (Ba not of detrital origin) are well correlated with one another in Atlantic and Indian sector surface sediments [*Fagel et al.*, 2002], suggesting that this trend should also hold for Pacific sector sediments.

Elevated Ba, C_{org}, and Si_{bio} fluxes that appear between 60-65°S (Figure 2.2a) identify the opal belt. Maximum Si net production [*Nelson et al.*, 2002] within the Southern ACC (61.5-65.5°S) corresponds to the zone of elevated productivity proxy (Ba, C_{org}, Si_{bio}) fluxes, supporting this identification. As noted in Section 2.3, interaction of the Southern ACC Front with the Pacific-Antarctic Ridge provides a strong impetus for enhanced accumulation of biogenic sediments near 62°S. Additionally, southward-propagating summer diatom blooms that begin at the ice edge and extend into the seasonal ice zone have been observed [*Brzezinski et al.*, 2001], and these blooms are hypothesized to be responsible for the creation of the opal belt. Therefore, high concentrations of Ba, C_{org}, and Si_{bio} in our data are consistent with oceanographic features that promote high phytoplankton productivity.

5.2 The Ag Record

Prior investigations of sedimentary Ag concentrations focused on continental margins within oxygen minimum zones and have produced mixed results with respect to the use of Ag as a proxy for diatom export production. The most promising results were produced at ODP Hole 1017E along the southern California margin [*Hendy and Pedersen*, 2005], where downcore concentrations of Ag correlated most closely with Cd and $\delta^{15}N$, supporting the idea that Ag is involved in biogeochemical cycling and might be useful as a paleoproductivity proxy. A

correlation observed between Ag/Al and Ba (i.e., biogenic barite) in eastern Pacific margin surface sediments [*McKay and Pedersen*, 2008] also suggests that sedimentary Ag accumulation may be linked to biogenic particle flux (although in comparison to Pacific sector sediments, these sediments contained higher C_{org} contents and were suboxic to anoxic). Straightforward application of Ag as a paleoproductivity proxy is complicated by several factors that affect the net amount of Ag buried in sediments. Several studies [*Böning et al.*, 2005; *McKay and Pedersen*, 2008; *Morford et al.*, 2008] have noted that bulk sediment Ag concentrations rise with increasing water depth. This trend has been interpreted to indicate that scavenging processes play an important role in Ag delivery, and that only a sufficiently long water column will result in significant Ag concentrations in sediments [*McKay and Pedersen*, 2008]. Furthermore, high bottom water oxygen concentrations result in oxidation of organic particles and significant release of Ag to pore waters [*Morford et al.*, 2008].

In the Pacific sector, long water columns (>2500 m) and high diatom productivity within the opal belt lead us to anticipate significant Ag delivery to underlying sediments. Bulk Ag concentrations are low at the deepest locations (i.e., below ~4000 m) and show a slight trend toward higher concentrations at shallower water depths (Figure 2.4), possibly reflecting a combination of export production and poor Ag preservation. Shallowest sites coincide with the Pacific-Antarctic Ridge ~62-64°S, and it is unclear whether higher Ag concentrations here are the result of Ag scavenging or stimulation of surface productivity by interaction of the Southern ACC Front with the ridge. High Southern Ocean O_2 concentrations potentially influence the Ag-depth relationship by remobilizing Ag, as discussed below. Previous studies that observed increasing sedimentary Ag concentrations with increasing water depth [*Böning et al.*, 2005; *McKay and Pedersen*, 2008; *Morford et al.*, 2008] were conducted along East Pacific continental

margins, where dissolved O_2 concentrations tend to be lower and thus sedimentary Ag is well preserved.

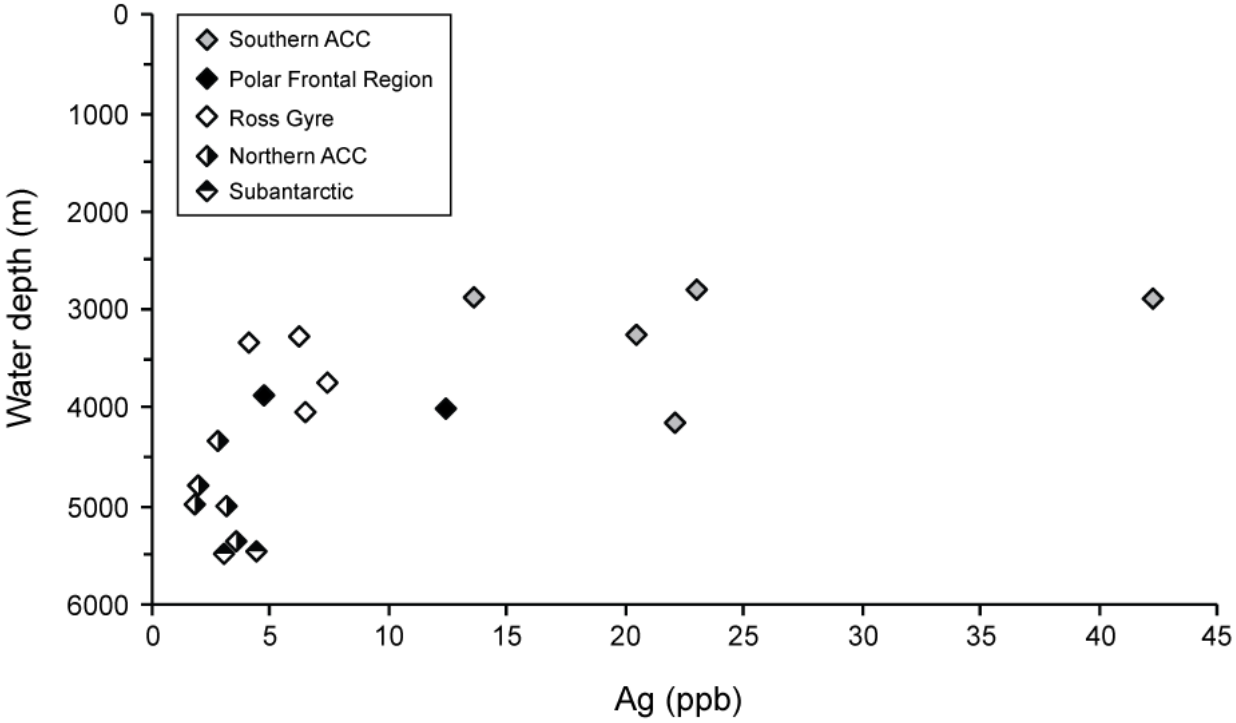

Figure 2.4. Bulk sediment Ag concentrations with depth. A slight trend toward higher Ag concentrations at shallower depths is observed, although shallow sites coincide with the Pacific-Antarctic Ridge.

A longstanding question about Ag has been its mode of delivery to sediments. A number of prior studies have reported similar Ag and Si water column profiles that imply an association of Ag with diatom hard parts [*Flegal et al.*, 1995; *Kramer et al.*, 2011; *Ndung'u et al.*, 2001; *Ranville and Flegal*, 2005; *Rivera-Duarte et al.*, 1999; *Zhang et al.*, 2001]. A compilation of dissolved Ag and silica profiles from the Pacific [*Kramer et al.*, 2011] shows a direct linear relationship in the South and Equatorial Pacific, implying primary control of seawater Ag concentrations by diatoms. However, studies conducted in the North Pacific [*Kramer et al.*, 2011; *Ranville and Flegal*, 2005; *Zhang et al.*, 2001] report a nonlinear correlation between Ag and silica. Other studies support an association of Ag with particulate organic carbon (POC). A strong association of Ag with C_{org} was reported for the Mexican margin [*Martin et al.*, 1983].

Consistent Ag:C molar ratios were observed throughout the upper water column, leading to the conclusion that Ag is complexed to organic matter. McKay and Pedersen [2008] also reported a strong correlation of Ag with C_{org} ($R^2 > 0.85$) in Mexican and Peruvian margin surface sediments. In Pacific sector surface sediments, Ag fluxes more closely follow Si net production and Si_{bio} fluxes (Figure 2.3), although an association between Ag and C_{org} cannot be ruled out because C_{org} and Si_{bio} are both components of diatom debris.

Although the exact association of Ag with C_{org} and/or Si_{bio} is not known, our study supports the use of Ag as a proxy for diatom export production. Bulk sediment Ag fluxes (Figure 2.2b) show elevated Ag delivery between 60-65°S, in agreement with surface primary productivity estimates and conventional productivity proxy fluxes that record the opal belt. The association of Ag with diatom debris implies that rates of particle transit to the seafloor and remineralization in the water column become important factors determining the amount of Ag delivered to sediments. High-density particles and slow recycling in the upper water column should encourage Ag enrichment in underlying sediments. Estimates of annual new production and POC export in the ACC are in line with global averages (on the order of 10^1 mol C m^{-2} yr^{-1}), but POC fluxes to 1000 m are about twice the global average. Additionally, about a quarter or more of the Si_{bio} exported from the photic zone reaches 1000 m water depth, and most of that also reaches the seafloor. Together these trends suggest relatively inefficient water column remineralization of Southern Ocean biogenic particles [*Nelson et al.*, 2002]. In the opal belt, this may result from diatom mats [*Honjo*, 2004] and large diatom frustules [*Honjo et al.*, 2000] that sink rapidly [*Bienfang and Ziemann*, 1992], potentially reducing the fraction of Ag lost to remineralization in the upper water column.

Although enhanced Ag delivery to sediments is expected, bulk sediment Ag

concentrations across the transect are lower than average shale, for example [70 ppb; *Turekian and Wedepohl*, 1961]. No appropriate comparison of Ag concentrations or fluxes reported in this study exists in the current literature. Most studies of sedimentary Ag concentrations have been conducted along continental margins where lithogenic input is high, and so do not provide good comparators for the open ocean. Koide et al. [1986] report Ag concentrations for Pacific Ocean pelagic sediments, but sediment composition is not given, so the influence of various processes on Ag accumulation cannot be evaluated. Reported Ag concentrations range from < 20 ppb to 310 ppb [*Koide et al.*, 1986].

Low Ag concentrations in Pacific sector surface sediments are possibly due to particle degradation by oxygenated bottom waters that can remobilize metals associated with organic-rich particles [*McKay and Pedersen*, 2008; *Morford et al.*, 2008]. One plausible scenario for the Southern Ocean is that Ag is delivered by summer diatom blooms and subsequently re-released to solution during winter due to a severe slowdown of organic matter delivery [*Honjo et al.*, 2000] and hence lower oxidant demand. Seasonal changes would therefore result in net low concentrations in sediments, as observed. Silver remineralization with biogenic particles compromises the integrity of the metal as an export production recorder where C_{org} or Si_{bio} concentrations may be unreliable. However, Ag may be useful in less well-oxygenated settings where other productivity proxies (C_{org}, Si_{bio}, Ba, ^{231}Pa) have not been measured, where barite ($BaSO_4$) may be unreliable because it can be reduced and remobilized [*Hendy*, 2010; *McManus et al.*, 1998], or to evaluate the contribution of different phytoplankton groups to biogenic input. Additionally, ^{231}Pa is a reliable proxy for opal flux [*Anderson et al.*, 2009; *Chase et al.*, 2003a], but Ag may be able to reveal past export production changes deeper in time, where ^{231}Pa concentrations are undetectable due to radioactive decay. It has also been proposed that Ag

concentrations might be compared to Re concentrations to disentangle past changes in export production from changes in bottom water ventilation [*Morford et al.*, 2008].

5.3 Redox-Sensitive Trace Metals

The Southern Ocean has traditionally been viewed as an unlikely environment for trace metal accumulation due to low sedimentation rates in the open ocean and the presence of well-ventilated bottom waters [*Crusius and Thomson*, 2000]. Muted enrichments of Ag, Cd and Re reported in this study support this prediction. However, it is possible to detect locally significant trace metal fluxes where sufficiently high export production—such as beneath the Southern Ocean opal belt—delivers elements associated with biodetritus (Ag and Cd). Locally significant Re fluxes ~62-63°S (Figure 2.2c) suggest that mildly suboxic conditions may exist seasonally in opal belt sediments due to elevated C_{org} fluxes, although this point cannot be resolved without more information about the provenance of lithogenic Re. Overall, Ag, Cd, and Re fluxes agree with productivity proxies, potentially recording the export and decomposition of the summer diatom bloom. Correlation between Mo fluxes and lithogenic content suggests that Mo has a primarily lithogenic source in the Pacific sector, perhaps in association with Mn oxides (see Section 2.1.4). For example, low Mo fluxes in the opal belt (Figure 2.2c) are consistent with reduced lithogenic detrital input [*Sayles et al.*, 2001; their Table 3]. Furthermore, Mo fluxes increase from the Antarctic Zone into the APFZ, in agreement with increased lithogenic content from ~12% (NBP9802-07) to ~32% (NBP9802-08). Hence, Mo fluxes in the Pacific sector do not support surface sediment anoxia, in agreement with pore water data [*Sayles et al.*, 2001].

We are unaware of similar open ocean, surface sediment estimates of trace metal fluxes in the Southern Ocean or elsewhere. Most other Southern Ocean trace metal studies employ authigenic U as a glacial-interglacial paleoproductivity indicator. As expected for sediments

overlain by well-oxygenated waters, Holocene-age Southern Ocean sediments typically have low authigenic U concentrations (< 0.5 ppm), while higher concentrations (up to ~5 ppm) are observed during glacial periods [e.g., *Anderson et al.*, 1998; *Bareille et al.*, 1998; *Frank et al.*, 2000]. Our trace metal results are supported by a study from the Indian sector of the Southern Ocean [*Rosenthal et al.*, 1995a] that found that high productivity south of the APF results in Cd and U enrichment during interglacials. However, Chase et al. [2003b], working on the same series of cores as this study, found no evidence from U that high organic matter fluxes produced suboxic pore water conditions, concluding instead that lateral redistribution of sediments focused C_{org} accumulation at particular sites. This conclusion does not contradict our findings that biodetritus delivers locally significant amounts of Ag and Cd to sediments in the opal belt, but the agreement between (1) Ag, Cd, and Re fluxes, (2) conventional productivity proxy fluxes, and (3) surface productivity leads us to conclude that high biogenic particle fluxes are responsible.

6. Conclusions

This study presents the first measurements of a suite of trace metals in Southern Ocean surface sediments. We show that preserved vertical fluxes of trace metals delivered with biogenic particles (Ag, Cd) accurately record the opal belt alongside productivity proxies (Ba, C_{org}, Si_{bio}). Thorium-normalized fluxes of all proxies except Mo rise between 60-65°S, in the highly productive Antarctic Zone near the Southern ACC Front. The locus of high productivity revealed by our results agrees with both ship-based [*Brzezinski et al.*, 2001] and satellite [*Comiso et al.*, 1993; *Moore and Abbott*, 2000] observations of phytoplankton activity, as well as surface productivity estimates [*Nelson et al.*, 2002]. We propose that seasonal export production in the Pacific sector opal belt is responsible for the detectable trace metal enrichments despite the well-

oxygenated bottom waters. The summer diatom bloom, fed by divergent upwelling and upward mixing of nutrients near the mid-ocean ridge, exports large amounts of organic matter over a short time period that result in locally elevated Ag, Cd, and Re fluxes to surface sediments. Significantly, Ag, Cd, and Re enrichments in opal belt sediments suggest that these proxies could be fruitfully applied downcore to generate long-term records of sediment chemistry and/or export production history in a crucially important region of the ocean.

This study also tested the utility of Ag as a productivity proxy. In Southern Ocean surface sediments, zonal Ag flux patterns are similar to Si net production, suggesting that Ag could be associated with diatom opal. Although the exact mechanism of sedimentary Ag enrichment remains unclear, Ag delivery appears tied to biogenic particle export. Well-oxygenated sediments make Ag burial as Ag_2S unlikely in the Pacific sector. We hypothesize that in the Southern Ocean, observed bulk sediment Ag concentrations reflect the competing effects of pulsed export production, water column transport and remineralization processes, and well-oxygenated bottom waters. Overall, Ag shows promise as a novel paleoproductivity proxy that can be used in conjunction with other proxies to support conclusions of export production changes through time.

Acknowledgements. This work was supported by grants to MW from the AAPG Foundation Grants-in-Aid program, the Scott Turner Awards in Earth Science, and Rackham Graduate School, University of Michigan. Pacific sector sediments were provided by the Oregon State University Marine Geology Repository, which is sponsored by the U.S. National Science Foundation. Jennifer McKay (Oregon State University) measured total carbon for all samples. Tom Pedersen (University of Victoria) contributed to trace metal analyses. MW wishes to thank Alice Chang (University of British Columbia) and Victoria Gray (University of Victoria) for

training and assistance. Comments from two anonymous reviewers regarding the current manuscript, and several additional reviewers regarding prior versions of this manuscript helped to substantially improve its quality.

Table 2.1. Core locations, water depths, and sampling depths for cores used in this study.

Cruise	Core	Latitude	Longitude	Water Depth (m)	Sample Depth (cmbsf)
KN7812	02-BC	57.813°S	174.232°E	5344	0-2
KN7812	05-BC	62.903°S	174.747°E	4139	3-5
KN7812	07-BC	66.828°S	174.238°E	3260	0-2
KN7812	08-BC	67.008°S	178.502°W	4030	0-2
KN7812	09-BC	68.407°S	176.365°W	3730	0-3
KN7812	11-BC	63.632°S	169.318°W	2783	2-4
KN7812	12-BC	63.322°S	169.73°W	2875	2-4
KN7812	13-BC	58.455°S	174.55°W	4980	0-2
KN7812	14-BC	54.13°S	177.4°W	5446	0-2
NBP9802	03-MC1	66.128°S	169.49°W	3322	2-4
NBP9802	05-MC2	63.166°S	169.852°W	2861	2-4
NBP9802	06-MC1	61.875°S	169.972°W	3243	2-4
NBP9802	07-MC1	60.244°S	170.186°W	3860	1.5-3.5
NBP9802	07-MC2	60.284°S	170.023°W	3995	2-3.5
NBP9802	08-MC1	58.688°S	169.979°W	4324	1-3
NBP9802	09-MC1	56.942°S	170.233°W	4778	1-3
NBP9802	09-MC3	56.881°S	170.171°W	4968	2-4
NBP9802	10-MC1	53.042°S	174.688°W	5470	1-3

Table 2.2. Replicate analyses (n = 8, trace metals; n = 2, Ba and Al) of the sediment standard MESS-3, ± 1σ standard deviation.

	Ag (ppb)	Cd (ppm)	Re (ppb)	Mo (ppm)	Ba (ppm)	Al (%)
Certified value	180	0.24	Not reported	2.78	Not reported[a]	8.59
Uncertainty	20	0.01	Not reported	0.07	Not reported[a]	0.23
Measured value	175	0.20	3.4	2.27	958	8.2
1 σ error	5	0.01	0.2	0.07	37	0.2

(a) The GeoReM database (http://georem.mpch-mainz.gwdg.de/) reports 945-973 ppm for Ba (2 values).

Table 2.3. Element concentration data for all cores.

	Productivity Proxies				Redox Proxies					
Sample	Al (%)	Ba (ppm)	C_{org} (%)	Si_{bio} (%)	Ag (ppb)	Cd (ppm)	Re (ppb)	Mo (ppm)	$^{230}_{xs}Th_0$ (dpm/g)[b]	Estimated $^{230}_{xs}Th_0$ uncertainty (± dpm/g)[c]
KN7812-02BC	5.7	1397	0.4	22.3	13	0.17	0.1	0.8	50.06	14.36
KN7812-05BC	1.0	1594	0.6	71.5	39	0.08	0.1	0.2	19.03	2.02
KN7812-07BC	6.3	2059	0.6	8.1	16	0.08	0.1	0.6	26.9	1.94
KN7812-08BC	6.2	2763	0.5	16.9	19	0.06	0.2	0.8	26.9	1.94
KN7812-09BC	6.8	967	0.4	n.d.[a]	20	0.09	0.2	0.6	26.9	1.94
KN7812-11BC	0.2	1654	0.5	83.9	24	0.07	0.1	0.2	7.77	2.59
KN7812-12BC	0.2	1565	0.6	85.1	43	0.11	0.2	0.1	7.77	2.59
KN7812-13BC	4.7	1818	0.4	31.8	12	0.11	0.3	2.0	50.06	14.36
KN7812-14BC	6.5	1077	0.3	13.5	10	0.11	0.1	1.2	33.82	0.27
NBP9802-03-MC1	4.2	6756	0.8	29.5	12	0.11	0.3	1.5	26.9	0.37
NBP9802-05-MC2	0.2	1590	0.4	71.6	14	0.07	0.1	0.1	7.77	0.33
NBP9802-06-MC1	0.1	1014	0.2	79.6	10	0.07	0.1	0.0	4.25	0.28
NBP9802-07-MC1	0.7	2084	0.7	49.3	9	0.08	0.1	0.4	18.74	1.45
NBP9802-07-MC2	0.7	2180	0.7	55.5	22	0.09	0.1	0.1	19.03	1.71
NBP9802-08-MC1	2.6	2725	0.9	36.5	8	0.09	0.0	0.9	33.37	1.67
NBP9802-09-MC1	5.6	1571	0.5	20.6	8	0.15	0.1	1.6	50.06	7.91
NBP9802-09-MC3	6.2	1670	0.5	18.0	8	0.11	0.1	2.5	55.58	0.39
NBP9802-10-MC1	6.7	970	0.4	10.1	7	0.07	0.0	0.7	33.82	0.27

(a) Concentration is below the detection limit of the method.
(b) Data from Chase et al. [2003b], their Table 2 for NBP9802 cores. KN7812 data taken from NBP9802 data as described in Section 3.2.
(c) Method for estimating errors given in Supplementary Information.

REFERENCES

Anbar, A. D., R. A. Creaser, D. A. Papanastassiou, and G. J. Wasserburg (1992), Rhenium in seawater: Confirmation of generally conservative behavior, *Geochimica et Cosmochimica Acta*, *56*(11), 4099-4103.

Anderson, R. F., N. Kumar, R. A. Mortlock, P. N. Froelich, P. Kubik, B. Dittrich-Hannen, and M. Suter (1998), Late-Quaternary changes in productivity of the Southern Ocean, *Journal of Marine Systems*, *17*(1-4), 497-514.

Anderson, R. F., S. Ali, L. I. Bradtmiller, S. H. H. Nielsen, M. Q. Fleisher, B. E. Anderson, and L. H. Burckle (2009), Wind-driven upwelling in the Southern Ocean and the deglacial rise in atmospheric CO_2, *Science*, *323*(5920), 1443-1448.

Bareille, G., M. Labracherie, P. Bertrand, L. Labeyrie, G. Lavaux, and M. Dignan (1998), Glacial-interglacial changes in the accumulation rates of major biogenic components in Southern Indian Ocean sediments, *Journal of Marine Systems*, *17*(1-4), 527-539.

Berner, R. A. (1981), A new geochemical classification of sedimentary environments, *Journal of Sedimentary Petrology*, *51*(2), 359-365.

Bienfang, P. K., and D. A. Ziemann (1992), The role of coastal high latitude ecosystems in global export production, in *Primary Productivity and Biogeochemical Cycles in the Sea*, edited by P. G. Falkowski and A. Woodhead, pp. 285-297, Plenum, New York.

Böning, P., S. Cuypers, M. Grunwald, B. Schnetger, and H.-J. Brumsack (2005), Geochemical characteristics of Chilean upwelling sediments at ~36°S, *Marine Geology*, *220*(1-4), 1-21.

Boyd, P. W. (2002), Environmental factors controlling phytoplankton processes in the Southern Ocean, *Journal of Phycology*, *38*(5), 844-861.

Boyle, E. A., F. Sclater, and J. M. Edmond (1976), On the marine geochemistry of cadmium, *Nature*, *263*(5572), 42-44.

Brzezinski, M. A., D. M. Nelson, V. M. Franck, and D. E. Sigmon (2001), Silicon dynamics within an intense open-ocean diatom bloom in the Pacific sector of the Southern Ocean, *Deep-Sea Research II*, *48*(19-20), 3997-4018.

Calvert, S. E., and T. F. Pedersen (1993), Geochemistry of recent oxic and anoxic marine sediments: Implications for the geological record, *Marine Geology*, *113*(1-2), 67-88.

Cavalieri, D. J., and C. L. Parkinson (2008), Antarctic sea ice variability and trends, 1979-2006, *Journal of Geophysical Research*, *113*(C07004), doi: 10.1029/2007JC004564.

Charles, C. D., P. N. Froelich, M. A. Zibello, R. A. Mortlock, and J. J. Morley (1991), Biogenic opal in Southern Ocean sediments over the last 450,000 years: implications for surface water chemistry and circulation, *Paleoceanography*, *6*(6), 697-728.

Chase, Z., R. F. Anderson, M. Q. Fleisher, and P. W. Kubik (2003a), Scavenging of ^{230}Th, ^{231}Pa, and ^{10}Be in the Southern Ocean (SW Pacific sector): the importance of particle flux, particle composition, and advection, *Deep-Sea Research II, 50*(3-4), 739-768.

Chase, Z., R. F. Anderson, M. Q. Fleisher, and P. W. Kubik (2003b), Accumulation of biogenic and lithogenic material in the Pacific sector of the Southern Ocean during the past 40,000 years, *Deep-Sea Research II, 50*(3-4), 799-832.

Colodner, D., J. Sachs, G. Ravizza, K. Turekian, J. Edmond, and E. Boyle (1993), The geochemical cycle of rhenium: a reconnaissance, *Earth Planet. Sci. Lett., 117*(1-2), 205-221.

Comiso, J. C., C. R. McClain, C. W. Sullivan, J. P. Ryan, and C. L. Leonard (1993), Coastal Zone Color Scanner pigment concentrations in the Southern Ocean and relationships to geophysical surface features, *Journal of Geophysical Research, 98*(C2), 2419-2451.

Constable, A. J., S. Nicol, and P. G. Strutton (2003), Southern Ocean productivity in relation to spatial and temporal variation in the physical environment, *Journal of Geophysical Research, 108 (C4)*(8079), doi: 10.1029/2001JC001270.

Crusius, J., and J. Thomson (2000), Comparative behavior of authigenic Re, U, and Mo during reoxidation and subsequent long-term burial in marine sediments, *Geochimica et Cosmochimica Acta, 64*(13), 2233-2242.

Crusius, J., and J. Thomson (2003), Mobility of authigenic rhenium, silver, and selenium during postdepositional oxidation in marine sediments, *Geochimica et Cosmochimica Acta, 67*(2), 265-273.

Crusius, J., S. Calvert, T. Pedersen, and D. Sage (1996), Rhenium and molybdenum enrichments in sediments as indicators of oxic, suboxic, and sulfidic conditions of deposition, *Earth Planet. Sci. Lett., 145*(1-4), 65-78.

de Baar, H. J. W., P. M. Saager, R. F. Nolting, and J. van der Meer (1994), Cadmium versus phosphate in the world ocean, *Marine Chemistry, 46*(3), 261-281.

Dezileau, L., G. Bareille, J. L. Reyss, and F. Lemoine (2000), Evidence for strong sediment redistribution by bottom currents along the southeast Indian ridge, *Deep-Sea Research I, 47*(10), 1899-1936.

Diekmann, B. (2007), Sedimentary patterns in the late Quaternary Southern Ocean, *Deep-Sea Research II, 54*(21-22), 2350-2366.

Eagle, M., A. Paytan, K. R. Arrigo, G. v. Dijken, and R. W. Murray (2003), A comparison between excess barium and barite as indicators of carbon export, *Paleoceanography, 18*(1), 1021, doi: 10.1029/2002PA000793.

Fagel, N., F. Dehairs, L. André, G. Bareille, and C. Monnin (2002), Ba distribution in surface Southern Ocean sediments and export production estimates, *Paleoceanography, 17*(2), 1011, doi: 10.1029/2000PA000552.

Falkowski, P. G., R. T. Barber, and V. Smetacek (1998), Biogeochemical controls and feedbacks on ocean primary production, *Science*, *281*(5374), 200-206.

Fisher, N. S., and M. Wente (1993), The release of trace elements by dying marine phytoplankton, *Deep-Sea Research I*, *40*(4), 671-694.

Flegal, A. R., S. A. Sañudo-Wilhelmy, and G. M. Scelfo (1995), Silver in the eastern Atlantic Ocean, *Marine Chemistry*, *49*(4), 315-320.

Francois, R., M. P. Bacon, M. A. Altabet, and L. D. Labeyrie (1993), Glacial/interglacial changes in sediment rain rate in the SW Indian sector of Subantarctic waters as recorded by ^{230}Th, ^{231}Pa, U, and δ^{15}N, *Paleoceanography*, *8*(5), 611-629.

Francois, R., M. Frank, M. M. R. van der Loeff, and M. P. Bacon (2004), Th-230 normalization: An essential tool for interpreting sedimentary fluxes during the late Quaternary, *Paleoceanography*, *19*(PA1018), doi: 10.1029/2003PA000939.

Frank, M., R. Gersonde, M. R. v. d. Loeff, G. Bohrmann, C. C. Nürnberg, P. W. Kubik, M. Suter, and A. Mangini (2000), Similar glacial and interglacial export bioproductivity in the Atlantic sector of the Southern Ocean: Multiproxy evidence and implications for glacial atmospheric CO_2, *Paleoceanography*, *15*(6), 642-658.

Friedl, G., and T. F. Pedersen (2001), Silver as a new tracer for diatom production, *EAWAG News*, *52*(D), 14-15.

Gille, S. T., E. J. Metzger, and R. Tokmakian (2004), Seafloor topography and ocean circulation, *Oceanography*, *17*(1), 47-54.

Hall, I. R., I. N. McCave, R. Zahn, L. Carter, P. C. Knutz, and G. P. Weedon (2003), Paleocurrent reconstruction of the deep Pacific inflow during the middle Miocene: Reflections of East Antarctic Ice Sheet growth, *Paleoceanography*, *18*(2), doi: 10.1029/2002PA000817.

Helz, G. R., and M. K. Dolor (2012), What regulates rhenium deposition in euxinic basins?, *Chemical Geology*, *304-305*, 131-141.

Helz, G. R., C. V. Miller, J. M. Charnock, J. F. W. Mosselmans, R. A. D. Pattrick, C. D. Garner, and D. J. Vaughan (1996), Mechanism of molybdenum removal from the sea and its concentration in black shales: EXAFS evidence, *Geochimica et Cosmochimica Acta*, *60*(19), 3631-3642.

Hendy, I. L. (2010), Diagenetic behavior of barite in a coastal upwelling setting, *Paleoceanography*, *25*(PA4103), doi: 10.1029/2009PA001890.

Hendy, I. L., and T. F. Pedersen (2005), Is pore water oxygen content decoupled from productivity on the California Margin? Trace element results from Ocean Drilling Program Hole 1017E, San Lucia slope, California, *Paleoceanography*, *20*(PA4026), doi: 10.1029/2004PA001123.

Honjo, S. (2004), Particle export and the biological pump in the Southern Ocean, *Antarct. Sci.*, *16*(4), 501-516.

Honjo, S., R. François, S. Manganini, J. Dymond, and R. Collier (2000), Particle fluxes to the interior of the Southern Ocean in the Western Pacific sector along 170° W, *Deep-Sea Research II*, *47*(15-16), 3521-3548.

Jahnke, R. A. (1996), The global ocean flux of particulate organic carbon: Areal distribution and magnitude, *Global Biogeochemical Cycles*, *10*(1), 71-88.

Koide, M., V. F. Hodge, J. S. Yang, M. Stallard, E. G. Goldberg, J. Calhoun, and K. K. Bertine (1986), Some comparative marine chemistries of rhenium, gold, silver, and molybdenum, *Applied Geochemistry*, *1*(6), 705-714.

Kramer, D., J. T. Cullen, J. R. Christian, W. K. Johnson, and T. F. Pedersen (2011), Silver in the subarctic northeast Pacific Ocean: Explaining the basin scale distribution of silver, *Marine Chemistry*, *123*(1-4), 133-142.

Martin, J. H., G. A. Knauer, and R. M. Gordon (1983), Silver distributions and fluxes in north-east Pacific waters, *Nature*, *305*(5932), 306-309.

Masuzawa, T., S. i. Noriki, T. Kurosaki, S. Tsunogai, and M. Koyama (1989), Compositional change of settling particles with water depth in the Japan Sea, *Marine Chemistry*, *27*(1-2), 61-78.

McKay, J. L., and T. F. Pedersen (2008), The accumulation of silver in marine sediments: A link to biogenic Ba and marine productivity, *Global Biogeochemical Cycles*, *22*(GB4010), doi: 10.1029/2007GB003136.

McManus, J., W. M. Berelson, S. Severmann, R. L. Poulson, D. E. Hammond, G. P. Klinkhammer, and C. Holm (2006), Molybdenum and uranium geochemistry in continental margin sediments: Paleoproxy potential, *Geochimica et Cosmochimica Acta*, *70*(18), 4643-4662.

McManus, J., et al. (1998), Geochemistry of barium in marine sediments: implications for its use as a paleoproxy, *Geochimica et Cosmochimica Acta*, *62*(21–22), 3453-3473.

Moore, J. K., and M. R. Abbott (2000), Phytoplankton chlorophyll distributions and primary production in the Southern Ocean, *Journal of Geophysical Research*, *105*(C12), 28709-28722.

Moore, J. K., M. R. Abbott, J. G. Richman, W. O. Smith, T. J. Cowles, K. H. Coale, W. D. Gardner, and R. T. Barber (1999), SeaWiFS satellite ocean color data from the Southern Ocean, *Geophysical Research Letters*, *26*(10), 1465-1468.

Morford, J. L., and S. Emerson (1999), The geochemistry of redox sensitive trace metals in sediments, *Geochimica et Cosmochimica Acta*, *63*(11/12), 1735-1750.

Morford, J. L., L. H. Kalnejais, P. Helman, G. Yen, and M. Reinard (2008), Geochemical cycling of silver in marine sediments along an offshore transect, *Marine Chemistry*, *110*(1-2), 77-88.

Mortlock, R. A., and P. N. Froelich (1989), A simple method for the rapid determination of biogenic opal in pelagic marine sediments, *Deep-Sea Research*, *36*(9), 1415-1426.

Mortlock, R. A., C. D. Charles, P. N. Froelich, M. A. Zibello, J. Saltzman, J. D. Hays, and L. H. Burckle (1991), Evidence for lower productivity in the Antarctic Ocean during the last glaciation, *Nature*, *351*(6323), 220-223.

Murray, R. W., D. J. Miller, and K. A. Kryc (2000), Analysis of major and trace elements in rocks, sediments, and interstitial waters by inductively coupled plasma-atomic emission spectrometry (ICP-AES), *ODP Tech. Note*, *29* [Online]. Available from World Wide Web: <http://www-odp.tamu.edu/publications/tnotes/tn29/INDEX.HTM>.

Ndung'u, K., M. A. Thomas, and A. R. Flegal (2001), Silver in the western equatorial and South Atlantic Ocean, *Deep-Sea Research II*, *48*(13), 2933-2945.

Nelson, D. M., et al. (2002), Vertical budgets for organic carbon and biogenic silica in the Pacific sector of the Southern Ocean, 1996-1998, *Deep-Sea Research II*, *49*(9-10), 1645-1674.

Orsi, A. H., T. I. Whitworth, and W. D. Nowlin, Jr. (1995), On the meridional extent and fronts of the Antarctic Circumpolar Current, *Deep-Sea Research I*, *42*(5), 641-673.

Orsi, A. H., G. C. Johnson, and J. L. Bullister (1999), Circulation, mixing, and production of Antarctic Bottom Water, *Progress in Oceanography*, *43*(1), 55-109.

Pedersen, T. F., R. D. Waters, and R. W. Macdonald (1989), On the natural enrichment of cadmium and molybdenum in the sediments of Ucluelet Inlet, British Columbia, *The Science of the Total Environment*, *79*(2), 125-139.

Pickard, G. L., and W. J. Emery (1990), *Descriptive Physical Oceanography: An Introduction*, 5th ed., Pergamon Press, New York.

Ragueneau, O., et al. (2000), A review of the Si cycle in the modern ocean: recent progress and missing gaps in the application of biogenic opal as a paleoproductivity proxy, *Global and Planetary Change*, *26*(4), 317-365.

Ranville, M. A., and A. R. Flegal (2005), Silver in the North Pacific Ocean, *Geochemistry Geophysics Geosystems*, *6*(3), Q03M01, doi: 10.1029/2004GC000770.

Rivera-Duarte, I., A. R. Flegal, S. A. Sañudo-Wilhelmy, and A. J. Véron (1999), Silver in the far North Atlantic Ocean, *Deep-Sea Research II*, *46*(5), 979-990.

Rosenthal, Y., P. Lam, E. A. Boyle, and J. Thomson (1995a), Authigenic cadmium enrichments in suboxic sediments: Precipitation and postdepositional mobility, *Earth Planet. Sci. Lett.*, *132*(1-4), 99-111.

Rosenthal, Y., E. A. Boyle, L. Labeyrie, and D. Oppo (1995b), Glacial enrichments of authigenic Cd and U in Subantarctic sediments: A climatic control on the elements' oceanic budget?, *Paleoceanography*, *10*(3), 395-413.

Sallée, J. B., K. G. Speer, and S. R. Rintoul (2010), Zonally asymmetric response of the Southern Ocean mixed-layer depth to the Southern Annular Mode *Nat. Geosci.*, *3*(4), 273-279.

Sayles, F. L., W. R. Martin, Z. Chase, and R. F. Anderson (2001), Benthic remineralization and burial of biogenic SiO_2, $CaCO_3$, organic carbon, and detrital material in the Southern Ocean along a transect at 170° W, *Deep-Sea Research II*, *48*(19-20), 4323-4383.

Scott, C., and T. W. Lyons (2012), Contrasting molybdenum cycling and isotopic properties in euxinic versus non-euxinic sediments and sedimentary rocks: Refining the paleoproxies, *Chemical Geology*, *324-325*, 19-27.

Smith, W. O., and D. M. Nelson (1985), Phytoplankton bloom produced by a receding ice edge in the Ross Sea: spatial coherence with the density field, *Science*, *227*(4683), 163-166.

Smith, W. O., and D. M. Nelson (1986), Importance of ice edge phytoplankton production in the Southern Ocean, *BioScience*, *36*(4), 251-257.

Tribovillard, N., T. J. Algeo, T. Lyons, and A. Riboulleau (2006), Trace metals as paleoredox and paleoproductivity proxies: An update, *Chemical Geology*, *232*(1-2), 12-32.

Trull, T., S. R. Rintoul, M. Hadfield, and E. R. Abraham (2001), Circulation and seasonal evolution of polar waters south of Australia: Implications for iron fertilization of the Southern Ocean, *Deep-Sea Research II*, *48*, 2439-2466.

Turekian, K. K., and K. H. Wedepohl (1961), Distribution of the elements in some major units of the earth's crust, *Geological Society of America Bulletin*, *72*(2), 175-192.

Whitworth, T., and W. D. Nowlin (1987), Water masses and currents of the Southern Ocean at the Greenwich Meridian, *Journal of Geophysical Research*, *92*(C6), 6462-6476.

Zhang, Y., H. Amakawa, and Y. Nozaki (2001), Oceanic profiles of dissolved silver: precise measurements in the basins of western North Pacific, Sea of Okhotsk, and the Japan Sea, *Marine Chemistry*, *75*(1-2), 151-163.

Zhang, Y., H. Obata, and Y. Nozaki (2004), Silver in the Pacific Ocean and the Bering Sea, *Geochemical Journal*, *38*, 623-633.

Zheng, Y., R. F. Anderson, A. van Geen, and J. Kuwabara (2000), Authigenic molybdenum formation in marine sediments: A link to pore water sulfide in the Santa Barbara Basin, *Geochimica et Cosmochimica Acta*, *64*(24), 4165-4178.

Chapter 3

Redox Chemistry of West Antarctic Peninsula Margin Surface Sediments

Abstract

Continental margin sediments are commonly studied using trace metal enrichments as proxies for characterizing their modern redox conditions and tracking past changes in bottom water ventilation and marine primary productivity. Currently little is known about the sedimentary redox history of the continental shelf west of the Antarctic Peninsula. Yet, environmental conditions of the West Antarctic Peninsula have changed rapidly in recent decades in response to global warming. Paleoclimate archives including bulk sediment trace metal enrichments can provide insight into both past and future environmental changes in this climatically sensitive region. Therefore, characterization of redox conditions in surface (modern) sediments is essential for establishing a framework for paleoredox interpretations. In this study we measured concentrations of trace metals (Ag, Cd, Re, and Mo) and productivity proxies (total Ba, organic carbon, and biogenic silica) in surface sediments from the Marguerite Bay, Gerlache Strait, and Bransfield Strait areas. Proxy concentrations suggest that sediments are generally suboxic due to seasonally high export of organic carbon from surface waters. Comparison of West Antarctic Peninsula trace metal enrichments to trace metal and pore water data from continental margins outside the Antarctic region demonstrates that although the West Antarctic Peninsula water column differs from other continental margins (e.g., it lacks a strong oxygen minimum zone), sedimentary redox chemistry is similarly controlled by organic matter

decomposition, through slow recycling of highly seasonal export production falling through a cold water column.

1. Introduction

Trace metal accumulation in continental margin sediments has been used as an effective tool for documenting past shifts in sedimentary redox chemistry caused by changes in bottom water oxygenation, ocean circulation, and primary productivity [e.g., *Hendy and Pedersen*, 2005; 2006; *Morford et al.*, 2001; *Muratli et al.*, 2010]. Often, redox changes at a single water depth or locality are interpreted to indicate larger-scale shifts in ocean-atmosphere circulation, biogeochemical cycling, and/or glacial processes that are used to provide insight into Earth's climate dynamics. Trace metal enrichments in continental margin environments have been better studied than open ocean environments because continental margins are more likely to accumulate trace metals preserved under reducing conditions. Typically, reducing conditions are produced by a combination of high sedimentation rates, high surface productivity, and the presence of a strong oxygen minimum zone.

For these reasons, most trace metal studies have focused on continental margins where strong wind-driven upwelling and an oxygen minimum zone are present, such as in the eastern Pacific. Despite seasonally high surface productivity, the West Antarctic Peninsula (WAP) continental shelf has been little studied in terms of its sedimentary redox chemistry because it differs in several ways that may bias or inhibit nonlithogenic trace metal accumulation. First, the phytoplankton growing season is light limited both by solar insolation and sea ice cover [*R C Smith et al.*, 1996]. Second, waters as cold as -1.8°C [*D A Smith et al.*, 1999] lower metabolic rates [*Gillooly et al.*, 2001] and potentially slow organic matter recycling. Third, glacial ice extends to the coast, and delivers ice-rafted debris to the shelf and slope [*Griffith and Anderson*,

1989]. Finally, well-ventilated waters are present [*Hofmann et al.*, 1996] that can remobilize trace metals precipitated under reducing conditions. Thus it is uncertain whether sediments of the WAP shelf and slope similarly accumulate trace metals.

The effects of future warming in the WAP environment can be explored through paleoclimate studies utilizing marine and terrestrial archives to examine past climatic variation. For example, recent studies have contributed to our understanding of current environmental changes by attempting to place modern climate change in the context of the last ~12,000 years [*Shevenell et al.*, 2011], and by evaluating the mechanisms responsible for climate change over this same timescale [*Bentley et al.*, 2009]. Trace metal studies of marine sediment paleoredox conditions could provide additional information about past ventilation and export production changes. However, interpreting downcore sedimentary trace metal enrichments requires first characterizing modern WAP sedimentary redox chemistry.

Therefore in order to determine the modern relationship between ventilation and productivity along the WAP shelf, we measured trace metal (Ag, Cd, Re, and Mo) and productivity proxy (total Ba, organic carbon [C_{org}], and biogenic silica [Si_{bio}]) concentrations in surface sediments from 35 box cores collected from WAP coastal areas and fjords. Furthermore, by comparing WAP sedimentary redox conditions and biogenic particle input with those from other continental margins, we infer that sedimentary suboxia is widespread on the WAP shelf, and that similar geochemical processes control redox conditions/trace metal accumulation in all margin environments.

2. Background

2.1 Oceanographic Setting

The West Antarctic Peninsula region can be divided into the shelf-slope area directly west of the peninsula, and Bransfield Strait, which is separated from Drake Passage by the South Shetland Islands. The southernmost front of the Antarctic Circumpolar Current (ACC) hugs the outer edge of the continental shelf (Figure 3.1), while the Antarctic Polar Front is found in the open ocean north of the South Shetland Islands [*Orsi et al.*, 1995]. Cyclonic surface circulation composed of two separate gyres is present near Gerlache Strait and Marguerite Bay, with the ACC flowing offshore to the northeast and a southwestward-flowing current returning along the coast [*Hofmann et al.*, 1996]. Cross-shelf water transport occurs between the two gyres and in association with bathymetric features [*Savidge and Amft*, 2009]. Cold, fresh Antarctic Surface Water occupies the upper water column [*D A Smith et al.*, 1999], but the most prominent water mass west of the peninsula is warm, nutrient-rich, and well-oxygenated Upper Circumpolar Deep Water (UCDW). This water mass floods the continental shelf to a depth of 150-200 m on the inner shelf and 400-700 m on the outer shelf [*Hofmann et al.*, 1996]. Bathymetric upwelling of UCDW at the shelf break has been shown to be an important source of nutrients for diatoms [*Prézelin et al.*, 2000].

Inside Bransfield Strait, clockwise surface circulation is also developed [*Savidge and Amft*, 2009]. Warm water from the ACC enters Bransfield Strait between Smith and Snow Islands [*Hofmann et al.*, 1996]. Additional inflow of cold water to the strait is from the Weddell Sea to the east and from Gerlache Strait to the west [*Hofmann et al.*, 1996; *D A Smith et al.*, 1999]. Consequently, the upper water column displays a complex water mass structure derived from mixing of different water types [*Hofmann et al.*, 1996]. Circumpolar Deep Water is recognizable primarily in the western part of the strait and along the southern margin of the South Shetland Islands [*Hofmann et al.*, 1996]. Elsewhere, cold deep waters are dominated by

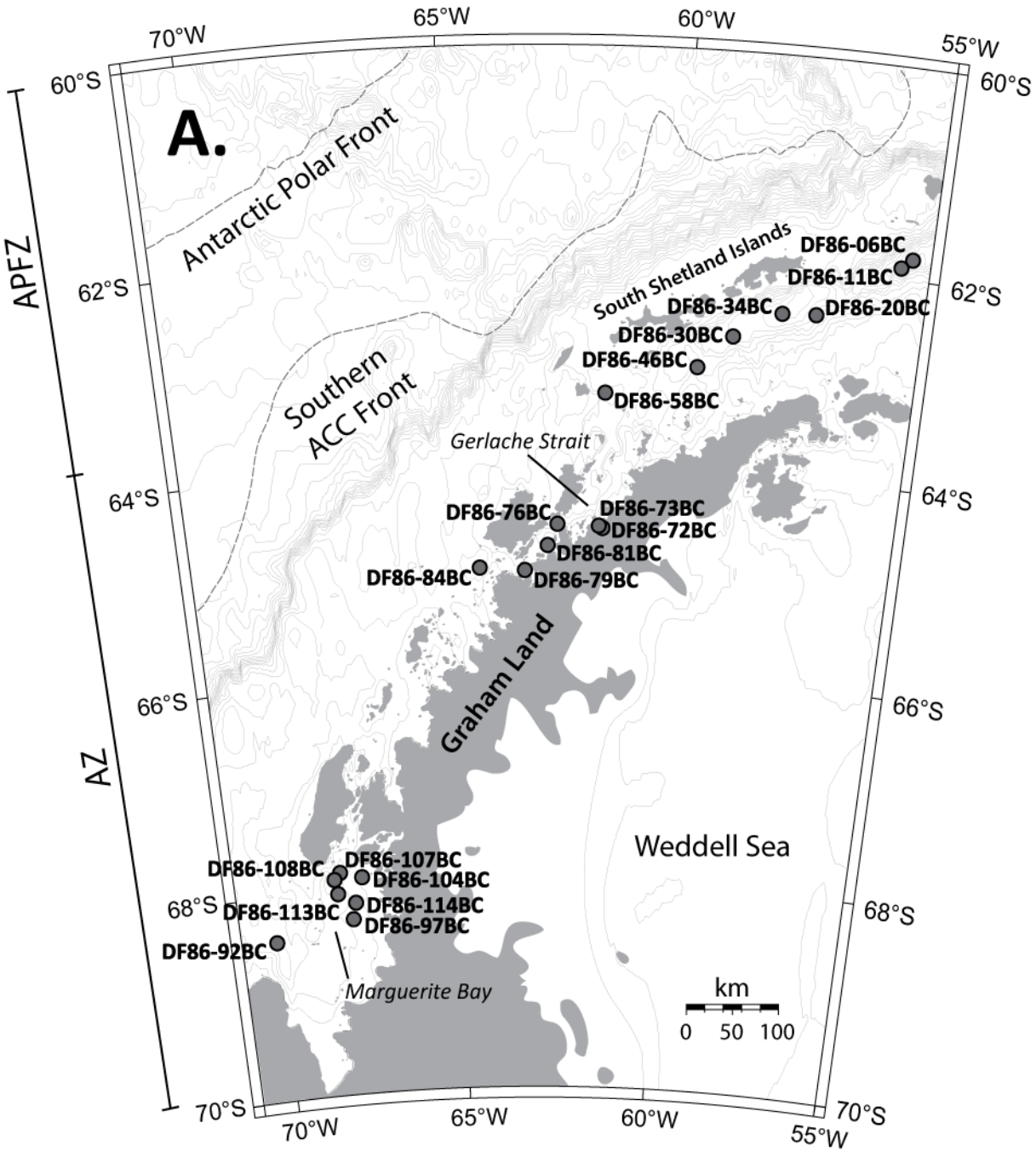
A.
70°W
65°W
60°W
55°W
60°S
62°S
64°S
66°S
68°S
70°S
APFZ
AZ
Antarctic Polar Front
Southern
ACC Front
South Shetland Islands
DF86-06BC
DF86-11BC
DF86-34BC
DF86-20BC
DF86-30BC
DF86-46BC
DF86-58BC
Gerlache Strait
DF86-73BC
DF86-76BC
DF86-72BC
DF86-81BC
DF86-84BC
DF86-79BC
Graham Land
Weddell Sea
DF86-108BC
DF86-107BC
DF86-104BC
DF86-113BC
DF86-114BC
DF86-97BC
DF86-92BC
Marguerite Bay
km
0 50 100

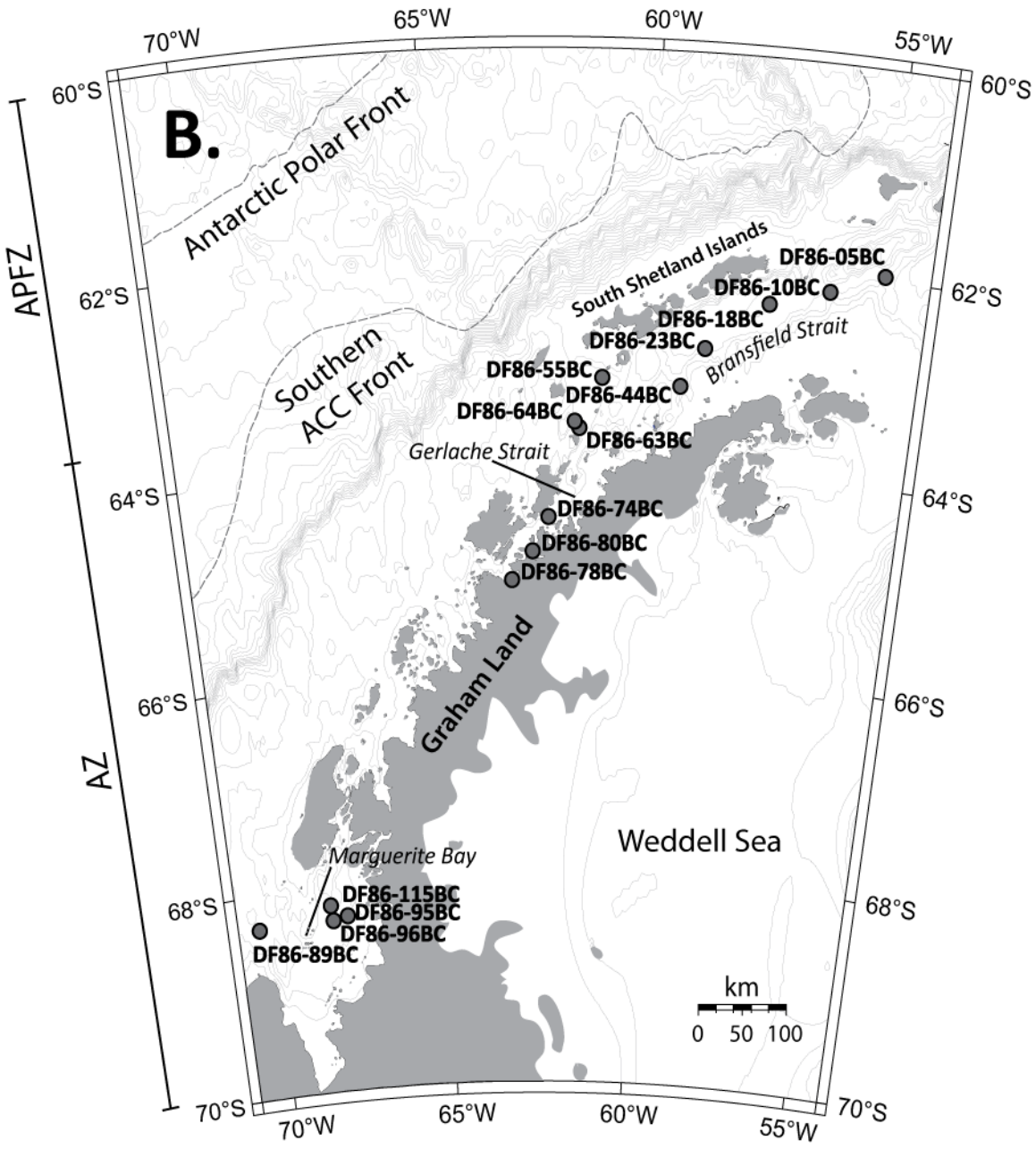

Figure 3.1. (Current and previous pages) Core locations, split into two maps for clarity (A and B). Fronts of the Antarctic Circumpolar Current (ACC) are indicated by dashed grey lines (after Orsi et al. [1995]). APFZ—Antarctic Polar Frontal Zone; AZ—Antarctic Zone; APF—Antarctic Polar Front.

Bransfield Strait Water, which may originate in the Weddell Sea [*Whitworth et al.*, 1994].

2.2 Sea Ice and Primary Productivity Patterns

West of the Antarctic Peninsula, the seasonal ice zone is characterized by substantial interannual variability, with maximum sea ice extent occurring during August and the minimum during March [*Stammerjohn and Smith*, 1996]. Primary productivity is also highly variable from year to year and shows a positive correlation with the timing of sea ice retreat [*Vernet et al.*, 2008]. Melt water from sea ice is thought to enhance primary productivity by stabilizing the upper water column and preventing mixing of phytoplankton out of the photic zone [*W O Smith and Nelson*, 1986]. Phytoplankton primary production is mostly limited to austral spring and summer months when increased solar irradiance and a lack of sea ice cover promote blooms [*R C Smith et al.*, 1996]. On the WAP shelf, chlorophyll concentrations and phytoplankton biomass decrease along an onshore-offshore gradient, with the highest chlorophyll concentrations found in coastal areas and in Marguerite Bay [*Garibotti et al.*, 2003a; *R C Smith et al.*, 1996]. Diatoms are responsible for a large proportion of carbon biomass (up to 86% in Marguerite Bay) [*Garibotti et al.*, 2003b] and predominate in coastal areas [*Garibotti et al.*, 2003a], the outer shelf, and Marguerite Bay. A mixed phytoplankton assemblage occupies the mid-shelf [*Garibotti et al.*, 2003b; *Prézelin et al.*, 2000].

2.3 Glacial Ice and Terrigenous Sedimentation

Cycles of glacial advance and retreat across the continental shelf have eroded the seafloor west of the Antarctic Peninsula, removing sediments in many locations and carving numerous submarine canyons and depressions, resulting in a rugged bathymetry [*J B Anderson*, 1999]. Terrigenous sedimentation from ice-rafting and melt water discharge to coastal areas is partly climatically controlled, with higher annual mean air temperature and/or precipitation (both

decrease toward the south) leading to higher sedimentation rates [*J B Anderson*, 1999; *Griffith and Anderson*, 1989]. Additionally, terrigenous material forms a greater proportion of the sediments in areas directly adjacent to a glacial ice front [*Domack and McClennen*, 1996].

The South Shetland Islands (Figure 3.1; Bransfield Strait subregion) occupy the northernmost part of the study area. The islands have a subpolar climate with relatively warm annual mean air temperatures, and receive frequent precipitation including rain [*J B Anderson*, 1999; *Griffith and Anderson*, 1989]. Less than 50% of the coast is occupied by tidewater glaciers, and where ice does reach the coast, it does so as piedmont and valley glaciers. Glacier ablation occurs primarily by calving near the waterline, although direct sublimation, advection, and melting also occur [*Griffith and Anderson*, 1989]. During the summer months, substantial amounts of melt water are discharged as sediment-laden plumes from tidewater glaciers [*Domack and Ishman*, 1993].

Western Graham Land (Figure 3.1; Marguerite Bay and Gerlache Strait subregions) experiences a polar climate, and is colder and drier than the South Shetland Islands [*Griffith and Anderson*, 1989]. The land is heavily glaciated with continuous ice cover along the coast in the form of outlet and valley glaciers that undergo ablation by calving near the waterline [*Griffith and Anderson*, 1989]. Tidewater glaciers are thought to introduce significant amounts of debris below sea level at the glacial terminus, and this process may account for the majority of sediment entering the marine environment [*Domack and Ishman*, 1993; *Griffith and Anderson*, 1989].

3. Materials and Methods

Box cores were collected from the West Antarctic Peninsula margin during the Deep Freeze 1986 cruise and obtained from the Antarctic Marine Geology Research Facility at Florida State University. Core locations, sampling depths, and water depths are given in Table 3.1.

Sediments are composed of diatomaceous mud and ooze, with volcanic ash and pebbles occasionally present [*Liu et al.*, 1992]. Continental margin surface sediments outside the WAP were selected based on the availability of the following: 1) surface sediments sampled from box cores or multicores (except for Saanich Inlet, for which information was sparse); 2) bulk sediment Ag, Cd, Re, and Mo concentrations, with at least 3 of 4 present; 3) sedimentation rate estimate; and 4) bottom water O_2 concentration.

Concentrations of Ag, Cd, Re, and Mo for all samples were determined at the University of Victoria by isotope dilution inductively coupled plasma-mass spectrometry (ID ICP-MS) using a Thermo X Series 2 quadrupole mass spectrometer. Prior to analysis, bulk sediment samples were freeze dried and homogenized, then spiked and subjected to total microwave digestion in Teflon vessels using an acid cocktail of trace metal grade HF, HCl, and HNO_3 (SeaStar), following Crusius et al. [1996]. An aliquot was removed from digested samples for Cd, Ag, and Re analysis and passed through a column of Dowex 1X-8 resin to remove interfering isotopes. Working spike concentrations and ratios of $^{109}Ag/^{107}Ag$, $^{111}Cd/^{113}Cd$, $^{185}Re/^{187}Re$, and $^{95}Mo/^{98}Mo$ were calibrated using natural element solutions (High-Purity Standards).

Total Ba and Al concentrations were measured at the University of Michigan's Environmental and Analytical Geochemistry Laboratory (EAGL) using a Jobin Yvon Horiba inductively coupled plasma-optical emission spectrometer (ICP-OES). Samples were prepared using the flux method [*Murray et al.*, 2000] and dissolved in 10% HNO_3. Reproducibility of measurements for trace metals, Ba, and Al, based on repeated analysis of the sediment standard MESS-3, are presented in Table 3.2. Biogenic silica (Si_{bio}) concentrations were determined by the method of Mortlock and Froelich [1989] (2% RSD). Organic carbon (C_{org}) was calculated as

the difference of weight percent total carbon minus weight percent inorganic carbon (6% RSD). Total carbon was measured at Oregon State University using a Carlo Erba NA1500 Series 1 elemental analyzer. Inorganic carbon was measured by coulometry at EAGL using a UIC, Inc. Coulometrics instrument. Relative standard deviations of Si_{bio} and C_{org} concentrations are based on 1-2 repeat measurements of ~10% of samples.

High sedimentation rates along the WAP result from a combination of biogenic material and ice-rafted debris input [*Griffith and Anderson,* 1989; *Isla et al.*, 2004], and thus the detrital component is anticipated to make a significant elemental contribution to our results. Therefore to estimate the nonlithogenic contribution to measured metal concentrations, we calculated excess values for each metal (Figure 3.2):

$$\text{Excess} = [M]_{smp} - ([M]_{bkg}/[Al]_{bkg} \times [Al]_{smp}) \quad (1)$$

where $[M]_{smp}$ is the concentration of the metal in the sample; $[M]_{bkg}$ is the detrital concentration of the metal; $[Al]_{bkg}$ is the detrital Al concentration; and $[Al]_{smp}$ is the concentration of Al in the sample. Without further information about the provenance and composition of the detrital material at each site, we assumed average shale concentrations [*Li,* 2000, his Table VI-5a] for detrital background. Negative excess values produced for some sites reflect uncertainty in the local detrital contribution, which is probably not accurately represented by average shale.

A second calculation was made to establish confidence that total metal concentrations are above that expected from lithogenic background, and therefore part of the biogenic or authigenic flux to sediments. This was assessed at all continental margin sites (Figure 3.3) by first estimating a background metal concentration (assumed to be 1σ background) from average shale [*Li,* 2000, his Table VI-5a] according to:

$$1\sigma = ([M]_{shale}/[Al]_{shale})*[Al]_{smp} . \quad (2)$$

This 1σ background was then multiplied by three to give the minimum concentration required to distinguish measured sample trace metal concentrations from lithogenic background, and hence considered significantly above background.

Cores recovered from the West Antarctic Peninsula (WAP) consist entirely of coastal and fjord sites (Figure 3.1). The region supports high annual primary productivity (182 ± 107 gC m^{-2} yr^{-1}) [*Vernet et al.*, 2008] and exhibits sedimentation rates centered ~200 cm kyr^{-1} [*Harden et al.*, 1992]. These characteristics should produce enhanced trace metal and productivity proxy preservation. However, proxy accumulation at individual sites is strongly influenced by bottom currents that redistribute sediments [*Abelmann and Gersonde*, 1991; *Bárcena et al.*, 2002; *Palanques et al.*, 2002] and concentrate particles in submarine canyons and depressions that act as sediment traps [*Isla et al.*, 2004]. This phenomenon makes it nearly impossible to correlate biogenic particle production in surface waters with accumulation in sediments directly below. Moreover, advected lithogenic particles can contribute to total trace metal concentrations, and not knowing their provenance and chemical composition introduces error into estimates of the nonlithogenic component. Therefore in order to draw the broadest possible conclusions, proxy data are hereafter grouped by subregion: Bransfield Strait, Gerlache Strait, or Marguerite Bay. Total concentrations of all proxies are presented in Table 3.3.

4. Results

4.1 West Antarctic Peninsula Surface Sediments

Figure 3.2 displays the data as box and whisker plots to fully encompass the range of enrichments observed for each subregion. Rhenium excess concentrations (Figure 3.2a) generally increase from Bransfield Strait (median excess 3.4 ppb) south to Marguerite Bay (median excess

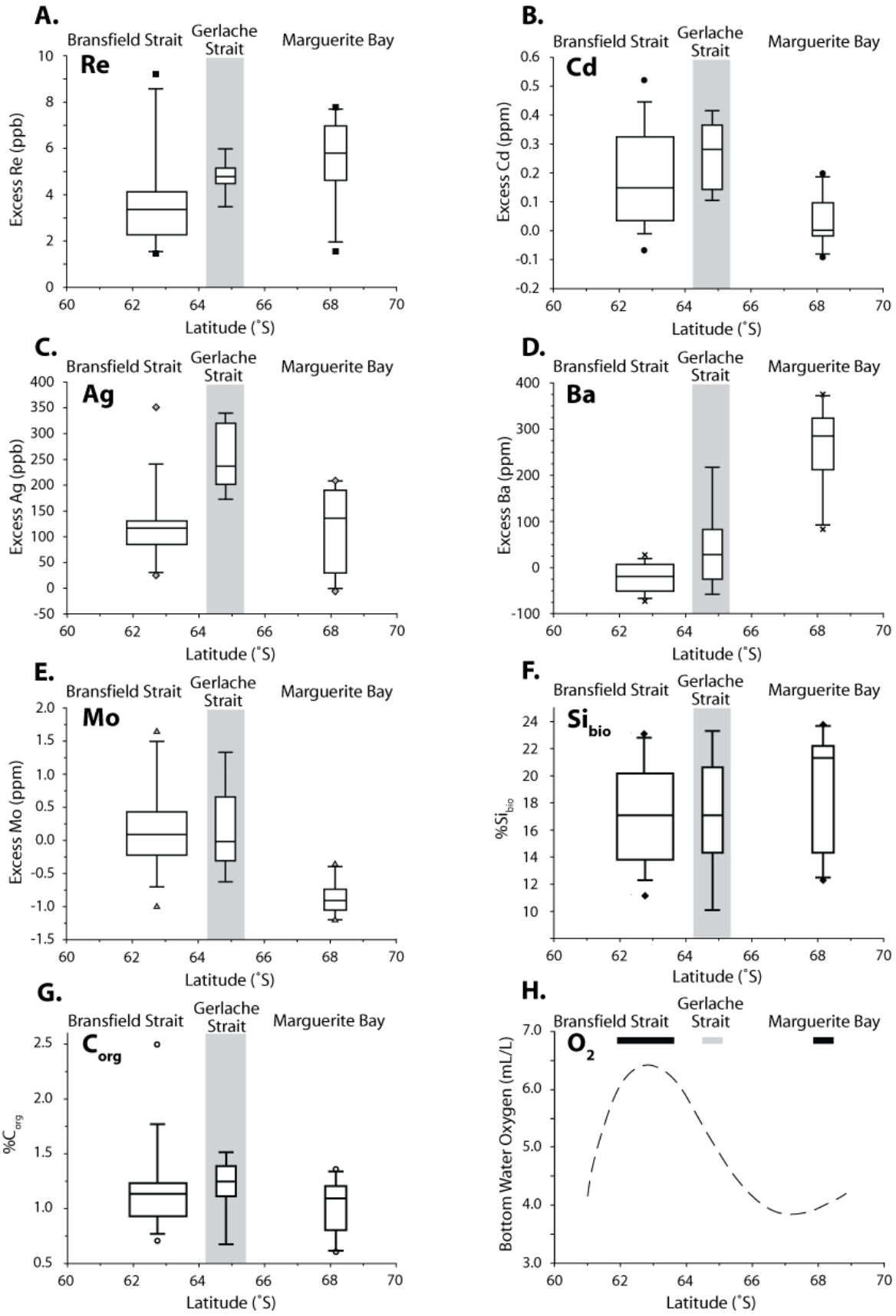
A.
Bransfield Strait
Gerlache Strait
Marguerite Bay
Re
Excess Re (ppb)
Latitude (˚S)
B.
Cd
Excess Cd (ppm)
C.
Ag
Excess Ag (ppb)
D.
Ba
Excess Ba (ppm)
E.
Mo
Excess Mo (ppm)
F.
Si$_{bio}$
%Si$_{bio}$
G.
C$_{org}$
%C$_{org}$
H.
O$_2$
Bottom Water Oxygen (mL/L)

Figure 3.2. (Previous page) Summary of trace metal and productivity proxy results from the West Antarctic Peninsula (WAP). Excess concentrations are plotted for (A) rhenium, Re; (B) cadmium, Cd; (C) silver, Ag; (D) barium, Ba; and (E) molybdenum, Mo; and weight percent of bulk sediment is plotted for (F) biogenic silica, Si_{bio}; and (G) organic carbon, C_{org}. Negative excess concentrations were calculated for some sites for Cd, Ag, Ba, and Mo due to uncertainty in background metal concentrations. Results are displayed as box and whisker plots due to large variability in proxy concentrations within each subregion. Grey shaded box in panels (A)-(G) highlights Gerlache Strait sediments, many of which were cored in bays and fjords. Panel (H) plots bottom water oxygen concentrations, oxygen data available at: http://www.nodc.noaa.gov/OC5/SELECT/dbsearch/dbsearch.html. Horizontal bars at top of plot indicate latitude ranges of cores used for this study.

5.3 ppb). The most tightly clustered excess concentrations occur in Gerlache Strait, which records a median Re excess of 4.8 ppb. Cadmium and Ag (Figure 3.2b and c, respectively) excess concentrations show a similar pattern in that both are slightly more enriched in Gerlache Strait sediments than in either Marguerite Bay or Bransfield Strait sediments, with median excess concentrations observed for Cd and Ag in Gerlache Strait sediments, respectively, at 0.28 ppm and 237 ppb; in Bransfield Strait, 0.15 ppm and 117 ppb; and in Marguerite Bay, 0.0 ppm and 136 ppb. Barium (Figure 3.2d) shows a different pattern, with median excess concentrations increasing from Bransfield Strait to Marguerite Bay (-19 ppm to 285 ppm, respectively). Molybdenum excess shows a roughly similar pattern to Cd and Ag (Figure 3.2e), although median excess concentrations in Gerlache Strait and Bransfield Strait are nearly equal (-0.02 ppm and 0.09 ppm, respectively), and median excess concentration is lower in Marguerite Bay (-0.91 ppm). Biogenic silica and organic carbon concentrations are moderately high, but vary little across the WAP (Figure 3.2f and g, respectively). Median biogenic silica content by weight is approximately 17% in Bransfield and Gerlache Straits. The highest concentrations are in Marguerite Bay, where the median increases to 21.3%. Median organic carbon concentrations range from 1.09-1.25 wt%. One extremely high concentration of 2.49 wt% is observed in surface sediments at site DF86-5BC, in Bransfield Strait.

4.2 Global Continental Margin Trace Metal Enrichments

Sedimentary Ag concentrations display a depth dependency [*McKay and Pedersen*, 2008; *Morford et al.*, 2008] that is not accounted for in Figure 3.3. Nevertheless, some broad trends are apparent. Most reported Ag concentrations are elevated above the 3σ background level (Figure 3.3a-b). Sites with Ag concentrations that are significantly above background tend to display low bottom water O_2 concentrations, high sedimentation rates, or both. Additionally, only the shallowest site from the Chile margin [*McKay and Pedersen*, 2008] reported Al concentrations, so a determination of significance was not possible for the deeper sites for Ag and other trace metals. Cadmium concentrations are only significantly above background under oxic ($[O_2] > 2$ mL L^{-1} or 63 μM) and hypoxic ($0.2 < [O_2] \leq 2$ mL L^{-1} or $10 < [O_2] \leq 63$ μM) bottom water O_2 concentrations at one site from the Mexican margin (Figure 3.3d) where sedimentation rates are 102 cm kyr^{-1} (107 m water depth); all other Cd concentrations significantly above background occur under dysoxic ($0 < [O_2] \leq 0.2$ mL L^{-1} or $0 < [O_2] \leq 10$ μM) bottom waters (Figure 3.3c-d). Furthermore, Cd concentrations tend to increase with decreasing bottom water O_2 concentration (Figure 3.3d). Similar to Ag, most reported Re concentrations are significantly above background (Figure 3.3e-f). Concentrations tend to increase with decreasing bottom water O_2 concentration and decreasing sedimentation rates, although at all sites except those from the W. Canada margin and one African margin site, sedimentation rates exceed 10 cm kyr^{-1}. The highest Re concentrations, up to 50 ppb, occur under dysoxic bottom water O_2 concentrations (Figure 3.3f). Unlike the other trace metals, Mo concentrations are only significantly above background at three sites: Saanich Inlet (Figure 3.3g), the Arabian Sea, and a single site from the Mexican margin (Figure 3.3h). Of these three, Saanich Inlet is a seasonally anoxic, restricted basin, and Arabian Sea sediments contain only 1.1% Al and are primarily biogenic. As with Re, Mo

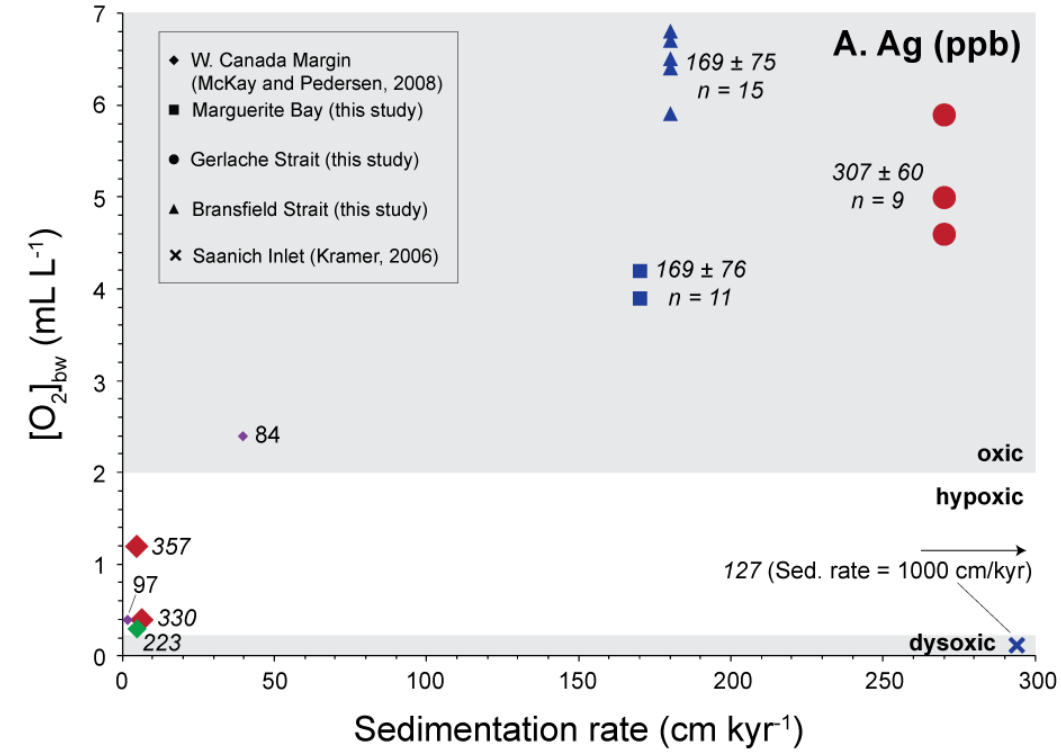

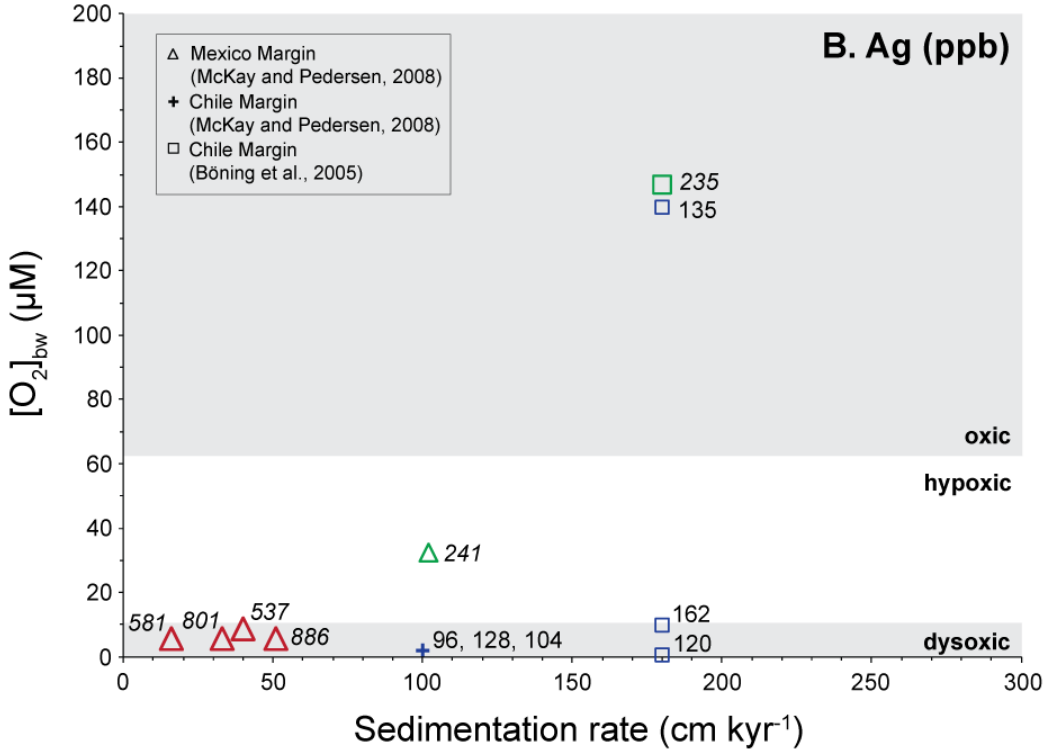

< 100 ppb 201-300 ppb

101-200 ppb > 300 ppb

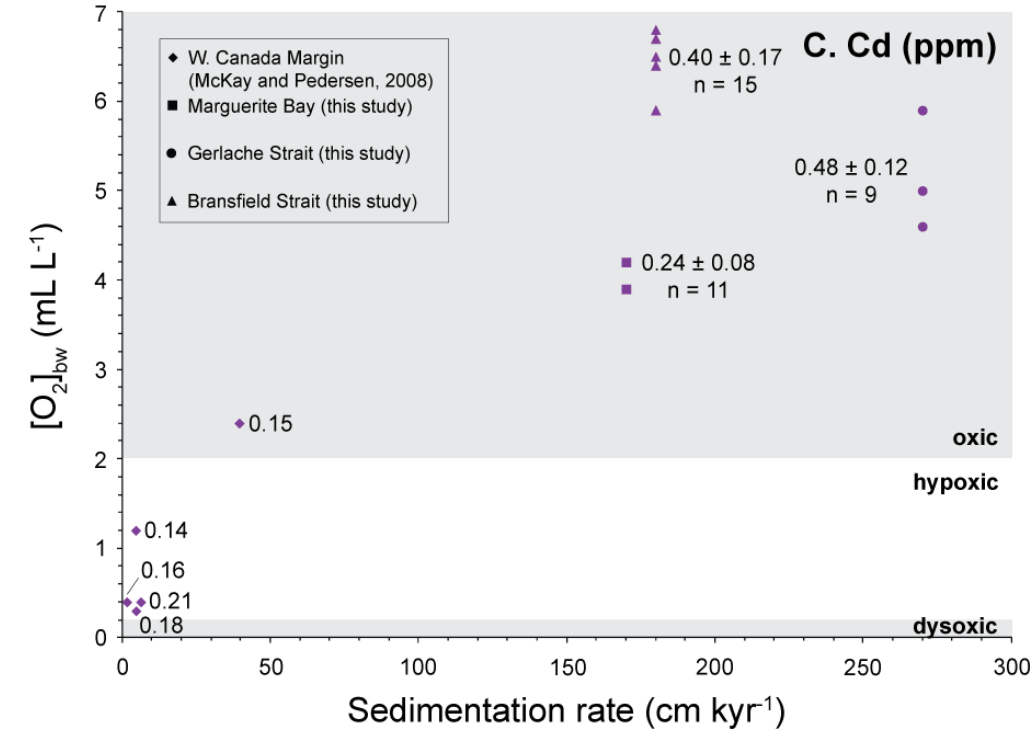

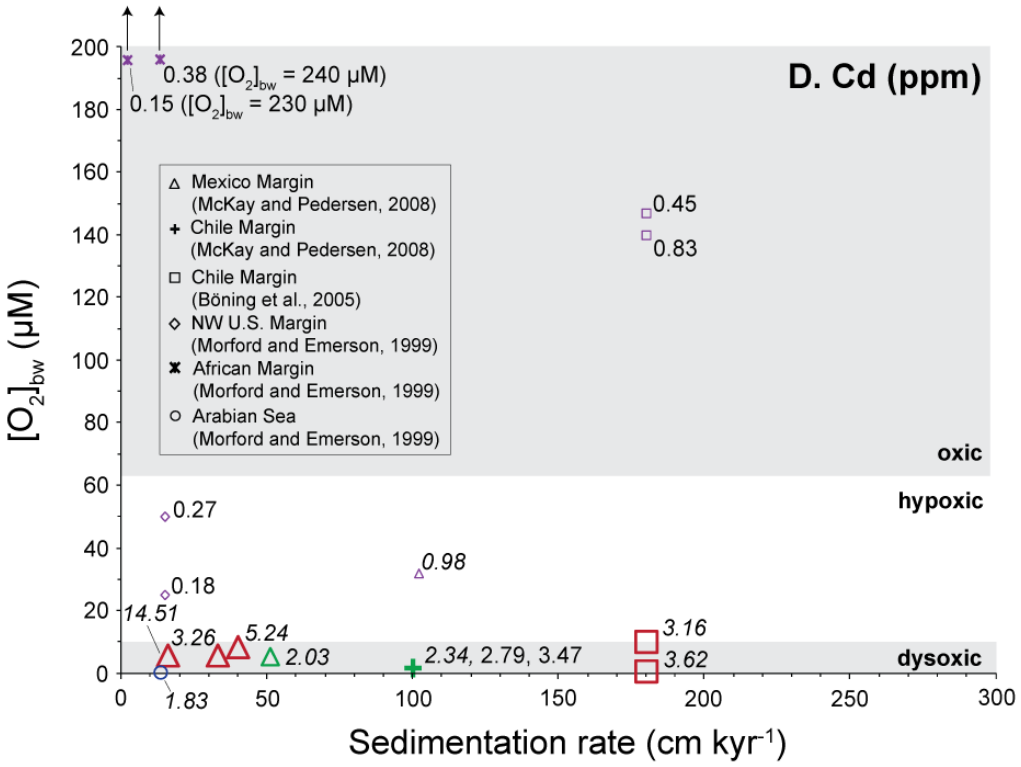

< 1 ppm 2-2.99 ppm

1-1.99 ppm > 3 ppm

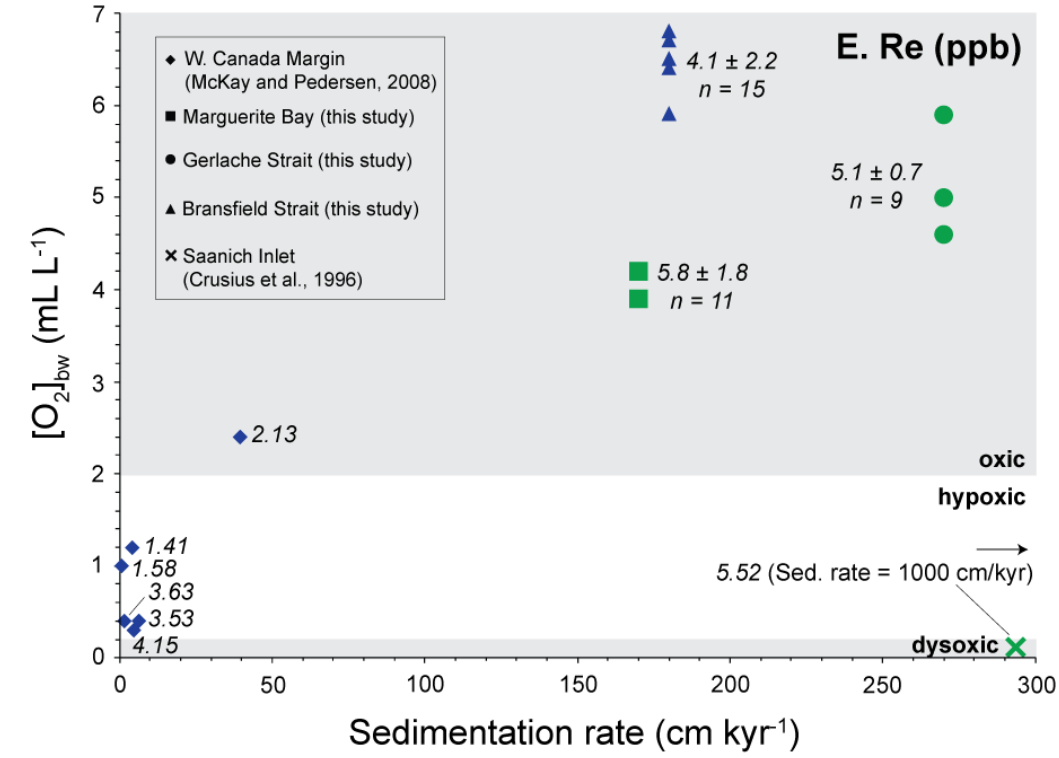

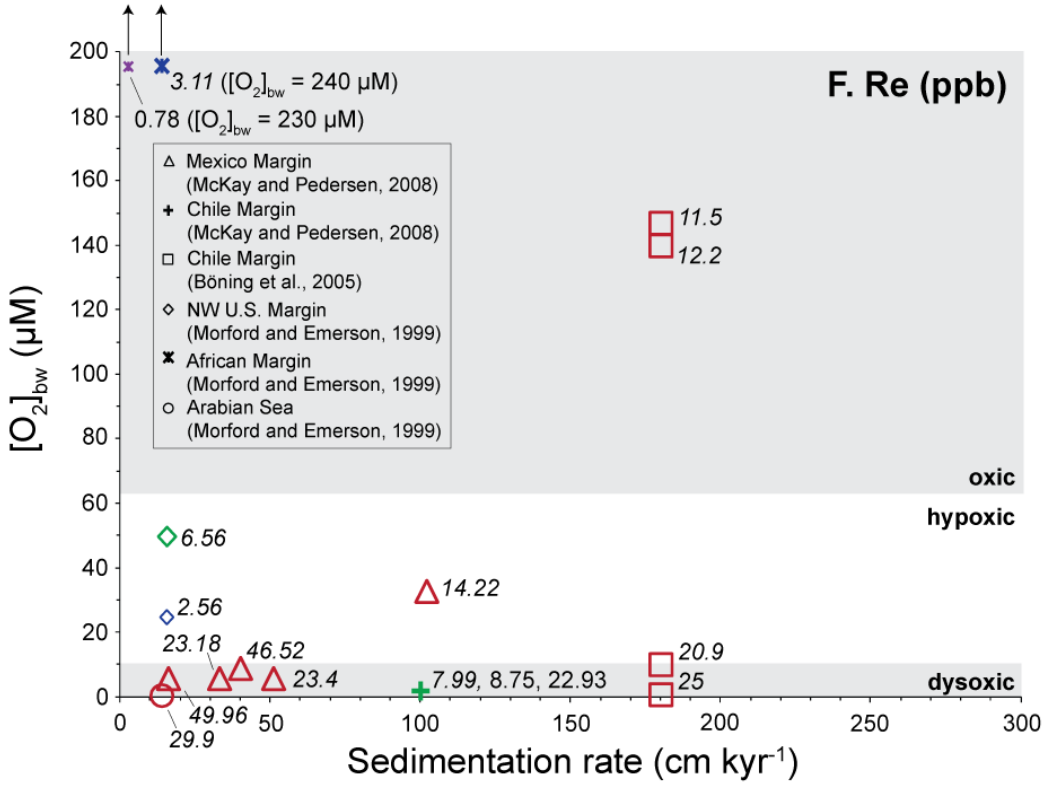

< 1 ppb 5-9.99 ppb

1-4.99 ppb > 10 ppb

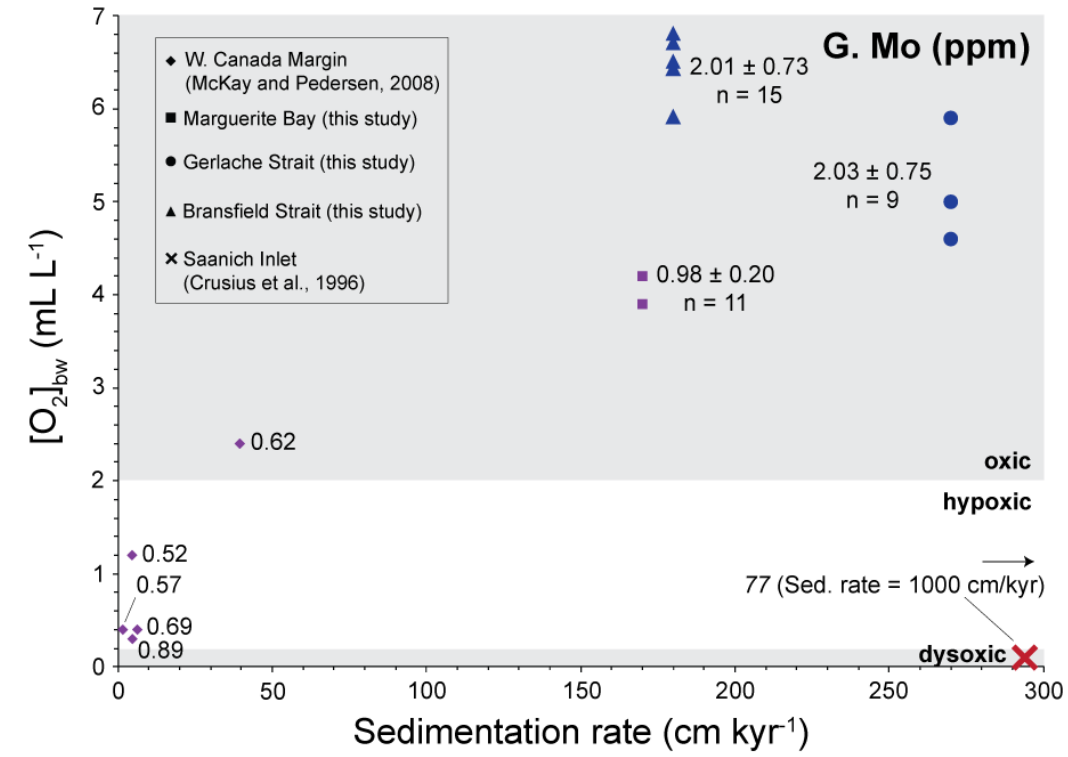

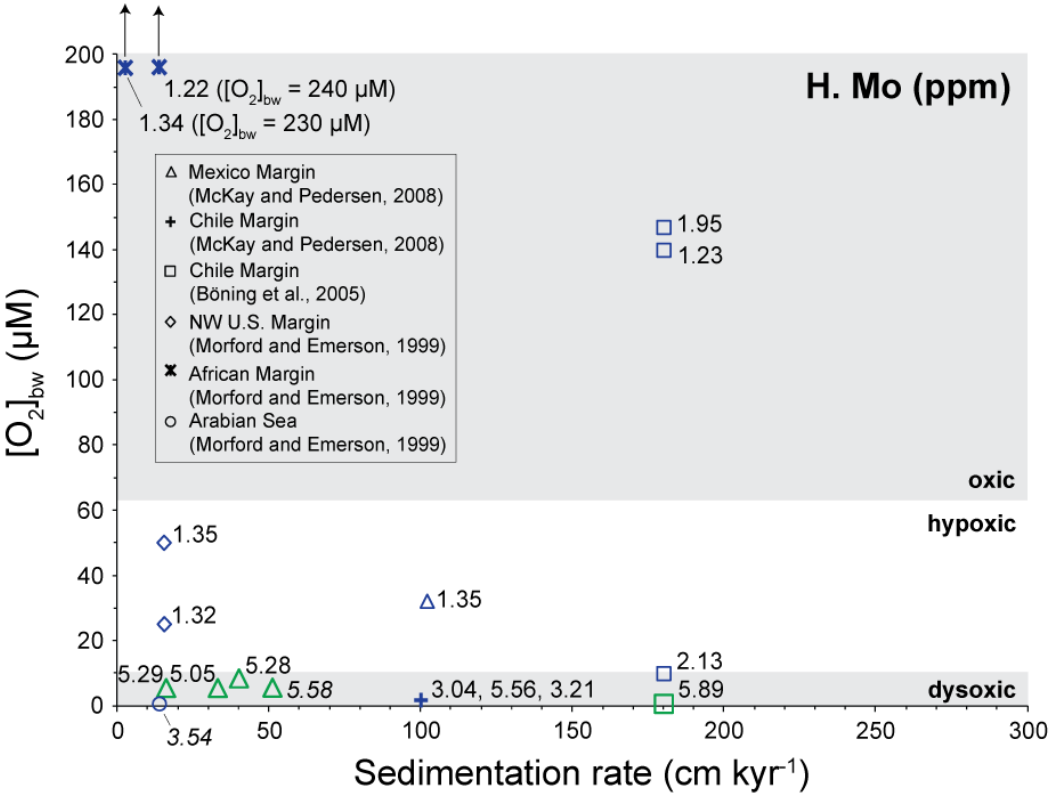

< 1 ppm 5-9.99 ppm

1-4.99 ppm > 10 ppm

Figure 3.3. (Previous four pages) Cores from this study (Table 3.1) and from the literature (Table 3.4) plotted according to sedimentation rate and bottom water oxygen concentration ($[O_2]_{bw}$). Bottom water oxygen was variably reported in units of mL L^{-1} and μM, hence there are two plots for each trace metal: (A) and (B) silver, Ag; (C) and (D) cadmium, Cd; (E) and (F) rhenium, Re; (G) and (H) molybdenum, Mo. Data labels indicate total trace metal concentrations, with concentrations significantly above background italicized (see Section 3). Size of data points scales with relative concentration of each trace metal. Total metal concentrations for WAP cores (this study) are reported by subregion as averages ± 1 standard deviation. Shading indicates transitions between oxic/hypoxic and hypoxic/dysoxic bottom water regimes. We have used the bottom water classification scheme given by Tribovillard et al. [2006] for panels A, C, E, and G (where we have substituted the terms hypoxic for suboxic, and dysoxic for anoxic). For panels B, D, F, and H we use the definition of hypoxia given by Middelburg and Levin [2009] to establish the oxic/hypoxic boundary (63 μM), and estimate the hypoxic/dysoxic boundary at 10 μM. The terms oxic, hypoxic, and dysoxic are used here to describe bottom water oxygen concentrations; and the terms oxic, suboxic, and anoxic are used to describe sedimentary pore waters.

concentrations tend to increase with decreasing bottom water O_2 concentration and decreasing sedimentation rates.

5. Discussion

Because solid phases are preserved in the geological record, bulk sediment concentrations of various trace metals are often used as proxies for paleoredox conditions at the time of deposition [*Tribovillard et al.*, 2006]. Additionally, by measuring a suite of trace metals, it is possible to elucidate the relationship between bottom water O_2 concentrations and C_{org} flux to sediments in controlling reducing conditions in pore waters. Although the terms oxic, suboxic, and anoxic are widely used to describe redox conditions, no universally accepted definition for classifying sediments and pore waters currently exists, introducing some ambiguity into the literature. To illustrate, one definition relies on the presence or absence of O_2 and H_2S [*Berner*, 1981], while others classify sediments by the chemical reactions occurring during the process of organic matter decomposition [*Canfield and Thamdrup*, 2009; *Froelich et al.*, 1979]. Canfield and Thamdrup [2009] propose a new terminology entirely (eliminating the terms suboxic and anoxic) by describing sediments where NO_3^- reduction is occurring as nitrogenous, where Fe reduction is occurring as ferruginous, and so on. Although this scheme provides the most

information, its use is restricted because the concentrations of all possible oxidants are rarely measured simultaneously within an individual sediment column due to resource limitations. The above definitions also fall short in terms of paleoredox studies because they rely on direct measurements of pore water chemistry, and there is no standard scheme for inferring the terminal electron acceptor(s) primarily in use by measuring only trace metals. To begin addressing this deficit, we propose a simple redox classification scheme for sediments using only bulk sediment concentrations of Ag, Cd, Re, and Mo. As a guide to developing this new scheme, we rely on the known geochemistry of the trace metals and their patterns of enrichment in continental margin sites from around the globe (Figure 3.3, Table 3.4).

5.1 Trace Metal Geochemistry

Silver, Cd, and Re have traditionally been considered suboxic indicators, and Mo an anoxic indicator [*Crusius et al.*, 1996; *Hendy and Pedersen*, 2005]. Rhenium behaves conservatively in seawater [*Anbar et al.*, 1992] and exists in pM concentrations as the perrhenate anion (ReO_4^-) [*Colodner et al.*, 1993]. It diffuses into sediments along concentration gradients and precipitates directly from seawater, possibly as ReO_2 [*Crusius et al.*, 1996], although the probability for this reaction to proceed spontaneously in typical seawater has recently been questioned [*Helz and Dolor*, 2012; and references therein]. Because Re requires only sufficiently reducing conditions to precipitate, its preservation does not depend on the presence of free sulfide. Due to its low crustal concentrations, nearly all sedimentary Re is authigenically precipitated [*Crusius et al.*, 1996], such that Re enrichment in the absence of Ag and/or Cd (elements associated with biogenic particles, discussed below) indicates that low bottom water O_2 concentrations rather than high organic matter delivery are responsible for O_2 depletion in underlying sediments.

Marine geochemical cycling of Ag is presently not well understood. In the water column it displays an intermediate behavior, resembling nutrient-type and scavenged elements [*Masuzawa et al.*, 1989]. Water column profiles that show increasing dissolved Ag concentrations with depth, and deep water Ag concentrations that increase from the North Atlantic to the North Pacific [*Flegal et al.*, 1995; *Kramer et al.*, 2011; *Martin et al.*, 1983; *Ndung'u et al.*, 2001; *Ranville and Flegal*, 2005; *Rivera-Duarte et al.*, 1999; *Zhang et al.*, 2001; *Zhang et al.*, 2004] suggest that it participates in biogeochemical cycles. Additionally, sedimentary Ag concentrations increase with water depth, implying concurrent Ag scavenging by sinking particles [*McKay and Pedersen*, 2008; *Morford et al.*, 2008]. Laboratory experiments [*Fisher and Wente*, 1993] and open ocean water column measurements [*Flegal et al.*, 1995] suggest that Ag may be delivered to sediments in association with diatom biodetritus, and preserved in the presence of trace quantities of sulfide as Ag_2S [*Friedl and Pedersen*, 2001]. However, studies conducted along the Mexican margin [*McKay and Pedersen*, 2008] and in the northeastern Pacific [*Martin et al.*, 1983] suggest instead that Ag is associated with organic carbon; if so, the preservation of Ag may not require sulfide. Due to its inferred association with biogenic particles, Ag concentrations higher than those expected from lithogenic background indicate that a high flux of organic matter drove reducing conditions in sediments [*Hendy and Pedersen*, 2005].

Similar water column profiles of Cd and PO_4^{3-} [*Boyle et al.*, 1976; *de Baar et al.*, 1994] suggest Cd cycling with biogenic particles that subsequently deliver Cd to the sediment-water interface. It is then released during early diagenesis, diffusing downward to the redox front where it is preserved as CdS in the presence of trace amounts of dissolved sulfide [*Rosenthal et al.*, 1995]. Like Ag, this behavior implies that Cd concentrations above those expected from

lithogenic background indicate that a high flux of organic matter produced reducing conditions and low-level sulfide concentrations in sediments [*Hendy and Pedersen,* 2005]. Unlike Ag, Cd displays a strong tendency toward authigenic precipitation where reducing conditions occur close to the sediment-water interface [*Calvert and Pedersen*, 1993; *Pedersen et al.*, 1989; *Rosenthal et al.*, 1995].

In seawater Mo is present as the conservative molybdate anion (MoO_4^{2-}). Under oxic conditions, Mo adsorbs to Mn-oxyhydroxides [*Calvert and Pedersen*, 1993; *Zheng et al.*, 2000] which produces minor enrichments unrelated to reductive processes. When redox conditions become favorable to Mn-oxyhydroxide reduction, adsorbed Mo can be released to pore waters [*Crusius et al.*, 1996], decreasing preserved solid-phase Mo. Molybdenum requires measureable sulfide concentrations to precipitate, and enrichments indicating reducing sediments are controlled by pore water H_2S concentrations [*Helz et al.*, 1996; *Zheng et al.*, 2000]. The conservative nature of MoO_4^{2-} in seawater and its reaction with sulfide imply that elevated Mo concentrations not coupled with increased Ag and/or Cd concentrations indicate that low bottom water O_2—rather than high organic carbon flux to sediments—caused reducing conditions in pore waters.

A plot of trace metal concentrations according to local sedimentation rate and bottom water O_2 concentration reveals that Ag and Re concentrations are likely to be significantly above background under hypoxic bottom waters (Figure 3.3a-b, 3.3e-f), consistent with the preservation of these elements in the absence of sulfide. In comparison, Cd and Mo concentrations are significantly above background almost exclusively under dysoxic bottom waters (Figure 3.3c-d, 3.3g-h), where the available O_2 can be more rapidly depleted. Cadmium concentrations are also much more likely than Mo concentrations to be significantly above

background, consistent with the conclusion that only trace quantities of sulfide are necessary for preservation. Because Re diffuses into sediments, high sedimentation rates may hinder Re accumulation, and this trend is reflected by higher Re concentrations at lower sedimentation rates (Figure 3.3f). Other trace metals are less obviously affected by sedimentation rate (at all sites above 10 cm kyr^{-1}).

5.2 Proposed Classification Scheme

Decomposition of organic matter in sediments proceeds using a series of oxidants, or terminal electron acceptors [*Froelich et al.*, 1979]. As available oxidants are consumed, sediments become more reducing, and enrichments of trace metals such as Ag, Cd, Re, and Mo increase. Sediment chemistry at the time of deposition is thereby linked to both trace metal enrichments and to the redox character of the sediments. Given the differences in trace metal delivery to and preservation in sediments, we propose the following scheme (Figure 3.4) to label the redox character of sediments as oxic, suboxic, or anoxic: *Oxic* sediments have no significantly elevated (above 3σ background) concentrations of Ag, Cd, Re, or Mo. *Suboxic* sediments have significantly elevated concentrations of Ag and/or Re. *Anoxic* sediments may have significantly elevated concentrations of Ag and/or Re but also include significantly elevated concentrations of Cd and/or Mo. Cadmium is re-classified as a weakly anoxic indicator due to its association with (trace) sulfide. Silver may not properly be a redox-sensitive trace metal if it is retained in sediments by association with organic matter. However, environmental conditions that are conducive to organic matter preservation—high export production, low bottom water O_2 concentrations, and high sedimentation rates—should therefore also promote Ag preservation. Silver also shows evidence of scavenging behavior [*Böning et al.*, 2005; *McKay and Pedersen*, 2008; *Morford et al.*, 2008] that is difficult to capture without normalizing to water depth, and

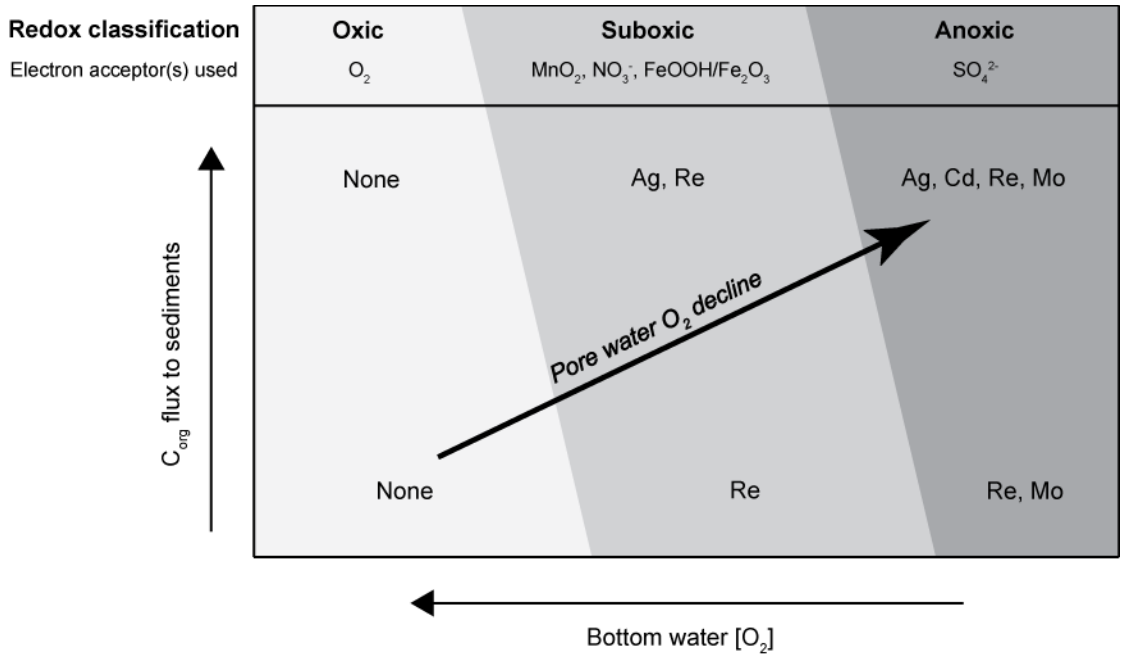

Figure 3.4. Proposed classification scheme for inferring paleoredox conditions using trace metal enrichments. Redox classification refers to sediments, not bottom waters. Electron acceptors used under oxic, suboxic, and anoxic conditions follow Froelich et al. [1979], and are in agreement with combined trace metal/pore water data discussed in Section 5.3.

this complicates interpreting sedimentary Ag enrichments. As implied in Section 5.1, the suite of trace metals considered here also allows for differentiation of the processes driving reducing conditions in pore waters by the presence (high C_{org} flux to sediments and possibly concurrent low bottom water O_2 concentrations) or absence (low bottom water O_2 concentrations) of Ag and Cd enrichments.

5.3 Sediment Chemistry from Combined Trace Metal/Pore Water Data

Trace metal-based redox classifications for surface sediments outside the WAP are listed in Table 3.4 and mapped in Figure 3.5. Examining available pore water profiles from the other continental margin sites can help to ground truth redox assignments and provide information about the relationship between observed trace metal enrichments and the electron acceptor(s) being used to degrade organic matter. The locations from which pore water data are available include W. Canada, the Northwest U.S., Africa, and Mexico.

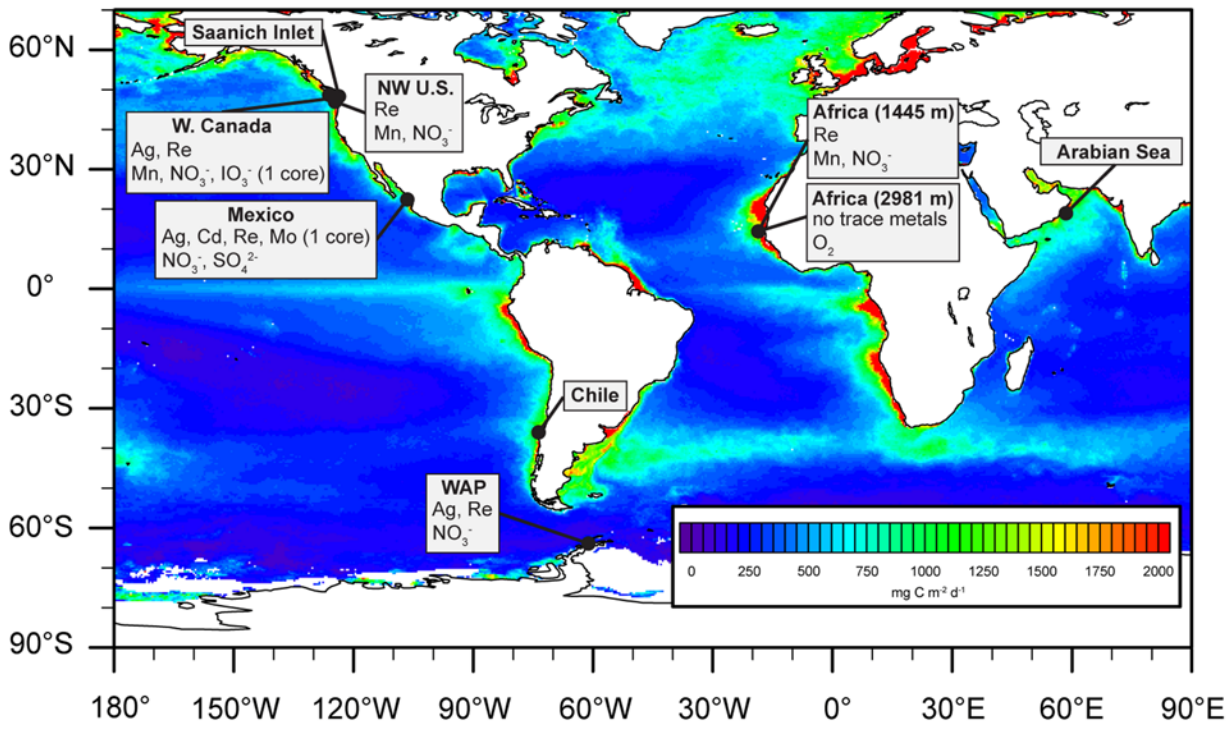

Figure 3.5. Continental margin locations considered in this study overlaid on 2007 SeaWiFS annual average net primary productivity. Boxes describe sedimentary redox chemistry: First line underneath name of margin gives trace metals with total bulk sediment concentrations above 3σ lithogenic background. Second line underneath name of margin gives electron acceptor(s) implied as being used for organic matter oxidation. References for pore water data appear in the main text. SeaWiFS data available at http://www.science.oregonstate.edu/ocean.productivity/.

On the W. Canada margin, sediments are classified as suboxic due to Ag and Re concentrations that are significantly above background (Table 3.4). McKay et al. [2007], however, qualify that these sediments are weakly suboxic, hovering between Mn and IO_3^- reduction. Pore water data reveal that NO_3^- and Mn reduction are occurring at multiple sites, and IO_3^- reduction is occurring at one site. Because Ag and Re concentrations are significantly above background at nearly all sites (Figure 3.3), the occurrence of IO_3^- reduction cannot be inferred from their enrichment. On the Northwest U.S. margin, sediments are also classified as suboxic using trace metal concentrations. Nitrate and Mn reduction are inferred to be occurring, but Fe/Al ratios indicate a lack of Fe diagenetic cycling within the sediments [*Hartnett and Devol*, 2003; *Morford and Emerson*, 1999]. The lack of Fe reduction indicates that this pathway for

organic matter oxidation cannot be assumed to occur for surface sediments with Re concentrations significantly above background. On the African margin, the two cores examined have distinctly different surface sediment chemistry. The shallower core is classified as suboxic using trace metals, and NO_3^- and probably Mn reduction are occurring [*Jahnke et al.*, 1989]. These sediments appear to have a reduction potential somewhere between Mn and Fe reduction, although trace metals (Ag, Cd, Re, and Mo) alone would be unable to make this distinction. The deeper core is classified as oxic using trace metals, consistent with a lack of NO_3^- and Mn reduction [*Jahnke et al.*, 1989]. The deeper African margin site is unique because trace metals are typically not measured in oxic sediments; this site is therefore the only available example where trace metals and pore water data are compared. Finally, on the Mexico margin, sediments are classified as weakly anoxic to anoxic using trace metals, consistent with undetectable pore water O_2 concentrations at sites deeper than ~100 m [*Hartnett and Devol*, 2003]. Active SO_4^{2-} reduction was measured in near-surface sediments [*Hartnett and Devol*, 2003], as expected for the presence of significantly elevated concentrations of Cd and Mo, which are preserved in association with sulfide.

In summary, trace metal (Ag, Cd, Re, and Mo) concentrations can be used to identify oxic (O_2 reduction occurring) and anoxic (SO_4^{2-} reduction occurring) sediments, but cannot be used to distinguish the reactions that fall under the label "suboxic" (Mn, NO_3^-, IO_3^-, and Fe reduction, similar to the definition of Froelich et al. [1979], Figure 3.4). One obvious solution to this problem is to also measure solid-phase Mn, Fe, and I concentrations in sediments. With the limited evidence presented here, Mn and NO_3^- reduction can be expected to occur in suboxic surface sediments, but Fe and IO_3^- reduction are less likely. Additionally, by utilizing a suite of trace metals that can distinguish between low bottom water O_2 concentrations and high C_{org} flux,

it should be possible to track changes in past continental margin sediment chemistry and infer the reasons behind these changes. With a structure now in place for evaluating continental margin sediment chemistry, we turn to the processes that control redox conditions along the West Antarctic Peninsula.

5.4 WAP Sedimentary Chemistry

5.4.1 Productivity proxies

Bulk sediment Si_{bio} and C_{org} concentrations (Table 3.3) are consistent with previous measurements from Bransfield Strait [*Bárcena et al.*, 2002] and Gerlache Strait [*Isla et al.*, 2004]. WAP C_{org} concentrations tend to be lower than those at other continental margin sites (Figure 3.6a), as expected based on a lower rate of surface primary productivity and a higher oxygen penetration depth [Figure 3.6b-c] (note that oxygen penetration depth is a function of the O_2 concentration at the sediment-water interface [*Rasmussen and Jorgensen*, 1992]). Barium has been shown to be a reliable recorder of export production in the open Southern Ocean [*Eagle et al.*, 2003]. However, persistently shallow water depths along the WAP (< 1000 m, Table 3.1) present insufficient water column lengths for particulate accumulation of barite, making excess Ba an unreliable proxy in this environment. The problems with Ba are also underscored by the observation that most of the deeper sites are located in Bransfield Strait (Table 3.1, Figure 3.1), but excess Ba concentrations are mostly negative here (Figure 3.2d).

5.4.2 Trace metal accumulation and sedimentary redox chemistry

Significantly elevated concentrations of only Ag and Re in all three subregions of the WAP imply that sediments are typically suboxic: Mn and NO_3^- reduction are expected, but near-surface SO_4^{2-} reduction is not. Positive excess concentrations of Ag, Cd, and Re (Figure 3.2a-c) tend to support this classification assignment. Excess Mo concentrations (Figure 3.2e) show no relation to either the suboxic indicators or to bottom water O_2 concentrations (Figure 3.2h), and

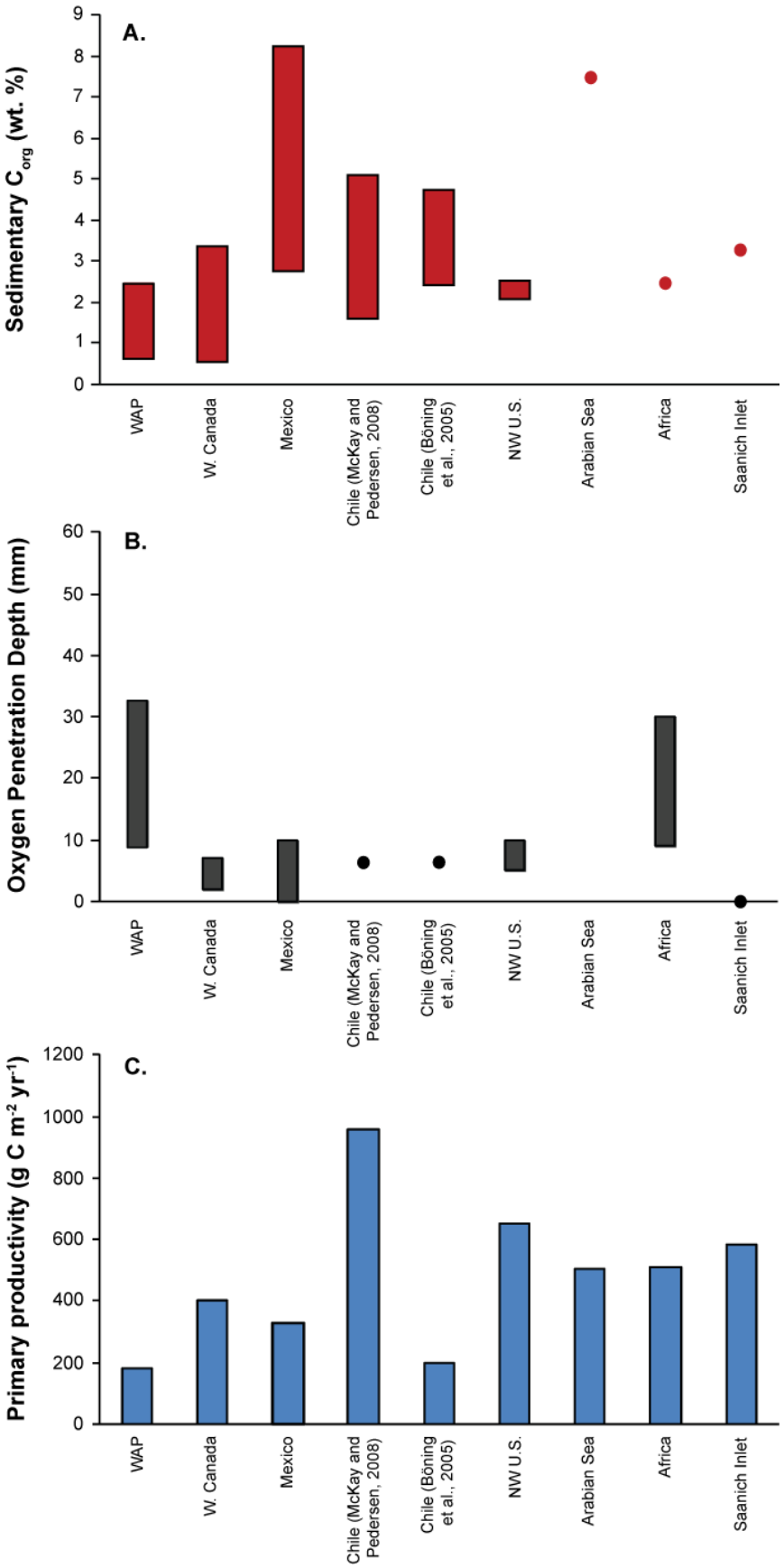
A.
Sedimentary C_{org} (wt. %)
0
1
2
3
4
5
6
7
8
9
B.
Oxygen Penetration Depth (mm)
0
10
20
30
40
50
60
C.
Primary productivity (g C m^{-2} yr^{-1})
0
200
400
600
800
1000
1200
WAP
W. Canada
Mexico
Chile (McKay and Pedersen, 2008)
Chile (Böning et al., 2005)
NW U.S.
Arabian Sea
Africa
Saanich Inlet

Figure 3.6. (Previous page) Comparison of the role of organic carbon at continental margin sites. (A) Sedimentary weight percent C_{org}. Data is presented as a range of available values for cores listed in Table 3.4. Dots represent sites with only one data point. Data sources: WAP—this study; W. Canada, Mexico, and Chile—[*McKay and Pedersen*, 2008]; Chile—[*Böning et al.*, 2005]; NW U.S.—[*Hartnett and Devol*, 2003]; Arabian Sea—Estimated from nearby sites [*Pedersen et al.*, 1992]; Africa—Estimated from graph [*Jahnke et al.*, 1989]; Saanich Inlet—Estimated from graph [*Calvert and Pedersen*, 1993]. (B) Oxygen penetration depth (OPD). Data is presented as a range of available values for cores listed in Table 3.4. Dots represent sites with only one data point. Data sources: WAP—Estimated from Palmer LTER data [*Hartnett et al.*, 2008]; W. Canada—[*McKay et al.*, 2007]; Mexico—[*Hartnett and Devol*, 2003]; Chile (all cores)—Estimated from nearby sites [*Glud et al.*, 1999]; NW U.S.—[*Hartnett and Devol*, 2003]; Arabian Sea—No data, but OPDs are assumed to be << 10 mm [*Morford and Emerson*, 1999]; Africa—[*Jahnke et al.*, 1989]; Saanich Inlet—Assigned a value of 0 mm because bottom waters frequently contain no oxygen and detectable H_2S during spring and summer [*J J Anderson and Devol*, 1973]. (C) Surface primary productivity. Data sources: WAP—[*Vernet et al.*, 2008]; W. Canada, Mexico, and Chile—[*McKay and Pedersen*, 2008]; Chile—[*Böning et al.*, 2005]; NW U.S.—[*Hartnett and Devol*, 2003]; Arabian Sea—[*Lee et al.*, 1998]; Africa—[*Jahnke et al.*, 1989]; Saanich Inlet—[*Timothy and Soon*, 2001].

are often negative. Bulk sediment Mo concentrations therefore likely reflect primarily detrital material, although it is possible that Mo depletions have occurred at some sites due to MnO_2 reduction and remobilization of associated Mo [*Crusius et al.*, 1996].

High bottom water O_2 concentrations (Figure 3.2h) should discourage suboxia and resultant trace metal accumulation in WAP surface sediments. However, C_{org} flux to sediments also influences trace metal accumulation by driving consumption of sedimentary oxidants during organic matter decomposition. The presence of nonlithogenic Ag and Cd suggests that enrichments result from elevated C_{org} flux to the sediment-water interface. Average primary production along the WAP is estimated to be about one-fourth that found in other coastal areas [*Vernet et al.*, 2008] (although literature-derived primary productivity estimates for the other margins place the WAP at closer to one-half to one-third [Figure 3.6c]). WAP export production differs from other margins in that it is highly pulsed and seasonal [*Abelmann and Gersonde*, 1991]. For example, elevated primary production has been observed in Bransfield Strait for a

short, ~60-day period during austral spring-summer [*Palanques et al.*, 2002]. Accumulation on the seafloor of phytodetritus resulting from spring-summer blooms is hypothesized to provide a "food bank" for detrivores during periods of low export production (austral winter), such that degradation of organic matter takes place throughout the year [*C R Smith et al.*, 2012]. This "food bank" may therefore act to maintain redox conditions in WAP sediments by holding C_{org} oxidation rates relatively constant [*Hartnett et al.*, 2008] despite seasonal changes in export production.

Our diagnosis of suboxia in WAP sediments is supported by O_2 and NO_3^- pore water data from the Gerlache Strait region [*Hartnett et al.*, 2008], and trace metal measurements from a site in Bransfield Strait [*Howe et al.*, 2007]. Inner-shelf pore water O_2 profiles near Gerlache Strait [*Hartnett et al.*, 2008] consistently show O_2 concentrations declining to zero $\leq$ 3 cm below the sediment-water interface. The decline in pore water NO_3^- concentrations closely follows O_2, especially during austral summer [*Hartnett et al.*, 2008], indicating active NO_3^- reduction. Downcore Mn/Li and Fe/Li profiles in Bransfield Strait [*Howe et al.*, 2007] increase from the sediment-water interface to maxima at 3.5 cm and 6.5 cm, respectively, suggesting that these are the modern redox boundaries. At the sediment-water interface, Mn/Li and Fe/Li ratios closely resemble upper continental crust [*Taylor and McLennan*, 1985], implying a purely lithogenic source of these metals. Therefore, Mn reduction may not be occurring at all sites.

In sum, trace metal evidence suggests that sedimentary suboxia on the WAP shelf is widespread, but corroborating evidence for this redox state is currently limited. Additional studies measuring Mn, Fe, and I in WAP sediments, as well as more widely distributed pore water measurements, are required to confirm widespread surface sediment suboxia. Observed trace metal enrichments occurring below highly oxygenated bottom waters suggest that C_{org}

remineralization is a more important control on sedimentary redox in this environment than bottom water oxygenation.

6. Conclusions

This study reports the first measurements of trace metal concentrations in surface sediments spanning Bransfield Strait, Gerlache Strait, and Marguerite Bay. Despite the presence of well-ventilated bottom waters, positive excess concentrations (i.e., nonlithogenic contributions) of Ag, Cd, and Re were found for all three subregions. Furthermore, total Ag and Re concentrations were in excess of three times average shale background, and therefore considered significant. Trace metal concentrations therefore imply that suboxic sediments commonly occur across the WAP inner shelf. Excess Ag and Cd in conjunction with moderately elevated bulk sediment C_{org} and Si_{bio} concentrations suggest that high C_{org} flux to sediments exerts primary control over sedimentary redox conditions. Additionally, WAP trace metal concentrations are within range of those measured at some other continental margins (Figure 3.3), suggesting that WAP sediment chemistry is influenced by similar processes. Finally, it is worth noting that surface sediments came mostly from the WAP inner shelf, and it is possible that different sediment chemistry exists along the middle and outer shelves, and on the continental slope. These areas require future investigation, especially through paleoceanographic studies to determine changes in phytoplankton productivity and bathymetric upwelling of Circumpolar Deep Water at the shelf break.

Drawing on known trace metal geochemical cycling, we propose a new scheme for classifying sedimentary (paleo)redox conditions based solely on Ag, Cd, Re, and Mo concentrations. Furthermore, coupled pore water-trace metal data from continental margin surface sediments outside the WAP are used to ground truth the most likely terminal electron

acceptor(s) used for organic matter remineralization under suboxic and anoxic conditions. The proposed scheme is intended to promote consistency in describing sedimentary paleoredox chemistry, and to provide a framework for interpreting paleoclimate/paleoceanographic studies utilizing trace metals as redox proxies.

Acknowledgements. This work was supported by grants to MW from the AAPG Foundation Grants-in-Aid program, the Scott Turner Awards in Earth Science, and Rackham Graduate School, University of Michigan. WAP surface sediment samples were provided by the Antarctic Marine Geology Research Facility at Florida State University (AMGRF), which is sponsored by the U.S. National Science Foundation. Jennifer McKay (Oregon State University) measured total carbon for all samples. Tom Pedersen (University of Victoria) contributed to trace metal analyses. Alice Chang (University of British Columbia) and Victoria Gray (University of Victoria) provided invaluable training and assistance to MW. Clay Tabor (University of Michigan) assisted with plotting the SeaWiFS data.

Table 3.1. Core locations, water depths, and sampling depths for cores used in this study.

Cruise	Core	Latitude	Longitude	Water Depth (m)	Sample Depth (cmbsf)
Bransfield Strait					
DF86	005-BC	61.96°S	55.002°W	1263	0-2
DF86	006-BC	61.888°S	55.59°W	2200	0-2
DF86	010-BC	62.173°S	56.145°W	1110	0-2
DF86	011-BC	62.08°S	56.19°W	1500	0-2
DF86	018-BC	62.347°S	57.442°W	1680	0-2
DF86	020-BC	62.423°S	57.222°W	927	0-2
DF86	023-BC	62.818°S	58.792°W	1080	1-3
DF86	030-BC	62.693°S	58.92°W	1460	0-2
DF86	034-BC	62.44°S	57.928°W	1880	0-2
DF86	044-BC	63.198°S	59.3°W	805	0-2
DF86	046-BC	63.007°S	59.632°W	899	0-2
DF86	055-BC	63.142°S	61.072°W	1180	0-2
DF86	058-BC	63.29°S	61.58°W	1217	0-2
DF86	063-BC	63.633°S	61.57°W	940	0-2
DF86	064-BC	63.568°S	61.685°W	1316	0-2
Gerlache Strait					
DF86	072-BC	64.585°S	61.57°W	471	0-2
DF86	073-BC	64.56°S	61.653°W	393	1-3
DF86	074-BC	64.493°S	62.273°W	693	0-2
DF86	076-BC	64.55°S	62.588°W	740	0-2
DF86	078-BC	65.102°S	63.167°W	650	1-3
DF86	079-BC	64.995°S	63.333°W	494	1-3
DF86	080-BC	64.825°S	62.653°W	366	0-2
DF86	081-BC	64.753°S	62.808°W	431	0-2
DF86	084-BC	64.963°S	64.373°W	1327	0-2
Marguerite Bay					
DF86	089-BC	68.328°S	70.4°W	695	0-2
DF86	092-BC	68.445°S	70.052°W	1370	0-2
DF86	095-BC	68.288°S	67.882°W	454	0-2
DF86	096-BC	68.318°S	68.298°W	723	4-6
DF86	097-BC	68.292°S	67.947°W	604	0-2
DF86	104-BC	67.893°S	67.637°W	300	0-2
DF86	107-BC	67.835°S	68.2°W	915	4-6
DF86	108-BC	67.895°S	68.363°W	840	0-2
DF86	113-BC	68.035°S	68.2998°W	470	2-4
DF86	114-BC	68.132°S	67.847°W	480	0-2
DF86	115-BC	68.173°S	68.335°W	630	2-4

Table 3.2. Replicate analyses (n = 8, trace metals; n = 2, Ba and Al) of the sediment standard MESS-3, ± 1σ standard deviation.

	Ag (ppb)	Cd (ppm)	Re (ppb)	Mo (ppm)	Ba (ppm)	Al (%)
Certified value	180	0.24	Not reported	2.78	Not reported[a]	8.59
Uncertainty	20	0.01	Not reported	0.07	Not reported[a]	0.23
Measured value	175	0.20	3.4	2.27	958	8.2
1 σ error	5	0.01	0.2	0.07	37	0.2

[a]The GeoReM database (http://georem.mpch-mainz.gwdg.de/) reports 945-973 ppm for Ba (2 values).

Table 3.3. Element concentration data for all cores.

		Productivity Proxies			Redox Proxies			
Sample	Al (%)	Ba (ppm)	C_{org} (%)	Si_{bio} (%)	Ag (ppb)	Cd (ppm)	Re (ppb)	Mo (ppm)
DF86-5BC	5.0	344	2.5	23.1	206	0.29	2.8	1.9
DF86-6BC	6.3	344	0.7	13.0	175	0.24	3.9	0.9
DF86-10BC	5.9	419	1.2	20.2	178	0.60	4.4	1.6
DF86-11BC	6.2	400	0.9	17.1	401	0.36	9.5	1.6
DF86-18BC	6.9	403	1.1	11.2	102	0.17	1.9	2.5
DF86-20BC	5.5	368	1.1	22.6	136	0.49	5.3	1.6
DF86-23BC	6.2	396	0.9	15.8	180	0.73	8.4	1.3
DF86-30BC	6.8	457	1.2	13.8	88	0.56	3.1	2.3
DF86-34BC	6.7	402	1.3	13.3	78	0.49	1.8	2.7
DF86-44BC	5.9	380	1.3	18.7	214	0.30	2.5	2.1
DF86-46BC	5.9	373	1.2	21.5	166	0.42	3.6	1.8
DF86-55BC	6.4	362	0.8	15.7	152	0.25	3.6	1.7
DF86-58BC	6.5	379	1.0	15.6	150	0.27	4.1	3.3
DF86-63BC	6.4	372	1.0	17.4	167	0.57	4.0	1.4
DF86-64BC	6.2	369	1.2	19.5	135	0.25	2.3	3.5
DF86-72BC	6.3	505	1.2	16.7	249	0.34	5.1	1.9
DF86-73BC	6.4	500	1.3	14.7	356	0.63	4.6	1.8
DF86-74BC	6.2	354	1.2	20.2	284	0.37	4.9	1.8
DF86-76BC	7.2	422	1.4	18.1	295	0.56	5.2	3.5
DF86-78BC	6.9	529	0.7	10.1	228	0.49	3.8	2.3
DF86-79BC	6.5	433	1.1	14.0	330	0.57	5.1	1.3
DF86-80BC	6.3	445	1.2	17.1	386	0.50	6.3	3.0
DF86-81BC	5.7	381	1.5	21.1	386	0.57	5.6	1.4
DF86-84BC	5.8	598	1.4	23.3	250	0.30	5.0	1.4
DF86-89BC	7.2	800	0.6	12.3	52	0.23	1.9	1.1
DF86-92BC	7.3	843	0.7	13.2	79	0.25	6.6	1.1
DF86-95BC	6.4	554	1.1	15.3	187	0.42	5.6	0.7
DF86-96BC	6.1	779	0.8	18.4	78	0.18	3.8	0.9
DF86-97BC	5.9	712	1.4	21.7	168	0.11	4.9	0.9
DF86-104BC	6.7	526	1.1	14.3	244	0.23	6.4	1.0
DF86-107BC	5.8	702	1.2	23.8	252	0.24	5.6	1.2
DF86-108BC	5.7	657	1.3	23.0	233	0.34	7.2	1.3
DF86-113BC	6.1	616	1.0	21.5	193	0.19	7.7	0.6
DF86-114BC	5.8	666	1.2	21.3	255	0.29	8.0	0.9
DF86-115BC	5.9	644	1.0	22.2	113	0.19	6.1	1.0

Table 3.4. Locations and water depths of cores from published literature.

Core	Location	Water depth (m)	Redox Classification	Reference
Pacific Ocean				
West Canada margin				
JT01mc	48.77°N 125.49°W	120	Suboxic	1
JT04mc	49.01°N 126.83°W	407	Suboxic	1
JT06bc	48.98°N 126.88°W	720	Suboxic	1
JT09mc	48.91°N 126.89°W	920	Suboxic	1
JT02mc	49.21°N 127.31°W	1340	Suboxic	1
JT05bc	49.13°N 127.55°W	1750	Suboxic	1
NW U.S. margin				
WEC213	46.5°N 124.7°W	620	Suboxic	2
WEC206	46.8°N 124.2°W	1004	Suboxic	2
Mexico margin				
NH3bc	22.7°N 106.3°W	107	Weakly anoxic	1
NH7bc	22.7°N 106.5°W	190	Weakly anoxic	1
NH12bc	22.7°N 106.5°W	322	Weakly anoxic	1
NH15bc	22.7°N 106.5°W	425	Weakly anoxic	1
NH6bc	22.6°N 106.5°W	620	Anoxic	1
Chile margin				
VG07mc	36.6°S 73.0°W	37	Weakly anoxic	1
VG18mc	36.5°S 73.1°W	87	*No Al data	1
VG26mc	36.4°S 73.4°W	122	*No Al data	1
Chile margin				
A	36.43°S 73.39°W	126	Weakly anoxic	3
B	36.04°S 73.07°W	367	Weakly anoxic	3
C	36.43°S 73.60°W	536	Suboxic	3
D	36.54°S 73.67°W	798	Suboxic	3
Saanich Inlet				
SS3	48.7°N 123.5°W	180	Anoxic	4
Not given	Not given	184	Anoxic	5
Indian Ocean				
Arabian Sea				
TN047-20	19.2°N 58.4°E	806	Anoxic	2
Atlantic Ocean				
African margin				
1BC1-2	14.7°N 17.8°W	1445	Suboxic	2

3BC8-1	14.7° 18.6°W	2981	Oxic	2

1) [*McKay and Pedersen*, 2008]
2) [*Morford and Emerson*, 1999]
3) [*Böning et al.*, 2005]
4) [*Kramer*, 2006]
5) [*Crusius et al.*, 1996]

REFERENCES

Abelmann, A., and R. Gersonde (1991), Biosiliceous particle flux in the Southern Ocean, *Marine Chemistry*, *35*(1-4), 503-536.

Anbar, A. D., R. A. Creaser, D. A. Papanastassiou, and G. J. Wasserburg (1992), Rhenium in seawater: Confirmation of generally conservative behavior, *Geochimica et Cosmochimica Acta*, *56*(11), 4099-4103.

Anderson, J. B. (1999), *Antarctic Marine Geology*, 289 pp., Cambridge University Press, New York.

Anderson, J. J., and A. H. Devol (1973), Deep water renewal in Saanich Inlet, an intermittently anoxic basin, *Estuarine and Coastal Marine Science*, *1*(1), 1-10.

Bárcena, M. Á., E. Isla, A. Plaza, J. A. Flores, F. J. Sierro, P. Masqué, J. A. Sanchez-Cabeza, and A. Palanques (2002), Bioaccumulation record and paleoclimatic significance in the Western Bransfield Strait. The last 2000 years, *Deep-Sea Research II*, *49*(4-5), 935-950.

Bentley, M. J., et al. (2009), Mechanisms of Holocene palaeoenvironmental change in the Antarctic Peninsula region, *The Holocene*, *19*(1), 51-69.

Berner, R. A. (1981), A new geochemical classification of sedimentary environments, *Journal of Sedimentary Petrology*, *51*(2), 359-365.

Böning, P., S. Cuypers, M. Grunwald, B. Schnetger, and H.-J. Brumsack (2005), Geochemical characteristics of Chilean upwelling sediments at ~36°S, *Marine Geology*, *220*(1-4), 1-21.

Boyle, E. A., F. Sclater, and J. M. Edmond (1976), On the marine geochemistry of cadmium, *Nature*, *263*(5572), 42-44.

Calvert, S. E., and T. F. Pedersen (1993), Geochemistry of recent oxic and anoxic marine sediments: Implications for the geological record, *Marine Geology*, *113*(1-2), 67-88.

Canfield, D. E., and B. Thamdrup (2009), Towards a consistent classification scheme for geochemical environments, or, why we wish the term 'suboxic' would go away, *Geobiology*, *7*(4), 385-392.

Colodner, D., J. Sachs, G. Ravizza, K. Turekian, J. Edmond, and E. Boyle (1993), The geochemical cycle of rhenium: a reconnaissance, *Earth Planet. Sci. Lett.*, *117*(1-2), 205-221.

Crusius, J., S. Calvert, T. Pedersen, and D. Sage (1996), Rhenium and molybdenum enrichments in sediments as indicators of oxic, suboxic, and sulfidic conditions of deposition, *Earth Planet. Sci. Lett.*, *145*(1-4), 65-78.

de Baar, H. J. W., P. M. Saager, R. F. Nolting, and J. van der Meer (1994), Cadmium versus phosphate in the world ocean, *Marine Chemistry*, *46*(3), 261-281.

Domack, E. W., and S. Ishman (1993), Oceanographic and physiographic controls on modern sedimentation within Antarctic fjords, *Geological Society of America Bulletin*, *105*(9), 1175-1189.

Domack, E. W., and C. E. McClennen (1996), Accumulation of glacial marine sediments in fjords of the Antarctic Peninsula and their use as Late Holocene paleoenvironmental indicators, in *Foundations for Ecological Research West of the Antarctic Peninsula*, edited by R. M. Ross, E. M. Hofmann and L. B. Quetin, pp. 135-154, American Geophysical Union, Washington.

Eagle, M., A. Paytan, K. R. Arrigo, G. v. Dijken, and R. W. Murray (2003), A comparison between excess barium and barite as indicators of carbon export, *Paleoceanography*, *18*(1), 1021, doi: 10.1029/2002PA000793.

Fisher, N. S., and M. Wente (1993), The release of trace elements by dying marine phytoplankton, *Deep-Sea Research I*, *40*(4), 671-694.

Flegal, A. R., S. A. Sañudo-Wilhelmy, and G. M. Scelfo (1995), Silver in the eastern Atlantic Ocean, *Marine Chemistry*, *49*(4), 315-320.

Friedl, G., and T. F. Pedersen (2001), Silver as a new tracer for diatom production, *EAWAG News*, *52*(D), 14-15.

Froelich, P. N., G. P. Klinkhammer, M. L. Bender, N. A. Luedtke, G. R. Heath, D. Cullen, P. Dauphin, D. Hammond, B. Hartman, and V. Maynard (1979), Early oxidation of organic matter in pelagic sediments of the eastern equatorial Atlantic: suboxic diagenesis, *Geochimica et Cosmochimica Acta*, *43*(7), 1075-1090.

Garibotti, I. A., M. Vernet, W. A. Kozlowski, and M. E. Ferrario (2003a), Composition and biomass of phytoplankton assemblages in coastal Antarctic waters: a comparison of chemotaxonomic and microscopic analyses, *Marine Ecology--Progress Series*, *247*, 27-42.

Garibotti, I. A., M. Vernet, M. E. Ferrario, R. C. Smith, R. M. Ross, and L. B. Quetin (2003b), Phytoplankton spatial distribution patterns along the western Antarctic Peninsula (Southern Ocean), *Marine Ecology--Progress Series*, *261*, 21-39.

Gillooly, J. F., J. H. Brown, G. B. West, V. M. Savage, and E. L. Charnov (2001), Effects of Size and Temperature on Metabolic Rate, *Science*, *293*(5538), 2248-2251.

Glud, R. N., J. K. Gundersen, and O. Holby (1999), Benthic *in situ* respiration in the upwelling area off central Chile, *Marine Ecology--Progress Series*, *186*, 9-18.

Griffith, T. W., and J. B. Anderson (1989), Climatic control of sedimentation in bays and fjords of the northern Antarctic Peninsula, *Marine Geology*, *85*(2-4), 181-204.

Harden, S. L., D. J. DeMaster, and C. A. Nittrouer (1992), Developing sediment geochronologies for high-latitude continental shelf deposits: a radiochemical approach, *Marine Geology*, *103*(1-3), 69-97.

Hartnett, H. E., and A. H. Devol (2003), Role of a strong oxygen-deficient zone in the preservation and degradation of organic matter: A carbon budget for the continental margins of northwest Mexico and Washington State, *Geochimica et Cosmochimica Acta*, *67*(2), 247-264.

Hartnett, H. E., S. Boehme, C. Thomas, D. DeMaster, and C. Smith (2008), Benthic oxygen fluxes and denitrification rates from high-resolution porewater profiles from the Western Antarctic Peninsula continental shelf, *Deep-Sea Research II*, *55*(22-23), 2415-2424.

Helz, G. R., and M. K. Dolor (2012), What regulates rhenium deposition in euxinic basins?, *Chemical Geology*, *304-305*, 131-141.

Helz, G. R., C. V. Miller, J. M. Charnock, J. F. W. Mosselmans, R. A. D. Pattrick, C. D. Garner, and D. J. Vaughan (1996), Mechanism of molybdenum removal from the sea and its concentration in black shales: EXAFS evidence, *Geochimica et Cosmochimica Acta*, *60*(19), 3631-3642.

Hendy, I. L., and T. F. Pedersen (2005), Is pore water oxygen content decoupled from productivity on the California Margin? Trace element results from Ocean Drilling Program Hole 1017E, San Lucia slope, California, *Paleoceanography*, *20*(PA4026), doi: 10.1029/2004PA001123.

Hendy, I. L., and T. F. Pedersen (2006), Oxygen minimum zone expansion in the eastern tropical North Pacific during deglaciation, *Geophysical Research Letters*, *33*(L20602), doi: 10.1029/2006GL025975.

Hofmann, E. E., J. M. Klinck, C. M. Lascara, and D. A. Smith (1996), Water mass distribution and circulation west of the Antarctic Peninsula and including Bransfield Strait, in *Foundations for Ecological Research West of the Antarctic Peninsula*, edited by R. M. Ross, E. M. Hofmann and L. B. Quetin, pp. 61-80, American Geophysical Union, Washington.

Howe, J. A., C. R. Wilson, T. M. Shimmield, R. J. Diaz, and L. W. Carpenter (2007), Recent deep-water sedimentation, trace metal and radioisotope geochemistry across the Southern Ocean and Northern Weddell Sea, Antarctica, *Deep-Sea Research II*, *54*(16-17), 1652-1681.

Isla, E., P. Masque, A. Palanques, J. Guillen, P. Puig, and J. A. Sanchez-Cabeza (2004), Sedimentation of biogenic constituents during the last century in western Bransfield and Gerlache Straits, Antarctica: a relation to currents, primary production, and sea floor relief, *Marine Geology*, *209*(1-4), 265-277.

Jahnke, R. A., S. R. Emerson, C. E. Reimers, J. Schuffert, K. Ruttenberg, and D. Archer (1989), Benthic recycling of biogenic debris in the eastern tropical Atlantic Ocean, *Geochimica et Cosmochimica Acta*, *53*(11), 2947-2960.

Kramer, D. (2006), An Exploration of the Marine Silver Cycle in Coastal and Open Ocean Environments of the North Pacific, 114 pp, University of Victoria, Victoria, BC.

Kramer, D., J. T. Cullen, J. R. Christian, W. K. Johnson, and T. F. Pedersen (2011), Silver in the subarctic northeast Pacific Ocean: Explaining the basin scale distribution of silver, *Marine Chemistry, 123*(1-4), 133-142.

Lee, C., et al. (1998), Particulate organic carbon fluxes: compilation of results from the 1995 US JGOFS Arabian Sea Process Study, *Deep-Sea Research II, 45*(10-11), 2489-2501.

Li, Y.-H. (2000), *A Compendium of Geochemistry: From Solar Nebula to the Human Brain*, 475 pp., Princeton University Press, Princeton.

Liu, X., H. Sun, D. C. Kelly, F. A. Kaharoeddin, C. J. Painter, and J. R. Bryan (1992), Descriptions of sediments recovered by the USCGC *Glacier* USARP Operation Deep Freeze 1986, Bransfield Strait, Gerlache Strait, Marguerite Bay. Sedimentology Research Laboratory Contribution No. 55, edited by J. R. Bryan, Florida State University, Tallahassee, FL.

Martin, J. H., G. A. Knauer, and R. M. Gordon (1983), Silver distributions and fluxes in north-east Pacific waters, *Nature, 305*(5932), 306-309.

Masuzawa, T., S. i. Noriki, T. Kurosaki, S. Tsunogai, and M. Koyama (1989), Compositional change of settling particles with water depth in the Japan Sea, *Marine Chemistry, 27*(1-2), 61-78.

McKay, J. L., and T. F. Pedersen (2008), The accumulation of silver in marine sediments: A link to biogenic Ba and marine productivity, *Global Biogeochemical Cycles, 22*(GB4010), doi: 10.1029/2007GB003136.

McKay, J. L., T. F. Pedersen, and A. Mucci (2007), Sedimentary redox conditions in continental margin sediments (N.E. Pacific)--Influence on the accumulation of redox-sensitive trace metals, *Chemical Geology, 238*(3-4), 180-196.

Middelburg, J. J., and L. A. Levin (2009), Coastal hypoxia and sediment biogeochemistry, *Biogeosciences, 6*(7), 1273-1293.

Morford, J. L., and S. Emerson (1999), The geochemistry of redox sensitive trace metals in sediments, *Geochimica et Cosmochimica Acta, 63*(11/12), 1735-1750.

Morford, J. L., A. D. Russell, and S. Emerson (2001), Trace metal evidence for changes in the redox environment associated with the transition from terrigenous clay to diatomaceous sediment, Saanich Inlet, BC, *Marine Geology, 174*(1-4), 355-369.

Morford, J. L., L. H. Kalnejais, P. Helman, G. Yen, and M. Reinard (2008), Geochemical cycling of silver in marine sediments along an offshore transect, *Marine Chemistry, 110*(1-2), 77-88.

Mortlock, R. A., and P. N. Froelich (1989), A simple method for the rapid determination of biogenic opal in pelagic marine sediments, *Deep-Sea Research, 36*(9), 1415-1426.

Muratli, J. M., Z. Chase, A. C. Mix, and J. McManus (2010), Increased glacial-age ventilation of the Chilean margin by Antarctic Intermediate Water, *Nature Geosci, 3*(1), 23-26.

Murray, R. W., D. J. Miller, and K. A. Kryc (2000), Analysis of major and trace elements in rocks, sediments, and interstitial waters by inductively coupled plasma-atomic emission spectrometry (ICP-AES), *ODP Tech. Note, 29* [Online]. Available from World Wide Web: <http://www-odp.tamu.edu/publications/tnotes/tn29/INDEX.HTM>.

Ndung'u, K., M. A. Thomas, and A. R. Flegal (2001), Silver in the western equatorial and South Atlantic Ocean, *Deep-Sea Research II, 48*(13), 2933-2945.

Orsi, A. H., T. I. Whitworth, and W. D. Nowlin, Jr. (1995), On the meridional extent and fronts of the Antarctic Circumpolar Current, *Deep-Sea Research I, 42*(5), 641-673.

Palanques, A., E. Isla, P. Masqué, P. Puig, J.-A. Sánchez-Cabeza, J. M. Gili, and J. Guillén (2002), Downward particle fluxes and sediment accumulation rates in the western Bransfield Strait: Implications of lateral transport for carbon cycle studies in Antarctic marginal seas, *Journal of Marine Research, 60*(2), 347-365.

Pedersen, T. F., R. D. Waters, and R. W. Macdonald (1989), On the natural enrichment of cadmium and molybdenum in the sediments of Ucluelet Inlet, British Columbia, *The Science of the Total Environment, 79*(2), 125-139.

Pedersen, T. F., G. B. Shimmield, and N. B. Price (1992), Lack of enhanced preservation of organic matter in sediments under the oxygen minimum on the Oman Margin, *Geochimica et Cosmochimica Acta, 56*(1), 545-551.

Prézelin, B. B., E. E. Hofmann, C. Mengelt, and J. M. Klinck (2000), The linkage between Upper Circumpolar Deep Water (UCDW) and phytoplankton assemblages on the west Antarctic Peninsula continental shelf, *Journal of Marine Research, 58*(2), 165-202.

Ranville, M. A., and A. R. Flegal (2005), Silver in the North Pacific Ocean, *Geochemistry Geophysics Geosystems, 6*(3), Q03M01, doi: 10.1029/2004GC000770.

Rasmussen, H., and B. B. Jorgensen (1992), Microelectrode studies of seasonal oxygen uptake in a coastal sediment: role of molecular diffusion, *Marine Ecology--Progress Series, 81*(3), 289-303.

Rivera-Duarte, I., A. R. Flegal, S. A. Sañudo-Wilhelmy, and A. J. Véron (1999), Silver in the far North Atlantic Ocean, *Deep-Sea Research II, 46*(5), 979-990.

Rosenthal, Y., P. Lam, E. A. Boyle, and J. Thomson (1995), Authigenic cadmium enrichments in suboxic sediments: Precipitation and postdepositional mobility, *Earth Planet. Sci. Lett., 132*(1-4), 99-111.

Savidge, D. K., and J. A. Amft (2009), Circulation on the West Antarctic Peninsula derived from 6 years of shipboard ADCP transects, *Deep-Sea Research I, 56*(10), 1633-1655.

Shevenell, A. E., A. E. Ingalls, E. W. Domack, and C. Kelly (2011), Holocene Southern Ocean surface temperature variability west of the Antarctic Peninsula, *Nature, 470*(7333), 250-254.

Smith, C. R., D. J. DeMaster, C. Thomas, P. Srsen, L. Grange, V. Evrard, and F. Deleo (2012), Pelagic-benthic coupling, food banks, and climate change on the West Antarctic Peninsula Shelf, *Oceanography*, *25*(3), 188-201.

Smith, D. A., E. E. Hofmann, J. M. Klinck, and C. M. Lascara (1999), Hydrography and circulation of the West Antarctic Peninsula continental shelf, *Deep-Sea Research I*, *46*(6), 925-949.

Smith, R. C., H. M. Dierssen, and M. Vernet (1996), Phytoplankton biomass and productivity in the western Antarctic Peninsula region, in *Foundations for Ecological Research West of the Antarctic Peninsula*, edited by R. M. Ross, E. E. Hofmann and L. B. Quetin, pp. 333-356, American Geophysical Union, Washington.

Smith, W. O., and D. M. Nelson (1986), Importance of ice edge phytoplankton production in the Southern Ocean, *BioScience*, *36*(4), 251-257.

Stammerjohn, S. E., and R. C. Smith (1996), Spatial and temporal variability of Western Antarctic Peninsula sea ice coverage, in *Foundations for Ecological Research West of the Antarctic Peninsula*, edited by R. M. Ross, E. E. Hofmann and L. B. Quetin, pp. 81-104, American Geophysical Union, Washington.

Taylor, S. R., and S. M. McLennan (1985), *The Continental Crust: its Composition and Evolution*, Blackwell Scientific Publications, Boston.

Timothy, D. A., and M. Y. S. Soon (2001), Primary production and deep-water oxygen content of two British Columbian fjords, *Marine Chemistry*, *73*(1), 37-51.

Tribovillard, N., T. J. Algeo, T. Lyons, and A. Riboulleau (2006), Trace metals as paleoredox and paleoproductivity proxies: An update, *Chemical Geology*, *232*(1-2), 12-32.

Vernet, M., D. Martinson, R. Iannuzzi, S. Stammerjohn, W. Kozlowski, K. Sines, R. Smith, and I. Garibotti (2008), Primary production within the sea-ice zone west of the Antarctic Peninsula: I--Sea ice, summer mixed layer, and irradiance, *Deep-Sea Research II*, *55*(18-19), 2068-2085.

Whitworth, T., W. D. Nowlin Jr, A. H. Orsi, R. A. Locarnini, and S. G. Smith (1994), Weddell Sea shelf water in the Bransfield Strait and Weddell-Scotia Confluence, *Deep Sea Research Part I: Oceanographic Research Papers*, *41*(4), 629-641.

Zhang, Y., H. Amakawa, and Y. Nozaki (2001), Oceanic profiles of dissolved silver: precise measurements in the basins of western North Pacific, Sea of Okhotsk, and the Japan Sea, *Marine Chemistry*, *75*(1-2), 151-163.

Zhang, Y., H. Obata, and Y. Nozaki (2004), Silver in the Pacific Ocean and the Bering Sea, *Geochemical Journal*, *38*, 623-633.

Zheng, Y., R. F. Anderson, A. van Geen, and J. Kuwabara (2000), Authigenic molybdenum formation in marine sediments: A link to pore water sulfide in the Santa Barbara Basin, *Geochimica et Cosmochimica Acta*, *64*(24), 4165-4178.

Chapter 4

Trace Metal Evidence for a Poorly Ventilated Glacial Southern Ocean: No Modern Analogue?

Abstract

Glacial benthic $\delta^{13}C$ and $\Delta^{14}C$ measurements from the Atlantic Ocean have been interpreted to indicate the existence of a poorly ventilated Southern Ocean with greater CO_2 and nutrient contents compared to present. Enhanced storage of CO_2 in the deep ocean predicts that oxygen concentrations should have declined at the same time, although no unequivocal evidence for glacial Southern Ocean suboxia has yet been found. Here we take a novel approach by using fluxes of redox-sensitive trace metals to show that Southern Ocean sediments from two cores in the Atlantic sector were suboxic during deglaciation and the last glacial period, implying reduced ventilation and/or elevated export production that significantly altered deep water chemistry. In the Cape Basin, maximum fluxes of the authigenically deposited trace metal Re coincide with oldest $\Delta^{14}C$ values at 3.8 km water depth in the Subantarctic Zone, indicating that poorest Southern Ocean ventilation occurred during the Last Glacial Maximum (~23-19 ka). Furthermore, trace metal results suggest that the vertical structure of the glacial Southern Ocean differed from modern deep water mass arrangement such that Lower Circumpolar Deep Water had lower O_2 concentrations, and therefore was the likely reservoir of glacial CO_2.

1. Introduction

Ice core records demonstrate that atmospheric CO_2 concentrations (pCO_2) were 80-100 ppm lower than preindustrial levels during glacial intervals of the last ~400,000 years [*Petit et al.*, 1999]. Of the ~40-50 ppm pCO_2 decrease currently unaccounted for, the most plausible storage location for this "missing" glacial CO_2 is the deep ocean because it is the largest easily exchangeable reservoir of carbon on the planet [*Sigman and Boyle*, 2000]. Paleoclimate studies have targeted the Southern Ocean as a primary regulator for glacial-interglacial atmospheric CO_2 changes because the CO_2 air-sea balance is set within the Antarctic Zone by gas exchange with the deep ocean and by downward CO_2 transfer via the biological pump [*Marinov et al.*, 2006]. Proposed physical mechanisms for drawing down atmospheric CO_2 during glacial intervals include increased Southern Ocean vertical stratification [*Francois et al.*, 1997] and (subsequently) decreased deep ocean ventilation rate [*Toggweiler*, 1999]. Because O_2 is only added at the sea surface, if glacial Southern Ocean ventilation was reduced, continuous organic matter respiration as deep waters "aged" would have caused CO_2 and nutrients to accumulate as O_2 was consumed. Hence bottom water O_2 concentrations provide an indirect assessment of whether the deep Southern Ocean CO_2 sink was enhanced during glacial intervals.

A recent compilation [*Jaccard and Galbraith*, 2012] of sedimentary oxygenation proxies documents increased deep ocean ventilation between the Last Glacial Maximum (LGM) and the early Holocene. Other studies [e.g., *Curry and Oppo*, 2005; *Herguera et al.*, 2010; *Hodell et al.*, 2003; *Ninnemann and Charles*, 2002] have sought to characterize global glacial-interglacial circulation and deep ocean ventilation changes using benthic $^{13}C/^{12}C$ ratios ($\delta^{13}C$) or $\Delta^{14}C$ derived from sedimentary $CaCO_3$. The longer a water mass is isolated from the surface and the more nutrients it accumulates, the lower its $\delta^{13}C$ [*Broecker and Peng*, 1982]. Similarly, surface waters dissolve CO_2 with an atmospheric ^{14}C signature, but once a water mass leaves the surface,

its ^{14}C content diminishes—increasing the offset from the atmosphere ($\Delta^{14}C$)—as the radiocarbon decays [*Broecker and Peng*, 1982].

In the Atlantic Ocean, glacial $\delta^{13}C$ and $\Delta^{14}C$ data imply different Southern Ocean chemistry potentially resulting from changes to deep ocean vertical stratification and mixing that have no modern analogue. South Atlantic benthic $\delta^{13}C$ values that are more than 1‰ lower than the modern ocean support the existence of strong vertical stratification and poorer ventilation [*Ninnemann and Charles*, 2002]. However, $\delta^{13}C$ is not a conservative tracer of water masses because it is influenced by a combination of air-sea gas exchange, export productivity, and water mass mixing [*Kroopnick*, 1985]. $\delta^{13}C$ also cannot uniquely identify whether bottom water masses were oxygen-poor and/or export productivity was high. Paired benthic-planktonic ^{14}C ventilation measurements from the northwest Atlantic Ocean [*Keigwin*, 2004; *Keigwin and Schlegel*, 2002; *Robinson et al.*, 2005] are also consistent with an "old" Southern-sourced water mass below ~2.5-3 km water depth. However, $\Delta^{14}C$ is not an unambiguous proxy because it is also affected by water mass mixing and interpretation requires accurate determination of reservoir age. As an added complication, both $\delta^{13}C$ and $\Delta^{14}C$ measurements require good carbonate preservation, but $CaCO_3$ is poorly preserved in the CO_2-rich waters south of the Antarctic Polar Front [*Howard and Prell*, 1994]. Thus, additional evidence for decreased bottom water O_2/increased CO_2 concentration in the glacial Southern Ocean must come from other proxies.

Redox-sensitive trace metals are reliable proxies for sedimentary pore water redox conditions (especially in the high latitude Southern Ocean where sediments contain primarily biogenic silica and little to no $CaCO_3$) and provide an alternative approach to reconstructing deep water ventilation. Additionally, by examining a suite of trace metals it is possible to tease apart

the relationship between low-oxygen bottom waters and sedimentary pore waters. In this study we measured the redox-sensitive trace metals Ag, Cd, Re, and Mo to reconstruct deep Southern Ocean oxygenation history over the last 30 kyr for two piston cores from the deep South Atlantic Ocean: RC13-254 (48.57°S, 5.127°E, 3636 m water depth), from the Cape Basin; and TN057-13-4PC (53.1728°S, 5.1275°E, 2848 m water depth), from the open ocean Antarctic Zone (Figure 4.1).

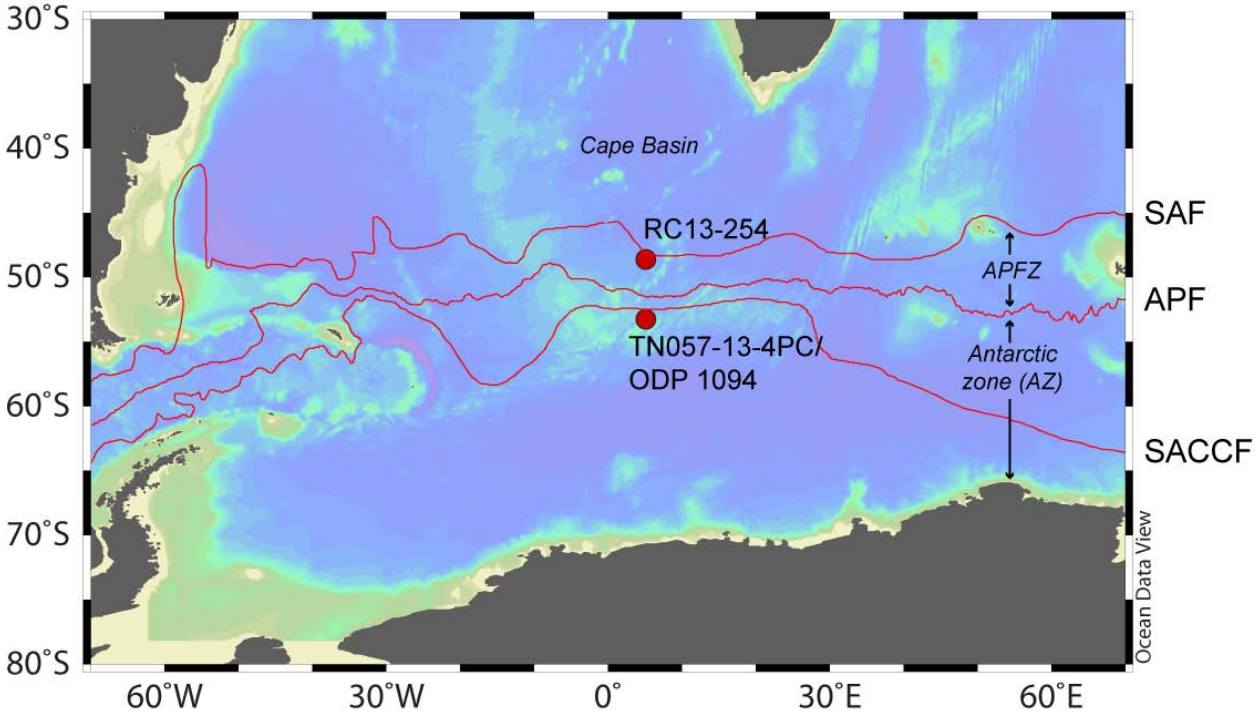

Figure 4.1. Locations of cores used for this study relative to fronts of the Antarctic Circumpolar Current (after [*Orsi et al.*, 1995]): SAF, Subantarctic Front; APF, Antarctic Polar Front; SACCF, Southern Antarctic Circumpolar Current Front; APFZ, Antarctic Polar Frontal Zone. Map created using Ocean Data View (R. Schlitzer, Ocean Data View, http://odv.awi.de, 2011).

2. Background

2.1 Trace Metal Enrichment Mechanisms

Because trace metals are delivered to sediments via a number of different delivery mechanisms, the use of a suite of trace metals is required to differentiate the processes that produce reducing conditions in pore waters. Here we follow the definition of Berner [1981], and

classify sediments whose pore waters contain no *measurable* dissolved oxygen or dissolved sulfide as suboxic, and those whose pore waters contain measurable dissolved sulfide as anoxic. Onset of suboxic conditions occurs between the reduction potentials of Mn and NO_3^- reduction [*Froelich et al.*, 1979]. Ag and Cd are thought to be delivered by sinking biogenic particles [*Hendy and Pedersen*, 2005] and preserved as their respective sulfides where trace quantities of dissolved sulfide are present [*Crusius and Thomson*, 2003; *Rosenthal et al.*, 1995a]. Hence, enhanced preservation of these metals indicates suboxic conditions caused by a high flux of organic matter [*Hendy and Pedersen*, 2005]. Cd also displays a strong tendency toward authigenic precipitation in sediments where reducing conditions occur close to the sediment-water interface [*Calvert and Pedersen*, 1993; *Pedersen et al.*, 1989; *Rosenthal et al.*, 1995a]. In contrast, authigenic Ag_2S precipitation appears to be negligible except in severely anoxic sediments where sulfate reduction is occurring [*McKay and Pedersen*, 2008]. Elevated preserved Re fluxes also indicate pore water suboxia. Re exists in seawater as the conservative perrhenate anion (ReO_4^-) [*Koide et al.*, 1986]. It diffuses into sediments along concentration gradients and precipitates directly from seawater under reducing conditions, possibly as ReO_2 [*Crusius et al.*, 1996], although the probability for this reaction to proceed spontaneously in typical seawater has recently been questioned [*Helz and Dolor*, 2012; and references therein]. Due to its low crustal concentrations, nearly all sedimentary Re is authigenically precipitated [*Crusius et al.*, 1996]. Hence, increases in Re accumulation without corresponding increases in Ag and/or Cd indicates that low bottom water O_2 concentrations were likely present, and this deficit was primarily responsible for suboxia in underlying sediments.

Mo enrichment occurs under anoxic conditions and requires measurable sulfide levels to precipitate. In seawater Mo is present as the conservative molybdate anion (MoO_4^{2-}). Under oxic

conditions, Mo associates with Mn-oxyhydroxides [*Calvert and Pedersen*, 1993; *Zheng et al.*, 2000] which produces low-level enrichments unrelated to reductive processes. When redox conditions become favorable to Mn-oxyhydroxide reduction, adsorbed Mo can be released to pore waters [*Crusius et al.*, 1996], decreasing preserved solid-phase Mo. Significant enrichments of Mo (up to tens of ppm in non-euxinic settings [*Scott and Lyons*, 2012]) above lithogenic background are controlled by pore water H_2S concentrations. At sulfide concentrations below ~11 μM, progressive substitution of S for O atoms occurs in molybdate, leading to the formation of multiple thiomolybdate species that co-precipitate as a labile Mo-Fe-S phase [*Erickson and Helz*, 2000; *Helz et al.*, 1996]. The substitution reaction is kinetically slow, but above the threshold value of 11 μM, a "geochemical switch" [*Helz et al.*, 1996] is flipped and complete conversion to MoS_4^{2-} (tetrathiomolybdate) occurs. Downcore measurements of Mo and H_2S in Santa Barbara Basin sediments provide empirical support for this theoretical "geochemical switch" [*Zheng et al.*, 2000]. Tetrathiomolybdate is highly particle-reactive and adsorbs to pyrite, after which it is retained in sediments as a Mo-Fe-S cubane compound [*Bostick et al.*, 2003]. Above sulfide concentrations of ~100 μM, direct precipitation of a discrete Mo-sulfide phase is hypothesized to occur [*Zheng et al.*, 2000]. Similar to Re, elevated Mo fluxes not coupled with increased Ag and/or Cd fluxes imply that low bottom water O_2 concentrations caused anoxic conditions in pore waters.

A linear relationship has yet to be shown between sedimentary trace metal accumulation and export production or bottom water ventilation due to the combined effects of biogenic particle remineralization, sedimentation rate, dilution by other phases, and post-depositional re-oxidation of trace metals. For this reason, trace metals can provide a qualitative determination of the relative importance of export production versus bottom water ventilation by comparing Ag

and Cd (metals associated with biodetritus) fluxes with Re and Mo (authigenic metals) fluxes. For this study, when Ag and/or Cd fluxes increase with increasing Re and/or Mo fluxes, we interpret this pattern as high export production that depletes sedimentary oxidants. When Ag and/or Cd fluxes decrease with increasing Re and/or Mo fluxes, we interpret this pattern as a relative decrease in export production and concomitant decrease in bottom water oxygenation.

2.2 Oceanographic Setting

Core TN057-13-4PC was recovered from a small sedimentary basin northeast of Bouvet Island, at the same location as ODP Site 1094 [*Kanfoush et al.*, 2002], so the two cores can be directly compared. Presently, TN057-13-4PC is located slightly to the south of the Southern ACC Front [*Orsi et al.*, 1995] and ~2° north of the average winter sea ice edge [*Kanfoush et al.*, 2002]. Primary productivity in this region is high [*Moore and Abbott*, 2000] and dominated by the heavily-silicified diatom *Fragilariopsis kerguelensis* [*Abelmann et al.*, 2006]. Sediments are composed primarily of diatomaceous ooze and diatom mud [*Shipboard Scientific Party*, 1999b]. Site RC13-254 is located southwest of Meteor Rise in the Cape Basin, on the northern edge of the Antarctic Polar Frontal Zone (APFZ), and within the Permanently Open Ocean Zone. Productivity within the APFZ is still high, but transitions from diatom-dominated in the south to coccolithophorid-dominated in the north [*Honjo et al.*, 2000]. Consequently, sediments in the upper portion of the core are composed primarily of $CaCO_3$ and transition to diatomaceous ooze during the deglacial [*Charles et al.*, 1991].

Today both cores are overlain by Lower Circumpolar Deep Water (LCDW) [Figure 4.2], a cold, saline, recirculating water mass of the Antarctic Circumpolar Current (ACC). Modern LCDW is a mixture of North Atlantic Deep Water (NADW), Antarctic Shelf Waters, and recirculated Pacific and Indian Deep Waters (PDW and IDW) that is exported to the three major

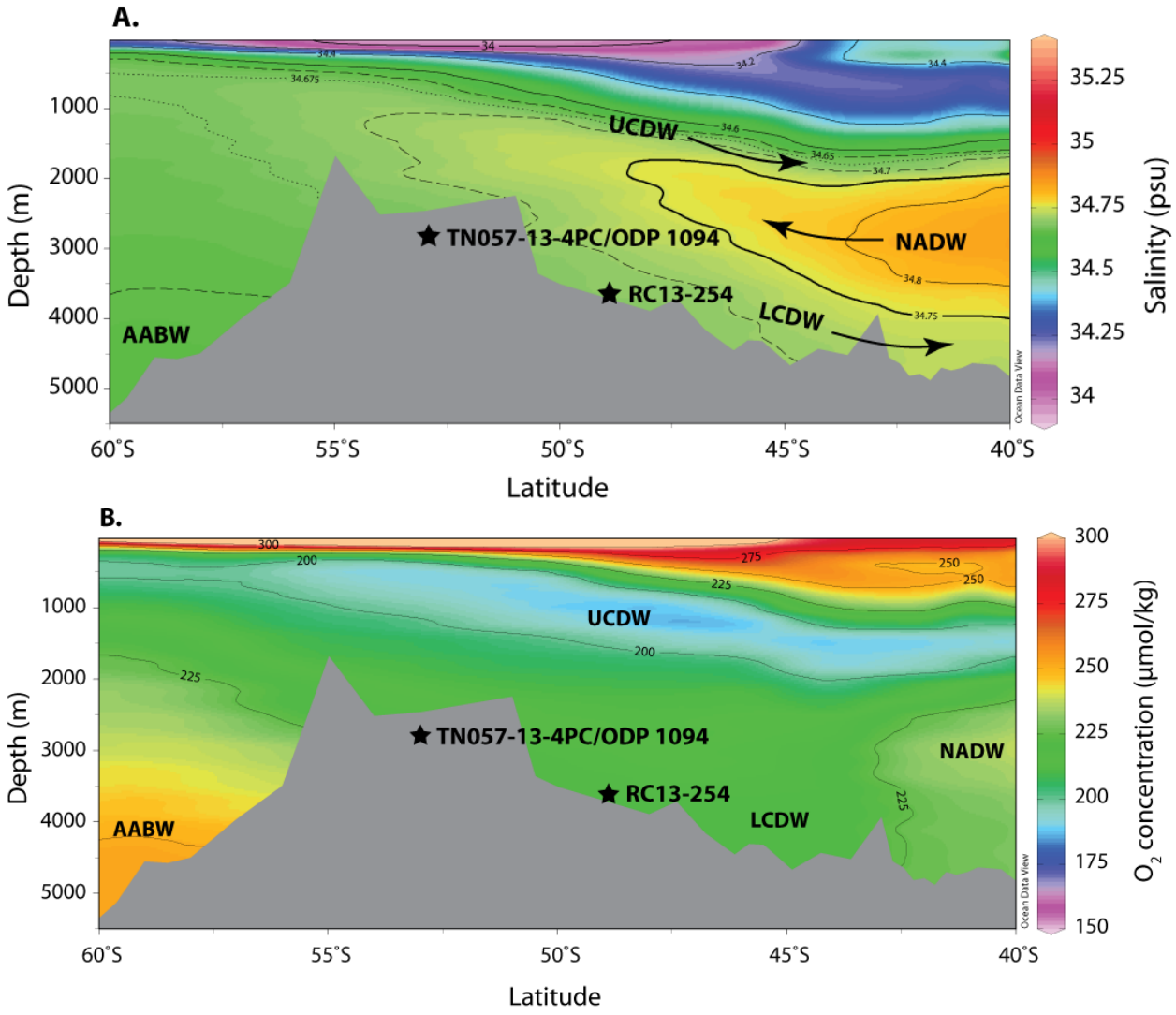

Figure 4.2. Locations of cores used for this study relative to water masses of the Southern Ocean. A: Salinity along WOCE Line A12. B: Oxygen concentration along WOCE Line A12. NADW, North Atlantic Deep Water; LCDW, Lower Circumpolar Deep Water; UCDW, Upper Circumpolar Deep Water; AABW, Antarctic Bottom Water. Map created using Ocean Data View (R. Schlitzer, Ocean Data View, http://odv.awi.de, 2011).

ocean basins through Deep Western Boundary Currents [*Talley*, 2008]. LCDW is ventilated from the north by penetration of NADW into the ACC, and from the south by upward mixing of Antarctic Bottom Water [*Orsi et al.*, 1999]. Note, however, that bottom waters overlying TN057-13-4PC receive less influence from NADW than sites further to the north [*Shipboard Scientific Party*, 1999a], such as RC13-254/ODP 1091. Once LCDW enters the Indian and Pacific basins, it upwells diapycnally to form the major volume of PDW and IDW. These subsequently re-enter

the Atlantic basin through Drake Passage, mix with ACC waters, and upwell isopycnally to form modern Upper Circumpolar Deep Water (UCDW) [*Talley*, 2008], a nutrient-rich and slightly lower-oxygen water mass. Thus in the modern ACC, waters are well ventilated but the vertical water column structure can be characterized as having a lower-oxygen water mass overlying a higher-oxygen water mass (Figure 4.2b).

3. Methods and Materials

3.1 Trace Metal Analysis

Cores were sampled at millennial- to submillennial-scale resolution from the core tops to ~30 ka. Concentrations of Ag, Cd, Re, and Mo were measured at the University of Michigan Keck Environmental Geochemistry Laboratory (KEGL) by isotope dilution inductively coupled plasma-mass spectrometry (ID ICP-MS) using a Finnigan Element mass spectrometer. Prior to analysis, samples were spiked and subjected to total microwave digestion in Teflon vessels using an acid cocktail of trace metal grade HF, HCl, and HNO_3 [*Crusius et al.*, 1996]. An aliquot was removed from digested samples for Cd and Ag analysis and passed through a column of Dowex 1X-8 resin to remove interfering isotopes. Working spike concentrations and ratios of $^{109}Ag/^{107}Ag$, $^{111}Cd/^{113}Cd$, $^{185}Re/^{187}Re$, and $^{95}Mo/^{97}Mo$ were calibrated using natural element ICP standards (Ricca Chemical Company). Errors are reported as one-sigma standard deviations for each run based on repeated analysis of the sediment standard MESS-3.

3.2 ^{230}Th Normalization

Trace metal concentrations (Tables 4.1 and 4.2) were normalized to ^{230}Th to correct for lateral sediment redistribution [*Francois et al.*, 2004]—which can deposit up to 20 times more sediment than the vertical rain in the Southern Ocean [*Chase et al.*, 2003; *Dezileau et al.*, 2000; *Francois et al.*, 1993]—and to generate fluxes of elements to the sediment-water interface. ^{230}Th

has a known production rate in the water column, and its expected flux to sediments is entirely a function of water depth. Preserved vertical fluxes of sedimentary components are calculated from measured excess ^{230}Th and normalized to the expected flux of ^{230}Th to sediments [*Francois et al.*, 2004]:

$$F_i = (\beta \times z \times f_i)/{}^{230}_{xs}\mathrm{Th}_0 \quad (1)$$

where F_i is the preserved vertical flux of component i; β is the production rate of ^{230}Th in the water column (2.63 x 10^{-5} dpm cm^{-3} kyr^{-1}); z is water depth in cm; f_i is the weight fraction of component i; and ${}^{230}_{xs}\mathrm{Th}_0$ is the measured sedimentary ^{230}Th not associated with the detrital component. Published ${}^{230}_{xs}\mathrm{Th}_0$ data [*Anderson et al.*, 2009, archived data; *Kumar et al.*, 1995, data not archived-see Table 4.3] and modern water depths for cores were used to calculate preserved vertical fluxes of trace metals to sediments. ${}^{230}_{xs}\mathrm{Th}_0$ values were linearly interpolated between data points, except for sampled intervals at the tops of the cores above the first data point, which were assigned the same ${}^{230}_{xs}\mathrm{Th}_0$ value as the first data point; and sampled intervals below the last data point (884 cm) in TN057-13-4PC, which were assigned the same ${}^{230}_{xs}\mathrm{Th}_0$ value as the last data point.

Errors for interpolated ${}^{230}_{xs}\mathrm{Th}_0$ values were estimated by calculating one standard deviation of the ${}^{230}_{xs}\mathrm{Th}_0$ values immediately above and below the sampled interval. Errors in ${}^{230}_{xs}\mathrm{Th}_0$ and trace metal concentrations were propagated at the 1σ level when calculating trace metal fluxes. Propagation at the 2σ level did not significantly change the results for TN057-13-4PC, and did not produce meaningful error envelopes for RC13-254 due to high uncertainties originating from the low density of ${}^{230}_{xs}\mathrm{Th}_0$ data points.

3.3 Age Models

Published age models were used for both cores. The initial age model for core RC13-254

[*Charles et al.*, 1991] was based on oxygen isotope chronostratigraphy. More recently, calibrated ^{14}C dates have been incorporated that indicate that the core top is ~7 kyr younger than originally estimated, and the age model for the upper ~190 cm of RC13-254 has been modified accordingly [R.F. Anderson, pers. comm.; *Anderson et al.*, 1998; *Kumar et al.*, 1995]. The age of the core top (0-1 cm) was set to 3500 years before present. A constant sedimentation rate was assumed between age-depth points provided by R.F. Anderson (pers. comm.). The age model for core TN057-13-4PC is based on a series of ^{14}C dates [*Shemesh et al.*, 2002] that were recalibrated using the program CALIB 6.0 and the Marine09 calibration, with an assumed 800-year reservoir effect. A constant sedimentation rate was assumed between age control points. Sedimentation rates varied from ~8-73 cm/kyr for TN057-13-4PC and ~1-55 cm/kyr for RC13-254. All dates are shown in calendar kyr.

4. Results

Although both cores are situated in the open ocean, trace metal concentrations in deglacial and glacial-age sediments are similar to concentrations found for continental margins (Tables 4.1 and 4.2) [e.g., *McKay and Pedersen*, 2008; *Morford and Emerson*, 1999]. Preserved vertical fluxes of trace metals in both cores are significantly higher downcore as compared to surface sediments (Figure 4.3a-d, 4.4a-d), where fluxes are often nearly zero. However, absolute magnitudes of preserved vertical fluxes are generally greater in RC13-254 (located in the APFZ). Ag and Cd fluxes (Figure 4.3a-b) are mutually consistent throughout the record. Maxima in Ag and Cd fluxes occur during the last glacial period at ~27.8, 26-25.4, and 21.8 ka. After ~21.8 ka, fluxes decrease slightly before increasing once again to record three distinct events during the deglacial interval (19-11 ka) at ~18.3, 17.7, and 16.1-15.6 ka. Following the youngest peak, fluxes decrease rapidly to near zero and remain at this level throughout the Holocene.

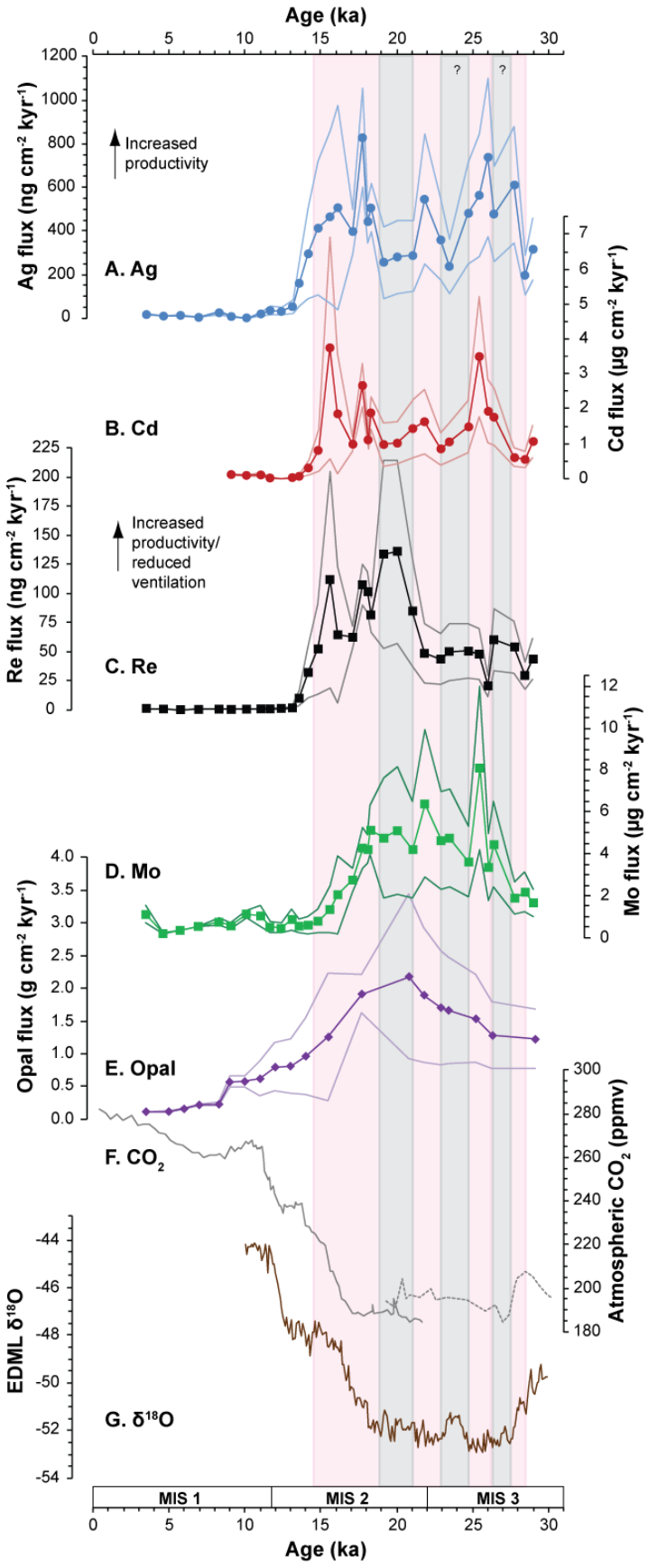
Age (ka)
Ag flux (ng cm-2 kyr-1)
Increased productivity
A. Ag
Cd flux (µg cm-2 kyr-1)
B. Cd
Re flux (ng cm-2 kyr-1)
Increased productivity/ reduced ventilation
C. Re
Mo flux (µg cm-2 kyr-1)
D. Mo
Opal flux (g cm-2 kyr-1)
E. Opal
Atmospheric CO2 (ppmv)
F. CO2
EDML δ18O
G. δ18O
MIS 1
MIS 2
MIS 3
Age (ka)

Figure 4.3. (Previous page) RC13-254 trace metal and productivity proxy fluxes, and regional paleoclimate records. A) Blue circles, Ag flux. B) Red circles, Cd flux. Cd flux data are truncated in the Holocene due to suspected contamination in the core top (see Table 4.2). C) Black squares, Re flux. D) Green squares, Mo flux. E) Purple diamonds, opal flux [opal concentration, *Charles et al.*, 1991; values, *Kumar*, 1994]; F) Solid grey line, atmospheric CO_2 concentration from EPICA Dome C ice core [*Flückiger et al.*, 2002]. Dotted grey line, atmospheric CO_2 concentration from Byrd ice core [*Ahn and Brook*, 2008]. G) Brown line, $\delta^{18}O$ for EPICA Dronning Maud Land (EDML) ice core, age synchronized to GICC05 chronology [*EPICA Community Members*, 2006]. Error envelopes in panels A-E show 1σ propagated uncertainty in proxy and $\mathbf{^{230}_{xs}Th_0}$ concentrations. Marine isotope stages (MIS) are denoted by boxes at the bottom of the figure. Pink vertical boxes denote time periods when sediments become reducing due primarily to high export production. Grey vertical boxes denote time periods when sediments become reducing due primarily to low bottom water O_2 concentrations.

Re fluxes (Figure 4.3c) in RC13-254 do not consistently increase with Ag and Cd fluxes. During late MIS 3, a local maximum of 54-60 ng cm^{-2} kyr^{-1} occurs from ~27.8-26.4 ka. Moderate fluxes then increase rapidly to 136 ng cm^{-2} kyr^{-1} beginning at ~21.8 ka. Two peaks corresponding to increased Ag and Cd fluxes are observed during the deglacial at ~17.7 and 15.6 ka. Mo fluxes (Figure 4.3d), in contrast, are dissimilar to other trace metals. A broad trend of elevated Mo fluxes is recorded from ~26-15 ka, although individual peaks only correlate with increased Ag and Cd fluxes at ~25.4, 21.8, and 18.3 ka. Increased Mo fluxes may also correspond with high Re fluxes at ~26.4, 20.0, and 18.3 ka. As with Ag and Cd fluxes, Re and Mo fluxes both decrease sharply to near zero by ~13.5 ka, although Mo fluxes reach minimum values earlier, ~15 ka.

TN057-13-4PC (located in the Antarctic Zone) records less variability in trace metal fluxes prior to the LGM than does RC13-254. Ag and Cd fluxes (Figure 4.4a-b) are relatively low until ~26.9 ka, when both increase to form broad peaks centered ~24-23 ka. Fluxes of both trace metals then decrease sharply during the LGM (23-19 ka). A step-like increase in Ag and Cd fluxes occurs beginning ~21.6 ka and lasting until ~6 ka. Ag, though perhaps not Cd, also shows three distinct peaks during the Holocene at ~10.2, 8.7, and 6.5 ka. Beginning ~6 ka, Ag and Cd fluxes decrease to low values equivalent to core top values.

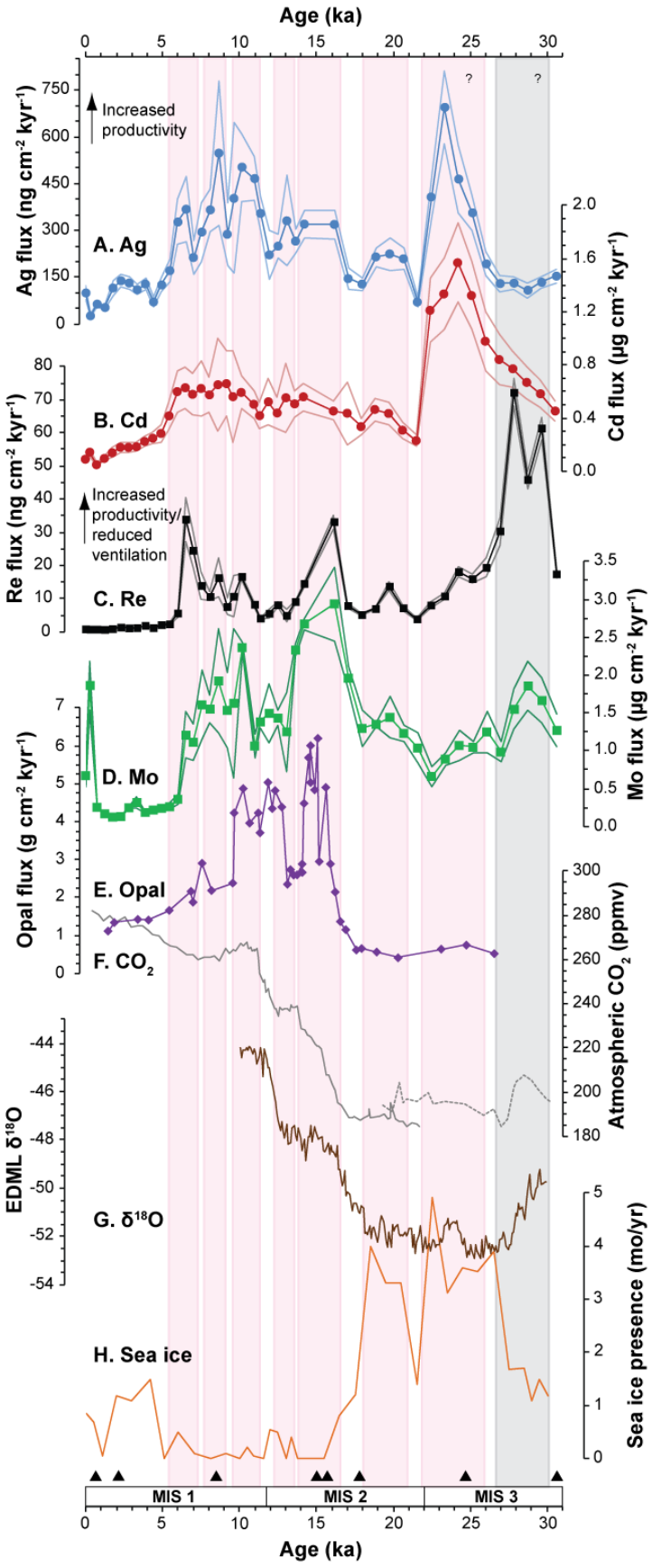
Age (ka)
Increased productivity
A. Ag
Ag flux (ng cm-2 kyr-1)
B. Cd
Cd flux (µg cm-2 kyr-1)
Increased productivity/ reduced ventilation
C. Re
Re flux (ng cm-2 kyr-1)
D. Mo
Mo flux (µg cm-2 kyr-1)
E. Opal
Opal flux (g cm-2 kyr-1)
F. CO2
Atmospheric CO2 (ppmv)
G. δ18O
EDML δ18O
H. Sea ice
Sea ice presence (mo/yr)
MIS 1
MIS 2
MIS 3
Age (ka)

Figure 4.4. (Previous page) TN057-13-4PC trace metal and productivity proxy fluxes, and regional paleoclimate records. A) Blue circles, Ag flux. B) Red circles, Cd flux. C) Black squares, Re flux. D) Green squares, Mo flux. E) Purple diamonds, opal flux [*Anderson et al.*, 2009]. F) Solid grey line, atmospheric CO_2 concentration from EPICA Dome C ice core [*Flückiger et al.*, 2002]. Dotted grey line, atmospheric CO_2 concentration from Byrd ice core [*Ahn and Brook*, 2008]. G) Brown line, $\delta^{18}O$ for EPICA Dronning Maud Land (EDML) ice core, age synchronized to GICC05 chronology [*EPICA Community Members*, 2006]. H) Orange line, sea ice presence [*Stuut et al.*, 2004]. Error envelopes in panels A-D show 1σ propagated uncertainty in trace metal and $^{230}_{xs}Th_0$ concentrations. Marine isotope stages (MIS) are denoted by boxes at the bottom of the figure. Black triangles at the bottom of the figure indicate calibrated, ^{14}C-dated age control points [*Shemesh et al.*, 2002]. Pink vertical boxes denote time periods when sediments become reducing due to high export production. Grey vertical boxes denote time periods when sediments become reducing due to low bottom water O_2 concentrations.

Re fluxes (Figure 4.4c) show a distinct double peak that occurs earlier (centered at ~29.6 and 27.8 ka) than the increases in Ag and Cd fluxes. As Ag and Cd fluxes increase at ~26.9 ka, Re fluxes decrease and remain close to core top values of near zero through the LGM. A small increase in Re, Ag, and Cd fluxes occurs during the glacial-interglacial transition from ~21.5-17.9 ka. Another single, broad Re peak that coincides with increased Ag fluxes occurs during the deglacial from ~17.1-13.6 ka. Re fluxes then decrease toward core top values, but as with Ag, Re fluxes exhibit three peaks during the Holocene at ~10.2, 8.7, and 6.5 ka. Subsequently, fluxes decrease to near zero in the uppermost part of the core. Mo fluxes (Figure 4.4d) display a small peak similar to Re fluxes from ~30.6-26.9 ka. Afterward, Mo fluxes decline but begin to increase again at ~22.5 ka. Fluxes reach a maximum of 2.94 μg cm^{-2} kyr^{-1} at 16.2 ka, in agreement with local Ag and Re flux maxima. Similarly to Ag and Re, three peaks are also observed during the Holocene at ~10.2, 8.7, and 6.5 ka. Mo fluxes then decline to near zero for most of the late Holocene.

5. Discussion

5.1 Oxidative Burndown

Large variations in trace metal fluxes throughout both cores suggest that sedimentary redox conditions have changed through time, raising the possibility that oxidative burndown has

altered the trace metal record. Oxidative burndown occurs when previously deposited sediments become re-exposed to oxygen, remobilizing reduced trace metal phases. It is more likely to occur in slowly accumulating sediments and during times of rapid environmental change, such as during a glacial-interglacial transition [*Tribovillard et al.*, 2006]. Once remobilized, trace metals can either diffuse downward into the sediment column if concentration gradients decrease in that direction, or diffuse upward out of sediments into the water column. In the former case, evidence of oxidative burndown usually presents as a sharp peak below a redox front. The effect has been observed downcore for Re in organic carbon-rich turbidites [*Crusius and Thomson*, 2003] and for Cd and U in Subantarctic sediments [*Rosenthal et al.*, 1995b] directly below the glacial-interglacial transition.

Burndown is very likely to have affected the upper ~200 cm of TN057-13-4PC and the upper ~60-70 cm of RC13-254. Evidence for oxidative burndown is clearest for RC13-254. An abrupt transition from nearly zero trace metal fluxes (oxic conditions) to glacial-level trace metal fluxes (suboxic conditions) occurs at ~70 cm core depth. This increase in trace metals coincides with downward decreases in pore water NO_3^- and increases in pore water Mn concentrations at a nearby core [*King et al.*, 2000]. Agreement among Ag, Cd, and Re fluxes (Figure 4.3a-c) during the deglacial provide confidence that oxidative burndown is not a significant issue further downcore, including at the glacial-interglacial transition. Trace metal fluxes in TN057-13-4PC that are close to zero from the core top to ~200 cm suggest the onset of oxidative burndown during the Holocene. However, NO_3^- and Mn pore water profiles [*King et al.*, 2000] indicate that the present oxic-suboxic transition occurs ~20-30 cm core depth, implying that a slowdown in trace metal delivery rather than re-oxidation may exert primary control over preserved vertical fluxes in the core top.

However, available proxy data fail to give an unambiguous determination of the existence of burndown in TN057-13-4PC at the glacial-interglacial transition. The sharp—though broad—nature of the Ag and Cd flux peaks observed in TN057-13-4PC between ~820-880 cm core depth (~26.9-21.6 ka) suggests the possible occurrence of burndown. If true, co-occurring Re peaks appear to have migrated further downcore. However, U fluxes increase slightly from ~832-884 cm (~26.5-22.1 ka) [*Anderson et al.*, 2009], suggesting that burndown was minimal or affected U in a similar—though less severe—manner to Ag and Cd. Changes in C_{org} flux can control the onset of burndown [*Crusius and Thomson*, 2000] and may help to diagnose when burndown began to occur. Sedimentary C_{org} concentration data from a nearby core, PS1768-8 (52.6°S, 4.5°E, 3299 m) [*Abelmann et al.*, 2006], show modest concentrations of about 0.2-0.3% from 30 ka to the end of MIS 3 (~24 ka). At the beginning of MIS 2, C_{org} concentrations increase and reach a maximum of almost 0.5% at ~16 ka. C_{org} concentrations in the Antarctic Zone therefore *increase* going into the LGM and a decrease in the intensity of organic matter respiration cannot be responsible for re-oxygenation of sediments. Therefore, with the evidence at hand, we assume that oxidative burndown has had a minimal effect on preserved vertical trace metal fluxes at the glacial-interglacial transition.

5.2 Glacial-Interglacial Changes in Southern Ocean Redox Conditions

Preserved trace metal fluxes in Holocene age sediments reported here for the Atlantic sector are similar to those estimated for Pacific sector core top sediments, both within and outside the opal belt [*Wagner et al., manuscript in revision*]. These data suggest that similar chemistry unfavorable to trace metal accumulation exists throughout the modern Southern Ocean. However, the obvious difference in the amplitudes of preserved vertical trace metal fluxes between late MIS 2 and the late Holocene implies that changes in water mass mixing and

stratification produced significantly different deep Southern Ocean chemistry at ~3 km during the last glacial period and the deglacial (19-11 ka). Core RC13-254 (Cape Basin) presents a strong case for pore water suboxia near the sediment-water interface prior to ~13.5 ka (Figure 4.3). Preserved Ag and Cd fluxes (on the order of 10-100 times greater than surface sediment fluxes) are most prominent between ~27.8-24.7 ka, ~22.9-21 ka, and ~19.1-14.8 ka, and indicate suboxic pore water conditions resulted from high organic matter flux to sediments. Prior to the beginning of the deglacial ~19 ka, preserved Re fluxes only increase convincingly with Ag and Cd fluxes from ~28.4-27.8 ka. However, until ~13.5 ka, Re fluxes were around 100 times higher than well-oxygenated late Holocene sediments, suggesting that low bottom water O_2 concentrations also contributed to suboxia in pore waters. Variations in primary productivity and bottom water oxygenation therefore acted synergistically to produce the observed trace metal record.

The significance of Mo fluxes at RC13-254 (Figure 4.3d) is unclear because fluxes do not closely track either Re or the productivity proxies Ag and Cd. Where Mo flux maxima coincide with high Ag and Cd fluxes, one possible explanation is that reducing conditions developed so rapidly that Re accumulation was suppressed [*Crusius et al.*, 1996]. However, in the absence of anoxic conditions, Mo fluxes may reflect an association with Mn oxides instead. The abrupt decline in all trace metal fluxes by ~13.5 ka reflects oxidative burndown, which has destroyed the more recent parts of the record.

High Re fluxes (Figure 4.4c) in TN057-13-4PC (Antarctic Zone) from ~30.6-27.8 ka indicate suboxic pore waters caused by low bottom water O_2 concentrations. Re fluxes then decrease and give way to broad peaks in Ag and Cd fluxes between ~26.9-21.6 ka (Figure 4.4a-b), indicating a change to suboxia driven by high export production. Increased fluxes of all trace

metals and opal [*Anderson et al.*, 2009] during deglaciation from ~17.1-13.6 ka (Figure 4.4a-e)—as well as increases in biogenic Ba [*Jaccard et al.,* 2013]—indicate pore water suboxia driven by strong export productivity. Similar increases in trace metal fluxes also point to sedimentary suboxia that developed during three discrete Holocene events. Well-oxygenated sediments similar to modern conditions appeared ~6 ka, coincident with the onset of the Neoglacial [*Hodell et al.,* 2001] and increased sea ice presence at the site [*Stuut et al.,* 2004; Figure 4.4h]. Burndown and/or a slowdown in trace metal delivery appears to be responsible for low trace metal fluxes after ~6 ka (see Section 5.1). The overall record of TN057-13-4PC therefore suggests that bottom waters at the site have been well ventilated for at least the last 27 kyr, with organic matter respiration primarily responsible for low-oxygen sediments.

5.3 Bottom Water Ventilation Changes

Variations in Re fluxes during the last glacial period suggest that bottom water ventilation was not constant through time. Therefore, we attempted to identify time periods of sedimentary suboxia that could be linked to physical changes in the ocean. Because Re precipitates directly from seawater under suboxic conditions and is not cycled with biogenic particles [*Colodner et al.*, 1993; *Crusius et al.*, 1996], it can provide a qualitative measure of the degree of bottom water ventilation when increased/decreased Re fluxes are not correlated with productivity increases/decreases. Hence we estimated the apparent Re removal depth as a proxy for the oxygen penetration depth by assuming that: 1) Re diffuses into sediments and precipitates at the depth where pore water O_2 concentration is zero—i.e., at the oxygen penetration depth; and 2) that the preserved vertical Re flux equals the downward pore water flux—i.e., a steady state situation is present [*Crusius et al.*, 1996]. The former assumption is reasonable given that suboxic conditions coincide with the onset of NO_3^- reduction [*Froelich et al.*, 1979]. Because a

permanent steady state situation in which the rate of O_2 consumption in sediments balances the influx of O_2 is unlikely, the apparent Re removal depth may not be equivalent to the oxygen penetration depth, and sediments can only be classified as more poorly oxygenated, or equally or better oxygenated than present. In other words, if the true O_2 flux into sediments is greater (less) than the O_2 consumption rate, then the apparent Re removal depth will be correspondingly greater (less) than the true oxygen penetration depth.

The apparent Re removal depth can be estimated by applying Fick's first law [*Berner*, 1980]:

$$J_s = -\phi D_s(\partial C/\partial z) \qquad (2)$$

where J_s is the diffusion flux into sediments, equivalent to the preserved vertical Re flux; ϕ is the sediment porosity; D_s is the whole sediment diffusion coefficient; and $\partial C/\partial z$ is the concentration gradient, with z taken here as the Re removal depth/oxygen penetration depth. Sediment porosity was unknown for RC13-254, but except for the upper ~30 cm the core material consists primarily of diatomaceous mud and ooze over the time interval studied, and so a constant porosity of 0.85—a typical value for this sediment type [*Hamilton,* 1976]—was assigned. An estimated porosity of 0.90 was applied to TN057-13-4PC based on porosity measurements at ODP 1094 [*Shipboard Scientific Party*, 1999b]. The ReO_4^- sediment diffusion coefficient, D_s, was estimated by Crusius et al. [1996] to be 5×10^{-6} cm^2 s^{-1}, a value similar to other oxyanions in seawater [*Li and Gregory*, 1974]. The concentration gradient $\partial C/\partial z$ is constrained by the following information: the Re concentration at the sediment-water interface should be equal to the seawater Re concentration of 4.59×10^{-14} mol cm^{-3} [*Colodner et al.*, 1993], the Re concentration at z equals zero, and if the depth at the sediment-water interface is set to zero, ∂z is simply equal to the Re removal depth. Equation (2) may then be rearranged and solved for z.

Estimated apparent Re removal depths and uncertainties are given in Tables 4.4 and 4.5. Sensitivity tests (Table 4.6) showed that the apparent Re removal depth is greatly affected by uncertainty in the Re flux, which can be large. In comparison, an applied percent change in the seawater Re concentration, sediment porosity, or diffusion coefficient produces a corresponding percent change in the apparent Re removal depth. However, these quantities are better constrained than the Re flux—especially in RC13-254 because of large intervals between measured $^{230}_{xs}\mathrm{Th}_0$ concentrations. Hence only the uncertainty in the Re flux was considered when estimating the error in apparent Re removal depths.

Modern oxygen penetration depths of 55 cm (RC13-254) and 37 cm (TN057-13-4PC) were estimated from nearby core data [*Sachs et al.*, 2009] and by comparison with pore water profiles [*King et al.*, 2000]. Modern oxygen penetration depths were then subtracted from estimated apparent Re removal depths to generate a residual to determine whether downcore sediments were less well oxygenated than present (Figure 4.5a-b). To estimate the uncertainty in the residual, the error in the apparent Re removal depth and in the modern oxygen penetration depth [*Sachs et al.*, 2009] were propagated at the 1σ level.

Re residuals indicate that TN057-13-4PC was nearly always well oxygenated during the last 30 kyr, with large Re residuals indicating burndown for the last ~6 kyr. The only Re residual excursion not clearly related to suboxia caused by high export production occurs from ~30.6-27.8 ka, when burndown may have affected the record. In contrast, sediments at RC13-254 were nearly always more poorly oxygenated during the deglacial and last glacial periods. Three events at ~27.8-26.4, 24.7-23.5, and ~21-19.1 ka (marked by boxes in Figure 4.5) correlate with time periods when Re fluxes increased, but Ag and Cd fluxes decreased, suggesting decreased bottom water O_2 concentrations.

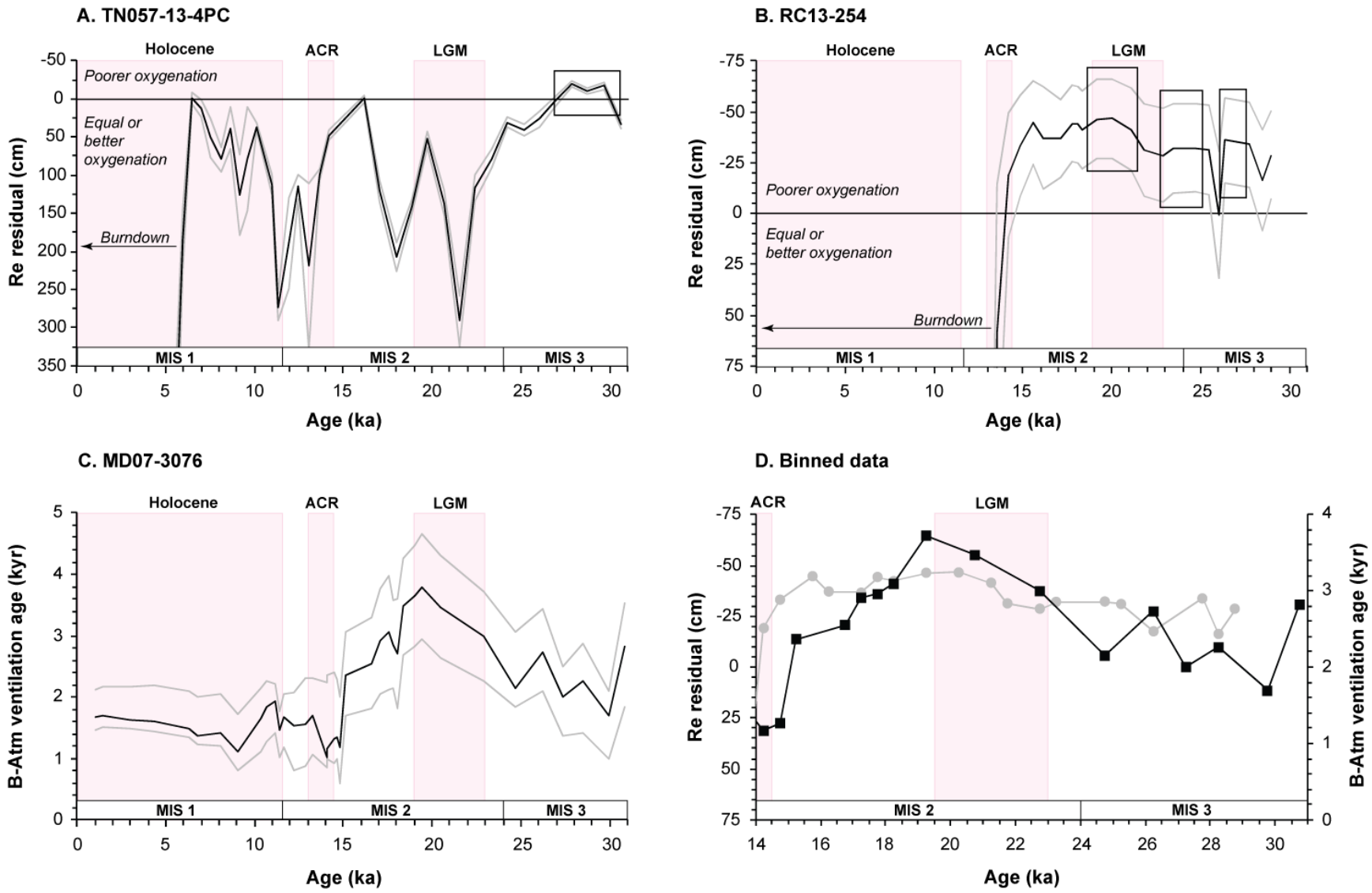
A. TN057-13-4PC
Holocene
ACR
LGM
Poorer oxygenation
Equal or better oxygenation
Burndown
Re residual (cm)
MIS 1
MIS 2
MIS 3
Age (ka)
B. RC13-254
Holocene
ACR
LGM
Poorer oxygenation
Equal or better oxygenation
Burndown
Re residual (cm)
MIS 1
MIS 2
MIS 3
Age (ka)
C. MD07-3076
Holocene
ACR
LGM
B-Atm ventilation age (kyr)
MIS 1
MIS 2
MIS 3
Age (ka)
D. Binned data
ACR
LGM
Re residual (cm)
B-Atm ventilation age (kyr)
MIS 2
MIS 3
Age (ka)

Figure 4.5. (Previous page) Re removal depth residuals (apparent Re removal depth – modern oxygen penetration depth) for A) TN057-13-4PC and B) RC13-254. Error bars (grey lines) in panels A and B are the propagated 1σ uncertainty in the Re residual from Re fluxes (this study) and the modern estimated oxygen penetration depth [*Sachs et al.*, 2009]. Black boxes mark time periods when suboxic conditions appear to be driven by decreases in bottom water ventilation, as evidenced by concurrent decreases in Ag and Cd fluxes and increases in Re fluxes. C) $\Delta^{14}C$ apparent ventilation age (B-Atm) for MD07-3076 (44.074°S, 14.208°W) [*Skinner et al.*, 2010]. D) Comparison of Re removal depth residual for RC13-254 (grey line and circles) with MD07-3076 $\Delta^{14}C$ apparent ventilation age (black line and squares), with data binned into 500-year intervals. Pink boxes in panels A-D mark significant climate events. ACR—Antarctic Cold Reversal. LGM—Last Glacial Maximum. Marine isotope stages (MIS) are denoted by boxes at the bottom of each panel.

The radiocarbon (^{14}C) content of deep ocean waters is an alternate, more common measure of water mass ventilation that has been applied to the last glacial period and deglacial [e.g., *Broecker and Barker*, 2007; *Marchitto et al.*, 2007; *Robinson et al.*, 2005]. The Re residual record from RC13-254 and $\Delta^{14}C$ apparent ventilation ages from Subantarctic core MD07-3076 (44.074°S, 14.208°W, 3770 m) [*Skinner et al.*, 2010] were binned into 500-year intervals to establish a common age scale, and were found to be significantly correlated at this temporal resolution (r = -0.64, p = 0.00423, n = 18; Pearson product moment correlation) [Figure 4.5b-d]. Most prominently, the lowest Re residuals from ~19-20 ka correspond to the highest measured benthic-atmospheric $\Delta^{14}C$ offsets of nearly 4 kyr (Figure 4.5d), thus supporting the conclusion of Skinner et al. [2010] that the carbon sequestration capacity of the Southern Ocean was enhanced at this time due to slower ventilation rates at the depth of modern LCDW.

5.4 Ocean Circulation Changes

$\Delta^{14}C$ (MD07-3076) and trace metal (RC13-254) results suggest that ocean circulation changes inhibited glacial LCDW from mixing with better ventilated waters. Glacial North Atlantic Intermediate Water penetrated only to ~30°S [*Curry and Oppo*, 2005], reducing LCDW ventilation from the north. If upward LCDW mixing was inhibited in the Indian and Pacific Oceans due to more extreme vertical density gradients created by colder, saltier deep waters

[*Adkins et al.*, 2002], relatively more LCDW would have recirculated into the ACC with its associated low oxygen and depleted ^{14}C characteristics (Figure 4.6). Benthic foraminiferal $\delta^{13}C$ from the western Pacific Ocean [*Keigwin*, 1998; *Matsumoto et al.*, 2002] suggest that glacial LCDW upwelled only to ~2500-3000 m, supporting this scenario. Indian Ocean $\delta^{15}N$ measurements [*Francois et al.*, 1997] also suggest that increased Southern Ocean vertical stratification was responsible for lowered bottom water O_2 concentrations in LCDW. Additionally, recent deep-sea coral $\Delta\Delta^{14}C$ measurements from Drake Passage [*Burke and Robinson*, 2012] tentatively support poor ventilation at depths corresponding to modern LCDW compared to UCDW during the LGM.

Because modern LCDW forms the bulk of Indian and Pacific Deep Waters [*Talley*, 2008], a low ^{14}C signature during the last glacial period is also expected for deep Pacific and Indian Ocean sites downstream of South Atlantic LCDW. In agreement with this prediction, apparent ventilation ages ~3600 yr older than modern values (and ~2500 yr older than those reported by Skinner et al. [2010]) were measured at Chatham Rise [*Sikes et al.*, 2000; *Vandergoes et al.*, 2012], where the Deep Western Boundary Current flows into the Southwest Pacific [*Carter and McCave*, 1997]. Additionally, increased LGM benthic-planktonic age differences were observed in a core from the deep North Pacific [*Galbraith et al.*, 2007]. Targeting LCDW and its downstream deep water products (IDW and PDW, as well as deep Atlantic waters [*Orsi et al.*, 1999]) allows for a radiocarbon-depleted Southern Ocean source to be diffused into a large volume of deep ocean water, thereby circumventing the need for a smaller, extremely depleted ^{14}C reservoir [*Broecker and Barker*, 2007].

Based on glacial age benthic-planktonic age differences from the western Pacific that are similar to modern values, it has been argued that an isolated, ^{14}C-depleted abyssal reservoir could

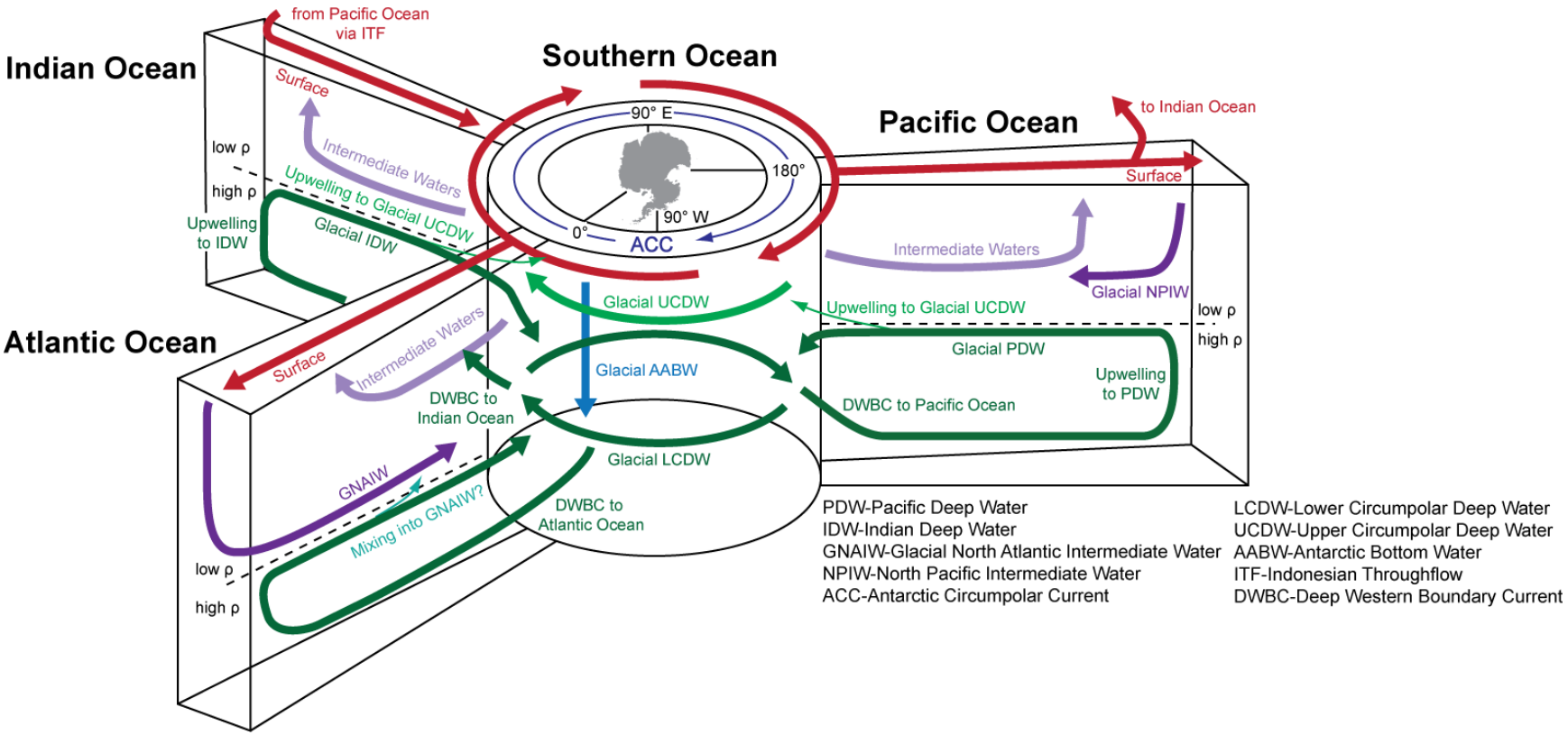

Figure 4.6. Conceptual diagram of hypothesized changes in glacial deep water circulation. Dashed lines in Pacific, Indian, and Atlantic Oceans represent a density boundary ~2500-3000 m water depth separating cold, salty deep waters (high ρ) below from warmer and/or fresher waters (low ρ) above. Stronger density stratification during the last glacial period could have produced changes in water mass mixing that reduced mixing of LCDW with better ventilated waters. Smaller arrows suggest a reduced volume of upwelled water compared to modern day.

only have existed below 2.8 km water depth [*Broecker et al.*, 2008]. This extremely "old" reservoir would then have dissipated by mixing into the global ocean at the deglaciation [*Broecker and Barker*, 2007]. However, Burke and Robinson [2012] point out that the age of such a reservoir would need to be less extreme if a portion of the trapped CO_2 is allowed to vent directly to the atmosphere, perhaps through increased Southern Ocean upwelling [*Anderson et al.*, 2009]. A simple calculation reveals that the total volume of the Atlantic, Indian, and Pacific Oceans below 2.8 km water depth is ~25% of global ocean volume. Because modern LCDW feeds all three basins, it is reasonable that recirculated glacial LCDW acted as the isolated reservoir, dispersing radiocarbon-depleted water throughout the deep ocean. Solid evidence for an "old" oceanic carbon reservoir is so far lacking. However, benthic-planktonic age differences often assume constant surface reservoir ages [e.g., *Galbraith et al.*, 2007]. If this assumption is not valid, and surface water reservoir ages are high, the "true" age of deep waters may not be apparent. Furthermore, $CaCO_3$ is not well preserved in the deep Pacific, and suitable samples from depths below 2.8 km are difficult to obtain [*Broecker et al.*, 2007].

Presently, LCDW bathes site TN057-13-4PC (Antarctic Zone); however, apparent Re removal depths persistently equal to or greater than the modern oxygen penetration depth (Figure 4.5a; Table 4.4) suggest that a different, well-ventilated water mass (perhaps a glacial equivalent of UCDW) existed at 2.8 km. The contrast with ventilation records from RC13-254 (Cape Basin) showing older, more O_2-depleted LCDW suggests that the modern water mass arrangement in which a lower-O_2 component of CDW overlies a higher-O_2 component may have been reversed during the last glacial period. The ventilation source at TN057-13-4PC is unclear, however, and the paucity of cores from all sectors of the Antarctic Zone leaves the glacial vertical water column structure an open question.

One plausible mechanism to increase Southern Ocean vertical stratification invokes increased sea ice extent and cooling of the open ocean water column as a driver for increased brine formation [*Keeling and Stephens*, 2001]. Average glacial winter sea ice extent that reached to approximately the modern APF [*Gersonde et al.*, 2003] could have resulted in deep water formation away from continental shelves [*Mackensen et al.*, 2001], where bottom water formation is restricted to today. Model studies indicate that brine export [*Bouttes et al.*, 2010] and reduced air-sea gas exchange [*Stephens and Keeling*, 2000] due to more extensive sea ice can also account for observed changes in atmospheric CO_2 and vertical oceanic $\delta^{13}C$ gradients.

5.5 Comparison to Other Trace Metal Records

Most other trace metal records available from the Southern Ocean utilize Cd or authigenic U as suboxic indicators, although interpreting bulk sediment U is not straightforward because its accumulation is influenced by a combination of bulk sedimentation rate/sediment focusing, organic carbon rain rate, and bottom water O_2 concentration [*Frank et al.*, 2000]. Higher Cd and U accumulation rates/concentrations in Subantarctic sediments during the last glacial period have been primarily interpreted to record suboxic conditions caused by a northward shift of the ACC high productivity zone [*Anderson et al.*, 1998; *Bareille et al.*, 1998; *Chase et al.*, 2001; *Frank et al.*, 2000; *Kumar et al.*, 1995; *Rosenthal et al.*, 1995b]. Elevated glacial Ag and Cd fluxes (Figure 4.3a-b) concur with previous work by demonstrating strong export production north of the modern APF. In comparison, Antarctic Zone sediments from the Indian and Atlantic sectors give inconsistent results. In the Atlantic sector, some studies show minima in bulk sediment U concentrations and C_{org} and Si_{bio} fluxes at the LGM before increasing during deglaciation [*Anderson et al.*, 1998; *Frank et al.*, 2000], when the high productivity zone shifted southward again. Other studies from the Indian sector demonstrate modest increases in

bulk sediment Cd and U accumulation rates during the LGM similar to deglacial accumulation rates [*Rosenthal et al.,* 1995b]. C_{org} accumulation rates also show a modest increase during the LGM, but afterward increase rapidly during the early deglaciation, suggesting that preservation issues could have influenced proxy accumulation. South Atlantic trace metal fluxes follow the results of Anderson et al. [1998] most closely by displaying minima during the LGM and higher fluxes during the deglacial and Holocene (Figure 4.4a-d).

A simple explanation of trace metal enrichment patterns involving glacial-interglacial shifts of the high productivity zone is complicated by the suggestion that the magnitude or pattern of Cd and U accumulation also implies decreased CDW oxygen concentrations [*Bareille et al.,* 1998; *Francois et al.,* 1997; *Rosenthal et al.,* 1995b]. Increasing Re fluxes coupled with decreasing Ag and Cd fluxes during the LGM (Figure 4.3a-c) support this conclusion, and suggest that export production and bottom water O_2 concentrations both influenced trace metal accumulation north of the modern APF. However, available data do not provide a clear indication of oxygenation levels in the glacial Antarctic Zone, and how they may have changed over time. Further studies employing a suite of redox proxies are needed from all three sectors of the Southern Ocean to sufficiently characterize glacial deep water ventilation.

5.6 Production vs. Preservation

Prior studies utilizing a variety of productivity proxies have concluded that the locus of Southern Ocean export productivity shifted north of the modern Antarctic Polar Front (APF) during the last glacial period [*Chase et al.,* 2003; *Dezileau et al.,* 2003; *Kumar et al.,* 1995]. This simple picture is challenged by our trace metal results and by diatom assemblage studies [*Abelmann et al.,* 2006], which suggest that preservation artifacts influence the records of productivity proxies such as biogenic silica (Si_{bio}) and organic carbon (C_{org}), and potentially also

proxies such as ^{231}Pa. Opal fluxes (Figure 4.3e, 4.4e) only partially support our interpretation of Ag and Cd flux data. At RC13-254, little structure is seen in the opal flux record (Figure 4.3e) [*Anderson et al.*, 1998; *Kumar et al.*, 1995], which is nearly identical to the C_{org} flux [*Anderson et al.*, 1998]. Maximum C_{org} fluxes occur ~20.8 ka, during the most intense period of bottom water O_2 depletion, as revealed by high Re fluxes (Figure 4.3c). However, C_{org} is better preserved under low O_2 and high sedimentation rate conditions [*Canfield*, 1994], and so low bottom water O_2 conditions at the LGM would favor enhanced C_{org} preservation. At TN057-13-4PC, an abrupt increase in opal flux (Figure 4.4e) occurs ~16 ka, after which reasonable agreement exists among Ag, Cd, and opal fluxes (Figure 4.4a-b, 4.4e). Conversely, no significant opal flux is seen prior to ~16 ka, although Ag and Cd fluxes record elevated export productivity between ~26.9-21.6 ka. Weight percent total C_{org} at PS1768-8 (52.6°S, 4.5°E, 3299 m) [*Abelmann et al.*, 2006] increases modestly from ~30-25 ka, overlapping broad peaks in Ag and Cd fluxes (Figure 4.4a-b). Moreover, total C_{org} concentrations that increase from approximately 0.35% to almost 0.5% capture deglacial productivity increases recorded by Ag and Cd fluxes (Figure 4.4a-b) between ~17.1-13.6 ka. Total C_{org} therefore appears more reliable than opal flux in recording last glacial period and early deglacial Antarctic Zone productivity changes. Although we cannot rule out the possibility of burndown at the glacial-interglacial transition as discussed above, one reason for this trend may be that Ag and Cd peaks ~26.9-21.6 ka reflect high C_{org} export by *Chaetoceros* spp. resting spores, which are poorly silicified and less well preserved in sediments [*Abelmann et al.*, 2006].

A plausible explanation of glacial-interglacial surface water ecological changes that may have contributed to the trace metal record was outlined by Abelmann et al. [2006]. At the LGM, the average winter sea ice edge expanded ~5° north of its present position to ~50°S [*Gersonde et*

al., 2003] to cover TN057-13-4PC during austral winter (Figure 4.4h), whereas this core is ~2° north of the present-day average winter sea ice edge [*Kanfoush et al.*, 2002]. Today the heavily silicified, robust, and well-preserved diatom *Fragilariopsis kerguelensis* occupies the Permanently Open Ocean Zone at the site of TN057-13-4PC. However, at the LGM expanded sea ice coverage altered local phytoplankton ecology such that the diatom *Chaetoceros* spp.—which inhabits the Seasonal Ice Zone—dominated surface waters in the vicinity of TN057-13-4PC. Proportionally greater export of *Chaetoceros* spp. resting spores from ~30-16 ka therefore resulted in export production with a lower Si_{bio}/C_{org} ratio [*Abelmann et al.*, 2006; their Figure 3]. After ~16 ka, the preserved sedimentary fraction of *F. kerguelensis* increased to >50% of the assemblage, in agreement with the increase in opal flux (Figure 4.4e). In comparison, RC13-254 remained within the Permanently Open Ocean Zone during the last glacial period, where *F. kerguelensis* was the dominant primary producer and hence biogenic sediments show higher Si_{bio}/C_{org} ratios [*Abelmann et al.*, 2006]. A cartoon illustrating the changes between glacial and interglacial periods is presented in Figure 4.7. When primary producer assemblage changes are considered alongside the trace metal record (Figure 4.3-4.4), we conclude that productivity proxies, even when ^{230}Th-normalized, are subject to significant preservation bias.

6. Conclusions

This study is the first to present a suite of trace metal (Ag, Cd, Re, and Mo) fluxes to Atlantic sector Southern Ocean sediments over the last 30 kyr, recording substantial changes in regional ventilation and export production history. When compared to late Holocene sediments, higher fluxes of all trace metals during the deglacial and last glacial period reveal significantly different past Southern Ocean chemistry. Cape Basin sediments (RC13-254) were suboxic from at least 30-13.5 ka due to a combination of high export production and reduced bottom water

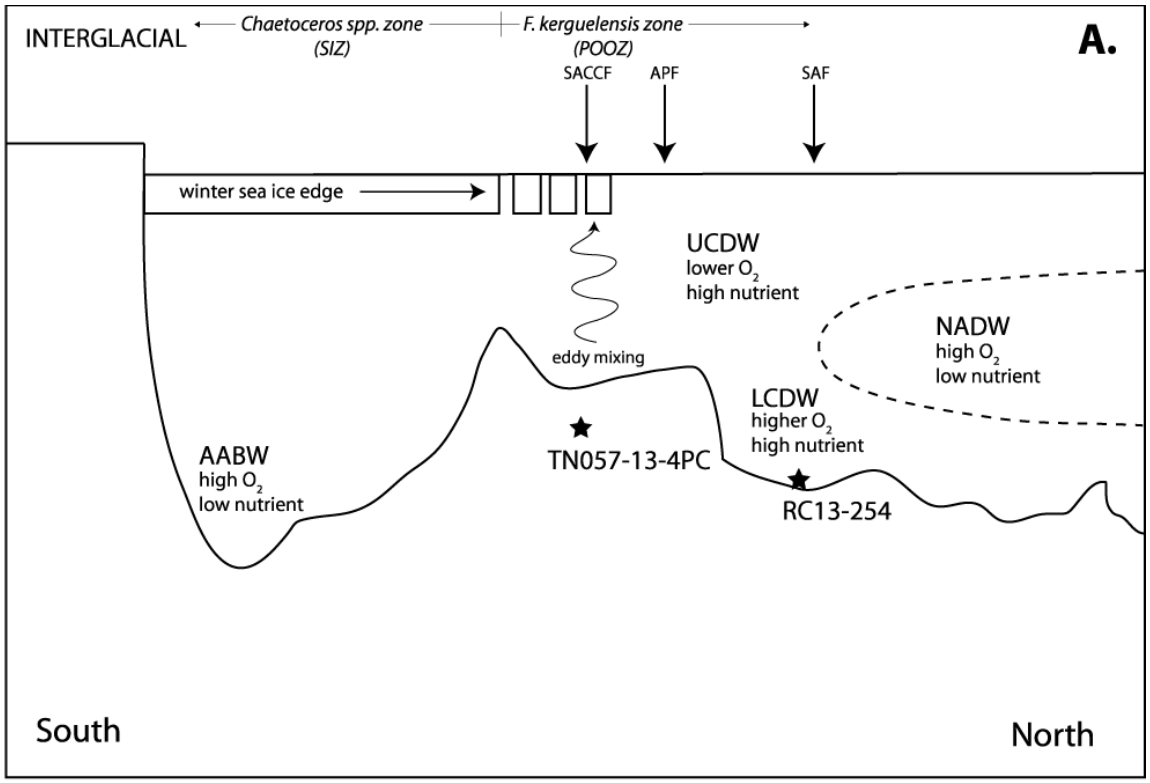
INTERGLACIAL
Chaetoceros spp. zone
(SIZ)
F. kerguelensis zone
(POOZ)
A.
SACCF
APF
SAF
winter sea ice edge
UCDW
lower O2
high nutrient
eddy mixing
NADW
high O2
low nutrient
LCDW
higher O2
high nutrient
AABW
high O2
low nutrient
TN057-13-4PC
RC13-254
South
North

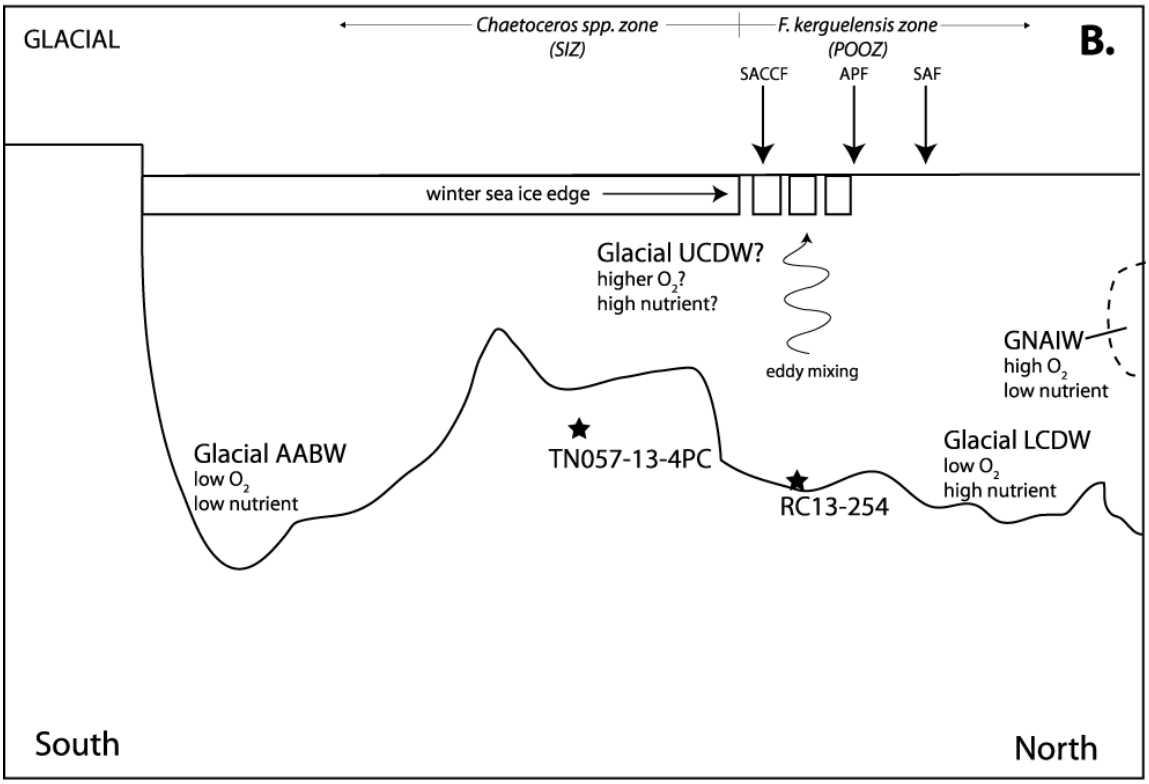
GLACIAL
Chaetoceros spp. zone
(SIZ)
F. kerguelensis zone
(POOZ)
B.
SACCF
APF
SAF
winter sea ice edge
Glacial UCDW?
higher O2?
high nutrient?
eddy mixing
GNAIW
high O2
low nutrient
Glacial AABW
low O2
low nutrient
TN057-13-4PC
RC13-254
Glacial LCDW
low O2
high nutrient
South
North

Figure 4.7. (Previous page) Cartoon depicting inferred ecological changes between A) interglacial and B) glacial stages in the Atlantic Sector of the Southern Ocean (after Abelmann et al. [2006]). Locations of cores used in this study are marked by stars. SACCF—Southern ACC Front; APF—Antarctic Polar Front; SAF—Subantarctic Front; SIZ—Seasonal Ice Zone; POOZ—Permanently Open Ocean Zone.

ventilation. After ~13.5 ka, trace metal fluxes fall to near zero as oxidative burndown erases the record. The presence of burndown underscores the glacial-interglacial redox shift in Southern Ocean water mass chemistry. Furthermore, during the LGM (23-19 ka) shallow apparent Re removal depths unconnected to export productivity coincide with oldest $\Delta^{14}C$ apparent ventilation ages [*Skinner et al.*, 2010].

Trace metal fluxes in the Antarctic Zone (TN057-13-4PC) are less intense than those from the Cape Basin and indicate suboxic sediments due to enhanced export production primarily from ~26.9-21.6 ka, during the deglacial from ~17.1-13.6 ka, and during three discrete Holocene events. Deglacial productivity increases inferred from higher Ag and Cd fluxes agree with previous opal flux estimates [*Anderson et al.*, 2009]. Increased Re fluxes indicate that sedimentary suboxia due to poor bottom water ventilation may have existed from ~30.6-26.9 ka, although burndown at the glacial-interglacial transition cannot be entirely ruled out.

Poorer ventilation of the glacial Southern Ocean requires changes in global deep ocean circulation. We hypothesize that colder, saltier glacial deep waters resulted in changes to water mass mixing and stratification that altered deep water chemistry, such that no modern analogue for the glacial Southern Ocean (and its deep water products) exists. Hence it may be an oversimplification to conceptualize glacial Southern Ocean circulation as similar to today, with only subtle shifts in the position of the westerly winds [cf. *Anderson et al.*, 2009]. Furthermore, our work suggests that glacial CO_2 was stored within LCDW and its downstream products, Indian and Pacific Deep Waters.

Conventional productivity proxies such as weight percent C_{org} and Si_{bio} have often been used to reconstruct glacial shifts in export productivity. However, these proxies are rapidly remineralized in the water column and during early sedimentary diagenesis, potentially introducing bias into any reconstruction. Trace metal productivity proxy (Ag, Cd) fluxes from the Antarctic Zone are not always consistent with available C_{org} and Si_{bio} data, suggesting that preservation bias is a real concern. Diatom assemblage studies [*Abelmann et al.*, 2006] show that the importance of poorly silicified *Chaetoceros* spp.—a low Si_{bio}/C_{org} ratio exporter—increased during the last glacial period. Hence this taxon may have exported large amounts of C_{org} relative to Si_{bio} that were recorded by Ag and Cd fluxes, although this export production would go unrecognized by measurement of opal flux or $^{231}Pa/^{230}Th$ ratios alone. Future studies should employ multiple productivity proxies to evaluate the impact of preservation bias.

Acknowledgements. This study was supported by a grant to MW from the Geological Society of America (GSA) and by the University of Michigan (to ILH). Samples were provided by the Lamont-Doherty Earth Observatory Core Repository. MW thanks Bob Anderson (Lamont-Doherty Earth Observatory) and Sam Jaccard (ETH Zürich) for sharing data, and Ted Huston and Kate Hanson (University of Michigan) for help with laboratory analyses. Comments from three anonymous reviewers regarding a prior version of the manuscript helped to improve its quality.

Table 4.1. TN057-13-4PC trace metal concentrations.

Depth (cm)	Age (yr)	Cd (ppm)	± 1σ (ppm)	Re (ppb)	± 1σ (ppb)	Ag (ppb)	± 1σ (ppb)	Mo (ppm)	± 1σ (ppm)
0-1	18	0.06	0.01	0.5	0.0	69	15	0.46	0.10
10-11	305	0.10	0.02	0.4	0.0	19	3	1.29	0.22
20-21	749	0.03	0.01	0.4	0.0	45	6	0.18	0.00
40-41	1259	0.07	0.01	0.4	0.0	37	5	0.12	0.00
60-61	1769	0.08	0.02	0.5	0.0	70	10	0.08	0.00
80-81	2295	0.10	0.02	0.7	0.0	79	11	0.08	0.00
100-101	2824	0.10	0.02	0.6	0.0	74	10	0.14	0.00
120-121	3353	0.10	0.02	0.6	0.0	61	9	0.18	0.04
140-141	3882	0.12	0.02	1.0	0.0	71	10	0.10	0.00
160-161	4410	0.13	0.02	0.6	0.0	38	8	0.12	0.00
180-181	4939	0.14	0.03	1.0	0.0	63	9	0.12	0.00
200-201	5468	0.20	0.04	1.0	0.0	81	11	0.12	0.00
220-221	5997	0.26	0.05	2.4	0.1	142	20	0.16	0.00
240-241	6526	0.25	0.04	13.3	0.6	145	31	0.47	0.08
260-261	6998	0.24	0.04	9.9	0.5	87	12	0.45	0.01
300-301	7549	0.19	0.03	4.1	0.2	88	12	0.48	0.01
340-341	8100	0.20	0.04	3.6	0.2	125	18	0.53	0.01
380-381	8651	0.18	0.07	4.4	0.2	148	32	0.52	0.01
420-421	9203	0.17	0.03	1.9	0.1	74	10	0.39	0.01
470-471	9631	0.11	0.02	2.1	0.1	82	11	0.33	0.05
510-511	10164	0.10	0.02	2.7	0.1	84	18	0.39	0.01
560-561	10988	0.10	0.02	1.6	0.1	94	13	0.22	0.03
580-581	11367	0.09	0.02	0.8	0.0	76	11	0.30	0.00
610-611	11936	0.09	0.02	1.0	0.0	40	9	0.27	0.00
640-641	12505	0.08	0.02	1.5	0.1	45	6	0.26	0.00
670-671	13073	0.14	0.03	1.2	0.1	82	11	0.31	0.00
700-701	13642	0.15	0.03	2.7	0.1	81	11	0.71	0.01

730-731	14211	0.16	0.03	4.2	0.2	95	13	0.79	0.01
760-761	16163	0.13	0.02	9.6	0.5	93	13	0.86	0.14
770-771	17062	0.26	0.14	4.6	0.2	87	19	1.17	0.02
780-781	17960	0.34	0.06	5.0	0.2	130	18	1.31	0.23
790-791	18859	0.43	0.08	6.4	0.3	200	28	1.25	0.02
800-801	19758	0.42	0.07	13.0	0.6	216	47	1.38	0.23
810-811	20657	0.32	0.06	7.3	0.3	218	31	1.28	0.02
820-821	21556	0.23	0.04	3.7	0.2	71	15	1.03	0.18
830-831	22454	1.13	0.20	7.4	0.4	382	53	0.62	0.11
840-841	23353	1.13	0.20	9.0	0.4	589	82	0.75	0.01
850-851	24252	1.24	0.22	14.2	0.7	366	81	0.84	0.14
860-861	25151	0.99	0.18	11.8	0.5	267	37	0.78	0.01
870-871	26050	0.78	0.14	15.3	0.7	154	22	0.99	0.17
880-881	26949	0.73	0.13	26.4	1.2	114	16	0.86	0.01
890-891	27847	0.69	0.12	64.8	3.1	119	17	1.39	0.23
900-901	28746	0.60	0.11	41.2	2.0	98	21	1.67	0.28
910-911	29645	0.52	0.09	55.1	2.6	121	17	1.50	0.26
920-911	30604	0.41	0.07	15.6	0.8	139	19	1.14	0.19

Table 4.2. RC13-254 trace metal concentrations.

Depth (cm)	Age (yr)	Cd (ppm)	± 1σ (ppm)	Re (ppb)	± 1σ (ppb)	Ag (ppb)	± 1σ (ppb)	Mo (ppm)	± 1σ (ppm)
0-1	3500	0.87	0.15	1.3	0.1	18	3	1.19	0.46
5-6	4625	8.97*	1.56	0.8	0.0	11	2	0.21	0.04
10-11	5750	1.80	0.30	0.2	0.0	14	3	0.38	0.01
15-16	6950	0.13	0.02	0.5	0.0	4	1	0.57	0.01
20-21	8293	3.70*	0.74	0.5	0.0	24	5	0.70	0.14
25-26	9100	0.10	0.02	0.4	0.0	7	1	0.50	0.10
30-31	10100	0.07	0.01	0.6	0.0	1	0	0.91	0.01
35-36	11050	0.08	0.01	0.6	0.0	14	2	0.76	0.01
41-42	11650	0.01	0.00	0.7	0.0	24	3	0.35	0.01
50-51	12393	0.00	0.00	0.8	0.0	20	3	0.28	0.00
61-62	13125	0.02	0.00	1.0	0.0	31	4	0.51	0.01
70-71	13575	0.04	0.01	5.6	0.3	90	13	0.31	0.00
81-82	14179	0.16	0.03	16.6	0.8	153	33	0.30	0.00
90-91	14821	0.38	0.07	24.8	1.1	195	27	0.37	0.01
101-102	15598	1.56	0.25	46.8	2.2	194	42	0.56	0.09
109-110	16120	0.71	0.13	24.6	1.1	193	27	0.78	0.01
125-126	17109	0.31	0.05	19.6	0.9	125	27	0.86	0.14
141-142	17745	0.76	0.13	30.6	1.5	235	53	1.21	0.20
161-162	18109	0.29	0.05	27.1	1.2	118	17	1.12	0.02
171-172	18291	0.48	0.08	21.1	1.0	130	18	1.32	0.21
181-182	19148	0.26	0.05	36.2	1.7	69	15	1.28	0.02
191-192	20041	0.29	0.05	38.5	1.8	79	11	1.44	0.24
205-206	21062	0.43	0.08	25.3	1.2	85	12	1.25	0.02
221-222	21829	0.50	0.10	15.0	0.7	168	24	1.97	0.32
240-241	22913	0.28	0.05	14.2	0.7	116	16	1.50	0.02
261-262	23466	0.35	0.07	16.7	0.8	79	17	1.58	0.03

290-291	24739	0.52	0.09	17.7	0.8	169	24	1.27	0.02
309-310	25440	1.26	0.25	17.3	0.8	204	46	2.92	0.50
330-331	26032	0.71	0.13	7.6	0.4	273	60	1.24	0.21
341-342	26402	0.66	0.12	22.7	1.1	179	25	1.67	0.27
361-362	27768	0.24	0.04	21.4	1.0	241	34	0.74	0.01
371-372	28451	0.22	0.04	12.0	0.6	80	17	0.88	0.14
379-380	28998	0.44	0.08	18.0	0.8	131	29	0.69	0.01

*Indicates suspected contamination.

Table 4.3. $^{230}_{xs}Th_0$ values for RC13-254 [*Kumar*, 1994].

Depth (cm)	$^{230}_{xs}Th_0$ (dpm g^{-1})
13	10.34
18	9.40
34	7.74
123	3.06
172	2.46
432	4.66

Table 4.4. Calculated Re removal depths and Re/Mo ratios for TN057-13-4PC.

Depth (cm)	Age (yr)	Re removal depth [z] (cm)	± (cm)	Re/Mo (mmol mol^{-1})
0-1	18	1665	37	0.6
10-11	305	2102	46	0.2
20-21	749	2116	46	1.1
40-41	1259	2330	51	1.6
60-61	1769	1613	215	3.1
80-81	2295	982	35	4.8
100-101	2824	1197	44	2.1
120-121	3353	1172	43	1.7
140-141	3882	685	3	4.9
160-161	4410	1177	120	2.4
180-181	4939	623	67	4.2
200-201	5468	549	87	4.3
220-221	5997	222	39	7.8
240-241	6526	36	7	14.4
260-261	6998	50	11	11.3
300-301	7549	88	25	4.4
340-341	8100	116	15	3.5
380-381	8651	75	27	4.3
420-421	9203	163	54	2.5
470-471	9631	115	67	3.3
510-511	10164	74	3	3.6
560-561	10988	150	13	3.9
580-581	11367	309	18	1.5
610-611	11936	225	60	1.9
640-641	12505	152	15	2.9
670-671	13073	256	108	2.0
700-701	13642	136	7	2.0
730-731	14211	85	5	2.8
760-761	16163	37	2	5.8
770-771	17062	158	14	2.0
780-781	17960	243	18	2.0
790-791	18859	177	8	2.6
800-801	19758	89	9	4.9
810-811	20657	173	16	2.9
820-821	21556	328	33	1.8
830-831	22454	154	16	6.1
840-841	23353	114	12	6.1
850-851	24252	68	6	8.6
860-861	25151	77	6	7.8

870-871	26050	63	10	7.9
880-881	26949	40	6	15.8
890-891	27847	17	1	23.9
900-901	28746	27	2	12.7
910-911	29645	20	1	19.0
920-911	30604	70	4	7.0

Table 4.5. Calculated Re removal depths and Re/Mo ratios for RC13-254.

Depth (cm)	Age (yr)	Removal depth [z] (cm)	± (cm)	Re/Mo (mmol mol^{-1})
0-1	3500	943	50	0.6
5-6	4625	1467	81	2.0
10-11	5750	5123	251	0.3
15-16	6950	2238	110	0.5
20-21	8293	2031	294	0.4
25-26	9100	2314	340	0.5
30-31	10100	1604	256	0.3
35-36	11050	1416	670	0.4
41-42	11650	1205	604	1.0
50-51	12393	949	514	1.4
61-62	13125	709	417	1.0
70-71	13575	114	71	9.5
81-82	14179	36	24	28.0
90-91	14821	22	16	34.7
101-102	15598	10	9	42.9
109-110	16120	18	16	16.3
125-126	17109	18	3	11.7
141-142	17745	11	2	13.0
161-162	18109	11	2	12.4
171-172	18291	14	2	8.2
181-182	19148	9	5	14.5
191-192	20041	8	5	13.7
205-206	21062	14	7	10.4
221-222	21829	24	13	3.9
240-241	22913	26	13	4.9
261-262	23466	23	11	5.5
290-291	24739	23	11	7.2
309-310	25440	24	11	3.0
330-331	26032	56	25	3.2
341-342	26402	19	8	7.0
361-362	27768	21	9	14.8
371-372	28451	39	16	7.1
379-380	28998	26	10	13.5

Table 4.6. Examples of outcomes for sensitivity tests in estimating apparent Re removal depths.

Parameter			Re removal depth (cm)
RC13-254, 81-82 cmbsf			
Porosity (φ)	Assigned value	0.85	36
	Maximum	0.94	39
	Minimum	0.77	32
D_s ($cm^2\ s^{-1}$)	Assigned value	5×10^{-6}	36
	Maximum	1.0×10^{-5}	72
	Minimum	2.5×10^{-6}	18
J ($mol\ cm^{-2}\ s^{-1}$)	Assigned value	1.90×10^{-20}	36
	Maximum	3.49×10^{-20}	21
	Minimum	3.22×10^{-21}	109
TN057-13-4PC, 760-761 cmbsf			
Porosity (φ)	Assigned value	0.90	37
	Maximum	0.99	40
	Minimum	0.81	33
D_s ($cm^2\ s^{-1}$)	Assigned value	5×10^{-6}	37
	Maximum	1.0×10^{-5}	74
	Minimum	2.5×10^{-6}	18
J ($mol\ cm^{-2}\ s^{-1}$)	Assigned value	5.62×10^{-21}	37
	Maximum	5.97×10^{-21}	35
	Minimum	5.26×10^{-21}	39

REFERENCES

Abelmann, A., R. Gersonde, G. Cortese, G. Kuhn, and V. Smetacek (2006), Extensive phytoplankton blooms in the Atlantic sector of the glacial Southern Ocean, *Paleoceanography*, *21*(PA1013), doi: 10.1029/2005PA001199.

Adkins, J. F., K. McIntyre, and D. P. Schrag (2002), The salinity, temperature, and $\delta^{18}O$ of the glacial deep ocean, *Science*, *298*(5599), 1769-1773.

Ahn, J., and E. J. Brook (2008), Atmospheric CO_2 and climate on millennial time scales during the last glacial period, *Science*, *322*(5898), 83-85.

Anderson, R. F., N. Kumar, R. A. Mortlock, P. N. Froelich, P. Kubik, B. Dittrich-Hannen, and M. Suter (1998), Late-Quaternary changes in productivity of the Southern Ocean, *Journal of Marine Systems*, *17*(1-4), 497-514.

Anderson, R. F., S. Ali, L. I. Bradtmiller, S. H. H. Nielsen, M. Q. Fleisher, B. E. Anderson, and L. H. Burckle (2009), Wind-driven upwelling in the Southern Ocean and the deglacial rise in atmospheric CO_2, *Science*, *323*(5920), 1443-1448.

Bareille, G., M. Labracherie, P. Bertrand, L. Labeyrie, G. Lavaux, and M. Dignan (1998), Glacial-interglacial changes in the accumulation rates of major biogenic components in Southern Indian Ocean sediments, *Journal of Marine Systems*, *17*(1-4), 527-539.

Berner, R. A. (1980), *Early Diagenesis: A Theoretical Approach*, 241 pp., Princeton University Press, Princeton, NJ.

Berner, R. A. (1981), A new geochemical classification of sedimentary environments, *Journal of Sedimentary Petrology*, *51*(2), 359-365.

Bostick, B. C., S. Fendorf, and G. R. Helz (2003), Differential adsorption of molybdate and tetrathiomolybdate on pyrite (FeS_2), *Environmental Science and Technology*, *37*(2), 285-291.

Bouttes, N., D. Paillard, and D. M. Roche (2010), Impact of brine-induced stratification on the glacial carbon cycle, *Climate of the Past*, *6*(5), 575-589, doi: 10.5194/cp-6-575-2010.

Broecker, W. S., and T.-H. Peng (1982), *Tracers in the Sea*, 690 pp., Lamont-Doherty Geological Observatory, Palisades, New York.

Broecker, W. S., and S. Barker (2007), A 190‰ drop in atmosphere's $\Delta^{14}C$ during the "Mystery Interval" (17.5 to 14.5 kyr), *Earth Planet. Sci. Lett.*, *256*(1-2), 90-99.

Broecker, W. S., E. Clark, and S. Barker (2008), Near constancy of the Pacific Ocean surface to mid-depth radiocarbon-age difference over the last 20 kyr, *Earth Planet. Sci. Lett.*, *274*(3-4), 322-326.

Broecker, W. S., E. Clark, S. Barker, I. Hajdas, G. Bonani, and E. Moreno (2007), Radiocarbon age of late glacial deep water from the equatorial Pacific, *Paleoceanography*, *22*(2), PA2206, doi: 10.1029/2006PA001359.

Burke, A., and L. F. Robinson (2012), The Southern Ocean's role in carbon exchange during the last deglaciation, *Science*, *335*(6068), 557-561.

Calvert, S. E., and T. F. Pedersen (1993), Geochemistry of recent oxic and anoxic marine sediments: Implications for the geological record, *Marine Geology*, *113*(1-2), 67-88.

Canfield, D. E. (1994), Factors influencing organic carbon preservation in marine sediments, *Chemical Geology*, *114*, 315-329.

Carter, L., and I. N. McCave (1997), The sedimentary regime beneath the Deep Western Boundary Current inflow to the southwest Pacific Ocean, *Journal of Sedimentary Research*, *67*(6), 1005-1017.

Charles, C. D., P. N. Froelich, M. A. Zibello, R. A. Mortlock, and J. J. Morley (1991), Biogenic opal in Southern Ocean sediments over the last 450,000 years: implications for surface water chemistry and circulation, *Paleoceanography*, *6*(6), 697-728.

Chase, Z., R. F. Anderson, and M. Q. Fleisher (2001), Evidence from authigenic uranium for increased productivity of the glacial Subantarctic Ocean, *Paleoceanography*, *16*(5), 468-478.

Chase, Z., R. F. Anderson, M. Q. Fleisher, and P. W. Kubik (2003), Accumulation of biogenic and lithogenic material in the Pacific sector of the Southern Ocean during the past 40,000 years, *Deep-Sea Research II*, *50*(3-4), 799-832.

Colodner, D., J. Sachs, G. Ravizza, K. Turekian, J. Edmond, and E. Boyle (1993), The geochemical cycle of rhenium: a reconnaissance, *Earth Planet. Sci. Lett.*, *117*(1-2), 205-221.

Crusius, J., and J. Thomson (2000), Comparative behavior of authigenic Re, U, and Mo during reoxidation and subsequent long-term burial in marine sediments, *Geochimica et Cosmochimica Acta*, *64*(13), 2233-2242.

Crusius, J., and J. Thomson (2003), Mobility of authigenic rhenium, silver, and selenium during postdepositional oxidation in marine sediments, *Geochimica et Cosmochimica Acta*, *67*(2), 265-273.

Crusius, J., S. Calvert, T. Pedersen, and D. Sage (1996), Rhenium and molybdenum enrichments in sediments as indicators of oxic, suboxic, and sulfidic conditions of deposition, *Earth Planet. Sci. Lett.*, *145*(1-4), 65-78.

Curry, W. B., and D. W. Oppo (2005), Glacial water mass geometry and the distribution of $\delta^{13}C$ of ΣCO_2 in the western Atlantic Ocean, *Paleoceanography*, *20*(PA1017), doi: 10.1029/2004PA001021.

Dezileau, L., J. L. Reyss, and F. Lemoine (2003), Late Quaternary changes in biogenic opal fluxes in the southern Indian Ocean, *Marine Geology, 202*(3-4), 143-158.

Dezileau, L., G. Bareille, J. L. Reyss, and F. Lemoine (2000), Evidence for strong sediment redistribution by bottom currents along the southeast Indian ridge, *Deep-Sea Research I, 47*(10), 1899-1936.

EPICA Community Members (2006), One-to-one coupling of glacial climate variability in Greenland and Antarctica, *Nature, 444*(7116), 195-198.

Erickson, B. E., and G. R. Helz (2000), Molybdenum (VI) speciation in sulfidic waters: Stability and lability of thiomolybdates, *Geochimica et Cosmochimica Acta, 64*(7), 1149-1158.

Flückiger, J., E. Monnin, B. Stauffer, J. Schwander, T. F. Stocker, J. Chappellaz, D. Raynaud, and J. M. Barnola (2002), High-resolution Holocene N_2O ice core record and its relationship with CH_4 and CO_2, *Global Biogeochemical Cycles, 16*(1), doi: 10.1029/2001GB001417.

Francois, R., M. P. Bacon, M. A. Altabet, and L. D. Labeyrie (1993), Glacial/interglacial changes in sediment rain rate in the SW Indian sector of Subantarctic waters as recorded by ^{230}Th, ^{231}Pa, U, and δ^{15}N, *Paleoceanography, 8*(5), 611-629.

Francois, R., M. Frank, M. M. R. van der Loeff, and M. P. Bacon (2004), Th-230 normalization: An essential tool for interpreting sedimentary fluxes during the late Quaternary, *Paleoceanography, 19*(PA1018), doi: 10.1029/2003PA000939.

Francois, R., M. A. Altabet, E. F. Yu, D. M. Sigman, M. P. Bacon, M. Frank, G. Bohrmann, G. Bareille, and L. D. Labeyrie (1997), Contribution of Southern Ocean surface-water stratification to low atmospheric CO_2 concentrations during the last glacial period, *Nature, 389*(6654), 929-935.

Frank, M., R. Gersonde, M. R. v. d. Loeff, G. Bohrmann, C. C. Nürnberg, P. W. Kubik, M. Suter, and A. Mangini (2000), Similar glacial and interglacial export bioproductivity in the Atlantic sector of the Southern Ocean: Multiproxy evidence and implications for glacial atmospheric CO_2, *Paleoceanography, 15*(6), 642-658.

Froelich, P. N., G. P. Klinkhammer, M. L. Bender, N. A. Luedtke, G. R. Heath, D. Cullen, P. Dauphin, D. Hammond, B. Hartman, and V. Maynard (1979), Early oxidation of organic matter in pelagic sediments of the eastern equatorial Atlantic: suboxic diagenesis, *Geochimica et Cosmochimica Acta, 43*(7), 1075-1090.

Galbraith, E. D., S. L. Jaccard, T. F. Pedersen, D. M. Sigman, G. H. Haug, M. Cook, J. R. Southon, and R. Francois (2007), Carbon dioxide release from the North Pacific abyss during the last deglaciation, *Nature, 449*(7164), 890-894.

Gersonde, R., et al. (2003), Last glacial sea surface temperatures and sea ice extent in the Southern Ocean (Atlantic-Indian sector): A multiproxy approach, *Paleoceanography, 18*(3), doi: 10.1029/2002PA000809.

Hamilton, E. L. (1976), Variations of density and porosity with depth in deep-sea sediments, *Journal of Sedimentary Petrology*, *46*(2), 280-300.

Helz, G. R., and M. K. Dolor (2012), What regulates rhenium deposition in euxinic basins?, *Chemical Geology*, *304-305*, 131-141.

Helz, G. R., C. V. Miller, J. M. Charnock, J. F. W. Mosselmans, R. A. D. Pattrick, C. D. Garner, and D. J. Vaughan (1996), Mechanism of molybdenum removal from the sea and its concentration in black shales: EXAFS evidence, *Geochimica et Cosmochimica Acta*, *60*(19), 3631-3642.

Hendy, I. L., and T. F. Pedersen (2005), Is pore water oxygen content decoupled from productivity on the California Margin? Trace element results from Ocean Drilling Program Hole 1017E, San Lucia slope, California, *Paleoceanography*, *20*(PA4026), doi: 10.1029/2004PA001123.

Herguera, J. C., T. Herbert, M. Kashgarian, and C. Charles (2010), Intermediate and deep water mass distribution in the Pacific during the Last Glacial Maximum inferred from oxygen and carbon stable isotopes, *Quaternary Science Reviews*, *29*(9-10), 1228-1245.

Hodell, D. A., K. A. Venz, C. D. Charles, and U. S. Ninneman (2003), Pleistocene vertical carbon isotope and carbonate gradients in the South Atlantic sector of the Southern Ocean, *Geochemistry Geophysics Geosystems*, *4*(1), 1004.

Hodell, D. A., S. L. Kanfoush, A. Shemesh, X. Crosta, C. D. Charles, and T. P. Guilderson (2001), Abrupt cooling of Antarctic surface waters and sea ice expansion in the South Atlantic sector of the Southern Ocean at 5000 cal yr B.P., *Quaternary Research*, *56*, 191-198.

Honjo, S., R. François, S. Manganini, J. Dymond, and R. Collier (2000), Particle fluxes to the interior of the Southern Ocean in the Western Pacific sector along 170° W, *Deep-Sea Research II*, *47*(15-16), 3521-3548.

Howard, W. R., and W. L. Prell (1994), Late Quaternary $CaCO_3$ production and preservation in the Southern Ocean: Implications for oceanic and atmospheric carbon cycling, *Paleoceanography*, *9*(3), 453-482.

Jaccard, S. L., and E. D. Galbraith (2012), Large climate-driven changes of oceanic oxygen concentrations during the last deglaciation, *Nat. Geosci.*, *5*(2), 151-156.

Jaccard, S. L., C. T. Hayes, A. Martínez-García, D. A. Hodell, R. F. Anderson, D. M. Sigman, and G. H. Haug (2013), Two modes of change in Southern Ocean productivity over the past million years, *Science*, *339*(6126), 1419-1423.

Kanfoush, S. L., D. A. Hodell, C. D. Charles, T. R. Janecek, and F. R. Rack (2002), Comparison of ice-rafted debris and physical properties in ODP Site 1094 (South Atlantic) with the Vostok ice core over the last four climatic cycles, *Paleogeogr. Paleoclimatol. Paleoecol.*, *182*, 329-349.

Keeling, R. F., and B. B. Stephens (2001), Antarctic sea ice and the control of Pleistocene climate instability, *Paleoceanography*, *16*(1), 112-131.

Keigwin, L. D. (1998), Glacial-age hydrography of the far northwest Pacific Ocean, *Paleoceanography*, *13*(4), 323-339.

Keigwin, L. D. (2004), Radiocarbon and stable isotope constraints on Last Glacial Maximum and Younger Dryas ventilation in the western North Atlantic, *Paleoceanography*, *19*, PA4012, doi: 10.1029/2004PA001029.

Keigwin, L. D., and M. A. Schlegel (2002), Ocean ventilation and sedimentation since the glacial maximum at 3 km in the western North Atlantic, *Geochemistry Geophysics Geosystems*, *3*(6), doi: 10.1029/2001GC000283.

King, S. L., P. N. Froelich, and R. A. Jahnke (2000), Early diagenesis of germanium in sediments of the Antarctic South Atlantic: In search of the missing Ge sink, *Geochimica et Cosmochimica Acta*, *64*(8), 1375-1390.

Koide, M., V. F. Hodge, J. S. Yang, M. Stallard, E. G. Goldberg, J. Calhoun, and K. K. Bertine (1986), Some comparative marine chemistries of rhenium, gold, silver, and molybdenum, *Applied Geochemistry*, *1*(6), 705-714.

Kroopnick, P. M. (1985), The distribution of ^{13}C of ΣCO_2 in the world oceans, *Deep-Sea Research Part A-Oceanographic Research Papers*, *32*(1), 57-84.

Kumar, N. (1994), Trace metals and natural radionuclides as tracers of ocean productivity, Ph.D. thesis, 336 pp, Columbia University.

Kumar, N., R. F. Anderson, R. A. Mortlock, P. N. Froelich, P. Kubik, B. Dittrichhannen, and M. Suter (1995), Increased biological productivity and export production in the glacial Southern Ocean, *Nature*, *378*(6558), 675-680.

Li, Y.-H., and S. Gregory (1974), Diffusion of ions in sea water and in deep-sea sediments, *Geochimica et Cosmochimica Acta*, *38*(5), 703-714.

Mackensen, A., M. Rudolph, and G. Kuhn (2001), Late Pleistocene deep-water circulation in the subantarctic eastern Atlantic, *Global and Planetary Change*, *30*(3-4), 197-229.

Marchitto, T. M., S. J. Lehman, J. D. Ortiz, J. Flückiger, and A. van Geen (2007), Marine radiocarbon evidence for the mechanism of deglacial atmospheric CO_2 rise, *Science*, *316*(5830), 1456-1459.

Marinov, I., A. Gnanadesikan, J. R. Toggweiler, and J. L. Sarmiento (2006), The Southern Ocean biogeochemical divide, *Nature*, *441*(7096), 964-967.

Matsumoto, K., T. Oba, J. Lynch-Stieglitz, and H. Yamamoto (2002), Interior hydrography and circulation of the glacial Pacific Ocean, *Quaternary Science Reviews*, *21*(14-15), 1693-1704.

McKay, J. L., and T. F. Pedersen (2008), The accumulation of silver in marine sediments: A link to biogenic Ba and marine productivity, *Global Biogeochemical Cycles, 22*(GB4010), doi: 10.1029/2007GB003136.

Moore, J. K., and M. R. Abbott (2000), Phytoplankton chlorophyll distributions and primary production in the Southern Ocean, *Journal of Geophysical Research, 105*(C12), 28709-28722.

Morford, J. L., and S. Emerson (1999), The geochemistry of redox sensitive trace metals in sediments, *Geochimica et Cosmochimica Acta, 63*(11/12), 1735-1750.

Ninnemann, U. S., and C. D. Charles (2002), Changes in the mode of Southern Ocean circulation over the last glacial cycle revealed by foraminiferal stable isotopic variability, *Earth Planet. Sci. Lett., 201*(2), 383-396.

Orsi, A. H., T. I. Whitworth, and W. D. Nowlin, Jr. (1995), On the meridional extent and fronts of the Antarctic Circumpolar Current, *Deep-Sea Research I, 42*(5), 641-673.

Orsi, A. H., G. C. Johnson, and J. L. Bullister (1999), Circulation, mixing, and production of Antarctic Bottom Water, *Progress in Oceanography, 43*(1), 55-109.

Pedersen, T. F., R. D. Waters, and R. W. Macdonald (1989), On the natural enrichment of cadmium and molybdenum in the sediments of Ucluelet Inlet, British Columbia, *The Science of the Total Environment, 79*(2), 125-139.

Petit, J. R., et al. (1999), Climate and atmospheric history of the past 420,000 years from the Vostok ice core, Antarctica, *Nature, 399*(6735), 429-436.

Robinson, L. F., J. F. Adkins, L. D. Keigwin, J. Southon, D. P. Fernandez, S.-L. Wang, and D. S. Scheirer (2005), Radiocarbon variability in the western North Atlantic during the last deglaciation, *Science, 310*(5753), 1469-1473.

Rosenthal, Y., P. Lam, E. A. Boyle, and J. Thomson (1995a), Authigenic cadmium enrichments in suboxic sediments: Precipitation and postdepositional mobility, *Earth Planet. Sci. Lett., 132*(1-4), 99-111.

Rosenthal, Y., E. A. Boyle, L. Labeyrie, and D. Oppo (1995b), Glacial enrichments of authigenic Cd and U in Subantarctic sediments: A climatic control on the elements' oceanic budget?, *Paleoceanography, 10*(3), 395-413.

Sachs, O., E. J. Sauter, M. Schlüter, M. M. R. v. d. Loeff, K. Jerosch, and O. Holby (2009), Benthic organic carbon flux and oxygen penetration reflect different plankton provinces in the Southern Ocean, *Deep-Sea Research I, 56*(8), 1319-1335.

Scott, C., and T. W. Lyons (2012), Contrasting molybdenum cycling and isotopic properties in euxinic versus non-euxinic sediments and sedimentary rocks: Refining the paleoproxies, *Chemical Geology, 324-325*, 19-27.

Shemesh, A., D. Hodell, X. Crosta, S. Kanfoush, C. Charles, and T. Guilderson (2002), Sequence of events during the last deglaciation in Southern Ocean sediments and Antarctic ice cores, *Paleoceanography, 17*(4), 1056, doi: 10.1029/2000PA000599.

Shipboard Scientific Party (1999a), Leg 177 summary: Southern Ocean paleoceanography, in *Proc. ODP., Init. Rpts.*, edited by R. Gersonde, D. A. Hodell and P. Blum, pp. 1-67, Ocean Drilling Program, College Station, TX.

Shipboard Scientific Party (1999b), Site 1094, in *Proc. ODP, Init. Repts.*, edited by R. Gersonde, D. A. Hodell and P. Blum, pp. 1-73, Ocean Drilling Program, College Station, TX.

Sigman, D. M., and E. A. Boyle (2000), Glacial/interglacial variations in atmospheric carbon dioxide, *Nature, 407*(6806), 859-869.

Sikes, E. L., C. R. Samson, T. P. Guilderson, and W. R. Howard (2000), Old radiocarbon ages in the southwest Pacific Ocean during the last glacial period and deglaciation, *Nature, 405*(6786), 555-559.

Skinner, L. C., S. Fallon, C. Waelbroeck, E. Michel, and S. Barker (2010), Ventilation of the deep Southern Ocean and deglacial CO_2 rise, *Science, 328*(5982), 1147-1151.

Stephens, B. B., and R. F. Keeling (2000), The influence of Antarctic sea ice on glacial-interglacial CO_2 variations, *Nature, 404*(6774), 171-174.

Stuut, J.-B. W., X. Crosta, K. van der Borg, and R. Schneider (2004), Relationship between Antarctic sea ice and southwest African climate during the late Quaternary, *Geology*, *32*(10), 909-912.

Talley, L. D. (2008), Freshwater transport estimates and the global overturning circulation: Shallow, deep, and throughflow components, *Progress in Oceanography, 78*, 257-303.

Toggweiler, J. R. (1999), Variation of atmospheric CO_2 by ventilation of the ocean's deepest water, *Paleoceanography, 14*(5), 571-588.

Tribovillard, N., T. J. Algeo, T. Lyons, and A. Riboulleau (2006), Trace metals as paleoredox and paleoproductivity proxies: An update, *Chemical Geology*, *232*(1-2), 12-32.

Vandergoes, M. J., et al. (2012), A revised age for the Kawakawa/Oruanui tephra, a key marker for the Last Glacial Maximum in New Zealand, *Quaternary Science Reviews*, http://dx.doi.org/10.1016/j.quascirev.2012.1011.1006.

Zheng, Y., R. F. Anderson, A. van Geen, and J. Kuwabara (2000), Authigenic molybdenum formation in marine sediments: A link to pore water sulfide in the Santa Barbara Basin, *Geochimica et Cosmochimica Acta*, *64*(24), 4165-4178.

Chapter 5

Characterizing Ag Uptake and Storage in the Marine Diatom *Thalassiosira pseudonana*: Implications for Ag Biogeochemical Cycling

Abstract

It has been hypothesized that diatoms accumulate Ag within their silica frustules, subsequently delivering Ag to underlying sediments as the organisms die and sink to the seafloor. Through this delivery mechanism, sedimentary Ag concentrations might serve as a useful record of past export production. However, the actual partitioning of Ag between diatom organic and frustule parts is unknown, and as such represents a considerable source of uncertainty in the development of Ag as a paleoproductivity proxy. Here we demonstrate using two different analytical methods that diatoms primarily store Ag in the organic fraction, with ≤ 8% of total Ag associated with the frustule matrix. Intracellular Ag appears to be concentrated in vacuoles, although the majority of Ag is widely distributed and likely associated with the cell membrane. These results therefore imply an alternate mechanism for marine Ag biogeochemical cycling whereby Ag is associated with decomposing organic particles rather than skeletal remains. Silver shows promise as a qualitative paleoproductivity proxy, but quantitative use is unlikely given variable uptake rates by diatoms in response to environmental conditions and the significant potential for remineralization in the water column.

1. Introduction

Diatoms—phytoplankton notable for their construction of a siliceous test—are

responsible for ~40% of total marine primary productivity [*Tréguer et al.*, 1995], making them significant players in the global carbon cycle. More importantly, diatoms are the dominant phytoplankton group in the Southern Ocean [*Ragueneau et al.*, 2000], an oceanic region where they influence the partitioning of carbon between its atmospheric and deep ocean reservoirs by a process known as the biological pump [*Marinov et al.*, 2006]. In surface waters, phytoplankton fix inorganic carbon as organic matter, which is subsequently transported to the deep ocean as the organisms die and sink. Once buried in sediments, organic matter can be removed from short term cycling; however, the majority of organic matter is respired back to CO_2 in the deep ocean where it may be stored for hundreds of years or longer [*Sarmiento and Gruber*, 2006]. The ability of diatoms and other phytoplankton to thus measurably impact carbon geochemical cycling—and by extension, global climate—has encouraged efforts to quantify the strength of the biological pump by reconstructing past export production. A solid quantitative understanding of biological pump strength is vital for accurate biogeochemical modeling experiments. One common approach to biological pump reconstruction measures bulk concentrations of proxies preserved in marine sediments, such as biogenic silica, calcium carbonate, and organic carbon. However, these proxies are subject to preservation bias as all undergo dissolution or degradation in the water column and at the sediment-water interface. Thus a new proxy that can accurately record phytoplankton export production and resist chemical remineralization has been sought.

Silver has been proposed as such a proxy for diatom export production in reducing environments [*Friedl and Pedersen*, 2001]. Open ocean water column measurements of dissolved Ag versus silica [*Flegal et al.*, 1995] and laboratory culture experiments [*Fisher and Wente*, 1993] suggest that diatoms might deliver Ag to sediments through Ag incorporation into their frustules. Friedl and Pedersen [2001] further hypothesized that at the seafloor, dissolution

of the biogenic silica carrier phase releases the bound Ag, and in the presence of dissolved sulfide, it precipitates as highly insoluble Ag_2S. Although some studies suggest that Ag might indeed be a reliable (paleo)productivity proxy [*Hendy and Pedersen*, 2005; *McKay and Pedersen*, 2008], Ag incorporation into the silica matrix of frustules has never been rigorously tested. Arguing against this hypothesis is the fact that Ag prefers soft bases such as S over O [*Nieboer and Richardson*, 1980]. Silver concentrations also correlate with organic carbon in marine sediments [*Böning et al.*, 2004; *McKay and Pedersen*, 2008] and open ocean waters [*Martin et al.*, 1983] suggesting instead that Ag associates with diatom soft parts. Accurate interpretation of Ag as a proxy requires a thorough understanding of its biogeochemical cycling, and the chemical and physical processes that control its water column distributions and accumulation in sediments.

In this study, we test the hypothesis that diatoms store Ag in their frustules for the first time, and show that most Ag accumulates intracellularly in the organic fraction. Subsequently we propose a modified mechanism by which Ag accumulates in marine sediments and suggest constraints on using Ag to record diatom export production. The location of Ag storage was investigated in both bulk cellular material and single cells. Rigorous quantitative results were not achieved, but qualitative results provide significant insight into how and where diatoms store Ag that should guide future development of Ag as a paleoproductivity proxy.

2. Methods

2.1 Bulk Diatoms

An axenic starter culture of the marine diatom *Thalassiosira pseudonana* (CCMP1014) was obtained from the Provasoli-Guillard National Center for Culture of Marine Phytoplankton (CCMP). Cultures were grown in 250-mL polycarbonate centrifuge bottles in f/2 medium

(CCMP) and maintained as batch cultures at approximately 23°C in the laboratory. Light was provided by two 26 W compact fluorescent light bulbs set on a 14:10 hour light:dark cycle, providing 50 µmol quanta m^{-2} s^{-1}. New centrifuge bottles were filled with 1 M HCl and allowed to stand for one week in order to remove any trace metals from the manufacturing process. Afterward, bottles were rinsed with double distilled water and microwave sterilized [*Keller et al.*, 1988]. All other plastic containers used for digestions were acid cleaned by filling with 1 M HCl and leaving in a 60°C oven overnight. Pipette tips were acid cleaned in a 3 M HNO_3 acid bath followed by a 1% trace metal grade HNO_3 bath, rinsed with double distilled water, and microwave sterilized.

Several transfers of cells to fresh growth medium were made before experiments commenced in order to establish a robust collection of cells and to acclimate cells to laboratory conditions. For each experimental culture, 1 mL of growth medium containing diatom cells was transferred to fresh medium and inoculated with $AgNO_3$ in a darkened hood to achieve nominal total Ag concentrations of 4, 12, 20, 32, and 48 nM ("regular" cultures). Control cultures contained no added Ag. Cultures were not stirred and culture vessels were loosely capped to allow gas exchange [*Yee and Morel*, 1996]. Cultures were monitored using optical density spectrometry to estimate when exponential growth was achieved. Approximately 24 hours after the onset of exponential growth, cells were collected by vacuum filtration onto 0.8 µm polycarbonate Isopore filters and washed with double distilled water to remove any adhering salts. Five mL of 1 mM diethylenetriaminepentaacetic acid (DTPA) was then added to each well of the filtration apparatus and allowed to stand for 10 minutes. DTPA is a good chelator for soft metals [*Hutchins et al.*, 1999] and was intended to remove any easily exchangeable Ag, especially Ag adsorbed to frustule surfaces. The DTPA solution was collected and saved for later

analysis. Cells were washed again with double distilled water and the filters were removed. Filters containing the diatoms were then placed into dry, acid-cleaned 50-mL centrifuge tubes and left in a 60°C oven overnight to dry.

Following published methods [*Ellwood and Hunter*, 2000], 4 mL of 50% w/w trace metal grade HNO_3 was added to each centrifuge tube and vortexed to mix. The centrifuge tubes were then placed in a 75°C oven for 1 hour, removed, vortexed again, and allowed to cool. Two 500-µL aliquots were taken from each tube for phosphate determination. The remaining HNO_3 solutions making up the organic fractions were centrifuged at 3500 rpms for 10 minutes and decanted into clean 50-mL centrifuge tubes. Frustules were washed three times with double distilled water and placed in a 65°C oven overnight to dry. Organic fractions were heated to evaporate the acid and 1 mL 30% H_2O_2 was added to each tube, sonicated, and allowed to stand for 1 hour. The samples were then heated again to remove the H_2O_2 and the remaining dry organics were re-dissolved in 1 mL 1% w/w trace metal grade HNO_3. Dry frustules were digested in 5 mL 1% w/w NaOH in an 85°C oven for 5 hours, similar to the method of Mortlock and Froelich [1989]. After digestion, samples were vortexed and allowed to cool. 200 µL concentrated trace metal grade HNO_3 was then added to neutralize the NaOH, followed by 1 mL 1% w/w HNO_3.

One set of cultures (4, 12, 20, 32, and 48 nM) was also established to determine the total amount of Ag in diatoms without separating the different fractions ("Total" cultures). These samples were not washed with DTPA during cell collection, and the entirety of each sample was carried through the same digestion process as described above. Two other sets of cultures were also established to test whether photoreduction of Ag is important for accumulation in diatoms ("Dark" cultures) and whether abiotic uptake is occurring ("Kill" cultures). Dark cultures had no

Ag added to the growth medium until cultures reached exponential growth, at which time $AgNO_3$ was added to produce cultures with nominal total Ag concentrations of 12 and 48 nM. Culture vessels were wrapped in aluminum foil and stored in a drawer with loosely capped lids. Approximately 24 hours later, cells were collected as for regular cultures, except that collection was performed in a darkened room. Kill cultures also had no Ag added to the growth medium until cultures reached exponential growth. At that time, cultures were poisoned with $HgCl_2$ or salt and left for ~2 days to die. $AgNO_3$ was then added to cultures to produce nominal total Ag concentrations of 12 and 48 nM. Kill cultures were collected ~2 days later as for regular cultures.

All samples were analyzed for Ag concentration by inductively coupled plasma-mass spectrometry (ICP-MS). In some cases, high salt content in DTPA and frustules samples interfered with ICP-MS analysis. When this occurred, samples were evaporated to dryness, aqua regia was added to remobilize any precipitated Ag, dried again, and re-dissolved in 1 mL 0.5 M HCl. The first run was analyzed at the Michigan State University ICP-MS Laboratory and the second run was analyzed at the University of Michigan Keck Environmental Geochemistry Laboratory (KEGL). Reproducibility of Ag measurements at KEGL was 11% RSD based on repeated analysis of a 5% solution of NIST Natural Water Standard 1640. Standard reference material recovery at Michigan State University varied between 94-96%. Total culture samples were spiked with an In solution before ICP-MS analysis to correct for evaporative loss while samples were stored; however, a correction was ultimately not possible and therefore Ag concentrations in Total culture samples are reported as minimum concentrations.

Silver contents were normalized to P, a proxy for biomass that assumes relative nutrient content is constant across all cells. Aliquots taken for phosphate determination were neutralized with 1.2 mL 5 M NaOH. Two mL 5% w/v potassium persulfate was added to oxidize any

organically bound P [*Menzel and Corwin*, 1965], and samples were diluted to 30 mL with double distilled water. Phosphate concentrations were determined by the method of Parsons et al. [1984]. Reproducibility of phosphate measurements was estimated as the relative standard deviation of the F value calculated from the three standards required by the method over a period of nine months (6.5% RSD).

2.2 Single Diatom Cells

Diatoms were also analyzed as single cells because while bulk analysis can reveal relative accumulation in various components, it cannot unequivocally establish chemical or spatial relationships. To address the latter we utilized a synchrotron micro-XRF microprobe to map cellular Ag distributions and explore any association with organelles or structural components. This analytical technique is ideal due to submicrometer beam dimensions and high brightness and brilliance of the synchrotron x-ray source that allow high sensitivity and spatial resolution [*Sutton et al.*, 2002]. Use of an x-ray source is also preferred for biological samples because electrons used in other microprobes are readily absorbed by light elements [*Twining et al.*, 2008].

Diatoms were cultured as for bulk experiments except that diatoms were first acclimated to Ag by transferring cells into fresh cultures containing ~300 nM and ~1 μM Ag in succession. For each experimental culture, 1 mL of growth medium containing Ag-acclimated diatom cells was transferred to fresh medium and $AgNO_3$ was added to produce nominal total Ag concentrations of 10, 50, 100, 200, and 500 ppb. However, cells grown at 200 ppb and 500 ppb Ag visually appeared to suffer from Ag toxicity and were not further investigated for Ag uptake. Silver has previously been shown to slow the growth rate of *T. pseudonana* to 50% of a control culture (i.e., EC_{50}) at ambient Ag concentrations ~1 μM [*Fisher et al.*, 1984]. Culture growth

was monitored by optical density spectrometry, and ~24 hours after exponential growth was achieved, diatoms were harvested by removing a 10 mL aliquot to a clean 50 mL centrifuge tube. Two mL of trace metal-cleaned, 10% glutaraldehyde [*Price et al.*, 1988/1989] was added to each sample and allowed to stand 3 days in a hood. Samples were then centrifuged, decanted, and washed three times with double distilled water, and subsequently resuspended in 500 μL double distilled water. Sample preparation followed published methods [*Twining et al.*, 2003] with the modification that cells were mounted on 400-mesh Au London Finder grids coated with a Formvar/C film (Electron Microscopy Sciences) using a 10 μL pipette instead of by centrifugation. Mounted drops were allowed to dry, after which samples were examined under an optical light microscope, and potential target cells were recorded.

Samples were analyzed at the 2-ID-D hard x-ray microprobe at the Advanced Photon Source, Argonne National Laboratory, according to the method developed by Twining et al. [2003]. A beam energy of 25.5 keV was chosen for Ag and 10 keV for other elements to excite Kα x-ray fluorescence. The x-ray beam was focused to a spot size of 0.56 μm × 0.36 μm for Ag analyses, and 0.2 μm × 0.2 μm for other elements. Target cells were scanned stepwise to give a pixel size of 0.15 μm x 0.15 μm and provide for some oversampling. Live time was 5 s for Ag and 1.5 s for other elements to ensure adequate counts. Calibration curves for converting peak areas to concentrations were constructed using standards made in-house (Ag) or NIST thin-film standards SRM 1832 and 1833 (other elements). Silver standards were made by placing a 1 μL drop of gravimetrically diluted Ag ICP standard (Ricca Chemical Company) onto a SiN window and allowing it to dry. Comparison of measured Ag standards with the expected mass of Ag deposited on the SiN window suggests that the quantified mass may be low by about a factor of two. However, the error appeared to be systematic.

Spectra were fit and elemental maps were created using the MAPS program (v1.7.3.05) [*Vogt*, 2003]. The program further allows elemental concentrations in the total cell and in hotspots to be quantified by user-defined regions of interest (ROIs). Beam time was insufficient to re-analyze cells, so no precision estimate for Ag measurements is possible. Precision of the synchrotron XRF method was previously estimated for Fe (0.9-1.5% RSD), Zn (0.9-8.3% RSD), and Si (0.2-2.4% RSD) [*Twining et al.*, 2003]. Previously, P quotas were also quantitatively determined for *T. pseudonana* and were not found to differ significantly from those measured using other methods [*Núñez-Milland et al.*, 2010].

3. Results

3.1 Bulk Diatoms

Most experimental cultures (i.e., those to which Ag was added to the growth medium) were set up in triplicate, although cultures at a given Ag concentration were spread between runs that were begun at different times. This produced inconsistent quantitative results between experimental runs, due to differences in the growth state of the seed culture. Qualitative results, however, are consistent. It is also therefore not possible to accurately compare the amount of Ag in Total cultures to the amount of Ag measured in one sample for the organics, frustules, and easily exchanged fractions combined. However, consistently lower Ag contents (nmol) calculated as the sum of organics, frustules, and easily exchanged (DTPA wash) fractions suggests some loss of Ag to culture vessel walls. Silver and P data for each experimental culture are given in Table 5.1.

Separating results by each time that experimental cultures were set up (run), Ag enrichment (Ag/P ratios) at each experimental concentration was averaged for each fraction—organics, frustules, and easily exchanged. For the organics and easily exchanged fractions, Ag/P

ratios at 48 nM from the first run were conspicuously higher than Ag/P ratios at lower growth medium Ag concentrations, and also higher than the Ag/P ratio at 48 nM from the second run. Because these high ratios may be in error, we have chosen to concentrate our analysis on Ag/P ratios from the second run. Ag/P ratios in the organics and easily exchanged fractions (Figures 5.1 and 5.2) show a strong linear correlation with growth medium Ag concentration when a regression line is fit to the data (R^2 = 0.98 and 0.95, respectively). Conversely, Ag/P ratios in the frustules fraction from the second run (Figure 5.3) show a weak linear correlation with growth medium Ag concentration (R^2 = 0.60). The organic fraction shows the greatest enrichment, with Ag/P ratios about an order of magnitude higher than the easily exchanged fraction. Silver enrichment in the frustules fraction from the second run is nearly absent, suggesting little to no Ag in diatom frustules. Total cellular Ag enrichment—including synchrotron-measured data at 927 nM—increases linearly (R^2 = 1) with growth medium Ag concentration (Figure 5.4, Table 5.2).

The percentage of Ag in each fraction was estimated by dividing Ag contents (nmol) in the organics, easily exchanged, or frustules by the total Ag (sum of all three fractions) for each culture from the second run in Table 5.1. The average amount of Ag in the organics fraction was found to be 93 ± 2% (1σ standard deviation), in the easily exchanged fraction 7 ± 2%, and in the frustules fraction 0.02 ± 0.37%. Control cultures were not included in averages. Silver contents in frustules were low enough that measured concentrations for samples at 0 and 4 nM were below the machine detection limit and so should not be considered reliable.

Phosphorus measurements for Kill and Dark cultures were extremely low. Kill cultures disintegrated rapidly after addition of poison, and Ag/P ratios (Table 5.3) are probably inflated.

However, we can compare the amount of Ag (nmol) in Kill and Dark cultures to those in regular cultures, assuming that a similar biomass of diatoms was achieved by the time cultures were

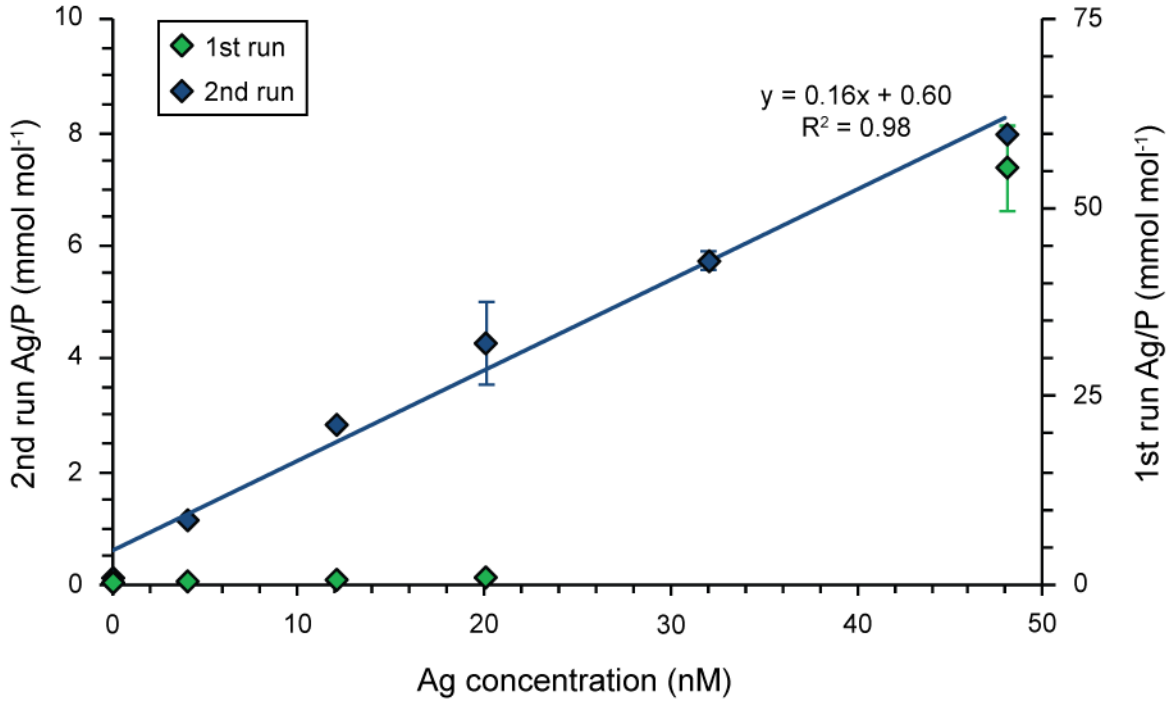

Figure 5.1. Ag enrichment (Ag/P ratios) in diatom organic matter for bulk culture samples. Replicate cultures were established at different times (see Table 5.1) and data are plotted as first run (green symbols) and second run (blue symbols) accordingly. Individual data points are averages of all cultures measured at a given Ag concentration for the appropriate run, and error bars show 1σ standard deviation where possible. A linear regression line was fit to the data from the second run.

collected—a reasonable assumption since all cultures were treated identically. For Dark cultures, Ag contents in the easily exchanged and organics fractions are the same order of magnitude as regular cultures; Ag contents in frustules are lower in Dark cultures. These results suggest that light, and hence photoreduction, is not important for Ag accumulation in diatoms. Silver contents in cultures killed with salt are more similar to regular cultures, although Ag contents in 48 nM cultures are an order of magnitude lower than regular cultures. Silver contents in cultures killed with Hg are at least an order of magnitude lower than regular cultures. Lowered Ag contents in Kill cultures suggest that biogenic uptake does play a role in diatom Ag accumulation, but Ag accumulation greater than that in control cultures suggests that abiogenic uptake may also occur.

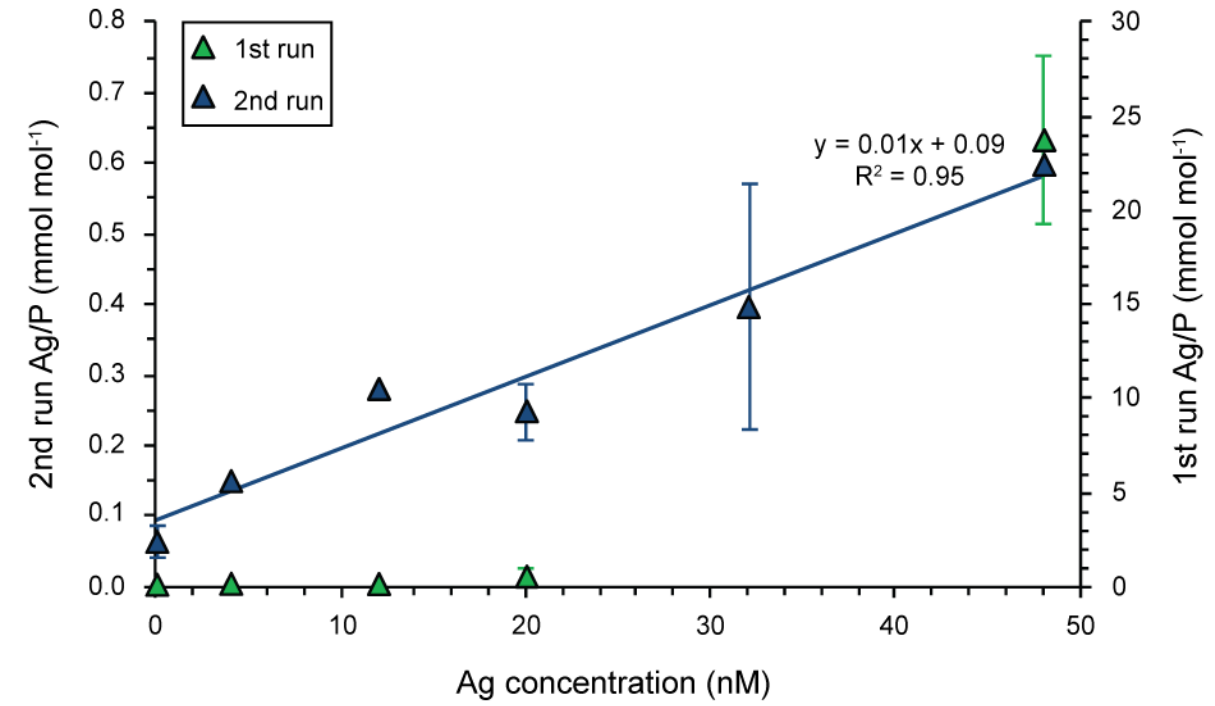

Figure 5.2. Ag enrichment (Ag/P ratios) in easily exchanged fraction for bulk culture samples. Data plotted as for Figure 5.1.

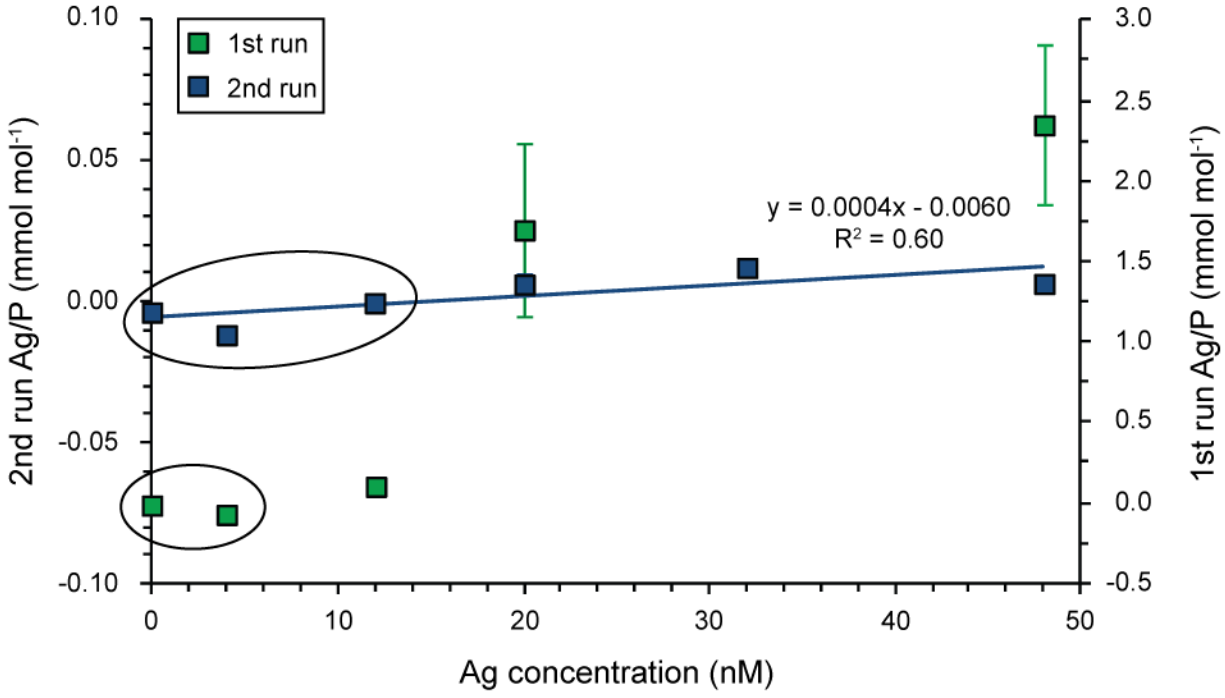

Figure 5.3. Ag enrichment (Ag/P ratios) in diatom frustules for bulk culture samples. Data plotted as for Figure 5.1. Circles around data points indicate that these samples were below the analytical detection limit.

3.2 Single Diatom Cells

Detection limits for Ag (and other elements) were determined as the average of 3 times the standard deviation of 15 background scans [*Twining et al.*, 2003] and are reported in Table 5.4. False color images of areal Ag concentration in single diatom cells show 1-2 Ag "hotspots" inside each cell (Figure 5.5). Mean areal hotspot Ag concentrations are 1.7-3.3 times greater than the average areal total Ag concentration (Table 5.5), indicating measurable localization of Ag in hotspots. However, in 3 of 4 cells measured, less than half of total cellular Ag resides inside hotspots (Table 5.5), and the remainder must therefore be dispersed intracellularly.

Except for one hotspot, Ag/P ratios are only 1.3-1.5 times greater than Ag/P ratios in the average total cell (Table 5.5), further implying Ag localization with P. Additionally, the areal cellular Ag distribution is more similar to the areal cellular P distribution than the Si distribution (Table 5.6), suggesting that Ag is localized in the same areas as P—i.e., part of the organic fraction. The amount of Ag outside of areas containing P is estimated to be no more than ~8% (Table 5.6), in agreement with bulk culture measurements indicating very low Ag concentrations in diatom frustules.

Other elements show a more centralized single hotspot (Figure 5.5), similar to previous observations [*Nuester et al.*, 2012; *Twining et al.*, 2004]. Areal concentrations of Fe, Zn, and S are up to 3.5 times higher inside hotspots compared to the total cell, although element/P ratios inside hotspots are approximately equal to or slightly lower than element/P ratios for the total cell (Table 5.7). Like Ag, a significant proportion of cellular Fe, Zn, and S is estimated to be unassociated with hotspots. In all four cells measured, at high energy (25.5. keV) Ag is possibly co-localized with Fe; at low energy (10 keV) Fe appears to be co-localized with Zn, S, and P. This pattern suggests that all five elements may be co-located, but because cells had to be

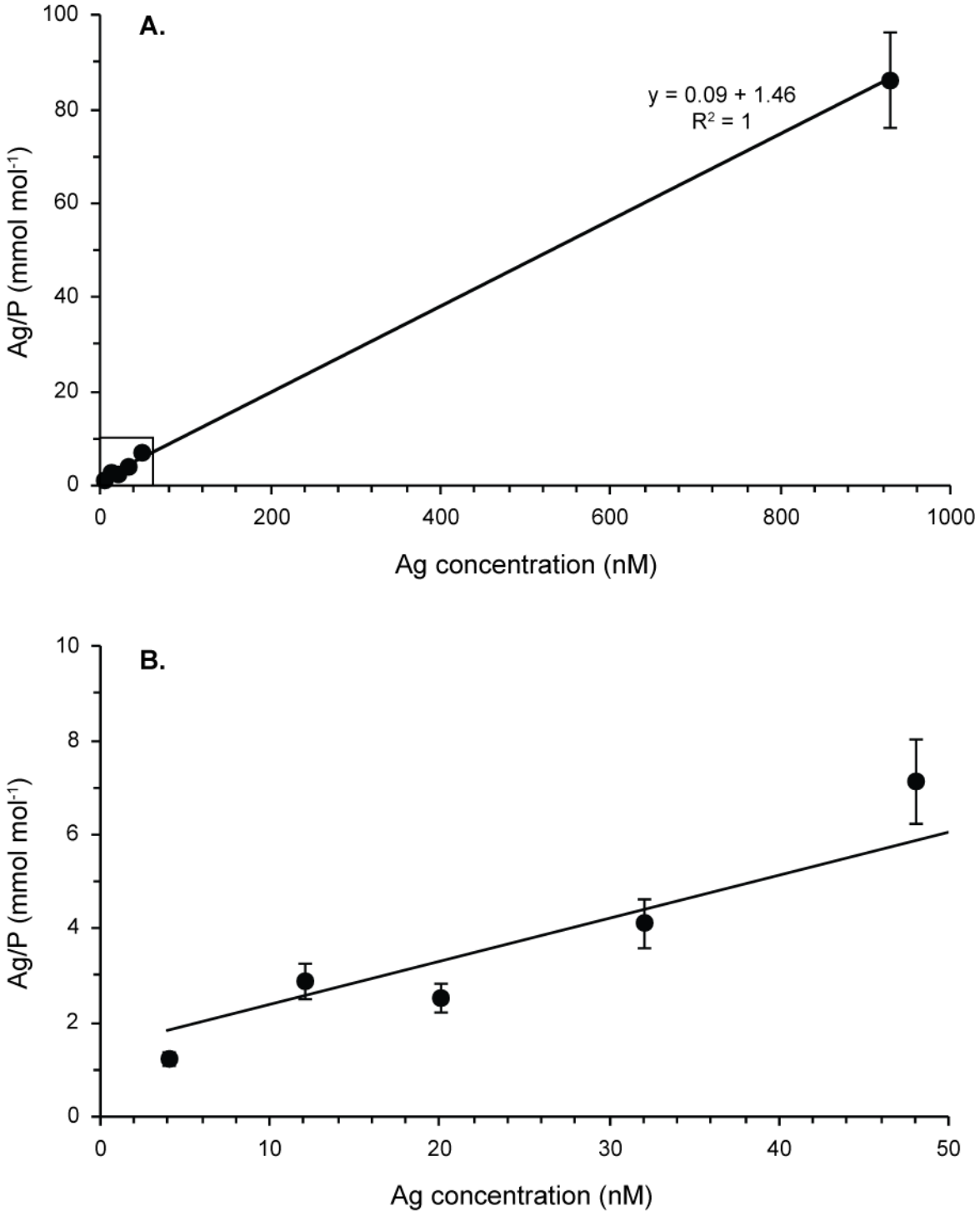

Figure 5.4. Total cellular Ag enrichment (Ag/P ratios), including data collected by synchrotron micro-XRF at 927 nM. Panel B is expansion of lower left corner of panel A. Error bar at 927 nM is one standard deviation of Ag/P measurements of four cells. Error bars for other points are propagated RSD of repeated measurement of NIST standards (10.7% RSD) for Ag and house-made standards (6.5% RSD) for P.

scanned twice, co-localization of Ag with other elements cannot be stated conclusively. No correction can be made for the possibility that Ag and nutrient element hotspots may actually be stacked on top of one another in 3-D space, and no chemical bonding of Ag with other elements can be shown by XRF. Total cellular contents for Ag, Fe, Zn, P, Si, and S are given in Table 5.8.

4. Discussion

Determining whether Ag delivery to marine sediments by diatoms occurs via the silica matrix of frustules or via organic matter has important implications for our understanding of Ag biogeochemical cycling and the reliability of Ag as a (paleo)productivity proxy. Silver concentrations in the open ocean are low (pM) [e.g., *Ndung'u et al.*, 2001], yet Ag can be enriched up to 15 times above lithogenic background in suboxic sediments [*McKay and Pedersen*, 2008]. Given that our results show primary Ag storage in the organic fraction of diatoms and very little Ag in the frustule fraction, delivery of organic matter to the seafloor must participate in concentrating Ag in marine sediments. The exact mechanism of Ag enrichment remains elusive; however, pinpointing where intracellular retention of Ag occurs allows us to begin to unravel its biogeochemical cycling in marine systems.

4.1 Comparison of Elemental Composition

Phytoplankton metal quotas are known to depend on factors such as ambient nutrient conditions, growth state [*Sunda and Huntsman*, 1998], and species [*Ho et al.*, 2003]. Variable experimental conditions therefore produce quantitative differences between our results and other studies measuring phytoplankton elemental concentrations. Nevertheless, such comparisons form a useful starting point for understanding Ag interaction with diatoms and support our approach using both bulk cultures and single cells.

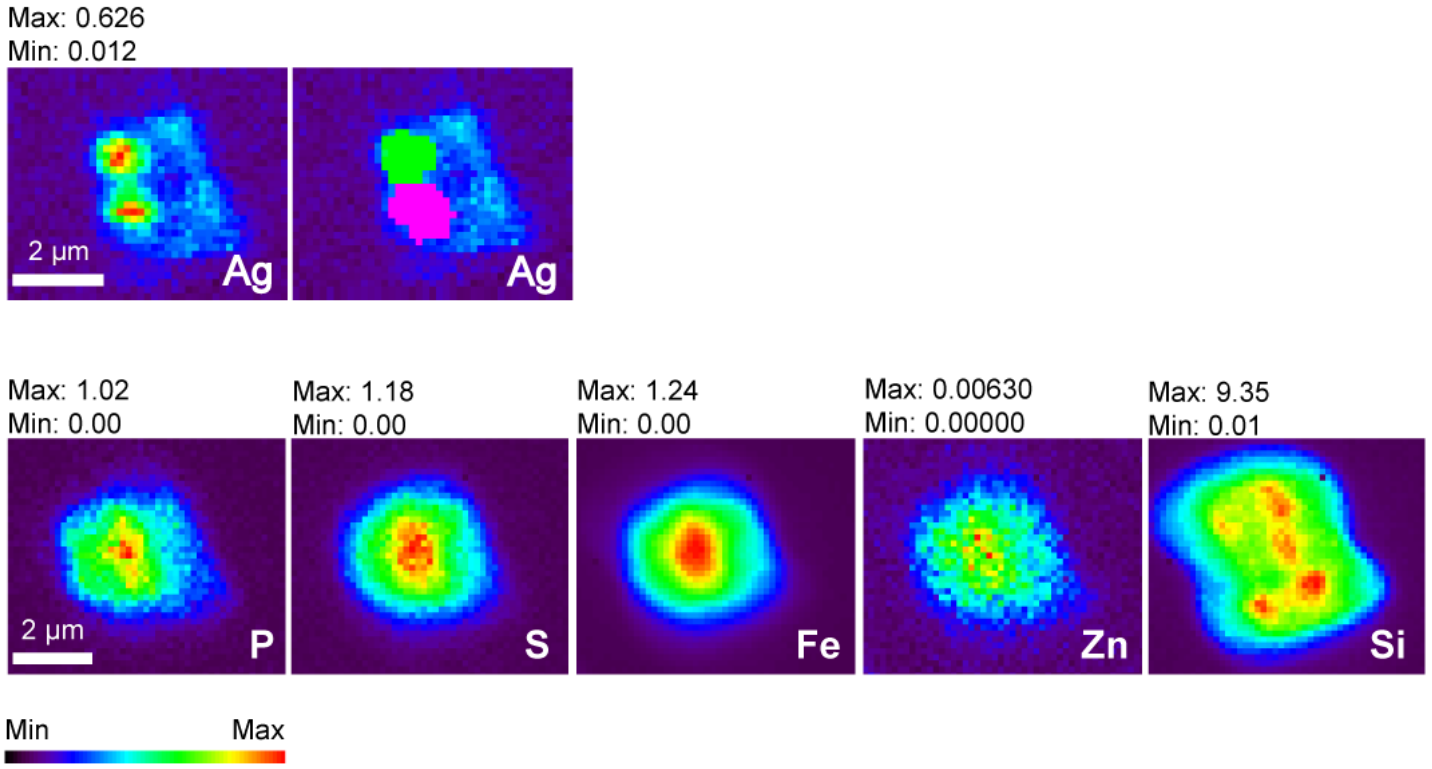

Figure 5.5. False-color images of element concentrations measured by synchrotron micro-XRF in a single diatom cell (Cell 2). Scale bar in Ag image (25.5 keV) is the same for both images in top row. Scale bar in P image (10 keV) is the same for all five images in the bottom row. MAPS program scales each panel to maximum concentration, so color scale is specific to each image. Concentrations given in µg cm^{-2}.

Silver concentrations measured in both wild and cultured cells support our conclusion that Ag is associated with organic matter. An analysis of phytoplankton collected in Monterey Bay, California, found detectable Ag concentrations only in the organic fraction [*Martin and Knauer*, 1973], similar to our bulk culture results. In another experiment, total Ag accumulation was measured in bulk cultures of *T. pseudonana*, although the method used could not determine the location of Ag storage [*Fisher et al.*, 1984]. Silver content per cell was found to increase in a log-linear fashion with Ag concentration in solution. Applying the relationship derived for *T. pseudonana* (their Table 3) at 927 nM yields an expected value of 1.1×10^{-15} mol Ag cell^{-1}, comparing well with our measured mean value of 1.4×10^{-16} mol Ag cell^{-1} (Table 5.8).

Other intracellularly accumulated metals may provide additional clues to how diatoms manage Ag. Toxic metals such as Ag can enter the cell through pathways similar to those of micronutrient metals and compete for micronutrient metal coordination sites [*Sunda and Huntsman*, 1998]. Iron and Zn have been found in both the organic and silica fractions of phytoplankton [*Martin and Knauer*, 1973]. However, the amount in the silica fraction was no more than 13.6% (Fe) and 10.0% (Zn), and usually much less than this. These results are in general agreement with those of Ellwood and Hunter [2000], who found that only 1-3% of the total amount of Zn, and ~3% of the total amount of Fe taken up by *T. pseudonana* is incorporated into frustules. Mean Fe and Zn contents measured for this study (Table 5.8) are within an order of magnitude (Fe) or ~10 times lower (Zn) than previous synchrotron XRF measurements (1.10-1.91 $\times 10^{-14}$ g cell^{-1} and 1.33-6.62 $\times 10^{-15}$ g cell^{-1}, respectively) for wild centric diatoms [*Twining et al.*, 2003]. Thus our results are in reasonable agreement. However, total Fe accumulation approaching ~1 mol mol^{-1} Fe/P is much higher than what would be expected for a typical Redfield ratio [*Ho et al.*, 2003]. Because Ag was the primary focus of this study, no precautions

were taken during the experiment to avoid Fe contamination. It is also possible that such accumulation is luxury Fe storage [*Sunda and Huntsman*, 1995], as has been previously speculated for high Fe contents measured by synchrotron micro-XRF in *Thalassiosira* [*Nuester et al.*, 2012].

4.2 Internal Ag Localization

Bulk and single cell analyses indicate that phytoplankton do not store large quotas of metals—including Ag—in their skeletons. Silver may therefore be expected to reach the seafloor with decomposing organic particles, but the amount of Ag delivered is influenced by the susceptibility of Ag to ligand exchange and remineralization. Therefore determining Ag localization and probable chemical bonding with organelles or other structures can provide further insight into Ag biogeochemical cycling. Silver "hotspots" visible in micro-XRF element maps (Figure 5.5) imply that a non-negligible portion (Table 5.5) of intracellular Ag is localized. By analogy with Fe localization and storage in diatoms [*Nuester et al.*, 2012] we hypothesize that these hotspots are vacuoles, with the remainder of intracellular Ag residing within the cell membrane [*Reinfelder and Fisher*, 1991]. Silver is not a known required nutrient, but rather is toxic to phytoplankton [*Fisher et al.*, 1984; *Ratte*, 1999], prompting the question of why diatoms would accumulate intracellular Ag.

Phytochelatins may provide a partial answer. Phytochelatins are peptides with the general structure $(\gamma\text{-Glu-Cys})_n\text{-Gly}$ (where n = 2-11) that are widely used by phytoplankton and plants to detoxify heavy metals by chelation and sequestration inside a vacuole [*Zenk*, 1996]. Their production is induced in the presence of toxic metals, although Ag appears less effective in stimulating phytochelatin production at low concentrations typical of seawater [*Ahner and Morel*, 1995]. *T. pseudonana* possesses genes for phytochelatin production [*Armbrust et al.*,

2004], suggesting that the observed Ag hotspots may indeed be vacuoles where phytochelatins have sequestered Ag. Silver accumulation appears to be at least partially an abiotic process, as suggested by our Kill cultures and by accumulation in heat-killed cells [*Fisher et al.*, 1984]. Additional experiments support Ag uptake as a passive process that depends on both ambient chloride concentration [*Reinfelder and Chang*, 1999] and nutrient levels [*Xu and Wang*, 2004].

Micro-XRF element maps further suggest that Ag may be co-localized with other intracellular micronutrient metals (Fe, Zn) and macronutrient elements (S, P). These elements could be contained in nutrient storage vacuoles, organelles that have evolved in centric diatoms to accumulate nutrients during high-nutrient conditions for later use [*Falkowski et al.*, 2004; *Raven*, 1997]. The presence of nutrient storage vacuoles would lend further support to vacuolar Ag storage by phytochelatins although it is unclear why toxic and essential nutrient elements would be stored together. Silver co-localization with S could also indicate the presence of Ag_2S, but speciation cannot be ascertained by XRF.

4.3 Marine Ag Biogeochemical Cycling

Silver storage inside vacuoles and with the cell membrane suggests that mechanisms invoking Ag delivery to sediments by incorporation into the silica matrix of diatom frustules are incorrect. Instead Ag is likely transported to deep water and sediments with diatom-associated organic matter. This conclusion is supported by studies showing a strong relationship between Ag and carbon in the water column [*Martin et al.*, 1983] and surface sediments [*McKay and Pedersen*, 2008]. Culture experiments [*Fisher and Wente*, 1993] suggest that diatoms may be particularly efficient at transporting Ag to deep water, as their biodetritus retains Ag longer than other phytoplankton. This phenomenon is attributed to retention of Ag by refractory organic matter (proteins) making up the cell membrane [*Lee and Fisher*, 1993; *Reinfelder and Fisher*,

1991]. Here we propose a modified mechanism for Ag delivery to sediments that may also explain increasing water column Ag concentrations with depth, similar to that previously proposed by Zhang et al. [2004]. Diatoms take up Ag in the photic zone, and as diatoms die and begin to sink, easily exchanged or loosely bound Ag is lost to the upper water column. Some of the remineralized Ag is then scavenged by diatom biodetritus or other particles, possibly existing as a separate phase (for example, Ag_2S) [*McKay and Pedersen*, 2008] to that hypothesized for intracellular Ag hotspots. In deeper waters, increasing amounts of Ag are remineralized along with organic matter, with fewer particles available to scavenge remineralized Ag. Ultimately, only the Ag most tightly bound to highly refractive organic matter will be buried and preserved in sediments (Figure 5.6).

The complexities of Ag biogeochemical cycling are underscored by previous studies implicating biogenic silica as the carrier phase based on open ocean water column profiles of Ag and silica [*Flegal et al.*, 1995; *Kramer et al.*, 2011]. This observation may reflect Ag association with phases that remain bound to the frustule even in deep water. The linear relationship between Ag and silica noted in the Atlantic Ocean [*Flegal et al.*, 1995] changes to a nonlinear relationship below ~1000 m in the North Pacific [*Zhang et al.*, 2001], suggesting more than a simple control on Ag concentrations by diatoms. Precipitation of Ag_2S within oxygen minimum zones [*Kramer et al.*, 2011] and scavenging of remineralized Ag by decomposing biogenic particles [*Zhang et al.*, 2004] have both been posited as explanations for Ag concentrations in the Pacific Ocean. An additional factor may be that organic matter is remineralized faster than biogenic silica, with only ~1% of organic carbon [*Jahnke*, 1996] and ~10% of biogenic silica [*Ragueneau et al.*, 2000] reaching the seafloor. Differential remineralization rates therefore could also contribute to dissolved Ag concentrations rising faster than dissolved silica concentrations with depth.

Similarly to Ag, a linear relationship was noted for Zn and silica in water column profiles [*Bruland*, 1980], yet insufficient Zn was found in diatom frustules to account for these profiles [*Ellwood and Hunter*, 2000]. Together the Zn and Ag data suggest that the details of these elements' biogeochemical cycling are not well represented by metal versus silica profiles.

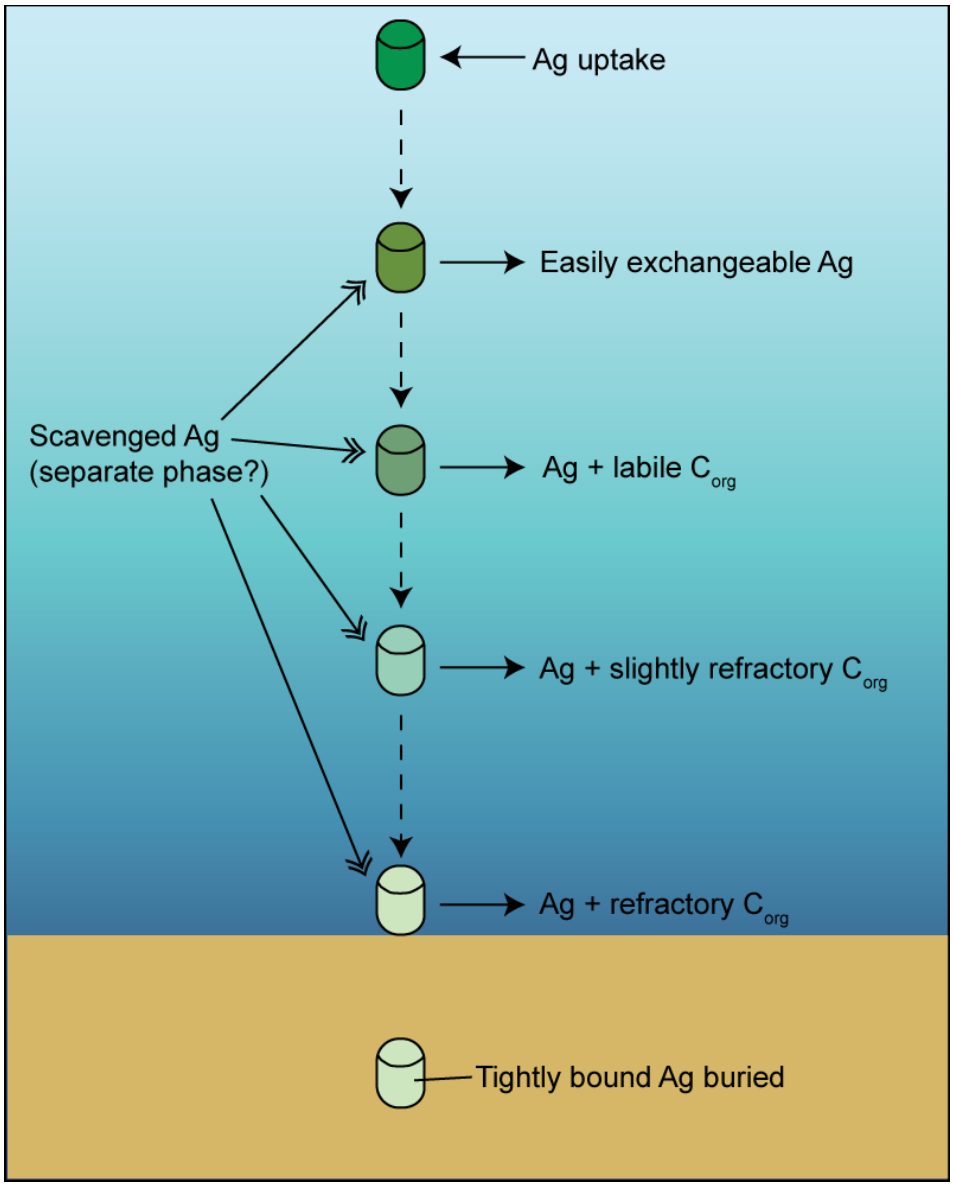

Figure 5.6. Cartoon depicting hypothesis for Ag transfer by diatoms from the surface ocean to deep water and sediments. Silver is also scavenged from the water column, and may be present in sinking particles as a different phase than Ag associated with diatom organic matter.

5. Conclusions

Two different analytical methods demonstrate that Ag is stored in the organic fraction of diatoms, contrary to previous hypotheses associating Ag with the inorganic silica matrix of the frustule. Single cell element maps reveal intracellular Ag localization, suggesting that phytochelatins sequester Ag inside one or more vacuoles as a detoxification mechanism. The remainder of the intracellular Ag is inferred to be associated with sulfhydryl groups in proteins comprising the cell membrane [*Reinfelder and Fisher*, 1991; *Reinfelder and Chang*, 1999]. Thus diatom organic matter is implied as the carrier phase for Ag delivery to marine sediments. In the open ocean, organic matter remineralization coupled with Ag scavenging is proposed to control Ag water column distributions.

Clarification of the Ag storage location in diatoms sheds new light on Ag biogeochemical cycling and contributes further evidence that sedimentary Ag potentially can serve as a reliable qualitative proxy for diatom export production. However, its use as a quantitative proxy is unlikely given that Ag uptake will likely vary depending on such factors such as diatom species, physical state of the diatom population, environmental conditions, etc., and the local balance between water column remineralization and scavenging of Ag. However, there is no evidence to suggest that these factors affect Ag partitioning between organic matter and frustules in surface waters. An association with diatom organic matter implies that in marine sediments, Ag and organic matter are likely to be preserved under similar conditions: high organic carbon flux, low bottom water oxygen, and high sedimentation rates. Silver may therefore be useful where organic carbon concentrations have not been measured, or as an additional productivity proxy to identify preservation biases in other commonly-used proxies such as biogenic silica. Pacific sector surface sediment studies [*Wagner et al., Earth and Planetary Science Letters, manuscript*

in revision; *Chapter 2*] suggest, however, that preservation of Ag may potentially be compromised by continued organic carbon remineralization at the seafloor and re-oxygenation of sediments after initial metal deposition. As early diagenesis of Ag in marine sediments is presently poorly characterized, future studies investigating the chemical reactions occurring should further improve the accuracy of Ag as a paleoproductivity proxy.

Acknowledgements. This study was supported by a Rackham Graduate Student Research Grant (Rackham Graduate School, University of Michigan) and a Scott Turner Award in Earth Sciences (Department of Earth and Environmental Sciences, University of Michigan) to MW, and a grant to ILH from the University of Michigan. Barry Lai (Argonne National Laboratory) provided beamline assistance in collecting the synchrotron micro-XRF element maps and fit the spectra. Karthik Anantharaman and Alex Voorhies assisted with data collection at the APS. The Advanced Photon Source at Argonne National Laboratory is a user facility operated for the U.S. Department of Energy Office of Science.

Table 5.1. Amounts of Ag and P in diatom fractions for all Regular cultures, and resulting Ag accumulation, given as Ag/P ratios. Stars by culture numbers indicate that these cultures were part of the first experimental run. No stars indicate that cultures were part of the second experimental run.

			Organics		*Exchanged*		*Frustules*	
Growth medium [Ag] (nM)	Culture #	P (μmol)	Ag (nmol)	Ag/P (mmol/mol)	Ag (nmol)	Ag/P (mmol/mol)	Ag (nmol)	Ag/P (mmol/mol)
0	1*	0.022	0.009	0.43	0.004	0.17	-0.0005	-0.021
	2	0.021	0.004	0.18	0.002	0.08		
	3	0.029	0.003	0.10	0.001	0.05	-0.0001	-0.004
4	1*	0.019	0.013	0.65	0.005	0.24	-0.0016	-0.081
	2*	0.025	0.014	0.56	0.005	0.20	-0.0022	-0.091
	3	0.016	0.019	1.16	0.002	0.15	-0.0002	-0.012
12	1*	0.029	0.027	0.94	0.005	0.18	0.0031	0.107
	2*	0.025	0.016	0.66	0.006	0.25	0.0024	0.098
	3	0.015	0.042	2.85	0.004	0.28	0.0000	-0.001
20	1*	0.018	0.022	1.22	0.016	0.88	0.0379	2.079
	2*	0.029	0.029	1.02	0.010	0.34	0.0378	1.314
	3	0.028	0.141	4.98	0.008	0.30	0.0001	0.002
	4	0.032	0.139	4.40	0.007	0.22	0.0003	0.009
	5	0.036	0.125	3.50	0.008	0.24	0.0003	0.007
32	1	0.038	0.211	5.59	0.008	0.20	0.0004	0.010
	2	0.016	0.094	5.73	0.008	0.52	0.0003	0.015
	3	0.018	0.109	5.93	0.009	0.48	0.0002	0.011
48	1*	0.017	0.998	59.57	0.452	26.98	0.0452	2.696
	2*	0.021	1.068	51.53	0.427	20.60	0.0415	2.002
	3	0.020	0.162	7.99	0.012	0.60	0.0001	0.006

Table 5.2. Total Ag enrichments in bulk cultures (growth medium [Ag] = 4-48 nM) and in single diatom cells (growth medium [Ag] = 927 nM = 100 ppb). Result for 927 nM is an average of 4 cells.

Growth medium [Ag] (nM)	Ag/P (mmol/mol)
4	1.25
12	2.90
20	2.54
32	4.14
48	7.16
927	86.38

Table 5.3. Amounts of Ag and P in diatom fractions for Kill and Dark cultures, and resulting Ag accumulation, given as Ag/P ratios.

			Organics		*Exchanged*		*Frustules*	
Growth medium [Ag] (nM)	Culture	P (μmol)	Ag (nmol)	Ag/P (mmol/mol)	Ag (nmol)	Ag/P (mmol/mol)	Ag (nmol)	Ag/P (mmol/mol)
12	dark	0.0007	0.067	100.63	0.0084	12.65	0.00011	0.168
	kill Hg	0.0005	0.007	14.55	0.0006	1.23	0.00000	0.008
	kill salt		0.017		0.0010		0.00020	
48	dark	0.0043	0.179	41.79	0.0181	4.22	0.00006	0.015
	kill Hg	0.0030	0.009	3.09	0.0006	0.20	0.00018	0.061
	kill salt		0.056		0.0027		-0.00009	

Table 5.4. Detection limits for elements measured by synchrotron micro-XRF microprobe.

Element	Detection limit (mol μm^{-2})
Ag	1.3×10^{-17}
Fe	4.0×10^{-18}
Si	1.0×10^{-16}
P	9.5×10^{-18}
S	9.2×10^{-18}
Zn	1.3×10^{-19}

Table 5.5. Ag concentration in hotspots (25.5 keV), and enrichment over total cellular concentrations.

	Average hotspot Ag concentration ($\mu g/cm^2$)	Enrichment factor compared to average total cell	Ag/P ratio in hotspots (mmol/mol)	Ag/P ratio in average total cell (mmol/mol)	Hotspot Ag/P enrichment factor compared to average total cell	% total Ag in hotspot
Cell 1	0.265 0.271	2.2 2.2	126.965 152.703	100.126	1.3 1.5	26.05 20.59
Cell 2	0.370 0.303	3.3 2.6	213.307 133.407	86.684	2.5 1.5	23.35 22.99
Cell 3	0.244 0.275	1.7 2.0	114.506 107.981	82.032	1.4 1.3	32.86 33.67
Cell 4	0.275	2.4	111.716	76.665	1.5	41.35

Table 5.6. Ag, P, and Si areas demonstrating that most Ag is located intracellularly (with P).

	Area (μm^2) [Si distribution]	Area (μm^2) [P distribution]	Area (μm^2) [Ag distribution]	Ag-P area (μm^2)	Ag outside P area (fg) [mean × area difference]	% of total Ag
Cell 1	28.5141	17.2867	18.4050	1.12	1.13	6.1
Cell 2	25.1726	14.5467	15.8175	1.27	1.25	8.0
Cell 3	21.4524	13.4106	11.6100	-1.80	-2.10	-15.5
Cell 4	21.5638	13.8784	11.6100	-2.27	-2.15	-19.5

Table 5.7. Fe, Zn, and S concentration in hotspots (10 keV), and enrichment over total cellular concentrations.

	Element	Average hotspot concentration (μg cm^{-2})	Enrichment factor compared to average total cell	Element/P ratio in hotspot (mmol mol^{-1})	Element/P ratio in average total cell (mmol mol^{-1})	Hotspot element/P enrichment factor compared to average total cell	% total in hotspot
Cell 1	Fe	1.038	2.8	949.836	1097.990	0.9	11.40
	Zn	0.007	2.6	5.222	6.514	0.8	10.57
	S	0.778	2.7	1239.517	1473.060	0.8	11.10
Cell 2	Fe	1.063	3.4	807.589	845.962	1.0	25.06
	Zn	0.004	3.3	2.539	2.787	0.9	23.91
	S	0.978	3.5	1294.149	1332.317	1.0	25.50
Cell 3	Fe	1.191	2.8	1002.749	1076.622	0.9	26.47
	Zn	0.007	2.7	4.806	5.377	0.9	25.41
	S	1.068	2.9	1566.397	1611.219	1.0	27.63
Cell 4	Fe	1.090	2.5	1056.226	1261.905	0.8	28.70
	Zn	0.007	2.7	5.993	6.678	0.9	30.77
	S	0.777	2.7	1310.928	1445.152	0.9	31.11

Table 5.8. Total elemental cellular contents.

Cell	Ag (g cell^{-1})	Fe (g cell^{-1})	Zn (g cell^{-1})	S (g cell^{-1})	Si (g cell^{-1})	P (g cell^{-1})
1	1.86×10^{-14}	1.05×10^{-13}	7.33×10^{-16}	8.12×10^{-14}	1.34×10^{-12}	5.33×10^{-14}
2	1.55×10^{-14}	7.84×10^{-14}	3.03×10^{-16}	7.09×10^{-14}	1.10×10^{-12}	5.14×10^{-14}
3	1.36×10^{-14}	9.22×10^{-14}	5.39×10^{-16}	7.92×10^{-14}	1.08×10^{-12}	4.75×10^{-14}
4	1.10×10^{-14}	9.39×10^{-14}	5.82×10^{-16}	6.17×10^{-14}	8.45×10^{-13}	4.13×10^{-14}
Average	1.47×10^{-14}	9.25×10^{-14}	5.39×10^{-16}	7.33×10^{-14}	1.09×10^{-12}	4.84×10^{-14}

REFERENCES

Ahner, B. A., and F. M. M. Morel (1995), Phytochelatin production in marine algae. 2. Induction by various metals, *Limnology and Oceanography*, *40*(4), 658-665.

Armbrust, E. V., et al. (2004), The genome of the diatom Thalassiosira pseudonana: Ecology, evolution, and metabolism, *Science*, *306*(5693), 79-86.

Böning, P., H.-J. Brumsack, M. E. Böttcher, B. Schnetger, C. Kriete, J. Kallmeyer, and S. L. Borchers (2004), Geochemistry of Peruvian near-surface sediments, *Geochimica et Cosmochimica Acta*, *68*(21), 4429-4451.

Bruland, K. W. (1980), Oceanographic distributions of cadmium, zinc, nickel, and copper in the North Pacific, *Earth Planet. Sci. Lett.*, *47*(2), 176-198.

Ellwood, M. J., and K. A. Hunter (2000), The incorporation of zinc and iron into the frustule of the marine diatom *Thalassiosira pseudonana*, *Limnology and Oceanography*, *45*(7), 1517-1524.

Falkowski, P. G., M. E. Katz, A. H. Knoll, A. Quigg, J. A. Raven, O. Schofield, and F. J. R. Taylor (2004), The evolution of modern eukaryotic phytoplankton, *Science*, *305*(5682), 354-360.

Fisher, N. S., and M. Wente (1993), The release of trace elements by dying marine phytoplankton, *Deep-Sea Research I*, *40*(4), 671-694.

Fisher, N. S., M. Bohé, and J.-L. Teyssié (1984), Accumulation and toxicity of Cd, Zn, Ag, and Hg in four marine phytoplankters, *Marine Ecology--Progress Series*, *18*, 201-213.

Flegal, A. R., S. A. Sañudo-Wilhelmy, and G. M. Scelfo (1995), Silver in the eastern Atlantic Ocean, *Marine Chemistry*, *49*(4), 315-320.

Friedl, G., and T. F. Pedersen (2001), Silver as a new tracer for diatom production, *EAWAG News*, *52*(D), 14-15.

Hendy, I. L., and T. F. Pedersen (2005), Is pore water oxygen content decoupled from productivity on the California Margin? Trace element results from Ocean Drilling Program Hole 1017E, San Lucia slope, California, *Paleoceanography*, *20*(PA4026), doi: 10.1029/2004PA001123.

Ho, T.-Y., A. Quigg, Z. V. Finkel, A. J. Milligan, K. Wyman, P. G. Falkowski, and F. M. M. Morel (2003), The elemental composition of some marine phytoplankton, *Journal of Phycology*, *39*(6), 1145-1159.

Hutchins, D. A., W.-X. Wang, M. A. Schmidt, and N. S. Fisher (1999), Dual-labeling techniques for trace metal biogeochemical investigations in aquatic plankton communities, *Aquatic Microbial Ecology*, *19*(2), 129-138.

Jahnke, R. A. (1996), The global ocean flux of particulate organic carbon: Areal distribution and magnitude, *Global Biogeochemical Cycles*, *10*(1), 71-88.

Keller, M. D., W. K. Bellows, and R. R. L. Guillard (1988), Microwave treatment for sterilization of phytoplankton culture media, *Journal of Experimental Marine Biology and Ecology*, *117*(3), 279-283.

Kramer, D., J. T. Cullen, J. R. Christian, W. K. Johnson, and T. F. Pedersen (2011), Silver in the subarctic northeast Pacific Ocean: Explaining the basin scale distribution of silver, *Marine Chemistry*, *123*(1-4), 133-142.

Lee, B.-G., and N. S. Fisher (1993), Release rates of trace elements and protein from decomposing planktonic debris. 1. Phytoplankton debris, *Journal of Marine Research*, *51*(2), 391-421.

Marinov, I., A. Gnanadesikan, J. R. Toggweiler, and J. L. Sarmiento (2006), The Southern Ocean biogeochemical divide, *Nature*, *441*(7096), 964-967.

Martin, J. H., and G. A. Knauer (1973), The elemental composition of plankton, *Geochimica et Cosmochimica Acta*, *37*(7), 1639-1653.

Martin, J. H., G. A. Knauer, and R. M. Gordon (1983), Silver distributions and fluxes in north-east Pacific waters, *Nature*, *305*(5932), 306-309.

McKay, J. L., and T. F. Pedersen (2008), The accumulation of silver in marine sediments: A link to biogenic Ba and marine productivity, *Global Biogeochemical Cycles*, *22*(GB4010), doi: 10.1029/2007GB003136.

Menzel, D. W., and N. Corwin (1965), The measurement of total phosphorus in seawater based on the liberation of organically bound fractions by persulfate oxidation, *Limnology and Oceanography*, *10*(2), 280-282.

Mortlock, R. A., and P. N. Froelich (1989), A simple method for the rapid determination of biogenic opal in pelagic marine sediments, *Deep-Sea Research*, *36*(9), 1415-1426.

Ndung'u, K., M. A. Thomas, and A. R. Flegal (2001), Silver in the western equatorial and South Atlantic Ocean, *Deep-Sea Research II*, *48*(13), 2933-2945.

Nieboer, E., and D. H. S. Richardson (1980), The replacement of the nondescript term ‘heavy metals’ by a biologically and chemically significant classification of metal ions, *Environmental Pollution Series B, Chemical and Physical*, *1*(1), 3-26.

Nuester, J., S. Vogt, and B. S. Twining (2012), Localization of iron within centric diatoms of the genus *Thalassiosira*, *Journal of Phycology*, *48*(3), 626-634.

Núñez-Milland, D. R., S. B. Baines, S. Vogt, and B. S. Twining (2010), Quantification of phosphorus in single cells using synchrotron X-ray fluorescence, *Journal of Synchrotron Radiation*, *17*, 560-566.

Parsons, T. R., Y. Maita, and C. M. Lalli (1984), *A manual of chemical and biological methods for seawater analysis*, Pergamon Press, Oxford.

Price, N. M., G. I. Harrison, J. G. Hering, R. J. Hudson, P. M. V. Nirel, B. Palenik, and F. M. M. Morel (1988/1989), Preparation and chemistry of the artificial algal culture medium Aquil, *Biological Oceanography, 6*, 443-461.

Ragueneau, O., et al. (2000), A review of the Si cycle in the modern ocean: recent progress and missing gaps in the application of biogenic opal as a paleoproductivity proxy, *Global and Planetary Change, 26*(4), 317-365.

Ratte, H. T. (1999), Bioaccumulation and toxicity of silver compounds: a review, *Environmental Toxicology and Chemistry*, *18*(1), 89-108.

Raven, J. A. (1997), The vacuole: a cost-benefit analysis, *Advances in Botanical Research*, *25*, 59-86.

Reinfelder, J. R., and N. S. Fisher (1991), The assimilation of elements ingested by marine copepods, *Science*, *251*(4995), 794-796.

Reinfelder, J. R., and S. I. Chang (1999), Speciation and microalgal bioavailability of inorganic silver, *Environmental Science and Technology*, *33*(11), 1860-1863.

Sarmiento, J. L., and N. Gruber (2006), *Ocean Biogeochemical Dynamics*, 503 pp., Princeton University Press, Princeton.

Sunda, W. G., and S. A. Huntsman (1995), Iron uptake and growth limitation in oceanic and coastal phytoplankton, *Marine Chemistry*, *50*(1–4), 189-206.

Sunda, W. G., and S. A. Huntsman (1998), Processes regulating cellular metal accumulation and physiological effects: Phytoplankton as model systems, *The Science of the Total Environment*, *219*(2-3), 165-181.

Sutton, S. R., P. M. Bertsch, M. Newville, M. Rivers, A. Lanzirotti, and P. Eng (2002), Microfluorescence and microtomography analyses of heterogeneous earth and environmental materials, in *Applications of Synchrotron Radiation in Low-Temperature Geochemistry and Environmental Sciences*, edited by P. A. Fenter, M. L. Rivers, N. C. Sturchio and S. R. Sutton, pp. 429-483, The Mineralogical Society of America, Washington, DC.

Tréguer, P., D. M. Nelson, A. J. V. Bennekom, D. J. DeMaster, A. Leynaert, and B. Quéguiner (1995), The silica balance in the world ocean: a reestimate, *Science*, *268*(5209), 375-379.

Twining, B. S., S. B. Baines, and N. S. Fisher (2004), Element stoichiometries of individual plankton cells collected during the Southern Ocean Iron Experiment (SOFeX), *Limnology and Oceanography*, *49*(6), 2115-2128.

Twining, B. S., S. B. Baines, S. Vogt, and M. D. de Jonge (2008), Exploring ocean biogeochemistry by single-cell microprobe analysis of protist elemental composition, *Journal of Eukaryotic Microbiology*, *55*(3), 151-162.

Twining, B. S., S. B. Baines, N. S. Fisher, J. Maser, S. Vogt, C. Jacobsen, A. Tovar-Sanchez, and S. A. Sañudo-Wilhelmy (2003), Quantifying trace elements in individual aquatic protist cells with a synchrotron x-ray fluorescence microprobe, *Analytical Chemistry*, *75*(15), 3806-3816.

Vogt, S. (2003), MAPS: A set of software tools for analysis and visualization of 3D X-ray fluorescence data sets, *J. Phys. IV*, *104*, 635-638.

Xu, Y., and W.-X. Wang (2004), Silver uptake by a marine diatom and its transfer to the coastal copepod *Acartia spinicauda*, *Environmental Toxicology and Chemistry*, *23*(3), 682-690.

Yee, D., and F. M. M. Morel (1996), In vivo substitution of zinc by cobalt in carbonic anhydrase of a marine diatom, *Limnology and Oceanography*, *41*(3), 573-577.

Zenk, M. H. (1996), Heavy metal detoxification in higher plants-a review, *Gene*, *179*(1), 21-30.

Zhang, Y., H. Amakawa, and Y. Nozaki (2001), Oceanic profiles of dissolved silver: precise measurements in the basins of western North Pacific, Sea of Okhotsk, and the Japan Sea, *Marine Chemistry*, *75*(1-2), 151-163.

Zhang, Y., H. Obata, and Y. Nozaki (2004), Silver in the Pacific Ocean and the Bering Sea, *Geochemical Journal*, *38*, 623-633.

Chapter 6

Conclusions

To conclude, the main results of each research chapter are summarized, and their overall significance toward understanding Ag biogeochemical cycling and (paleo)productivity proxy use is synthesized. Finally, future research directions are considered.

1. Surface Sediments: Pacific Sector and West Antarctic Peninsula Margin

Surface sediment studies explored the relationship between modern diatom surface productivity patterns and Ag enrichment in underlying sediments. **Chapter 2** focused on the open ocean Pacific sector and the influence of the highly productive opal belt. Fluxes of Ag and Cd—trace metals delivered with biogenic particles—were found to increase within the opal belt (60-65°S) alongside more conventional productivity proxies: organic carbon (C_{org}), biogenic silica (Si_{bio}), and total Ba. Rhenium fluxes also increased within the opal belt, though bulk sediment Re concentrations were very low, and we tentatively concluded that Re fluxes reflect weakly reducing conditions in sediments caused by high export production. Additionally, the pattern of Ag fluxes across the transect more closely followed Si net production in surface waters, similar to other studies linking Ag to diatom silica [e.g., *Ndung'u et al.*, 2001]. However, low bulk sediment Ag concentrations suggested significant Ag remineralization resulting from the seasonal nature of export production in the high-latitude Southern Ocean and high-oxygen bottom waters. Nevertheless, this study demonstrated that Ag concentrations/fluxes reliably

record diatom surface productivity patterns. More importantly, the potential for Ag and other trace metals to be present in the modern Southern Ocean environment was recognized for the first time, opening the door for the work described in **Chapter 4**.

Chapter 3 considered trace metal and productivity proxy enrichments in a different Southern Ocean environment, the West Antarctic Peninsula (WAP) continental margin. Trace metal and productivity proxy concentrations indicated suboxic conditions driven by a high flux of C_{org} to sediments. Although WAP bottom water oxygen concentrations are comparable to the open ocean Pacific sector, the magnitude of total trace metal concentrations was similar to those reported for other continental margins. This novel finding suggested that processes controlling redox conditions along the WAP are not different to those in other margin settings. Additionally we proposed a system for inferring past sedimentary redox chemistry/pore water chemistry at the time of trace metal deposition. This system provides a much-needed link between trace metal enrichments and terms commonly used to indicate sedimentary redox conditions, as well as a framework for interpreting paleoredox records along the WAP. Given the dynamic, complex environment of the WAP continental margin, future studies should concentrate on producing records recovered from well-characterized depositional settings.

2. Downcore Sediments: South Atlantic Ocean

Having established that Ag tracks diatom productivity patterns in modern sediments, **Chapter 4** examined Ag as a paleoproductivity proxy by comparing Ag enrichments to other paleoproductivity indicators in Southern Ocean sediments over the past 30 kyr. Furthermore by combining Ag data with redox-sensitive trace metal (Cd, Re, and Mo) enrichments, deep Southern Ocean redox chemistry was investigated independently of carbon isotopes. Trace metals demonstrated a major shift in Southern Ocean chemistry between the mid-Holocene

(TN057-13-4PC) or deglacial (RC13-254) and the late Holocene, shown most clearly by burndown in RC13-254. Past reducing conditions in TN057-13-4PC (modern Antarctic Zone) sediments appear to have been driven by increased export production. In comparison, past reducing conditions in RC13-254 (Cape Basin/modern Antarctic Polar Frontal Zone) sediments appear to have been caused by a combination of increased export production and lower bottom water oxygen concentrations. The trace metal record at RC13-254 suggested that glacial Lower Circumpolar Deep Water (LCDW) stored greater amounts of CO_2, and that enhanced storage was an effect of ocean circulation changes that isolated LCDW and its downstream products, Pacific Deep Water and Indian Deep Water. Moreover Ag fluxes were shown to be an effective paleoproductivity proxy—tracking Cd fluxes and sometimes biogenic silica (opal) fluxes—that may be able to identify preservation biases associated with other proxies. Future studies should take into account that glacial water mass distribution may not have been a modified form of the present day, the interconnected nature of the global ocean, and the potential for proxy preservation biases.

3. Diatom Culture Studies

The culture studies described in **Chapter 5** disproved the assumption that diatoms store Ag in their frustules. Analysis of bulk cultures demonstrated that Ag is primarily associated with diatom organic matter. Single cell analysis further suggested that some Ag is contained with vacuoles, with the remainder assumed to be associated with proteins making up the cell membrane [*Reinfelder and Fisher*, 1991]. Some portion of preserved sedimentary Ag must therefore be delivered to sediments with diatom organic matter, and the rest delivered as an uncharacterized scavenged phase. Although this study clarified the location of Ag storage and pointed to a slightly modified conception of marine Ag geochemical cycling, the question of why

Ag follows silica in the water column and in sediments (**Chapter 2**) has not been fully answered and deserves further study.

4. Synthesis

At the outset of this dissertation, Ag was proposed as a more robust (paleo)productivity proxy for determining the (past) strength of the biological pump. The research presented in the preceding chapters indicates that Ag can be an effective new tool for reconstructing spatial and temporal diatom export production patterns, and their relationship to marine geophysical processes (e.g., upwelling, deep water circulation) that determine the air-sea partitioning of CO_2. Furthermore, the discovery that Ag enrichments occur in Southern Ocean sediments—past and present—expands the range of environments in which trace metals are known to accumulate. Low bottom water oxygen concentrations are not required for trace metal enrichments, but can be achieved where C_{org} flux to the seafloor is periodically high. However, beginning with a bottom water oxygen deficit tends to promote greater trace metal and C_{org} preservation in sediments (Figures 3.3 and 3.5).

Like all proxies, Ag has its own set of biases and limitations. In order to fully reconstruct the strength of the biological pump, a quantitative relationship between sedimentary proxy enrichments and surface productivity is needed. Presently this relationship remains elusive partly as a result of elemental recycling within the water column. Yet Ag may work as a productivity proxy because it is a non-nutrient element whose biogeochemical cycling is uncomplicated by competition for uptake by various organisms. Nevertheless, questions concerning early diagenesis of Ag remain: How does the speciation of Ag change between arrival at the sediment-water interface and permanent burial? Does Ag associate with pyrite or other minerals, and if so,

does this association enhance Ag preservation? Does the geochemical behavior of Ag confer an advantage to its use as a proxy over other metals?

5. Future Directions

Several potential directions for future research arise from this dissertation. Clearly, the details of Ag marine biogeochemical cycling have not been fully worked out, including the phase association and speciation of marine Ag with increasing water depth. Sediment trap studies utilizing filtration to isolate different particle size fractions followed by sequential chemical digestions (H_2O_2, aqua regia, HF, etc.) may be able to provide additional information. Some of this work is already being carried out by my collaborator, Dr. Jennifer McKay of Oregon State University. Stable Ag isotopes are another tool that could be used to investigate Ag cycling. Silver exhibits isotopic fractionation in environmental materials which is measurable using multicollector-ICP-MS [*Luo et al.*, 2010]. Significantly, Ag has the potential to undergo mass independent fractionation (MIF), having two odd-numbered stable isotopes with nonzero nuclear spins and being easily photoreduced [*Buchachenko,* 2013]. MIF of stable mercury (Hg) isotopes has been used successfully to trace that element's biogeochemical cycling [e.g., *Sherman et al.*, 2010], suggesting that a similar approach may prove useful for Ag. Like Hg, Ag is toxic to phytoplankton and invertebrates [*Ratte,* 1999]. Silver nanoparticles are being produced in ever-increasing quantities as antimicrobial agents and finding their way into the environment [*Hendren et al.*, 2011], and remediating any toxicity effects will likely require a more complete understanding of Ag biogeochemical cycling.

In regard to glacial-interglacial CO_2 changes, the ocean circulation changes and resulting deep water chemistry that were discussed in **Chapter 4** can only be conclusively demonstrated as arising from glacial LCDW by further trace metal measurements from cores in all three

sectors of the Southern Ocean, and the deep Indian and Pacific Oceans. Because trace metal measurements do not require well-preserved carbonate samples, greater access to the deep Indo-Pacific should be available than for stable isotope studies, which currently provide the bulk of our information concerning glacial hydrography [e.g., *Curry and Oppo*, 2005; *Keigwin*, 1998]. Additionally, further characterization of glacial Antarctic Zone redox chemistry would assist in determining vertical water mass distributions and properties, as well as changes in deep water formation. Lastly, in order to more accurately interpret proxies, more direct evidence is needed about the speciation and enrichment mechanisms of trace metals in sediments, along with chemical changes that occur during early diagenesis. Sophisticated analytical techniques such as XAFS are currently little used by the paleoceanographic community but could be a next step. Where possible, laboratory experiments should be coupled with observations from natural samples. This approach would allow for identification of probable geochemistry in a controlled setting, followed by field tests to confirm whether similar behavior occurs in a more complex, uncontrolled system.

REFERENCES

Buchachenko, A. L. (2013), Mass-independent isotope effects, *Journal of Physical Chemistry B, 117*(8), 2231-2238.

Curry, W. B., and D. W. Oppo (2005), Glacial water mass geometry and the distribution of $\delta^{13}C$ of ΣCO_2 in the western Atlantic Ocean, *Paleoceanography, 20*(PA1017), doi: 10.1029/2004PA001021.

Hendren, C. O., X. Mesnard, J. Dröge, and M. R. Wiesner (2011), Estimating production data for five engineered nanomaterials as a basis for exposure assessment, *Environmental Science and Technology, 45*(7), 2562-2569.

Keigwin, L. D. (1998), Glacial-age hydrography of the far northwest Pacific Ocean, *Paleoceanography, 13*(4), 323-339.

Luo, Y., E. Dabek-Zlotorzynska, V. Celo, D. C. G. Muir, and L. Yang (2010), Accurate and precise determination of silver isotope fractionation in environmental samples by multicollector-ICPMS, *Analytical Chemistry, 82*(9), 3922-3928.

Ndung'u, K., M. A. Thomas, and A. R. Flegal (2001), Silver in the western equatorial and South Atlantic Ocean, *Deep-Sea Research II, 48*(13), 2933-2945.

Ratte, H. T. (1999), Bioaccumulation and toxicity of silver compounds: a review, *Environmental Toxicology and Chemistry, 18*(1), 89-108.

Reinfelder, J. R., and N. S. Fisher (1991), The assimilation of elements ingested by marine copepods, *Science, 251*(4995), 794-796.

Sherman, L. S., J. D. Blum, K. P. Johnson, G. J. Keeler, J. A. Barres, and T. A. Douglas (2010), Mass-independent fractionation of mercury isotopes in Arctic snow driven by sunlight, *Nat. Geosci., 3*(3), 173-177.

Appendix A

Supplementary Information for Chapter 2

Without normalization, sedimentary components of interest may be diluted by other components, masking their signal. For example, on the Ross Sea continental shelf, high lithogenic input dilutes C_{org} (DeMaster et al., 1996; NBP9802-01-MC1, $\%C_{org} = 0.44$, %lithogenic ≈ 90.47); and in the opal belt ~62°S in the Pacific sector, Si_{bio} dilutes essentially all other components (Table 2.3). Below we describe several possible methods of data normalization or comparison, demonstrate that we reach the same conclusion with our data no matter the method chosen, and explain our rationale for preferring the ^{230}Th normalization method.

One common method normalizes elemental data to Al, an element presumed to reside entirely within the aluminosilicate fraction [*Calvert and Pedersen*, 1993; *Tribovillard et al.*, 2006]. Al-normalization assumes a constant flux of detrital aluminosilicates to sediments. With increasing distance from sources of detrital input (i.e., in oceanic environments), the assumption of constant Al input may not be valid [*Murray and Leinen*, 1996] particularly if variable or pulsed opal rain delivers a significant quantity of sedimentary Al [*Dymond et al.*, 1997]. Al-normalized trace metal concentrations (Figure A.1) show highest (Ag, Cd, Re)/Al ratios between ~60-65°S, coincident with the northern limit of sea ice and the opal belt. Mo/Al ratios show a less pronounced increase between these latitudes. However, the coefficient of variation (standard deviation divided by the mean) is greater for Al than the coefficient of variation of any of the

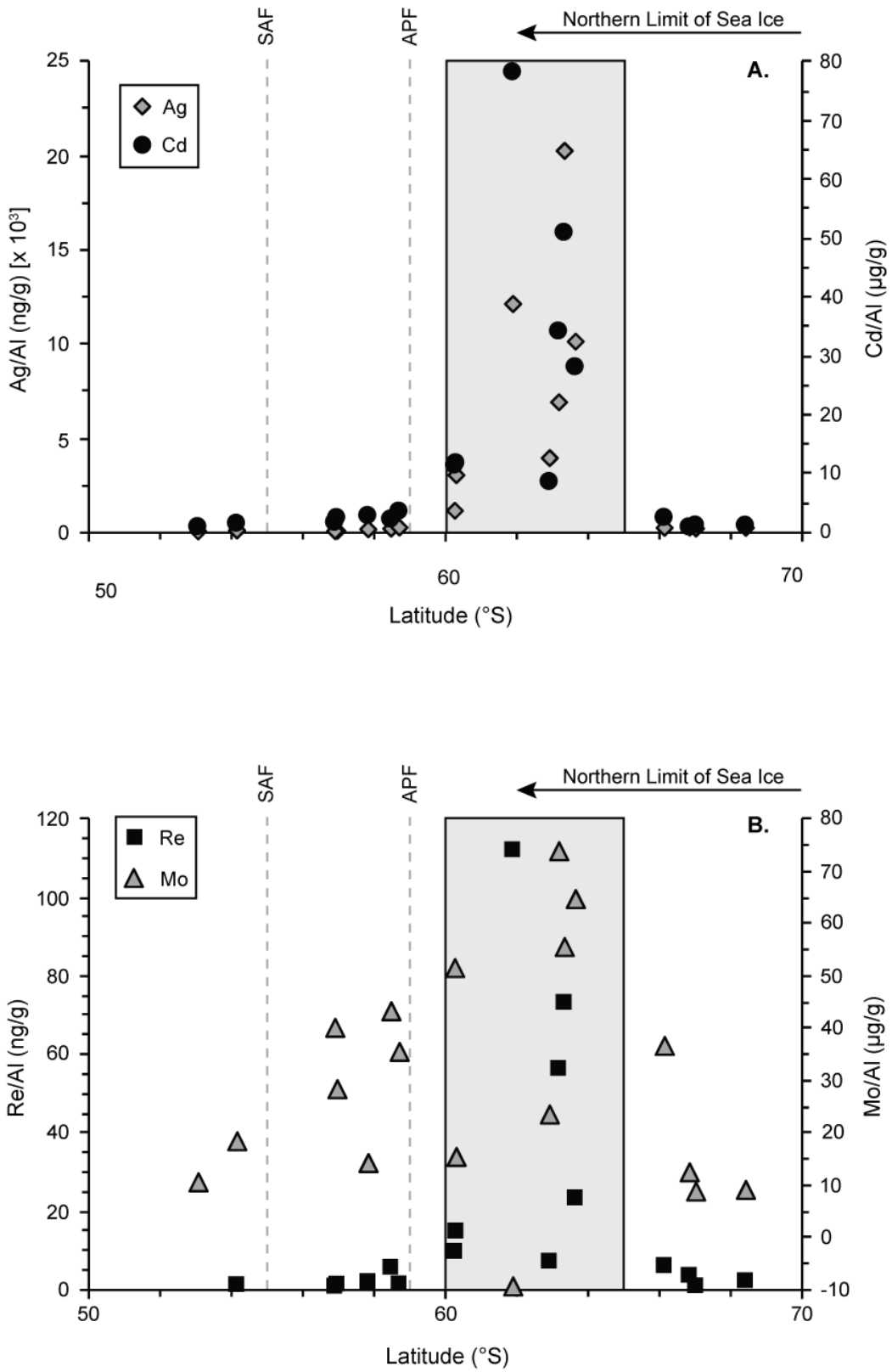

Figure A.1. Total trace metal concentrations normalized to weight percent Al. A) Ag/Al and Cd/Al ratios. B) Re/Al and Mo/Al ratios. Grey box denotes opal belt. Dashed grey lines indicate approximate locations of the Antarctic Polar Front (APF) and Subantarctic Front (SAF).

proxies except Mo (Table 2.3), increasing the possibility of creating a spurious correlation mathematically [*Van der Weijden*, 2002].

Calculating excess concentrations is another common method of comparing geochemical data whereby the concentration "in excess" of the lithogenic component is estimated by the following equation [*Tribovillard et al.*, 2006]:

$$[M]_{xs} = [M]_{smp} - (([M]/[Al])_{bkg} * [Al]_{smp})$$

where $[M]_{xs}$ is the excess concentration of the metal; $[M]_{smp}$ is the measured concentration of the metal in the sample; $([M]/[Al])_{bkg}$ is the background metal/Al ratio (often assumed to be average shale); and $[Al]_{smp}$ is the measured Al concentration in the sample. Notably, this method relies on measured Al concentrations, with similar issues to those discussed in the previous paragraph. Very low Al concentrations will drive higher excess concentrations, as occurs in the opal belt samples. More problematic is that the true $([M]/[Al])_{bkg}$ ratio for each core must be assumed when calculating excess concentrations. Without specific information about the provenance and chemical composition of the lithogenic material at each site, the appropriate background ratio is always uncertain. Excess concentrations are plotted in Figure A.2, with average shale [*Li*, 2000] assumed as the background for simplicity. Excess Ag, Cd, and Re concentrations are generally only greater than zero within the opal belt. Excess Mo concentrations, in contrast, average approximately zero within the opal belt and are highest at two sites within the Antarctic Polar Frontal Zone. Because many excess concentrations are calculated as less than zero, average shale composition is clearly not an appropriate choice for background composition in this polar setting. Equally, it is not clear what could be used as a better choice.

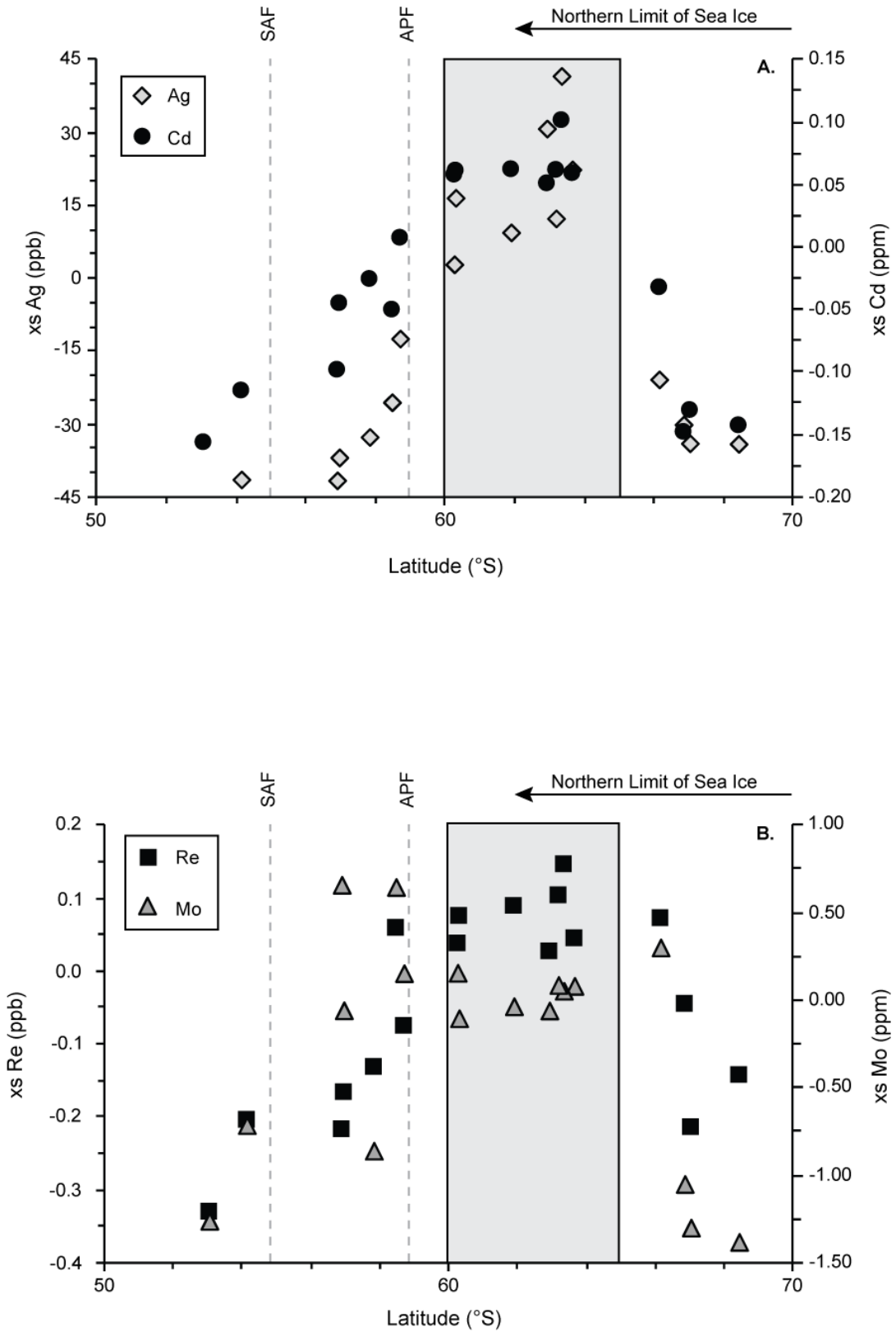

Figure A.2. Excess trace metal concentrations. A) Ag and Cd. B) Re and Mo. Grey box and dashed lines as in Figure A.1.

Aluminum concentrations tend to track lithogenic content across the transect (Figure A.3a), suggesting that productivity does not drive Al accumulation in this region. Based on this observation, total Ag concentrations are plotted alongside Ag excess concentrations assuming both average shale and upper continental crust background compositions in Figure A.3b to illustrate that the choice of background composition is most important for samples at the northern and southern ends of the transect, where lithogenic input is higher. Within the high productivity zone (60-65°S) where elevated Ag fluxes exist, lithogenic input makes a relatively minor contribution to total Ag and other trace metal concentrations, justifying the decision not to use excess concentrations when normalizing to ^{230}Th.

Bulk mass accumulation rates are another commonly used method but rely on both good age control and sediment dry bulk density measurements, neither of which are available for Pacific sector surface sediments. Furthermore, another set of assumptions is required to determine age including estimates of the average regional surface ocean reservoir age if radiocarbon dating is used. Moreover, upwelling conditions change significantly across the transect, and episodic addition of old dissolved inorganic carbon from upwelled deep water may create spurious radiocarbon ages. Additionally, Southern Ocean sediments are difficult to date due to the paucity of biogenic carbonate. Therefore we are not able to calculate bulk mass accumulation rates for individual trace metals.

Another possibility is to normalize to ^{232}Th, an isotope considered to have a solely lithogenic source [*Brewer et al.*, 1980]. This method should produce results similar to Al normalization. ^{232}Th concentrations were not measured for samples used in this study, but Chase et al. [2003a] report surface sediment ^{232}Th concentrations for the NBP9802 cores. The same

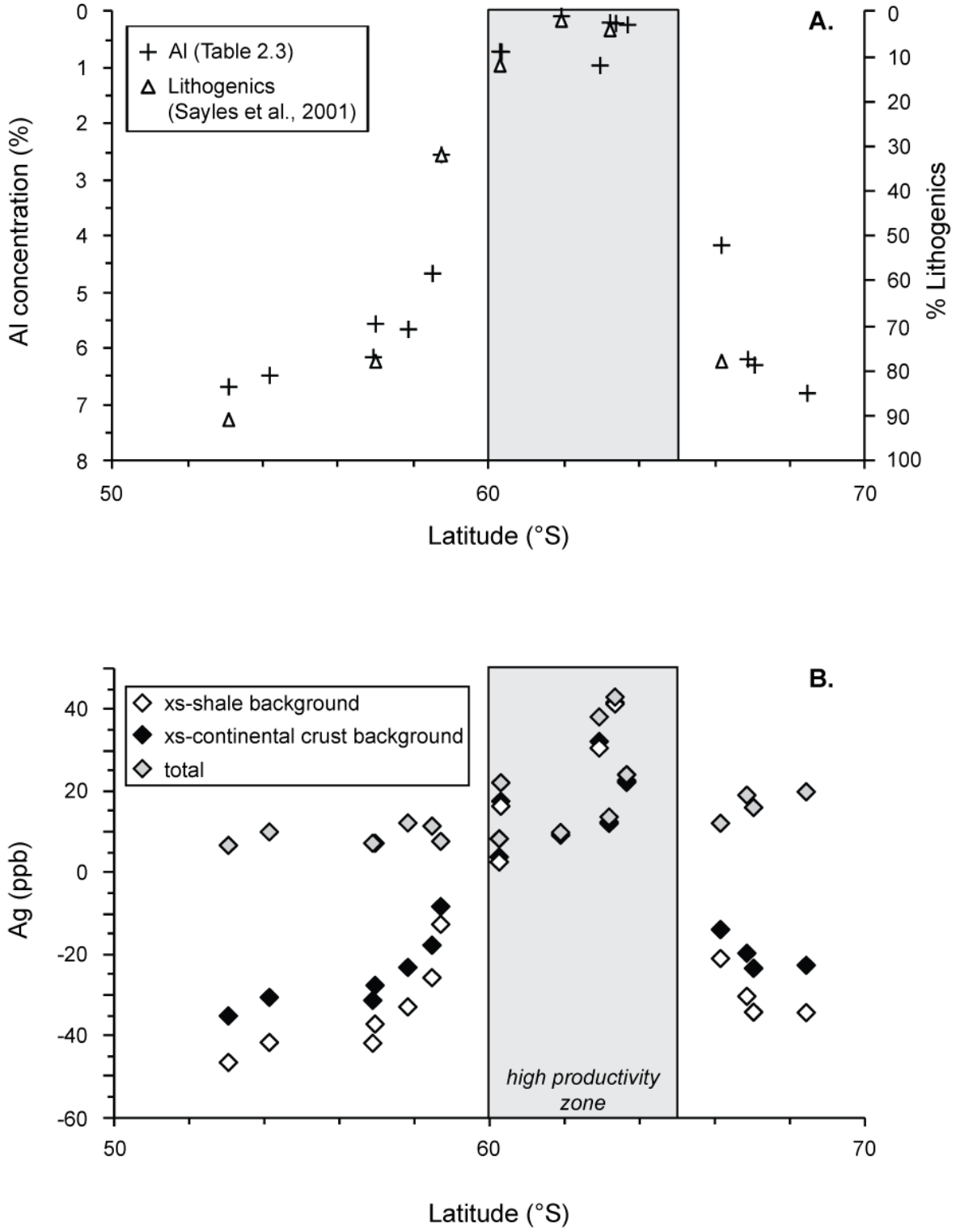

Figure A.3. Expected lithogenic contribution to trace metal excess concentrations. A) Al concentrations closely track lithogenic content, implying that the assumption that Al is associated solely with the aluminosilicate fraction is reasonable. B) Effect of applying different background concentrations on calculated trace metal excess concentrations. Note that lithogenic input makes a comparatively small contribution to opal belt sediments (~60-65°S) compared to sites outside this zone.

cores and intervals chosen for ^{230}Th concentrations (see Chapter 2) were chosen for ^{232}Th concentrations. As expected, a similar pattern to Al-normalization emerges when normalizing to ^{232}Th (Figure A.4). Highest (Ag, Cd, Re)/^{232}Th ratios occur between ~60-65°S, but Mo/^{232}Th ratios show no clear trend.

All three methods considered above (omitting bulk mass accumulation rates) result in a slight increase in relative sedimentary abundance of Ag, Cd, and Re within the opal belt compared to regions north and south of ~60-65°S, in agreement with flux estimates derived from ^{230}Th normalization. To illustrate, Ag data are plotted in Figure A.5 using all three methods described above, plus Ag flux estimates. While the details are slightly different, the general conclusion holds that Ag input to opal belt sediments is greater than can be expected only from detrital sources.

Ultimately ^{230}Th profiling was chosen as the preferred method of comparing data across the transect because it has the advantage of correcting for effects of dilution and sediment redistribution, as well as estimating metal fluxes to the sediment-water interface. This approach presents the fewest potential problems. Although we did not measure ^{230}Th concentrations on splits of our samples—anticipating that Al normalization would be sufficient—the coefficient of variation (standard deviation divided by the mean) of $_{xs}^{230}Th_0$ concentrations is 9% or less within the upper 5 cm of each core (with the exception of NBP9802-09-MC1 at 15.8%, although of the two data points given, one has large error bars) [*Chase et al.*, 2003a]. This implies that our application to surface samples is reasonable, as discussed further below. It is also worth noting that opal belt $_{xs}^{230}Th_0$ concentrations are also several times lower (depending on the sites compared) than $_{xs}^{230}Th_0$ concentrations at the northern and southern ends of the transect.

Uncertainties in $_{xs}^{230}Th_0$ values were estimated as follows: For NBP9802 cores, $_{xs}^{230}Th_0$

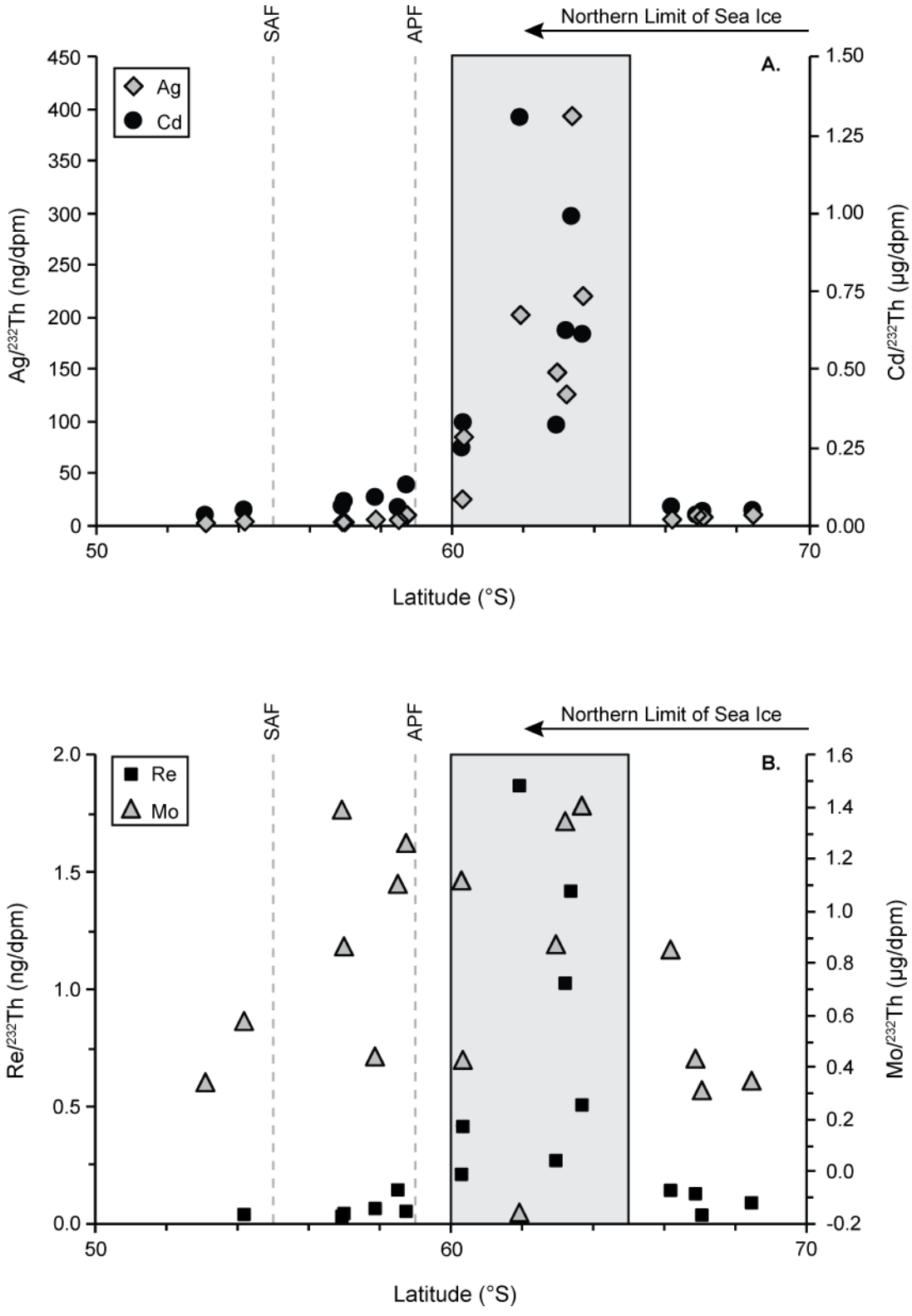

Figure A.4. Total trace metal concentrations normalized to ^{232}Th concentrations. A) Ag/^{232}Th and Cd/^{232}Th ratios. B) Re/^{232}Th and Mo/^{232}Th ratios. Grey box and dashed lines as in Figure A.1.

values were only affected by differences in sample depth, so the $_{xs}^{230}Th_0$ coefficient of variation for the upper 5 cm of each core was multiplied by the chosen $_{xs}^{230}Th_0$ (Table 2.3) to give an uncertainty in dpm/g. Exceptions include NBP9802-03-MC1, for which the sample depth given by Chase et al. [2003a] is the same as for this study; and NBP9802-09-MC3, for which there is only one data point. In both cases, the uncertainties given in Chase et al. [2003a] were used. For KN7812 cores, latitudinal variation is also expected to contribute significantly to uncertainty in assigned $_{xs}^{230}Th_0$ values. Cores were divided into the Northern ACC, Polar Frontal Region, Southern ACC, and Ross Gyre zones, after Nelson et al. [2002]—except for core NBP9802-10-MC1 which is located north of the Subantarctic Front and formed its own category. The $_{xs}^{230}Th_0$ coefficient of variation was then calculated for each zone, using all cores and sample depths within the zone. The coefficient of variation for each zone was then multiplied by the relevant $_{xs}^{230}Th_0$ value chosen for each KN7812 core to give an uncertainty in dpm/g. For example, cores KN7812-07BC, -08BC, and -09BC are within the Ross Gyre zone, where the coefficient of variation is 7.2% and the uncertainty = 0.072 × 26.9 dpm/g = 1.94 dpm/g. Cores KN7812-02BC and KN7812-05BC likely present the greatest uncertainty because they are located westward of the main north-south transect of the other cores. The Southern Ocean is more zonally homogeneous [*Nelson et al.*, 2002], but because ^{230}Th production is a function of water depth [*Francois et al.*, 2004], $_{xs}^{230}Th_0$ values for these cores were taken from NBP9802-09-MC1 and NBP9802-07-MC2, respectively. And although KN7812-05BC is sited within the Southern ACC, NBP9802-07-MC2 falls within the Polar Frontal Region, and for consistency, the coefficient of variation for this region was applied to KN7812-05BC.

For the authigenic metals Re and Mo, fluxes were calculated identically to other elements that are assumed to be part of the sinking particulate flux in order to compare all proxies on the

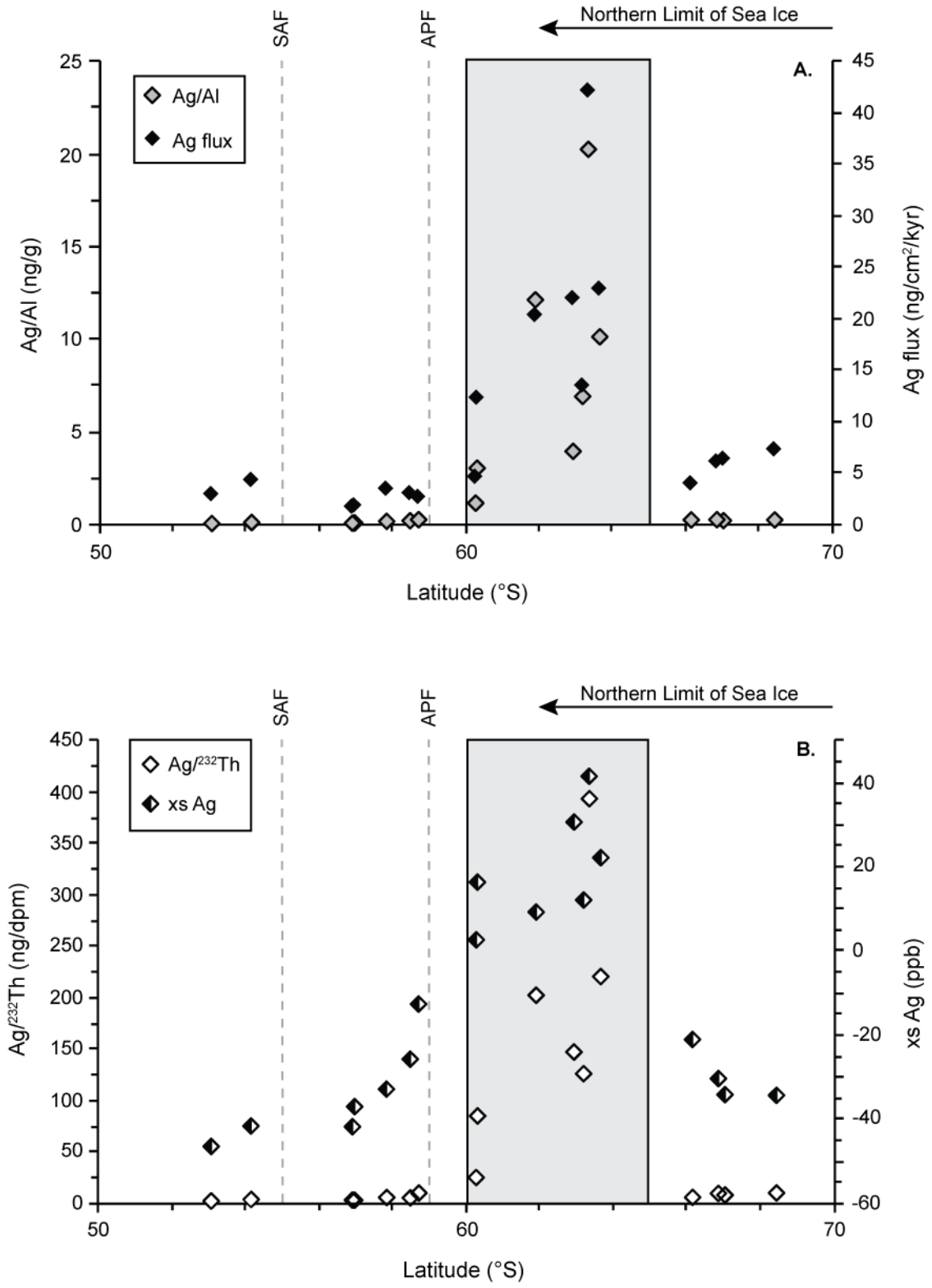

Figure A.5. Ag data compared using all four methods described in the Supplementary Information. A) Ag flux and Ag/Al ratios. B) Ag/^{232}Th ratios and xs Ag. Grey box and dashed lines as in Figure A.1.

same basis and to correct for syndepositional sediment redistribution. Although the term "preserved vertical flux" is not strictly applicable to authigenically precipitated elements, metals diffuse into and are precipitated within the sediments or are scavenged from the overlying water column, so a "vertical component" conceptually exists. A more important consideration is that Re and Mo precipitation from pore waters may occur deeper in the sediment column than deposition of ^{230}Th, which is delivered to the sediment-water interface. However, in sediments that are sufficiently reducing for Re and/or Mo accumulation, precipitation occurs within the upper ~1 cm of sediments [*Crusius et al.*, 1996], minimizing the impact of this offset. Moreover, applying ^{230}Th profiling to Re and Mo does not violate any assumptions of the method—it may, in principle, be applied to any sedimentary component. The main assumption underlying the method is that the flux of scavenged ^{230}Th reaching the seafloor equals the ^{230}Th production rate in the water column [*Francois et al.*, 2004]. In the Pacific sector, scavenged ^{230}Th fluxes appear to be similar to the water column production rate [*Chase et al.*, 2003b].

REFERENCES

Brewer, P. G., Y. Nozaki, D. W. Spencer, and A. P. Fleer (1980), Sediment trap experiments in the deep North Atlantic: isotopic and elemental fluxes, *Journal of Marine Research, 38*, 703-728.

Calvert, S. E., and T. F. Pedersen (1993), Geochemistry of recent oxic and anoxic marine sediments: Implications for the geological record, *Marine Geology*, *113*(1-2), 67-88.

Chase, Z., R. F. Anderson, M. Q. Fleisher, and P. W. Kubik (2003a), Accumulation of biogenic and lithogenic material in the Pacific sector of the Southern Ocean during the past 40,000 years, *Deep-Sea Research II*, *50*(3-4), 799-832.

Chase, Z., R. F. Anderson, M. Q. Fleisher, and P. W. Kubik (2003b), Scavenging of ^{230}Th, ^{231}Pa, and ^{10}Be in the Southern Ocean (SW Pacific sector): the importance of particle flux, particle composition, and advection, *Deep-Sea Research II*, *50*(3-4), 739-768.

Crusius, J., S. Calvert, T. Pedersen, and D. Sage (1996), Rhenium and molybdenum enrichments in sediments as indicators of oxic, suboxic, and sulfidic conditions of deposition, *Earth Planet. Sci. Lett.*, *145*(1-4), 65-78.

Dymond, J., R. Collier, J. McManus, S. Honjo, and S. Manganini (1997), Can the aluminum and titanium contents of ocean sediments be used to determine the paleoproductivity of the oceans?, *Paleoceanography*, *12*(4), 586-593.

Francois, R., M. Frank, M. M. R. van der Loeff, and M. P. Bacon (2004), Th-230 normalization: An essential tool for interpreting sedimentary fluxes during the late Quaternary, *Paleoceanography*, *19*(PA1018), doi: 10.1029/2003PA000939.

Li, Y.-H. (2000), *A Compendium of Geochemistry: From Solar Nebula to the Human Brain*, 475 pp., Princeton University Press, Princeton.

Murray, R. W., and M. Leinen (1996), Scavenged excess aluminum and its relationship to bulk titanium in biogenic sediment from the central equatorial Pacific Ocean, *Geochimica et Cosmochimica Acta*, *60*(20), 3869-3878.

Nelson, D. M., et al. (2002), Vertical budgets for organic carbon and biogenic silica in the Pacific sector of the Southern Ocean, 1996-1998, *Deep-Sea Research II*, *49*(9-10), 1645-1674.

Tribovillard, N., T. J. Algeo, T. Lyons, and A. Riboulleau (2006), Trace metals as paleoredox and paleoproductivity proxies: An update, *Chemical Geology*, *232*(1-2), 12-32.

Van der Weijden, C. H. (2002), Pitfalls of normalization of marine geochemical data using a common divisor, *Marine Geology*, *184*(3-4), 167-187.

Appendix B

Supplementary Figures for Chapter 5

The following figures show the micro-XRF scans of Cells 1, 3, and 4 and a relationship between cell size and Ag enrichment (Ag/P ratio).

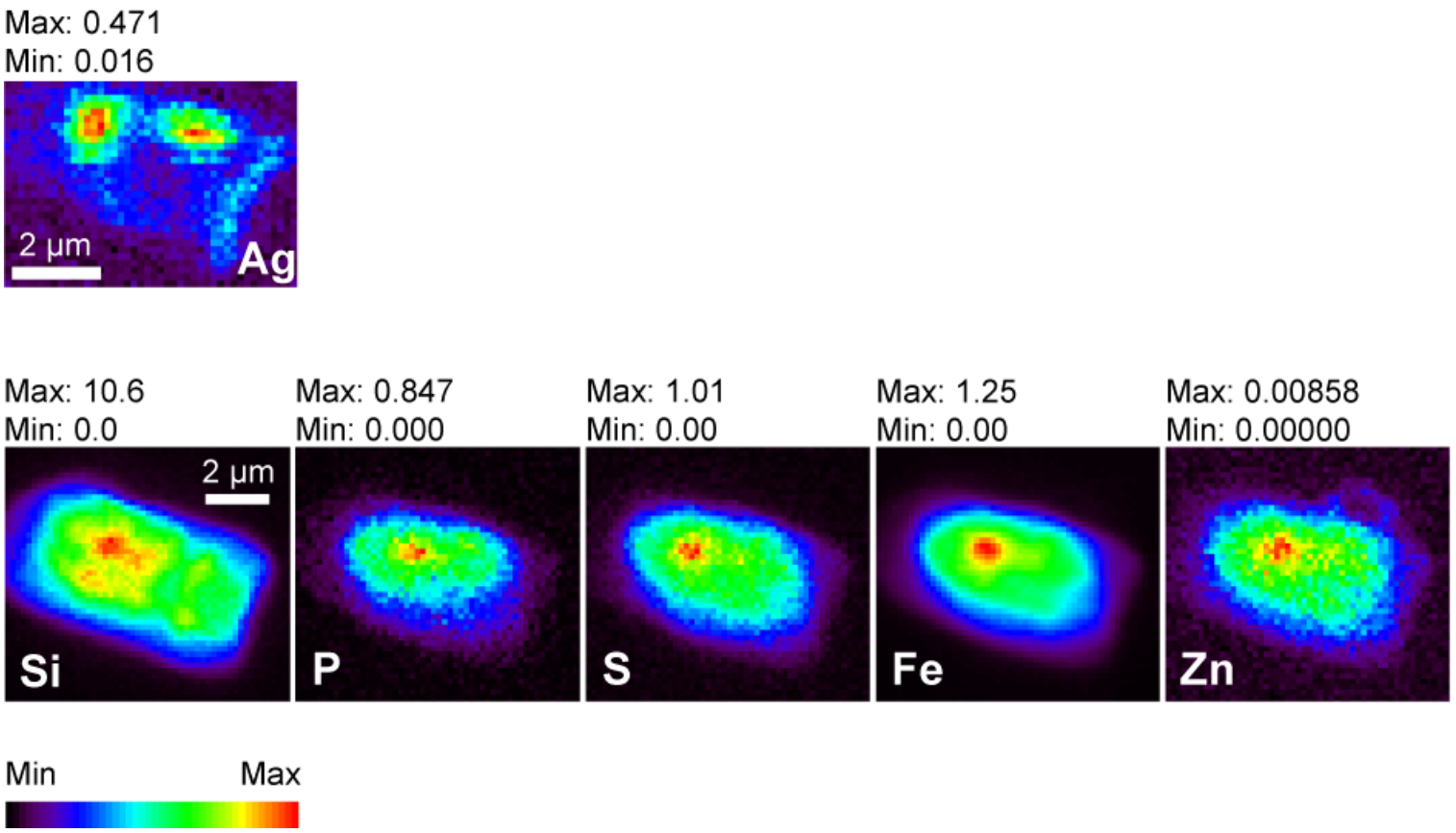

Figure B.1. Cell 1. Color scale is scaled to maximum concentration in each panel. Concentrations given in µg cm^{-2}. Scale bar in Ag image (25.5 keV) is the same for both images in top row. Scale bar in Si image (10 keV) is the same for all five images in the bottom row.

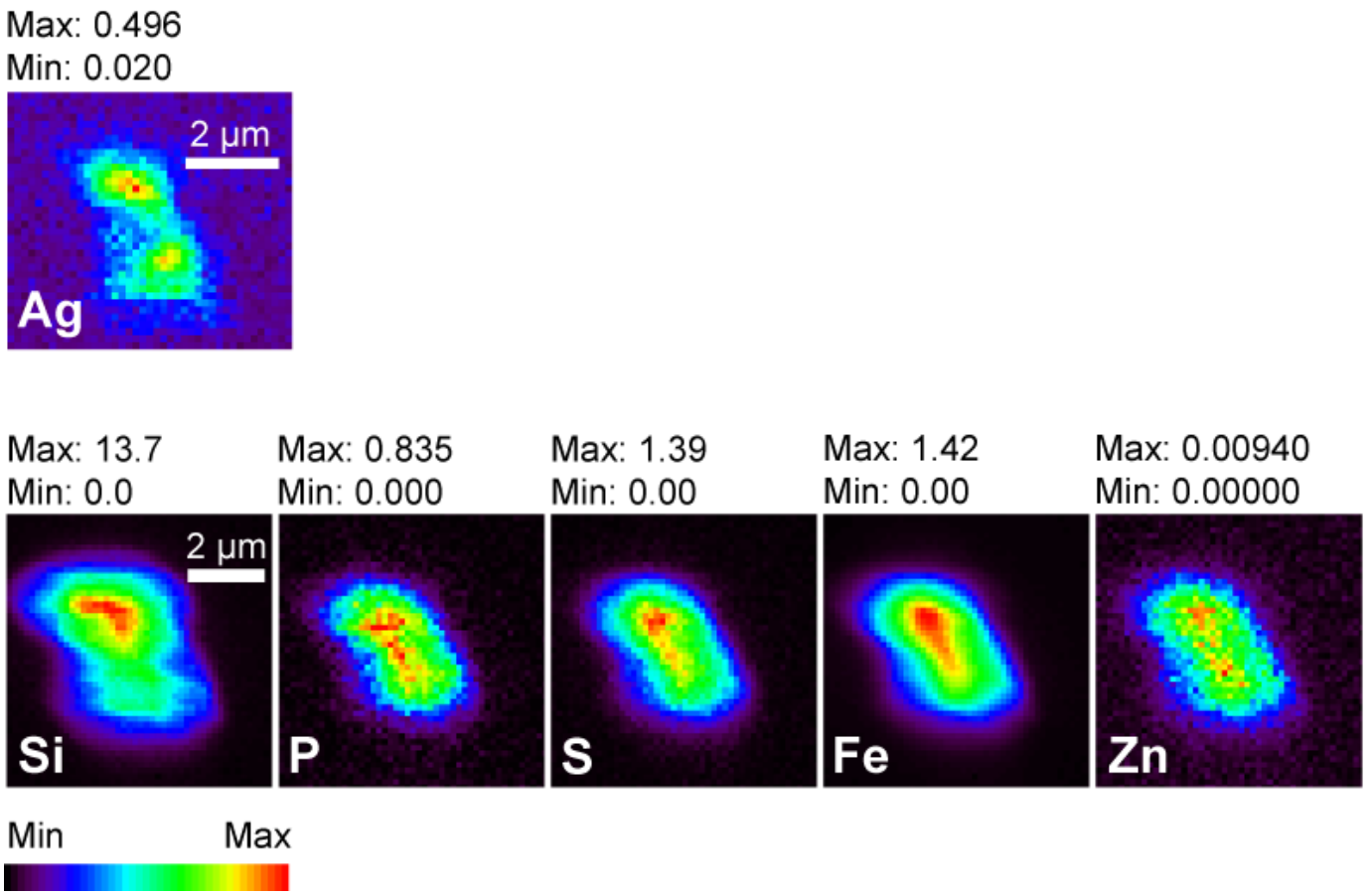

Figure B.2. Cell 3. Color scale is scaled to maximum concentration in each panel. Concentrations given in µg cm^{-2}. Scale bars as in Figure B.1.

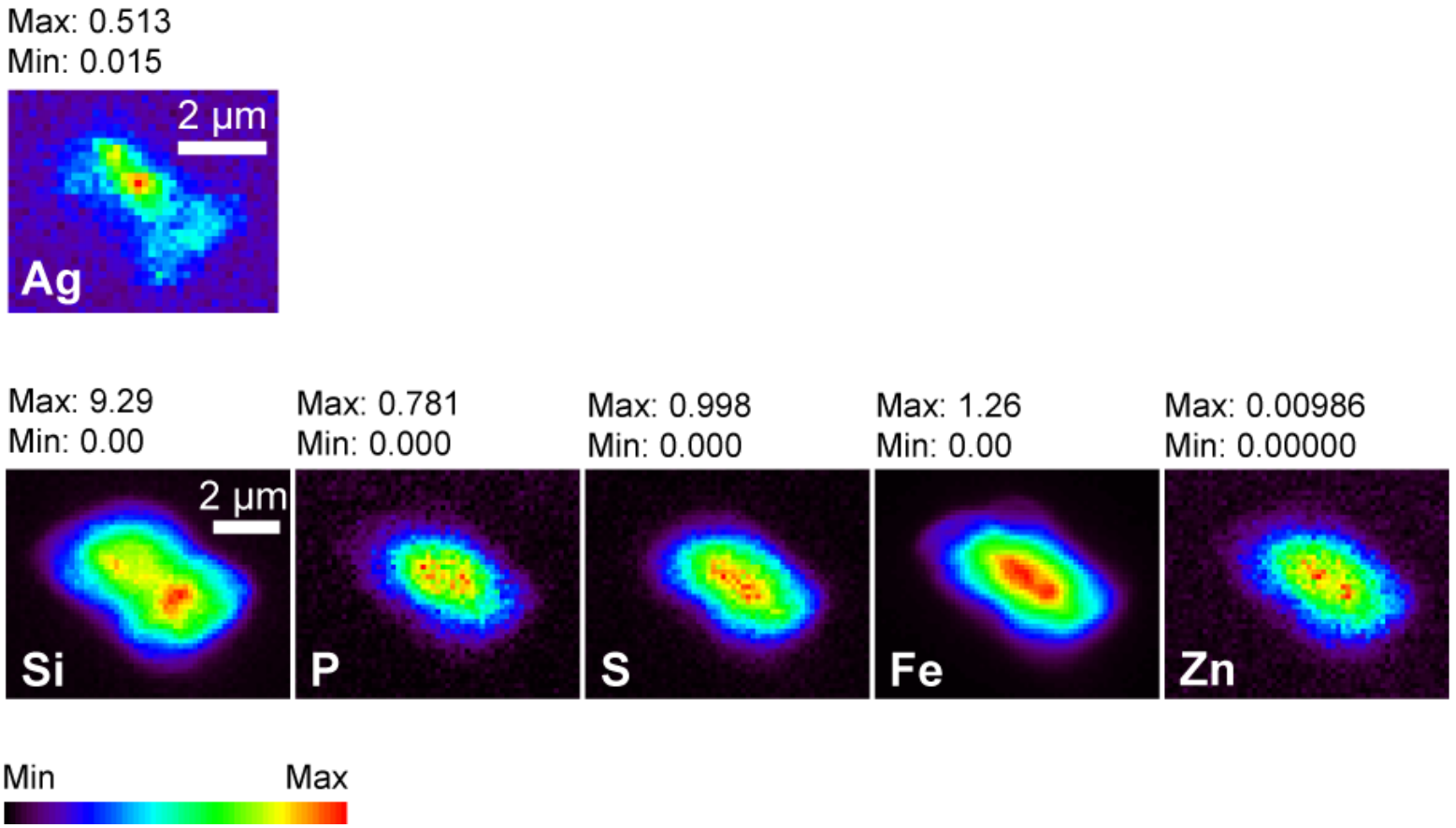

Figure B.3. Cell 4. Color scale is scaled to maximum concentration in each panel. Concentrations given in µg cm^{-2}. Scale bars as in Figure B.1.

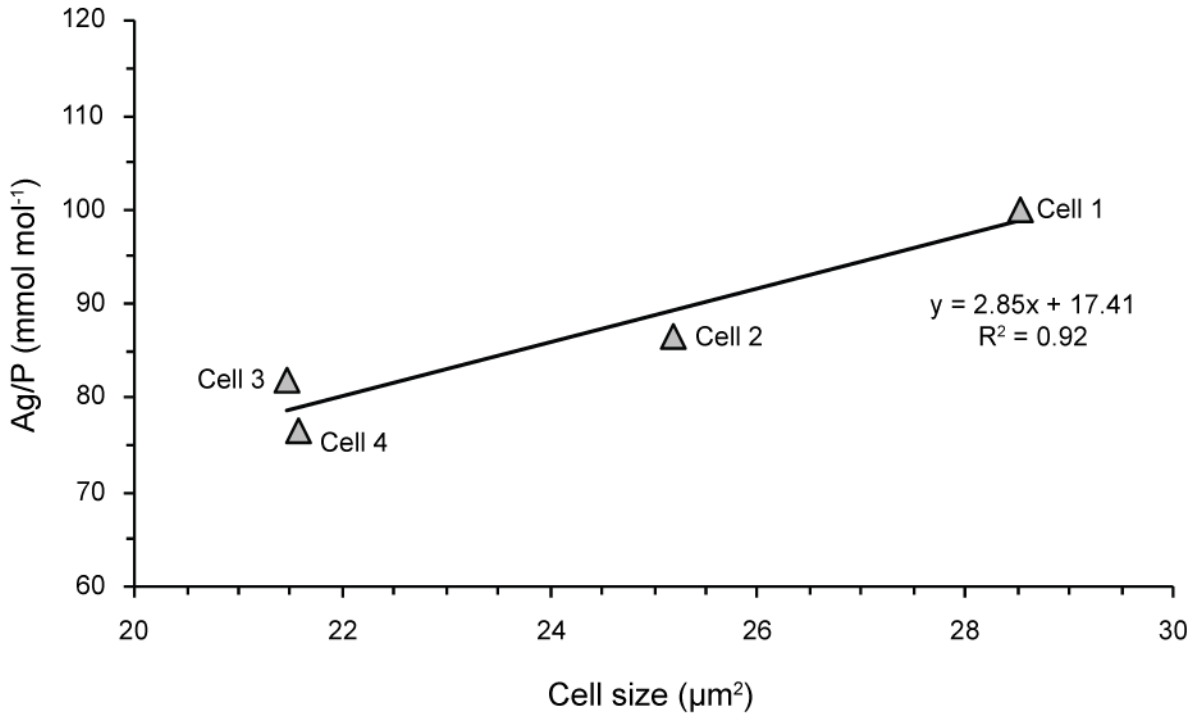

Figure B.4. Ag enrichment (Ag/P ratio) as a function of areal cell size.